A toolkit to study mechanisms of liver disease associated with hepatitis C virus genotype 3 infection

Anya Kerry Morrison (BSc(Hons)MRes)

Submitted in accordance with the requirements for the degree of Doctor of Philosophy

University of Leeds
Faculty of Biological Sciences
School of Molecular and Cellular Biology
February 2024

I confirm that the work submitted is my own and that appropriate credit has been given where reference has been made to the work of others.

Acknowledgements

I would like to thank my supervisors Professors Mark Harris and Fiona Oakley for the continued support and advice throughout this project.

Thank you to all Oakley lab members, in particular Amy Collins and Hannah Paish, for answering all my emails and teaching me the ropes of spheroids and liver slices at Newcastle University. And a special shoutout for everyone who had to undertake the BSL-3 out-of-hours training for me. Thank you to Julia Spoors and Fiona who fought very hard to get me into the Newcastle BSL-3, infection of the liver slices wouldn't have been accomplished without you both!

I would like to thank past and present members of Garstang 8.61 and Level 9 at the University of Leeds. Kate, Ellie, Paul, Sarah, James and Ollie, thank you for providing lots of activities throughout the years, it provided lots of laughs and enjoyment, making the past couple of years a unique and fun experience.

Thank you to my family for always supporting me no matter what task I put my mind to and later complain about. Thank you to Alison and Jeremy for the support, desserts, and providing lots of cuddles with the dogs, especially when feeling homesick.

Tim, I am unbelievably lucky to have had you by my side throughout the PhD. The process has not been easy and without you, I would never have come this far. Feeling lucky I chained you down to tie the knot before final year really kicked in! I won't ever be able to thank you enough

for all the support, patience and love you give me. I am so excited to start the next chapter of our lives together.

I would like to dedicate my PhD to my family. A lot has happened in these few years, something which will always remain is the unwavering support and love we have for each other.

And thank you Jamie Balls, just because.

Abstract

Hepatitis C virus (HCV) infection is the leading cause of liver transplantation, cirrhosis and cancer. HCV genotype 3 (GT3), the second most common genotype worldwide, shows a high level of resistance to direct-acting antivirals and a more rapid progression to chronic liver disease. Currently, tools available to study GT3 are limited and needed to achieve a greater understanding of the mechanisms driving disease pathology. Molecular biology techniques include modification of subgenomic replicons and infectious cell culture virus clones by inserting epitope tags into domain III of NS5A to assess protein plasticity, alluding to different functional roles of NS5A in different GTs, and comparison of GT2 and GT3 NS5A interactome to host proteins. Contradictory to GT2, assessment of tagged GT3 clones for genome replication and virus production showed that tags are best tolerated at the very C terminus of NS5A, suggesting that GT3 NS5A domain III may have different functions compared to other HCV GTs. Recapitulating the complexity of HCV interactions *in vitro* has been investigated by infecting monolayer and spheroid cultures of Huh7 (hepatocyte), LX-2 (stellate) and THP1 (monocyte) cells. Maintenance of liver architecture and the gold standard for studying liver fibrosis was investigated by infecting human precision cut liver slices (PCLS). Altering the complexity of possible HCV-cell interactions (monolayer vs spheroid infections), exposes the difficulty of recapturing cell-cell interactions *in vitro* and the mechanisms required for the progression of fibrosis. The data suggests differences between GT2 and GT3 capabilities to infect in the presence of Huh7, LX-2 and THP1 cells that may be indicative of the poor PCLS infection observed for GT3. By independently investigating the viral genome separately from altering the composition of cell culture experiments, various layers of the human liver physiology during HCV infection can be investigated. This is a crucial requirement for studying the progression of fibrosis in HCV patients.

Table of Contents

List of Tables.

List of Figures.

Abbreviations

αSMA – Alpha Smooth Muscle Actin
3D – 3-Dimensional
5'UTR – 5' Untranslated Reading Frame
aa – Amino Acid
AKR1C2 – Aldo-Keto Reductase Family 1 Member C2
AMPK – AMP-Activated Protein Kinase
Apo – Apolipoproteins
AST – Aspartate Aminotransferase
Bax – Bcl-2-Associated X-Protein
Bcl-2 – B-Cell Lymphoma-2
CCL2 – C-C Motif Chemokine Ligand 2
CD81 – Cluster Of Differentiation 81
CLDN1 – Claudin-1
CM – Conditioned Media
Col1A1 – Collagen Type 1 A1
CRISPR - Clustered Regularly Interspaced Short Palindromic Repeats
DAA – Directly Acting Antiviral
DAMPS – Damage-Associated Molecular Pattern Molecules
DBN3a – Developed HCV Genotype 3A Full-Length Genome
DMSO – Dimethyl Sulfoxide
Ds-RNA – Double Stranded RNA
E. cColi – *Escherichia Coli*
ECM – Extracellular Matrix
Edu – 5-Ethynyl-2'-Deoxyuridine
eGFP – Enhanced Green Fluorescent Protein
EMT – Epithelial-Mesenchymal Cell Transition
FAS – Fatty Acid Synthase
FFA – Focus Forming Assay
FFU/mMLl – Focus Forming Units Per Millilitre
FKBPS – FK506-Binding Proteins
GFP – Green Fluorescence Protein
Grb2 – Growth Factor Receptor-Bound Protein 2
GRP78 – Glucose Regulated Protein 78 Kda
GSK-3 – Glycogen Synthase Kinase-3
GT – Genotype
h – Hours
h.p.e – Hours Post Electroporation
h.p.i – Hours Post Infection
HCV – Hepatitis C Virus
HM -– Hepatic Myofibroblasts
hr – Humanised Renilla
HSC – Hepatic Stellate Cells
HSP70 – Heat Shock Protein 70
HSPGS – Heparan Sulphate Proteoglycans

IL – Interleukin
IL13Rα2 – Interleukin 13 Receptor Subunit Alpha 2
IRES – Internal Ribosome Entry Site
IRF1 – Interferon Regulatory Factor 1
ISGs – Interferon Stimulating Genes
ISRE – IFN-Stimulated Response Element
Jak-STAT – Janus Kinase/Signal Transducers And Activators Of Transcription
JFH-1 – Japanese Fulminant HCV Genotype 2A
LDH – Lactate Dehydrogenase
LSC – Low Short Complexity
MASLD – Metabolic Dysfunction–Associated Steatotic Liver Disease
Mir-192 – Microrna-192
MMP1 – Matrix Metalloprotease 1
MOI – Multiplicity Of Infection
MTTP – Microsomal Triglyceride Transfer Protein Inhibition
NAFLD – Non-Alcoholic Fatty Liver Disease
NAP1L1 – Nucleosome Assembly Protein 1-Like 1
NS – Non-Structural
NTP – Neomycin Phosphotransferase
OCLN – Occludin
ORF – Open Reading Frame
P53 – Tumour Protein P53
PBS – Phosphate Buffered Saline
PCLS – Precision Cut Liver Slices
PDK1 – PH Domain-Containing Kinase
PI – Propidium Iodide
PI3K-AKT – Phosphinositide-3-Kinase And Protein Kinase B
PIP3 – Phosphatidylinositol-3,4-Diphosphate
PKR – Ds-RNA-Dependent Protein Kinase
PMA – Propidium Monoazide
PPAR-α – Peroxisome Proliferator Associated Receptor Alpha
RAS – Resistance Associated Substitutions
RCU – Red Calibrated Unit
RIG-1 – Retinoic-Acid-Inducible Gene-I
RISC – RNA-Induced Silencing Complex
ROS – Reactive Oxygen Species
RT-qPCR – Real Time Quantitative Polymerase Chain Reaction
SGR – Subgenomic Replicon
SR-BI – Scavenger Receptor, Class B Type 1
SREBP-1c – Sterol Regulatory Element-Binding Protein 1c
ssRNA – Single Stranded Ribonucleic Acid
TIMP1 – Tissue Inhibitor Of Metalloproteinases 1
TLR3 – Toll-Like Receptor 3
TNF-A – Tumour Necrosis Factor Alpha
TST – Twin Streptavidin Tag
VLDL – Very Low Density Lipoproteins
WHO – World Health Organisation
ZEB-1 – Zinc Finger E-Box-Binding Homeobox 1

Chapter 1. Introduction

1.1. Introduction to hepatitis C virus

1.1.1. Impact of HCV discovery

Since its discovery in 1989, hepatitis C virus (HCV) remains a global health burden with an estimated 1% of the global population (equating to 71.1 million viraemic individuals) currently suffering from persistent HCV infection. Despite developments in antiviral treatments, only 12 of 194 countries in 2018 were on target to accomplish the WHO goal of eliminating HCV infection by 2030. By 2030, WHO strategy to eliminate infection include reduction of HCV infections by 80 %, reduced HCV-related mortality by 65 %, diagnose 90 % of HCV patients and treat 80 % of HCV infections (Spearman et al., 2019). Despite efforts to eradicate the infection, which can cause liver pathology such as fibrosis, cirrhosis, steatosis and hepatocellular carcinoma (HCC), an estimated 1.5 million people were infected globally in 2015 (Spearman et al., 2019). The most common route of transmission is intravenous drug injection. However, invasive procedures or injection based therapies using contaminated instruments are a common route of transmission (Hauri et al., 2004). Other modes of HCV infection include mother-to-child and sexual transmission routes (Spearman et al., 2019). Since the discovery of the virus over 30 years ago, major advancements in treating the infection have been made. However, key biological questions underpinning the mechanisms which HCV induces pathogenesis have still to be fully elucidated.

1.1.2. HCV molecular biology and replication

1.1.2.1. Replication

The *Flaviviridae* family contains four genera, HCV is a member of the *Hepacivirus* genus. Similar to other *Flaviviridae* viruses, HCV is enveloped in a lipid bilayer which holds a nucleocapsid containing a positive-sense single stranded RNA genome (ssRNA) (Tan, 2006). The nature of the RNA genome allows it to serve directly as messenger RNA (mRNA). The presence of an internal ribosomal entry site (IRES), mediates binding to the ribosomal subunits and initiation of viral genome translation (Fukushi et al., 1994; Morozov & Lagaye, 2018). The genome contains conserved 5' - 3' non-coding regions flanking a single open reading frame (ORF) of approximately 9030 - 9099 nucleotides. A polyprotein, approximately 3010 - 3033 amino acids (aa) dependent on the GT, is translated from the single ORF and co- and post-translationally cleaved by viral and cellular proteases (Dustin et al., 2016; Fraser & Doudna, 2007; Morozov & Lagaye, 2018) (Figure 1.1, Table 1.1). Viral entry into the cell can be described in two phases. Primarily, viral glycoproteins E1 and E2 alongside host derived lipids and apolipoproteins (Apo) allowing the first interaction with ApoE with the cell surface heparan sulphate proteoglycans (HSPGs) or with the scavenger receptor, class B type 1 (SR-BI). Secondly, the E1-E2 complex is primed by a chain of interactions/co-interactions involving different components such as SR-BI, cluster of differentiation 81 (CD81) and tight junction proteins; claudin-1 (CLDN1) and occludin (OCLN) (Alazard-Dany et al., 2019).

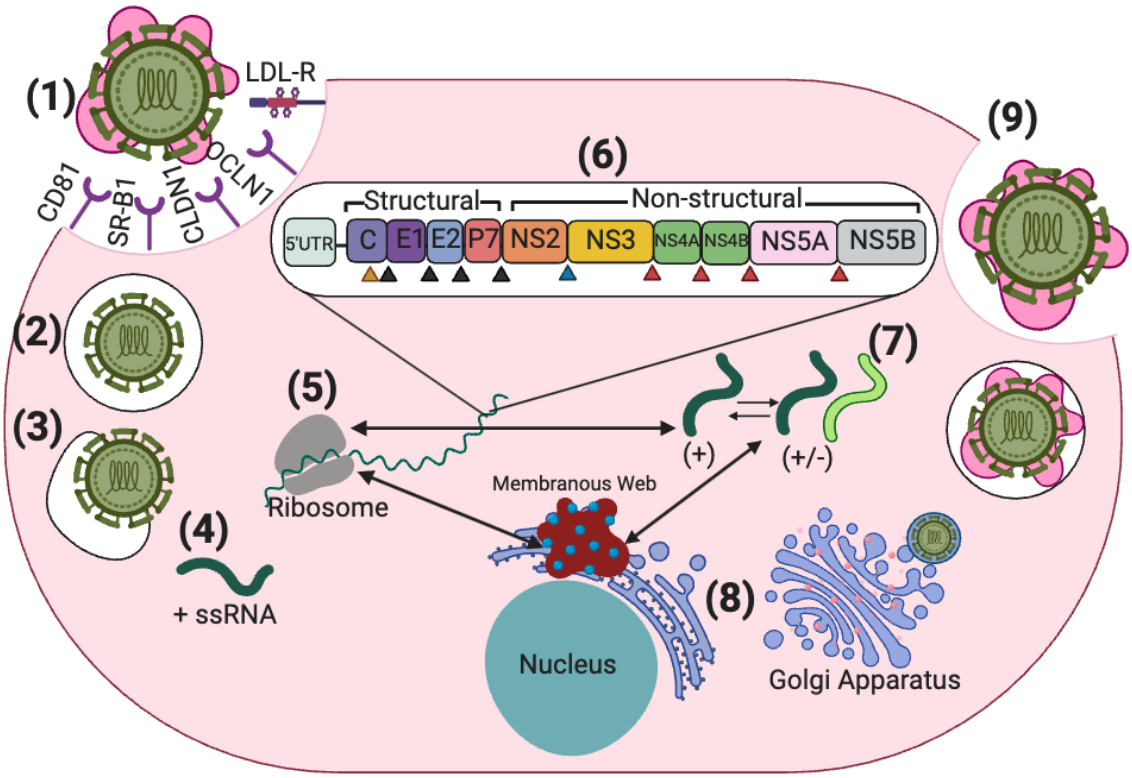

Figure 1.1 Hepatitis C virus life cycle.

The hepatitis C virus (HCV), surrounded by lipoprotein, attaches to a hepatocyte cell via various receptors. (2) After viral attachment, the virus enters the cell through clathrin-mediated endocytosis. (3) Uncoating of the viral particle is triggered by low pH in the endosome. This results in virus and host membranes fusion followed by disintegration of the viral capsid. Consequently, the positive (+) single stranded (ss) RNA viral genome is released into the cytoplasm (4). (5) The genomic viral RNA is directly translated into a polyprotein which undergoes cleavage into single proteins by viral and host proteases (6). HCV genome can be categorised into structural and non-structural proteins. Triangles refers to the method of protein cleavage; yellow – signal peptide peptidase, black – signal peptidase, blue NS2/NS3 protease and red - NS3 protease. (7) A membranous web forms via the synthesis of virus proteins, particularly NS4A and NS5B, interacting with host factors causing the reorganization of host membranes. The membranous web promotes the replication of the virus RNA genome via the production of a negative (-) sense RNA intermediate. (8) Viral progeny obtain E1 and E2 glycoproteins (the envelope) as it is packaged inside the endoplasmic reticulum (ER). The progeny mature and obtain endogenous lipoproteins to complete the formation of lipoviral particles. (9) The newly synthesised virus can then leave the hepatocellular cell via exocytosis prior to the infection of a new cell. Abbreviations; CD81 - cluster of differentiation 81, SR-B1 – scavenger receptor, class B type 1, CLDN1 – claudin 1, - OCLN1 – occludin 1 and LDL-R – low density lipoprotein receptor. Figure was created by information from Dustin et al. (2016), Lange et al. (2014) and Alazard-Dany et al. (2019).

Protein	Function
Core	• Aggregates to form the viral capsid. • Once mature, promotes the binding to host-derived lipid membrane and HCV RNA.
E1, E2	• Highly glycosylated transmembrane proteins which are tightly associated together to form a E1-E2 heterodimer. This forms the viral envelope. • Believed to play multiple roles in the HCV replication cycle; attachment to host cell, endosome-lipid membrane fusion and assembly.
P7	• Hydrophobic transmembrane protein involved in viral assembly and release. • Characterised as a viroporin due to ability to oligomerize as hexamers to form ion channels in host cell membranes.
NS2	• Acts as a cysteine protease; catalyses a single cleavage between NS2 and NS3. • Co-factor in viral assembly.
NS3	• Bi-functional enzyme activity; serine protease and helicase activity. • Serine protease cleaves most of the viral polyprotein into free non-structural proteins. • Helicase activity unwinds viral RNA promoting viral replication.
NS4A	• Attaches the NS3-4A complex to the outer shell of the ER and outer mitochondrial membrane. • Co-factor for NS3 serine protease. • Enhances NS3 helicase activity. • Regulates NS5A hyperphosphorylation. • Interacts with NS4B to control genome replication.
NS4B	• Promotes changes to the cytoplasmic membrane of the host cell. • Mediates virus-host interactions. • Component of the replication complex and formation of membranous web.
NS5A	• Essential component of replication complex. • Key protein regulating the interaction of viral and host cell proteins. • Crucial in the formation of double membrane vesicles originating from the ER. • Believed to play a key role in HCV pathogenesis.
NS5B	• Essential for viral replication; RNA-dependent RNA polymerase.

Table 1.1 Summary of HCV protein functions.

Outlines the roles of HCV viral proteins. Abbreviations; NS – non-structural, ER – endoplasmic reticulum. Table was created by information gathered from Dubuisson (2007).

1.1.2.2. Defining genotypes and subtypes

Lengths of the viral genome differ depending on the genotype and subtype of HCV being investigated. Additionally, nucleotide sequence identity varies by 30-35% between genotypes (GT), and 20-25% between subtypes. Subtypes act as a more detailed classification within each

GT, for example, GT1 is known to have several subtypes with differences in genetic makeup. Subtypes are designated by a lowercase letter following the GT number; GT1a and GT1b. Sequence variability is scattered evenly throughout the viral genome, apart from the highly conserved 5' untranslated reading frame (5'UTR), core regions and the hypervariable envelope proteins (Takamizawa et al., 1991; Zein, 2000). Complex genetic variants with 10% differing nucleotide sequence identity from a host are termed as a 'quasispecies'. Quasispecies can occur in an individual host as a result of an accumulation of mutations during viral replication (Okamoto et al., 1992; Zein, 2000).

1.1.2.3. Global distribution of HCV genotypes

The number of HCV GT isolates identified is currently debated. As many as 11 GTs have been identified with some scientists suggesting isolates should be grouped and regarded as variants. This was discussed for GT7 through to GT11 which was previously described as GT6 variants in the late 1990's (de Lamballerie et al., 1997; Zein, 2000). However, as HCV research has advanced, more GTs have been discovered such as GT7 and GT8 (Borgia et al., 2018; Murphy et al., 2015). Geographic distribution of HCV can split GTs and subtypes HCV into two groups; epidemic and endemic strains.

Epidemic strains are widely distributed on a global scale and are specific to GT1a, 1b, 3a and 4a. These strains account for a high portion of HCV infections worldwide. Epidemic strains are believed to have spread extensively and rapidly during the 1970's and 80's through blood products, transfusions, intravenous injecting drug abusers and human migration (Messina et al., 2015; Simmonds, 2013). Despite a global presence, their prevalence differs between different geographic areas (Figure 1.2). Epidemic strains only account for a small part of HCV diversity. Extensive heterogeneity within a region is termed as "endemic". Endemic strains are believed to be the result of the long-term presence of a HCV GT which has diversified within a region (Messina et al., 2015; Simmonds, 2013).

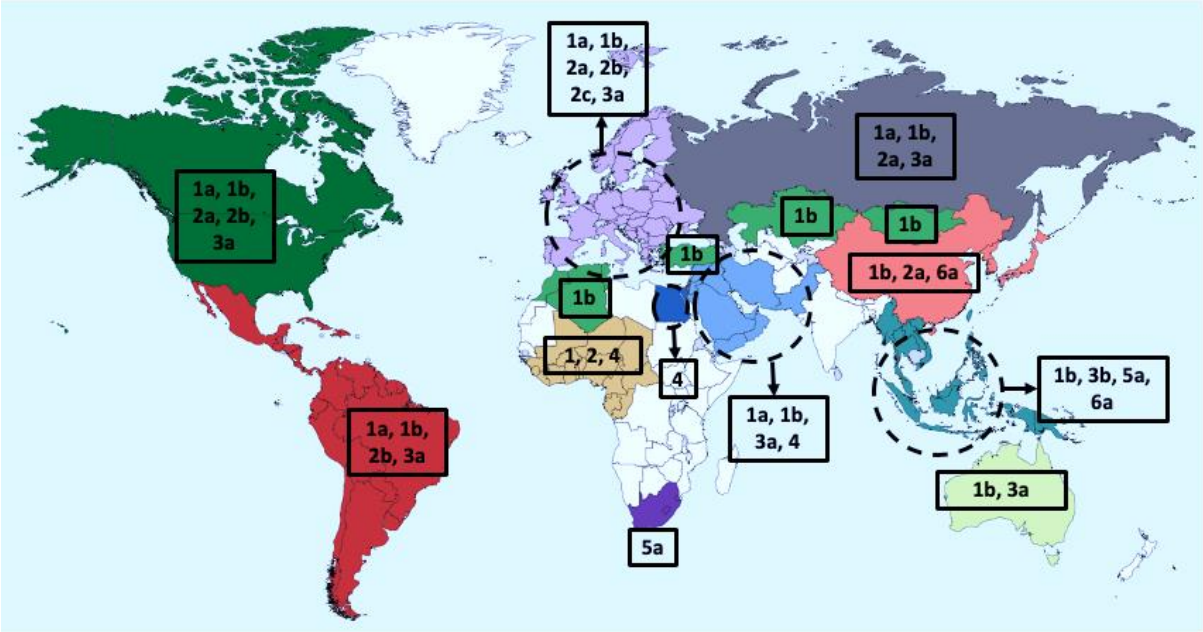

Figure 1.2 Global geographic distribution of HCV genotypes.

Numbers and colour outline the genotype present in that region. Lowercase letters outline the subtype of that genotype present. Figure was adapted from Messina et al. (2015).

1.2. Hepatic pathogenesis of HCV

1.2.1. Defining HCV pathology

The crucial mechanisms of HCV pathology are still to be determined, particularly in relation to specific GTs and subtypes. However, it is speculated to have two arms; host mediated pathology and viral mediated pathology. It is believed that both the inflammatory immune response and metabolism of the host is affected, independent of which arm is driving the pathology. As a result, livers may be described as having various grades of fibrosis, cirrhosis, and steatosis. Additionally, chronic infection increases the risk of HCC (Li et al., 2018). Multiple factors are believed to play a role in the severity of liver pathology such as age, gender, co-infection with human immunodeficiency virus (HIV) or hepatitis B virus (HBV), alcohol intake and the HCV GT also plays a role (Chan et al., 2017). Additionally, HCV infection may be described as “acute” or “chronic”, this also alters pathology of disease as the infection may be resolved by the host naturally (Figure 1.3).

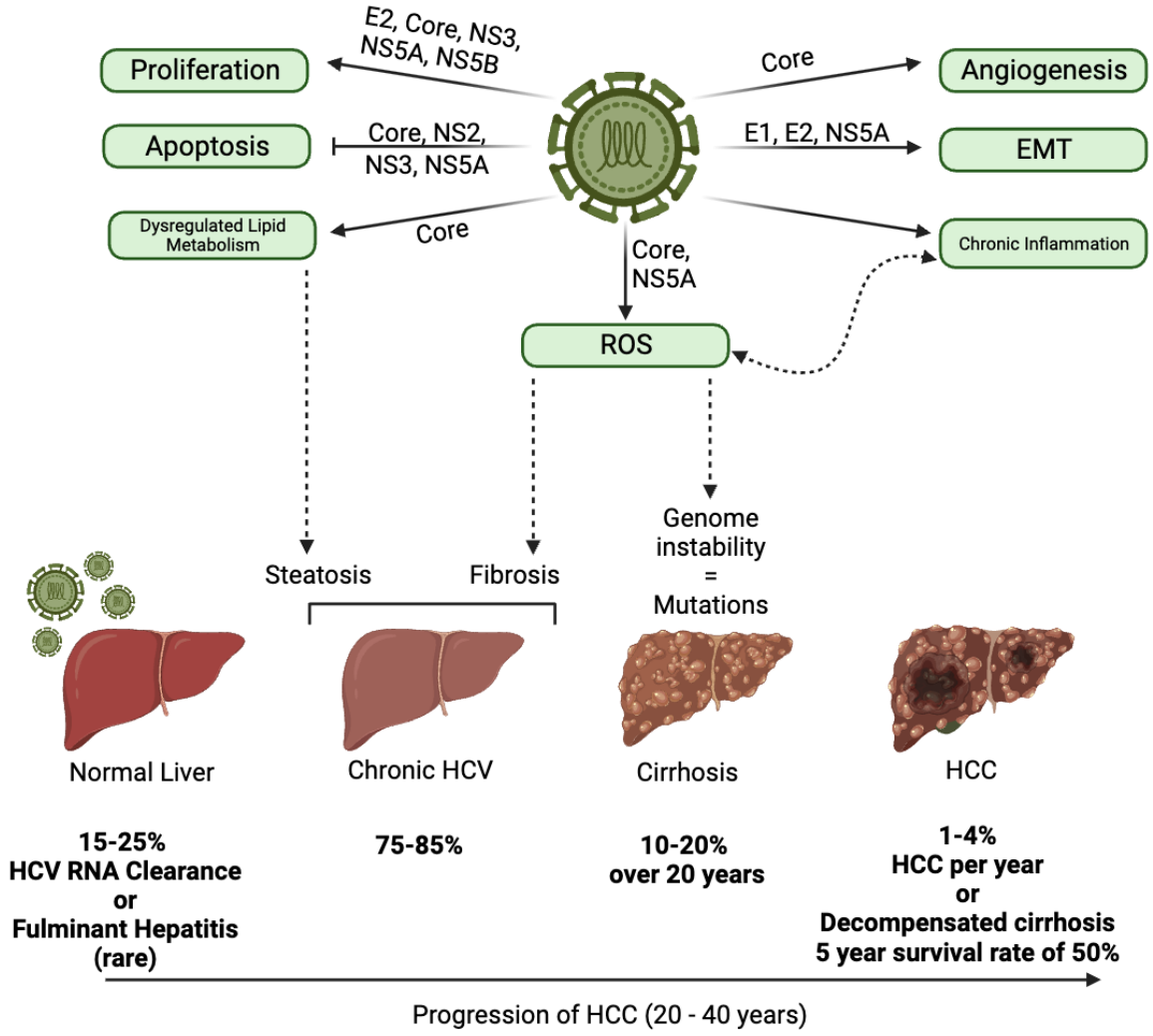

Figure 1.3 Disease progression of HCV.

HCV infection induces mitogenic, angiogenic, epithelial/mesenchymal transition (EMT) and metastatic pathways resulting in persistent inflammation, reactive oxygen species (ROS), dysregulation of host lipid metabolism and inhibition of cell death. Disease progression of HCV without therapeutic interference can result to fibrosis and steatosis progression prior to development of hepatocellular carcinoma (HCC). Figure was created by information gathered from Chen and Morgan (Chen & Morgan, 2006), Vescovo et al. (2016) and Axley et al. (2018).

1.2.1.1. Steatosis

Commonly described as a fatty liver, steatosis is the accumulation of fat in the liver triggering an inflammatory response. Importantly to note, steatosis itself does not induce an inflammatory state but instead reflects the presence of lipogenic pathways which enhance pro-

fibrogenic stimuli (Chan et al., 2017). While it can be mediated metabolically as a result of obesity, raised fat blood levels, insulin resistance and type 2 diabetes, it may also be directly associated with the presence of HCV. Both steatosis types can simultaneously be present in an individual which increases the risk of HCV disease progression, reduces the response to HCV therapeutics and promotes the progression of HCC (Chan et al., 2017; Yoon & Hu, 2006). The accumulation of fat in the liver results to increased oxidative stress, increased cell susceptibility to apoptosis by immune cells and abnormal liver cell regeneration (Yoon & Hu, 2006). The precise mechanisms of HCV inducing steatosis is unknown, but it is believed that the virus modulates lipid and fat metabolism as well as transportation. It is advantageous for the virus to interfere with the host lipid and fat metabolism as lipids play an essential role in several aspects of the HCV lifecycle; formation of the virion structure, cell receptor recognition, membrane fusion, viral replication, assembly and export.

Viral components prompting steatosis have been demonstrated by the anchoring of the core protein to the ER of hepatocytes gaining virus access to lipid droplets (Boulant et al., 2006) as well as overexpression of the core protein sufficiently inducing steatosis in mice (Moriya et al., 1997). Shimizu *et al.* (2018) further demonstrates virus mediated steatosis as treatment of chronically infected HCV patients decreased steatosis severity after eradication of the virus. However, steatosis was not completely eliminated suggesting the contribution of a host mediated steatosis process. Unlike steatosis, the direct association of HCV infection and fibrosis progression is limited.

1.2.1.2. Fibrosis and cirrhosis

Fibrosis is defined as an accumulation of scar matrix, characterised by excessive production and accumulation of extracellular matrix (ECM) proteins because of persistent injury. As well as scar tissue performing no function in the liver, the condition is typically non-symptomatic with patients only experiencing symptoms with complications and end-stage liver disease. This is known as cirrhosis and typically occurs in 10 -20 % of chronically infected HCV

patients (Chen & Morgan, 2006). Cirrhosis is the presence of widespread and severe fibrosis whereby the scar matrix destroys the internal structure which impairs the livers ability to function and regenerate (Chen & Morgan, 2006). The major cell types promoting fibrosis in the liver included human stellate cells (HSC), hepatocytes and Kupffer cells (resident liver macrophages) (Figure 1.4).

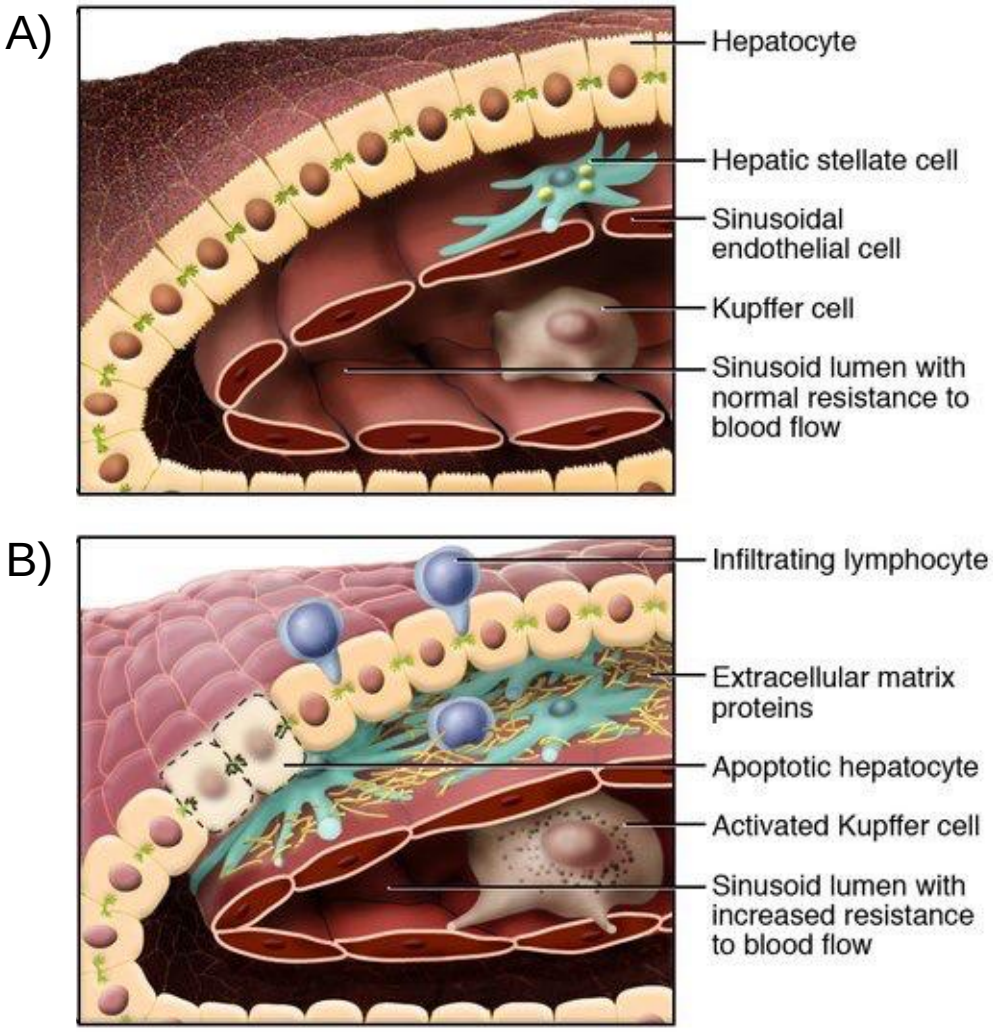

Figure 1.4 Comparison of a healthy and fibrotic liver architecture.
A) Healthy liver. B) Associated with chronic liver damage. Stellate and Kupffer cells become activated resulting in increased inflammation and increased production of the extracellular matrix. Due to increased resistance to blood flow in the hepatic sinusoid, hepatocyte access to oxygen is reduced resulting in cell death. Figure adapted from Bataller *et al.* (2005).

HSC play a key role in fibrosis progression as both the activation of the cell type by cytokines and chemokines as well as liver injury result to transdifferentiation of quiescent stellate cells to their activated phenotype, myofibroblast-like cells, namely hepatic myofibroblasts (HM). Persistence of HM results in fibrosis progression due to the secretion of ECM proteins after complete transformation into myofibroblasts expressing alpha smooth muscle actin (αSMA) (Akil et al., 2019; Y. A. Lee et al., 2015; Morozov & Lagaye, 2018). It is believed HCV may indirectly activate HSC by oxidative stress and steatosis which is induced directly by viral proteins (Clément et al., 2010; Ming-Ju et al., 2011). HCV promotes apoptosis which drives the activation of HSC through the presence of apoptosis bodies which increases damage-associated molecular pattern molecules (DAMPs) resulting in HSC activation (Ignat et al., 2020). Additionally, there is evidence that HCV promotes the release of transforming growth factor beta 1 (TGF- β1), the most potent pro-fibrotic cytokine, by infecting hepatocytes (Figure 1.5). TGF-β1 acts by modulating the expression of key genes controlling liver fibrosis in hepatic stellate cells (HSC) (Shin et al., 2005). Akil *et al.* (2019), successfully demonstrated an increased expression of HCV-dependent fibrogenic genes in stellate cells during the infection of a three cell co-culture model system containing hepatocytes (Huh7), HSCs (LX-2) and primary macrophages with HCV (H77, GT1a).

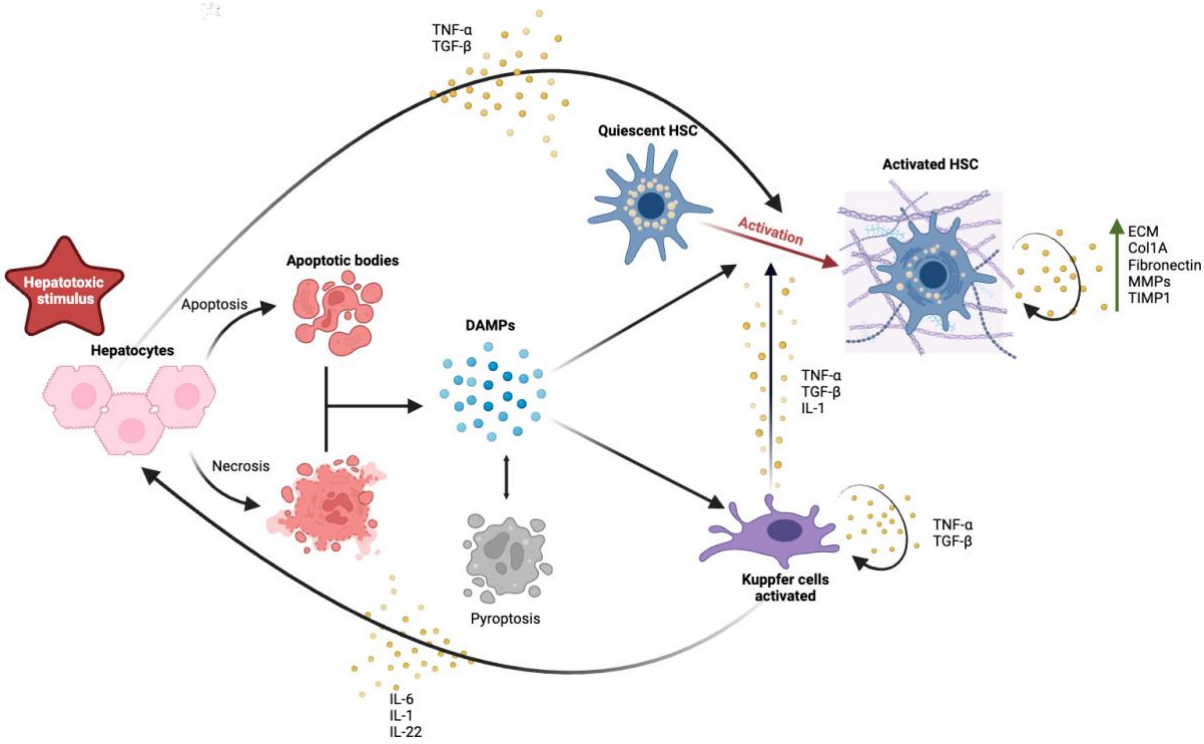

Figure 1.5 Summary of human hepatic stellate cells activation resulting in fibrosis.
Hepatocytes drive the activation of human stellate cells (HSC) through cell death resulting in increased expression of damage associated molecular patterns (DAMPs) which activates Kupffer cells and HSC. DAMPs may also promote cell death of inflammatory cells, known as pryoptosis. Soluble factors released by hepatocytes and activated Kupffer cells also contribute to the activation of HSC (tumour necrosis factor- alpha – TNF- α, transforming growth factor-beta – TGF-B and interleukins – IL). Kupffer cells can remain activate through the excretion of their soluble factors as well as communicate to other cell types. Activated HSC results to an increased production of fibrogenic markers (fibronectin, Collagen type 1 – Col1A, metalloproteinase – MMPs, tissue inhibitor of metalloproteinases – TIMP-1) and accumulation of the extracellular matrix (ECM). Figure adapted from Ignat (2020).

1.2.1.3. Hepatocellular carcinoma

HCV infection is a major risk factor to developing hepatocellular carcinoma (HCC), the leading cause of liver-related death worldwide and fifth most common cancer. The disease comes hand-in-hand with advanced HCV induced fibrosis and steatosis pathogenesis, with the risk of HCC development occurring despite successful treatment of HCV infection (Luna-Cuadros et al., 2022; Marrero et al., 2018). The development of HCC after HCV infection may span between 20 to 40 years, and like fibrosis and steatosis, advanced by both viral-induced factors

and host-induced immunological response. Viral proteins trigger host cell signalling pathways involved in the upregulation of cell growth and division in addition to inhibiting tumour suppression genes and cell cycle check points (Axley et al., 2018; Vescovo et al., 2016) (Figure 1.3). Virus induced mechanisms specifically promoting HCC development, independent of fibrosis and steatosis, include the interaction of the core and NS3 protein with tumour suppression genes such as protein 53 (p53) and retinoblastoma protein which significant increases HCC progression. It was suggested HCV core protein regulates the expression and function of p53, altering the cell's response to genomic damage and promoting immortalization of infected hepatocytes. The expression levels of p53 fluctuate during HCV infection depending on the levels of HCV core expression; low levels endorsed p53 expression, high levels suppressed p53 expression (Poole et al., 2018). The presence of NS3 supresses actinomycin D induced apoptosis which is believed to be connected to p53 interaction; described as NS3 sequence dependent demonstrated through site-specific mutagenesis experiments in the N terminus of NS3 (Deng et al., 2006; Tanaka et al., 2006). Research investigating HCV direct vs indirect carcinogenic mechanisms has been described as limited by experimental systems. For example, it remains unclear if infected proliferating hepatocytes are driving HCC or if it is driven by uninfected hepatocytes cells responding to hepatocyte stress signals. During HCV infection, it is estimated less than 30% of hepatocytes contain replicating HCV, observed by HCV genome copy number of livers from infected-chimpanzees (Bigger et al., 2004). In liver human tissue, frozen and non-malignant, only 2-20% expressed HCV antigen (Liang et al., 2009). Presence of HCV in malignment cells in HCC patients is not a reliable marker of infection driving the disease as there may be a high number of virions circulating in the blood. Due to the presence of HCV in the blood, any vascular tissue may test positive for HCV infection (McGivern & Lemon, 2011).

1.3. Treatment of HCV

1.3.1. Historic treatment

HCV was primarily treated using pegylated interferon alpha (PEG-IFN) and ribavirin. The PEG-IFN stimulated the host immune response, rendering infected cells more susceptible to cell death. Ribavirin, a synthetic antiviral nucleoside analogue, acted alongside PEG-IFN, inhibits viral growth by being incorporated into the viral RNA during replication resulting in errors in viral RNA synthesis; disrupting the production of functional viral proteins and reducing the ability of the virus to replicate accurately (Feld & Hoofnagle, 2005). Despite the long treatment course, typically lasting 24 – 48 weeks, a sustained virological response (SVR) of 45 – 85% was accomplished with patients suffering a range of intolerable side effects such as psychiatric disturbances, anaemia and flu-like symptoms. (Hunyady et al., 2011; Liver, 2011). It was not until the development of directly acting antivirals (DAAs), that treatment for HCV was brought to the modern era.

1.3.2. Development of direct-acting antivirals

There has been a dramatic advancement in the treatment for HCV, resulting in therapeutics which directly targets the replication of HCV (Table 1.2). Overall these treatments are safer, more effective than PEG-IFN and ribavirin, have a shorter treatment time of typically 8 – 12 weeks with more tolerable side effects (Kish et al., 2017). In theory, these treatments may be broadly used independently of the GT a person is infected by. However, SVR does differ depending on the GT, for example the combination of sofosbuvir/simeprevir/ribavirin (Lawitz et al., 2014) and the fixed-dose combinations of ledipasvir/sofosbuvir (Kowdley et al., 2014) results to SVR rates of 92 – 100 % for GT1 infected patients and 85 – 100 % for other GT infected patients. Additionally, the effect of some DAAs on harder to treat circumstances such as presence of cirrhosis and particular GTs, such as GT3, may determine the antiviral drugs used

and the treatment length. Treatments are typically regimented based on clinical trials such as FUSION (Jacobson et al., 2013) and ALLY-3 (Nelson et al., 2015). However, despite these advances, Chhatwal *et al.* (2018) predicted 7 % of patients will fail to achieve SVR and will have limited retreatment options. Treated individuals are also at risk of reinfection with the incidence varying between 7 – 13 / 100 person-years reported among gay and bisexual men in Europe (Ingiliz et al., 2017). This highlights the requirement for further research into the GTs, natural polymorphisms and mutations circulating which are associated with drug resistance.

Drug name ending	Example of drug	Target
' – previr '	Simeprevir	NS3/4 protease
' – buvir '	Sofosbuvir	NS5B polymerase
' – asvir '	Declatasvir	NS5A

Table 1.2 Breakdown of directly acting antiviral targets.
Outlining of different drugs against HCV infection characterised by their targeted viral proteins. Table was created based on information provided by Kish et al. (Kish et al., 2017).

1.4. Progress to HCV elimination

The introduction of DAA treatments has provided greater confidence in the accomplishment of the WHO target of eliminating HCV infections by 2030. DAAs have been associated with a reduction in the number of HCV infected patients at liver clinics and an increase in treatment uptake (Samur et al., 2018). However, as HCV infection may only be tested in chronic patients exhibiting symptoms possibly >10 years after infection, DAA treatment may only result to minimal improvements contributing the WHO targets. Prior to the COVID-19 pandemic, only 9 of 45 high-income countries where on track to accomplish the WHO target by 2030 (Razavi et al., 2020). It is believed the COVID-19 pandemic has only worsened the progression of eliminating the infection. It has been suggested, at the current rate, the target may only be achieved by 2050. This has been credited to a lack of national screening programmes (Gamkrelidze et al., 2021). Until there is an increase in HCV screening and

diagnosis, the significance of DAA treatment will not be translated to the number of patients cured of HCV nor a reduction in the HCV-related morbidity and mortality (Manns & Maasoumy, 2022; Razavi et al., 2014). Such an example of an effective screening programme and translation of DAA treatment success was observed in Egypt. In 2018, Egypt aimed to screen all citizens above 18 years of age or older within 1 year. After 7 months, 79% of the population was screened, 4.6% of patients tested were anti-HCV positive, therefore were further HCV RNA tested and linked to DAA treatment. The success of the programme was partially linked to the discount on DAA treatment provided by pharmaceutical companies (Waked et al., 2020). This suggests a hand-in-hand relationship between screening programmes and treatment costs required to accomplish the elimination of HCV. Despite changes to screening programmes and DAA treatment access, HCV resistance to treatment has not been factored into the WHO 2030 targets. To eliminate the risk of HCV resistance increasing, there must be continual development of DAA treatment and a prophylactic vaccine. A vaccine to HCV would greatly improve the outcome of eliminating HCV infection, particularly for countries with lack of resources for screening programmes, to eradicate HCV DAA resistant infections and high-risk groups (such as needle injecting drug users) with a particular risk of reinfection.

1.5. HCV GT3 halting HCV eradication

GT3 is the second most common GT (after GT1) accounting for 22 - 30 % of all HCV infections. Geographically, GT3 accounts for 50% of cases in the UK, and up to 70% of all cases in low-income countries including Pakistan, India and Thailand (Messina et al., 2015). It is characterised as having a more rapid progression to chronic liver disease with higher rates of liver fibrosis, severity of steatosis and a higher frequency of HCC. Additionally, GT3 has a high level of resistance against DAAs. However, like the characterisation of HCV pathogenesis independent of HCV GT, the reasons for why HCV GT3 is harder to treat and results to a more rapid progression to liver disease are still to be fully determined. Furthermore, the development

of a GT3 SGR, in 2020, and cell-cultured virus clone, in 2016, were only recently produced (Ramirez et al., 2016; Ward et al., 2020), therefore the majority of GT3 studies are limited to analysing patient databases.

1.5.1. Promotion of steatosis

Despite steatosis being both viral and host mediated, HCV GT3 is believed to promote the condition more so than other GTs. Severity of steatosis has been linked to the viral load of GT3 infection. For example, a link between HCV RNA levels in comparison to steatosis grades have not been linked to other GTs like it has been for GT3 (Adinolfi, Gambardella, et al., 2001). Adinolfi *et al.* (2001) also suggests GT3 infection plays a more direct role promoting steatosis than host mediated factors, such as obesity. This is suggested as obesity levels did not exaggerate steatosis progression in GT3 infection. Despite the exact mechanisms promoting steatosis remaining unknown, it is believed GT3 infection influences the steatosis progression by interacting with fat metabolism and transportation pathways within the liver (Chan et al., 2017).

1.5.1.1. Microsomal triglyceride transfer protein inhibition (MTTP).

This pathway plays a key role modulating triglyceride secretion from the liver by production of ApoB. ApoB forms the very low density lipoproteins (VLDL) required to export the triglycerides into the bloodstream. The MTTP pathway is inhibited during HCV GT3 infection by restricting the transfer of lipid molecules to ApoB resulting in the degradation of ApoB and a decreased reduction in VLDL production (Figure 1.6) (Perlemuter et al., 2002). Research has shown this to be HCV-core protein mediated with all GTs capable of inhibiting the pathway. However, Jhaveri *et al*. (2008) expresses that particular polymorphisms in the core protein of GT3 may be the reason why the MTTP is more greatly affected during GT3 infection.

1.5.1.2. Peroxisome proliferator associated receptor alpha (PPAR-α).

PPAR-α induces hepatic fatty acid oxidation and ketogenesis while upregulating hepatic glucose production. In brief, when PPAR-α is activated it acts on metabolic regulation of the liver (Chan et al., 2017). However, in the presence of the HCV GT3 core protein, the pathway is inhibited resulting in a reduction in triglyceride breakdown and the accumulation of intrahepatic fatty acids (Figure 1.6) (de Gottardi et al., 2006). Similar to the MTTP pathway, other GTs may inhibit this pathway, such as GT1. However, the extent by which the pathway is disrupted does not reach the same severity as when GT3 is present (Dharancy et al., 2005).

1.5.1.3. Sterol regulatory element-binding protein 1c (SREBP-1c).

SREBP-1c is a transcription factor which regulates lipogenic pathways such as fatty acid synthesis and cholesterol by the modulation of downstream enzymes, such as fatty acid synthase (FAS). FAS uses acetyl-CoA and malonyl-CoA catalysing reactions to modulate triglyceride accumulation and lipid synthesis in hepatocytes. It is believed presence of GT3 core protein, upregulates the SREBP-1 and FAS activation increasing the production of triglycerides in the liver (Jackel-Cram et al., 2007). The exact mechanisms of this is unknown however, it is speculated upstream factors may be affected such as phosphinsitide-3-kinase (PI3K) and protein kinase B (AKT) as well as the involvement of insulin receptors (Figure 1.6)(Chan et al., 2017; Jackel-Cram et al., 2007). The PI3K-AKT axis is highly conserved playing key roles in cell proliferation, genetic stability and apoptosis (Chan et al., 2017).

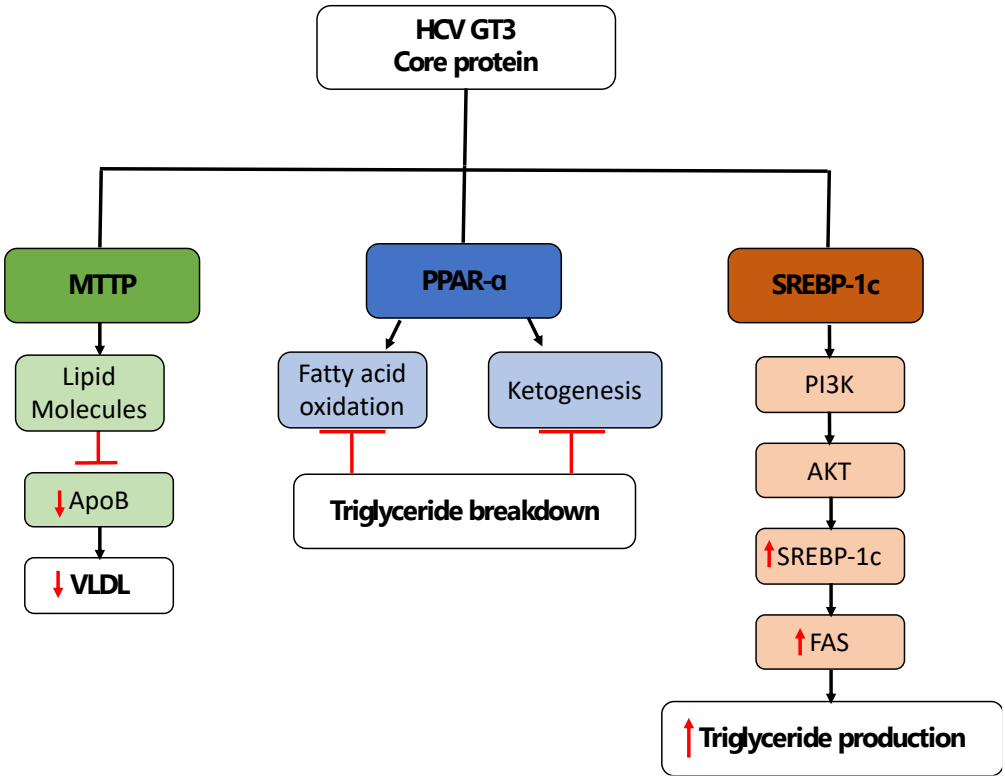

Figure 1.6 Summary of HCV GT3 influencing steatosis progression.
HCV GT3 core protein influences the steatosis progression by interacting with fat metabolism and transportation pathways within the liver. Red lines indicate the blocking of pathways and red arrows indicate either a decrease (facing downwards) or increase (facing upwards) of pathway components. Abbreviations; MTTP - microsomal triglyceride transfer protein inhibition, PPAR-α - peroxisome proliferator associated receptor alpha, SREBP-1c - sterol regulatory element-binding protein 1c, ApoB – apolipoprotein B, VLDL – very low density lipoproteins, PI3K – phosphoinositide 3-kinases, AKT – protein kinase B, FAS – fatty acid synthase.

1.5.1.4. Promotion of fibrosis and cirrhosis

The research elucidating the HCV specific mechanisms to fibrosis progression is currently lacking, especially in relation to why GT3 infection demonstrates a higher fibrosis progression in comparison to the other HCV GTs. Chan *et al*. (2017) reviews retrospective studies whereby an association of GT3 and fibrosis progression was observed. However, these studies were limited by small cohorts and/or inconsistencies involving patient characterisations, such as BMI index (Adinolfi, Gambardella, et al., 2001; Probst et al., 2011; Westin et al., 2002). Importantly, these studies did not take steatosis grades into account while associating fibrosis

to GT3. Multiple studies have suggested increased fibrosis progression is linked to increased steatosis grades (Adinolfi, Utili, et al., 2001). When comparing GT3 mediated fibrosis and steatosis pathogenesis, research has predominantly only reported steatosis as being directly correlated to GT3 pathogenesis (Adinolfi, Gambardella, et al., 2001; Rubbia-Brandt et al., 2004).

To determine whether GT3 directly impacts fibrosis progression, or whether it is steatosis driven, a direct experimental approach is required. Such research is demonstrated by Akil *et al*. (2019), whereby five inflammatory and fibrogenic genes including C-C motif chemokine ligand 2 (CCL2), interleukin 1 alpha (IL1α), interleukin 1 beta (IL1β), interleukin 13 receptor subunit alpha 2 (IL13Rα2) and matrix metalloprotease 1 (MMP1) may be monitored. Expression of these genes in comparison to other GTs could determine whether GT3 directly impacts fibrosis progression more so than other GTs. For example, GT1a (H77) upregulated these genes by more than 1.9 fold (Akil et al., 2019). Steatosis factors could also be monitored to greater understand the association between steatosis and fibrosis progression.

1.5.1.5. Promotion of hepatocellular carcinoma

HCC is believed to be driven by a multitude of factors, such as virus-specific, host genetics, immune-related (driven by the host and virus), and host environmental factors, but it remains undefined how HCV may promote HCC regardless of GT specific mechanisms. The evaluation of HCC large patient cohorts within America, France and Korean populations suggest patients infected with GT3 are at greater risk of developing HCC in comparison to other GTs, suggested by a higher prevalence of HCC patients infected by HCV GT3 (Kanwal et al., 2014; Lee et al., 2019; Nkontchou et al., 2011). Further investigation is required to define if GT3 patients are at greater risk due to HCV GT3 specific HCC-driven mechanism or if there is an association of greater HCC risk due to a more rapid progression of fibrosis and steatosis. There are conflicting reports that DAA treatment increases the risk of HCC development. Tayyab *et al.* (2020) explores this possibility in GT3 patients, concluding that GT3 infected should be screened

earlier and more frequently for HCC in comparison to non-GT3 infected patients, especially if cirrhosis was present. However, this research was limited to a small non-GT3 cohort and did not validate the contribution of other possible HCC risk factors, such as non-alcoholic fatty liver disease. Additionally, data was collected on patients between 2014 and 2017, during a time period with treatment guidelines not conforming to the most recently required treatment guidelines of GT3 patients. Therefore, greater research is required to define GT specific mechanisms which may drive HCC.

1.5.2. HCV treatment plan manipulated by GT3 infection

Prior to the development of the DAAs, GT3 was believed to be less pathogenic as it was readily cured by IFN-based treatments, in comparison to GT1. This was defined by differences in SVR rates after treatment; GT1 patients SVR between 38 to 52 % in comparison to GT3. Patients 66 – 88% after IFN-treatment (Ferenci et al., 2005; Hadziyannis et al., 2004). This has been associated with the belief GT3 alters the immune response more than other GTs , however, the mechanisms for this are not fully understood (Zarębska-Michaluk et al., 2016). Despite DAAs being a major advancement for the treatment of HCV, treatment of individuals infected by GT3 are relatively harder to treat than other GTs. It was not until the advancement of daclatasvir and sofosbuvir, in 2015, that there was an effective treatment against GT3 (Chan et al., 2017). The precise reason for GT3 being harder to treat by DAAs has still not been resolved. There is evidence to believe GT3 is harder to treat due to the additional risk factors such as advanced fibrosis, cirrhosis and the presence of resistant associated substitutions (RASs) (Nelson et al., 2015).

Resistance associated substitutions ((RAS) or variants / polymorphisms) are defined as point mutations which are associated with drug resistance. The presence of a RAS does not directly relate to a phenotypic treatment failure, however, should be considered as an overall aspect of treatment outcome (Chan et al., 2017). There are two clinically relevant RASs

associated with GT3 found within NS5A; Y93H and A30K which are estimated to be present in 8.3 % and 6.3 % of all GT3 patients. Presence of these RASs alongside cirrhosis alters the treatment plan for these patients; administration of ribavirin alongside DAAs has been suggested (Bhattacharya et al., 2023). Due to the continual emergence and persistence of RASs in DAAs failure, it has been suggested direct resistance testing is recommended prior to re-treating treatment-failing patients (Mushtaq et al., 2022). In respect to future DAA therapies, research has now focused on harder to treat HCV infected patients such as GT3 infections involving second generation DAAs such as ABT-493, a NS3/4 protease inhibitor (Muir et al., 2016), and MK-3682, an NS5B inhibitor (Gane et al., 2015).

1.6. Role of NS5A promoting disease progression

NS5A is an RNA binding phosphoprotein consisting of 3 domains separated by short-low complexity sequences (LSCs) (Tellinghuisen et al., 2004) (Figure 1.7). Domain I defined as a structured domain with an amphipathic alpha helix that hooks the protein to the cytoplasmic membrane. Domain II and III are defined as intrinsically disordered (Brass et al., 2002; Penin et al., 2004). Like the multi-functional ability of the protein, NS5A has been suggested to play a key role in facilitating HCV pathogenesis.

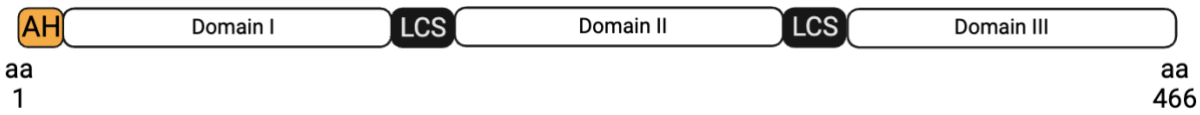

Figure 1.7 Summary of NS5A organisation.
NS5A consists of three domains. Domain I consists of a amphipathic alpha helix (AH) at the 5' with a low complexity sequence (LCS) at the 3' end. The protein is approximately 466 amino acids (aa), size varying dependent on the genotype.

1.6.1. NS5A modulating the host immune response.

NS5A has been described as a protein crucial for the evasion of the host innate immune response required for HCV replication and chronic infection. Targeting of the host immune response may result in a range of different consequences as more than one pathway is required to be targeted for complete shut-down of an antiviral pathway. Relevant to this is NS5A targeting of PKR, double stranded RNA (ds-RNA)-dependent protein kinase, has had conflicting literature as the interaction has been described as both advantageous and disadvantageous to the virus life cycle. Pro-viral effects include the inhibition of host translation supporting HCV genome replication and diminishes the expression of antiviral effectors by blocking the interferon effector function (Arnaud et al., 2010; Garaigorta & Chisari, 2009). However, PKR may also inhibit virus assembly (Chen & Harris, 2023), host factors required for HCV replication and cell growth survival limiting HCV persistence and inducing IFN- β and interferon stimulating genes (ISGs) (Noguchi et al., 2001; Pflugheber et al., 2002) (Pflugheber et al., 2002). PKR also drives anti-viral responses such as the activation of the interferon regulatory factor 3 (IRF3) and nuclear factor-κB (NF-κB) (Waris et al., 2003), despite research investigating HCV interaction with PKR functions and activation/suppression during HCV infection remains unclear.

NS5A has also demonstrated the ability to supress STAT1 phosphorylation (pSTAT1) restricting the expression of ISGs however, the molecular mechanisms of which were not fully elucidated (Gong et al., 2007; Kumthip et al., 2012; Lan et al., 2007). Kumthip *et al.* (2012) used overexpression of NS5A from GT1 and GT3 and infectious virus clones (JFH-1) as well as an NS5A inhibitor to investigate the effect of HCV NS5A on the IFN-α-induced Janus kinase/signal transducers and activators of transcription (Jak-STAT) signalling pathway, specifically the mechanism of pSTAT1 interaction with NS5A. Jak-STAT is a signalling pathway which mediates the cellular response to cytokines, interleukins, and growth factors. It was discovered HCV NS5A c-terminus binds to STAT1 reducing levels of pSTAT1, IFN-induced IFN-stimulated response element (ISRE) signalling, and ISG transcription. Additionally, inhibition of this pathway is an

independent mechanism for greater HCV replication. Furthermore, the interaction was compared to GT1 and GT3 NS5A constructs generated from HCV patients to recapitulate the possible differences between GT1 and GT3 HCV patients receiving IFN-treatment, GT3 patients associated with a greater SVR rate than GT1 patients as described previously in "1.5.2 HCV treatment plan manipulated by GT3 infection". Results suggested GT1 NS5A has a higher binding affinity to STAT1 than GT3 NS5A. This further alludes to differences between HCV GTs and that the same interactions may occur but differences in binding affinities can lead to variations in disease progression.

1.6.2. NS5A promoting liver steatosis.

An example of NS5A promoting steatosis is its interaction with AMP-activated protein kinase (AMPK), a major mediator of lipid metabolism including fatty acid synthesis and oxidation. AMPK is composed of α, β and γ subunits; phosphorylation of the threonine 172 (Thr172) residue within the α subunit regulates AMPK activation (Willows et al., 2017). Once activated, AMPK promotes fatty acid oxidation and reduces lipogenesis by modulating the expression of lipogenic gene transcription levels (Smith & Steinberg, 2017; Zhang et al., 2018). The transcription factor sterol regulatory element binding protein-1c (SREBP-1c), is the main transcription factor promoting lipogenic enzymes in the liver. In a high glucose environment, AMPK phosphorylates SREBP-1c which supresses SREBP-1c cleavage and translocation to the nucleus in hepatocytes resulting in a reduction of the SERBP-1c target gene expression and a reduction in lipogenesis and lipid accumulation. Meng *et al.* (2019) investigated NS5A promotion of hepatic lipid accumulation through the AMPK/SREBP-1c pathway via recombinant lentivirus particles containing NS5A of GT3a and observing changes in the accumulation of lipid droplets and expression of lipogenic genes. It was suggested NS5A can promote lipid droplet accumulation by inhibiting the phosphorylation of AMPK allowing an increased expression of SERBP-1c (Figure 1.8).

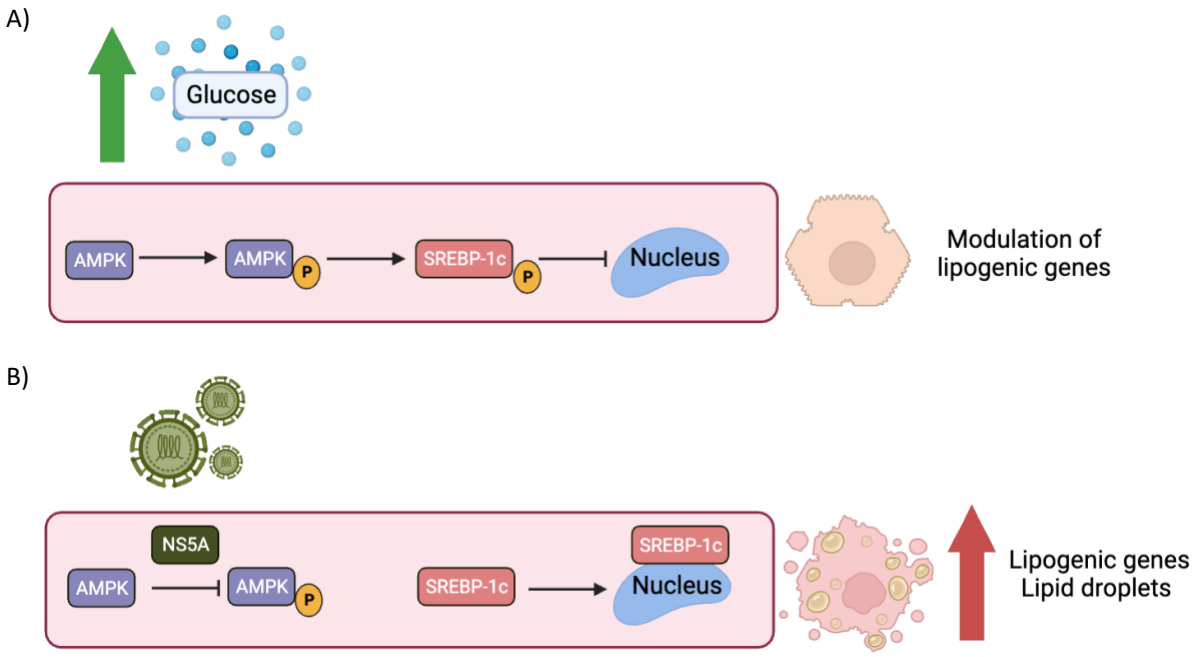

Figure 1.8 NS5A manipulating the expression of lipogenic genes.
A) The phosphorylation (P) of AMP-activated protein kinase (AMPK) results to phosphorylation of sterol regulatory element binding protein-1c (SREBP-1c) inhibiting translocation to the nucleus allowing regulation of lipogenic gene transcription and reducing the progression steatosis in a high glucose environment. B) Presence of the virus, specifically NS5A, inhibits the phosphorylation of AMPK allowing SREBP-1c cleavage and translocation to the nucleus. This promotes steatosis allowing increased expression of lipogenic genes and lipid droplet accumulation.

1.7. NS5A promoting liver fibrosis.

The progression of fibrosis has been greatly associated to a chronic HCV infection driving chronic inflammation. There is much debate about the progression of fibrosis and cirrhosis directly promoted by HCV proteins (Brenner, 2009). However, activation of stellate cells driven by oxidative stress and apoptosis are likely to be contributing factors, both of which may be driven by NS5A.

1.7.1.1. Oxidative stress

Oxidative stress is measured by reactive oxygen species (ROS), including superoxide anion, hydroxyl radical, and hydrogen peroxide, which when elevated promotes an excessive

production of the extracellular matrix by activated HSCs (Hao et al., 2022). Both core and NS5A are key promoters of ROSs, with the promotion of ROS being more elusive than the mechanisms demonstrated by core; induction of a calcium efflux from the endoplasmic reticulum to the mitochondria disrupting normal functioning of the mitochondria. Smirnova *et al.* (2016) demonstrated the inhibition of calcium flux from the endoplasmic reticulum did not impact the NS5A-induction of oxidative stress. Instead, NS5A mediated the induction of NADPH oxidases 1 and 4 (NOX1 and NOX4), resulting in an increase in transforming growth factor-B (TGF-B) production, conducted utilising the expression of GT1a NS5A within Huh7 cells. As a result, TGF-B may directly activate stellate cells in addition to the promotion of ROS production (Figure 1.9).

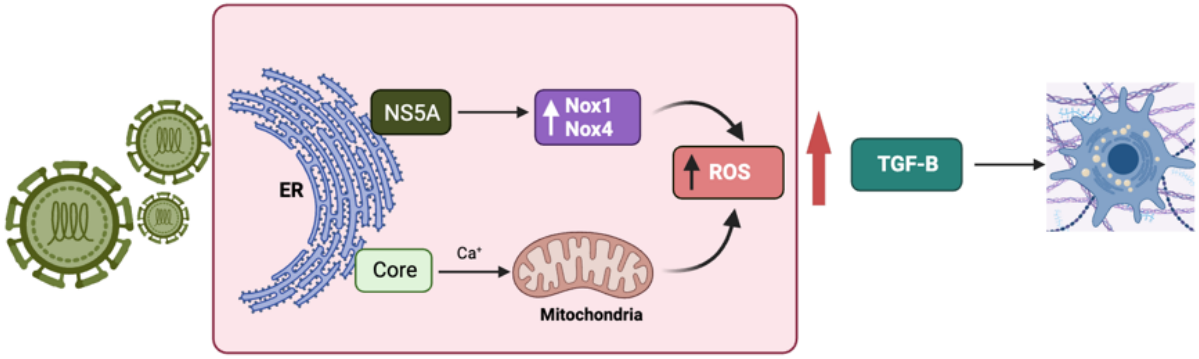

Figure 1.9 NS5A promotion of fibrosis independent of a calcium efflux.
In the presence of NS5A, within the endoplasmic reticulum (ER), NS5A induces the expression of NADPH oxidases 1 and 4 (NOX1 and NOX4) allowing increased expression of reactive oxygen species (ROS). HCV core protein induces the expression of ROSs via a calcium efflux impacting the mitochondria. Increased expression of ROS resulting in increased expression of TGF-B which activates stellate cells inducing fibrosis.

1.7.1.2. Apoptosis

An example of NS5A driving an anti-apoptotic pathway is the binding to FKBP38, a membrane -anchored member of the FK506-binding proteins (FKBPs), activated by calcium and calmodulin, playing a role in cell regulation of apoptosis via the intrinsic apoptosis pathway of mitochondria. Wang *et al*. (2006) demonstrated NS5A binding to FKBP38 and localisation to the mitochondria membrane. Direct mechanisms of inhibiting apoptosis were not explored

however, it may be suggested localisation of NS5A and FKBP38 to the mitochondria membrane results to the anchoring of B-cell lymphoma-2 (Bcl-2) to the membrane inhibiting apoptosis. It has been demonstrated that FKBP38 interaction with Bcl-2, inhibits apoptosis by anchoring Bcl-2 to the mitochondria where Bcl-2 can prevent the mitochondrial permeability transition via inhibiting the actions of Bax, Bcl-2-associated X-protein (Chung et al., 2003; Shirane & Nakayama, 2003). The mitochondrial permeability transition results in the swelling of the mitochondria rupturing the outer membrane of the organelle leading to apoptotic cell death (Bernardi et al., 2023). Bax, another member of the family B-cell lymphoma family, promotes apoptosis by piercing the mitochondria membrane promoting the mitochondrial permeability transition. Bcl-2 binds Bax to the mitochondria membrane inhibiting rupturing of the membrane (Kale et al., 2018) (Figure 1.10).

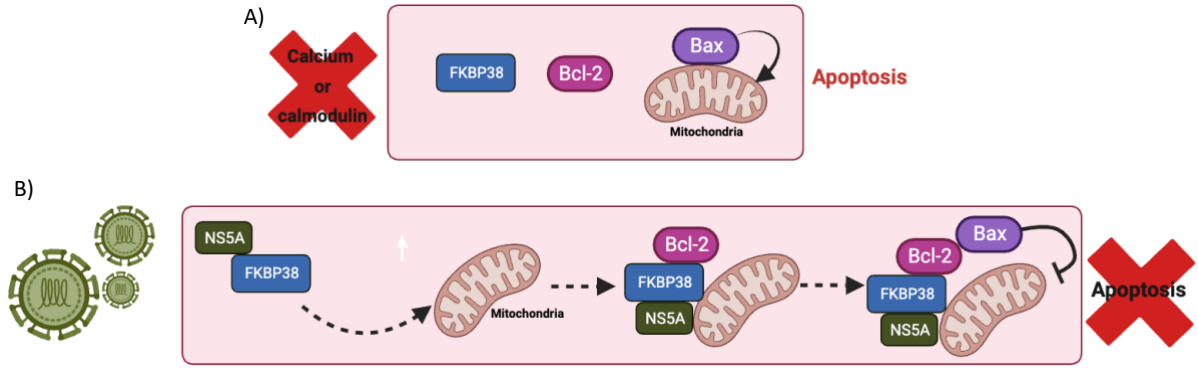

Figure 1.10 NS5A inhibiting mitochondria dysregulation.

A) In the absence of HCV, FK506-binding proteins (FKBPs) FKBP38 does not inhibit cell apoptosis unless activated by calcium or calmodulin. B) NS5A binding to FKBP38 inhibits mitochondrial permeability transition via the binding of Bcl-2-associated X-protein (Bax) to B-cell lymphoma-2 (Bcl-2) on the mitochondrial surface.

1.7.1.3. Hepatocellular carcinoma

NS5A has been directly linked to alteration of the phosphatidylinositol 3-kinase-mediated signalling pathways. PI3K are lipid kinases that regulate the proliferation, adhesion, survival, and motility of cells; its multitude of roles distinguishes dysregulation of the pathway

as important for the promotion of cancer. PI3K is composed of a p85 subunit and a p110 catalytic subunit which phosphorylates phosphatidylinositol-3,4-diphosphate (PIP2) into the second messenger PIP3. PIP3 may be bound by pleckstrin homology (PH) domains resulting in the recruitment of PH domain-containing proteins to the plasma membrane, such as PH domain-containing kinase (PDK1). A downstream effector of the PI3K is the Akt/PKB pathway, serine/threonine kinase Akt, also known as protein kinase B (PKB), once activated can inhibit apoptosis and triggering of the cell cycle allowing cell proliferation via targeting of pro-apoptotic proteins (He et al., 2021; Macdonald & Harris, 2004). For example, a member of the Bcl-2 protein family Bad, and glycogen synthase kinase-3 (GSK-3) by cytosolic sequestration or inactivation by phosphorylation. GSK-3 is particularly associated with the progression of HCC (Lee et al., 2020). Akt/PKB activation can occur by PIP3 binding to Akt/PKB resulting in Akt/PKB phosphorylation by PDK1 (He et al., 2021; Macdonald & Harris, 2004).

During HCV infection, it is believed NS5A binds to PI3K promoting PI3K activity, both *in vivo* and *ex vivo*, resulting in higher Akt/PKB activation. Street *et al*. (2004) demonstrated NS5A mediated activation of AKT resulted in the inhibition of Bad and GSK-3 via phosphorylation. Phosphorylation of GSK-3 promotes stabilisation of the proto-oncogene beta-catenin which has been associated with the inhibition of tumour necrosis factor-alpha induced apoptosis (Shang et al., 2004) which has been associated with a range of tumours (Kramer et al., 2023; Schön et al., 2014), in particular, HCC (Cui et al., 2003) (Figure 1.11).

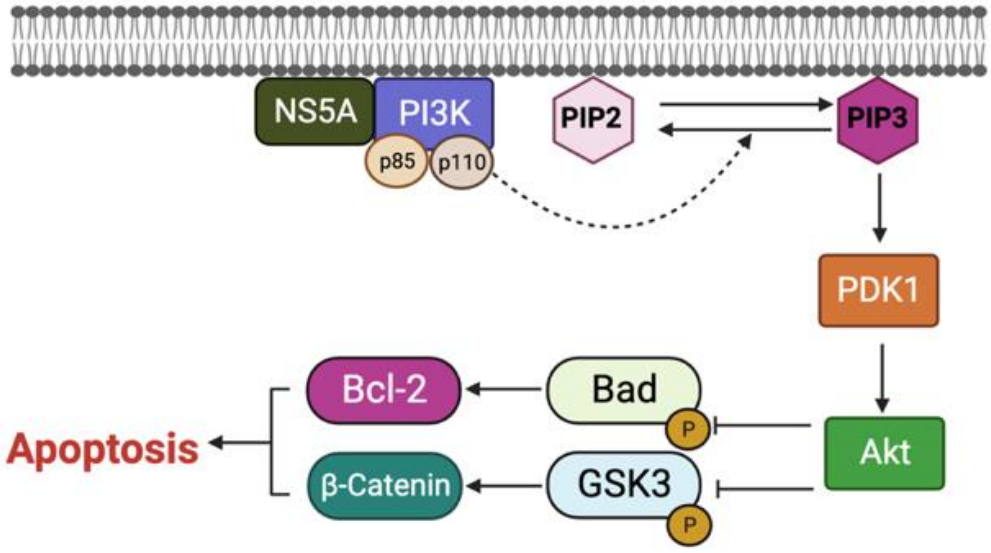

Figure 1.11 NS5A influencing cell survival.
NS5A binding to phosphatidylinositol 3-kinase (PI3K) promotes PI3K activity and downstream effectors of the Akt pathway; inhibiting phosphorylation of the member of the Bcl-2 protein family, Bad, and glycogen synthase kinase-3 (GSK-3). This alters the regulation of anti-apoptotic factors altering cell survival.

1.8. Investigating HCV in the laboratory

The establishment of sub-genomic replicon (SGR) and cell culture infectious clones allowed the development of new HCV therapy; antiviral efficacy and drug resistance profiles to DAAs, as well as the ability to study HCV molecular mechanisms promoting disease progression (Ramirez et al., 2016). Cell culture systems (SGR) and infectious virus) have now been developed for a range of HCV GTs, initially driven by the development of the GT1b SGR (Lohmann et al., 1999), and the GT2a (JFH-1) and 2B (J8) infectious cell-culture systems (Y. P. Li et al., 2012; Lindenbach et al., 2005; Wakita et al., 2005). Relevant to this research a GT3a cell culture infectious clone (Ramirez et al., 2016) from which an SGR was developed (Ward et al., 2020). These tools enabled the direct experimental comparison of GT2a (JFH-1) and GT3a (DBN3a).

Both SGR and cell-cultured virus systems have been used in conjunction with molecular techniques to explore protein specific functions, exposing how individual HCV proteins play a role in HCV infection and disease progression.

1.8.1. Infectious virus culture systems

Development of infectious clones for *in vitro* experiments remain the only way to recapitulate the infectious HCV life cycle *in vitro*. As such, experiments are limited to the GTs of which cell culture adapted clones have been developed. Not all GTs have cell culture infectious clones due to lack of understanding of the mutations required allowing infection of *in vitro* cell lines and efficient virus production between different GTs. The infectious JFH-1 system, developed in 2005 (Lindenbach et al., 2005; Wakita et al., 2005), was the only available efficient infectious system of HCV allowing the full virus life cycle *in vitro* until 2012; the development of JFH-1-independent J6 cell culture system whose virus replication and propagation was as efficient as JFH-1 was published (Y. P. Li et al., 2012). Additionally, Li *et al.* (2012) developed the J8 (representative of GT2b) cell-culture virus, containing 9 adaptive mutations, 3 of which discovered through the development of the J6 clone. Infectious virus clones J6 and J8 differ in nucleotide sequence by 24%. Relevant to this is the development of the Jc1 infectious clone, a chimeric virus containing J6 structural and JFH-1 non-structural (Steinmann et al., 2013). Chimeric viruses act as useful tools to determine GT specific protein functions such as, protein interactome and functions differing dependent on the HCV GT infected. The development of Jc1 by Steinmann *et al.* (2013), demonstrated the HCV glycoproteins E1 and E2 important role during viral membrane envelopment and a cell-cultured HCV virus that can produce significantly higher virus titres than the parental JFH-1 virus.

The GT3a infectious system with virus propagation mimicking that of JFH-1 with limited cell culture adaptions proved to be more difficult. For example, the infectious clone S52 clone, originally found to lack infectivity of Huh7.5 cells however fully functional in chimpanzees (Gottwein et al., 2010), was further developed to include cell and virus specific adaptions within NS5A (Kelly et al., 2017). Due to the adaptions required, investigation of protein function and interaction, such as within NS5A, results to limitations of using the virus clone.

When developing a GT3a infectious clone, emphasis was placed on limiting the number of cell culture adaptions, to allow for greater comparisons to the clinical strain, and virus propagation efficiency like that of JFH-1. As such, a GT3a infectious clone only became available in 2016 (Ramirez et al., 2016). Prior to 2021, when utilising techniques used to develop other GT cell culture systems, GT1b cell cultured virus either failed to propagate or had too low a virus titre to support autonomous virus propagation in culture (Date et al., 2012; Mori et al., 2016; Pietschmann et al., 2009). Li *et al.* (2015), developed an infectious clone of the most prominent HCV GT, GT1b, by primarily utilising the HCV-1/SF9_A and H77C *in vivo* infectious clones and adapting the HCV-1 genome with of the 5'UTR-NS5A and the JFH-1 NS5B-3'UTR. HCV-1 recombinant contains 17 cell-culture adapted mutations allowing the production of a high virus titre.

Infectious clones developed for other GTs however, are deemed not to be viable or comparable to JFH-1 cell culture experiments due to poor virus replication levels (Ramirez & Bukh, 2018). Patient sera cannot be used directly as a method to study HCV GTs as it cannot be cultured in the laboratory unless using hepatoma cell lines with adaptive mutations, allowing only marginal virus production (Saeed et al., 2015). Saeed *et al.* (2015), hypothesised cell cultured cells lacked uncharacterised factors required for efficient HCV replication from clinical isolates. A single mutation was identified, SEC14L2, when expressed in Huh7.5 cells allowed HCV replication following inoculation with patient sera. It is believed SEC14L2 allowed HCV replication by enhancing the vitamin E-mediated protection against lipid peroxidation. There is potential to use cell cultured adapted cell lines to greater understand different HCV infectious clones and the mechanisms of the virus adapted mutations.

1.8.2. Sub-genomic replicons

The SGR system allows research of the non-structural proteins of HCV. By not containing all virus proteins (no structural proteins present), different components of the virus lifecycle can

be investigated, such as genome replication and virus-host protein interactions, without the risk of producing infectious virus. The first SGR system was established in 1999, for GT1b strain Con1 (Lohmann et al., 1999), which accelerated the development of multiple SGR systems for different HCV GTs (Ramirez & Bukh, 2018). Respectively, the JFH-1 and DBN3a SGR systems were established by Kato *et al.* (2003) and Ward *et al.* (2020). In comparison to the development of infectious cell culture systems, SGR systems are much faster to develop after the establishment of an infectious clone containing the required cell culture mutations. When developing an infectious clone there are greater limitations between *in vivo* and *in vitro* virus viability; infectious virus propagation from clinical patient samples without an accumulation of cell culture adapted mutations. (Ramirez & Bukh, 2018).

1.9. Utilising *in vitro* models to greater understand HCV pathology

The development of HCV infectious cell cultured clones and SGR systems allowed investigation of HCV infection in a plethora of different disease model systems. Research fixated on understanding molecular mechanisms of virus infection may not require recapitulation of organ characteristics, for example, investigating the entry of HCV in hepatocytes. However, recapitulation of organs and microenvironments is crucial when investigating the development of disease pathology. Particularly the development of fibrosis during HCV infection as the infection of hepatocytes and the activation of HSC are required for production and accumulation of the extracellular matrix is required.

1.9.1. Monolayer

Primary hepatocytes are not typically used in laboratories due to difficulty isolating the cells, inability to maintain long-term culture and cell proliferation mimicking that of a human liver, due to rapid differentiating rate into mesenchymal phenotypes after 1-2 days of culture

(Duan et al., 2007). Stem cell derived hepatocytes show greater differentiation than primary hepatocytes, showing greater similarities to a fetal liver than an adult liver as well as a mixed phenotype displaying that of the intestines, fibroblasts and non-differentiated stem cells. Cancerous cell lines allow a limitless amount of biological material for the completion of *in vitro* experiments while maintaining their genetic properties (Mirabelli et al., 2019).

HCV research changed dramatically after Blight *et al.* (2002) utilised the SGR system to identify Huh-7 cells susceptible to HCV replication. This resulted to the identification of Huh 7 clones (Huh7 and Huh7.5) being discovered and much of our understanding of HCV infection can be attributed to these cells lines. Particularly the Huh-7.5 cell line allows for efficient HCV replication due to a defect to the retinoic-acid-inducible gene-I (RIG-I), which is part of the cell innate immune response, due to a missense mutation (Sumpter et al., 2005). In addition to high levels of HCV genome replication, Huh7 cell line clones allow the investigation of virus entry and release ensuring all components of HCV infection can be investigated. However Huh7 cell lines are HCC derived resulting in poor differentiation, abnormal proliferation and gene regulation as well as altered signally pathways in comparison to *in vivo* hepatocytes (Durantel & Zoulim, 2007). Furthermore, Huh7 cell lines are phenotypically different between different laboratories. Sainz *et al* (2009) compared Huh7 cells lines from different laboratories, discovering cells differed in morphology, cell growth and permissiveness to infection suggesting an additional variable to consider when comparing HCV research.

To mimic *in vivo* hepatocytes, Sainz *et al.* (2006) treated Huh7 cells with dimethyl sulfoxide (DMSO), a chemical shown to induce the differentiation of primary cell lines (Chang et al., 2006), including hepatocytes (Azuma et al., 2003; Cable & Isom, 1997) and tumour cell lines *in vitro* (Aninat et al., 2006; Cheung et al., 2006; Sainz Jr & Chisari, 2006). Culturing Huh7 cells with 1% DMSO resulted in altered cell differentiation, observed by a change in cell morphology, a non-dividing state confirmed by hepatocyte specific genes. Furthermore, cells remained

susceptible to long-term HCV infection concluding treatment of Huh7 cells with DMSO may more closely mimic *in vivo* hepatocytes.

Other hepatoma cell lines have also been used to investigate HCV biology, differing from Huh7 cell clones by the susceptibility to HCV genome replication, expression of HCV receptors and origins (Table 1.3). Despite not all cell lines being fully susceptible to all stages of the HCV lifecycle, it is possible to explore specific elements of HCV infection in greater detail than if only fully susceptible cell lines were used. For example, Huh 6 cells are not submissive to HCV infection due to low expression levels of claudin-1, however Huh 6 cells allow HCV genome replication when transfected with the HCV SGR. Additionally, Huh 6 cell interferon resistance makes the cell line desirable for the research of anti-viral compounds (Haid et al., 2010) and PLC/PRF/5 cells were utilised to gain greater understanding of HCV internalization by clathrin-mediated endocytosis (Blanchard et al., 2006).

1.9.1.1. Hepatocyte polarisation

In vivo hepatocytes demonstrate a high level of polarisation; forming tight protein junctions between two hepatocytes creating a narrow lumen acting as a site for bile secretion defining the apical canalicular domain (containing the bile duct) and the basolateral sinusoidal membrane required for correct functioning of the liver (Figure 1.12). Key functions of hepatocytes in the liver include; protein and bile secretion, detoxification, urea and cholesterol metabolism, glucose/glycogen metabolism and storage, and secretion of clotting factors.

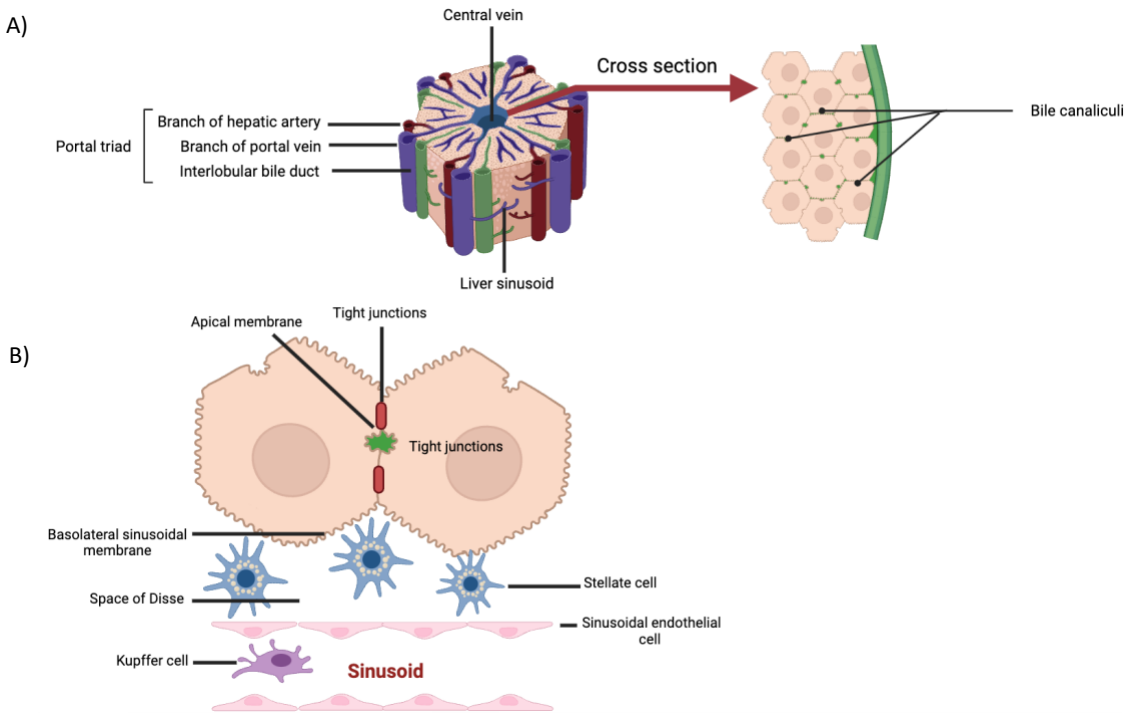

Figure 1.12 Structure of the liver lobule and liver sinusoids.

A) Hepatocytes are organised in a radial form allowing the exchange of materials within sinusoids; hepatic artery carrying oxygenated blood to hepatocytes, portal vein carrying blood with nutrients from the small intestine and, the bile duct carrying bile products away from hepatocytes to the larger duct and gall bladder. B) The sinusoids are lined with endothelial cells interspaced with Kupffer cells. The space between the endothelial cells and hepatocytes is known as the Space of Disse and contains extracellular matrix components such as stellate cells. Hepatocytes allow exchange of materials; basolateral domain shared between neighbouring cells or the sinusoids and the apical domain allowing formation of the bile canicular for bile secretion. Tight junctions seal the lumen of the bile canicular between adjacent hepatocytes.

An essential challenge in translating HCV and hepatocyte biology *in vivo* is the completion of experiments using polarised cell types of hepatocyte origin with high susceptibility to HCV infection. Polarisation of hepatocytes during the conduction of *in vitro* experiments is particularly important to examine the full function of hepatocytes such as bile homeostasis and cholestatic toxicity. Non-hepatic polarising cell line Caco2, expressing HCV entry receptors and supporting HCV replication, demonstrated tight junctions acting as a barrier limiting HCV entry, nevertheless is not a hepatic cell line and so not desirable for further study

of HCV pathology mechanisms. The HepG2 cell line is polarising and of hepatoma cell origin however, must be grown with exogenous CD81 to allow virus entry and only allows a very low level of HCV infection. Therefore, HepG2 cells have been used to demonstrate HCV entry in a polarised cell architecture, particularly as the receptor distribution mimics that of the receptors expressed in human liver tissue. Promotion of polarised Huh7 cells was optimised by Saran *et al*. (2022), by culturing Huh7 cells with 0.5% dexamethasone and 0.5% DMSO prior to the addition of a Matrigel overlay, completed within 2 weeks. Dexamethasone is a known ligand of the glucocorticoid receptor, involved in the regulation of genes controlling cell development, metabolism and immune response. Treatment of Huh 7 cells with dexamethasone induces the expression of constitutive androstane receptor (CAR) and pregnane X receptor (PXR) – two receptors required for sensing of endobiotic an xenobiotic substances, a crucial function of the liver to protect against bile acids as well as drug metabolism of the liver (Lickteig et al., 2019; Pascussi et al., 2000). Matrigel promotes Huh7 cells maturation resulting in a change in cell shape, from epithelium-like to cuboidal, expressing bile canaliculi structures (Kang et al., 2019). Research by Saran *et al*. resulted in a shorter and improved differentiation process of Huh7 cells in comparison to protocols using only dexamethasone and Matrigel requiring a 4 week culture (Kang et al., 2019; Saran et al., 2022).

Cell line	Derived tissue	Susceptibility to HCV lifecycle	Comments	Reference
Study of HCV biology				
Huh 7	HCC	Full lifecycle	Interferon response to infection.	(Blight et al., 2002)
Huh 7.5	HCC	Full lifecycle	Defective RIG-I pathway.	(Blight et al., 2002)
Huh 6	Hepatoblastoma	Entry/replication	Interferon resistance.	(Haid et al., 2010; Windisch et al., 2005)
PLC/PRF/5	Primary liver carcinoma	Entry	Low HCV replication.	(Blanchard et al., 2006; Sainz et al., 2012)
Study of HCV in polarised cells				
HepG2	Hepatoblastoma	Entry/replication	HCV entry requires exogenous CD81. Forms hepatic polarity.	(Mee et al., 2010; Mee et al., 2009; Wilson et al., 2012)
Caco2	Colorectal adenocarcinoma	Entry/replication	Non-hepatic origin. Demonstrates epithelial polarity.	(Mee et al., 2008)
293-T	Kidney	Entry/replication	HCV entry requires exogenous Claudin-1. Non-hepatic origin.	(Evans et al., 2007)

Table 1.3 Selection of *in vitro* hepatoma cell lines utilised in HCV research.
Adapted from Wilson *et al.* (2012)

1.9.2. Mixed cell culture

To better understand HCV pathogenesis *in vitro*, different elements of the hepatic microenvironment have been mimicked, allowing the crosstalk between particular cell lines to be distinguished. To fully recapitulate HCV pathology *in vitro*, mixed cell cultures are required as stellate cells are not susceptible to HCV infection (Florimond et al., 2015). Cell types of particular importance are hepatocytes, HSC and macrophages.

Hepatocytes comprise up to 80% of the total cell population of the liver (Blouin et al., 1977), HSC comprises 5-8% of total cells in a healthy liver (Friedman, 2008) and the rest of the

liver is comprised of endothelial cells, lymphocytes and Kupffer cells. Kupffer cells are liver resident macrophages that situate between liver sinusoids and are adherent to the endothelial cells lining the blood vessels. Kupffer cells differ from monocyte-derived-macrophages as they have a proliferative capacity, allowing replenishment of the cell population (Schulze et al., 2019). As liver fibrosis is a result of chronic hepatic injury, Kupffer cells play a crucial role in the liver wound-healing mechanisms. In the presence of HCV, Kupffer cells become activated expressing tumour necrosis factor alpha (TNF-α), interleukins and chemoattractants (Fletcher et al., 2014; Mandal et al., 2010). As such immune cells, are recruited to the organ resulting in a pro-inflammatory state driving the synthesis of profibrogenic factors such as TGF-B (Roth et al., 1998). This defines both hepatocyte and Kupffer cells as capable of activating HSC. Additionally, the activation of macrophages resulting in an increased expression of TNF-α directly impacts HCV entry into hepatocytes; TNF-α relocalises occludin, disrupting the integrity of the tight junctions, and increases the lateral diffusion speed of CD81, promoting the entry of HCV into hepatocytes (Fletcher et al., 2014).

To recapitulate these different cell lines, Huh7 cell clones are typically used to mimic hepatocytes, LX-2 cells behave as an immortalised cell line of HSC and, THP1, a non-activated immortalised monocyte-like cell line, may be used to mimic the function of Kupffer cells (Bility et al., 2016).

1.9.2.1. Conditioned media

Breakdown of crosstalk between cell types may be determined through conditioned media experiments which defines soluble factors required for the communication between cells. Lin *et al.* (2011) demonstrated crosstalk between hepatocytes and HSC via the treatment of LX-2 cells with supernatant collected from Huh7.5 cells infected with JFH-1. Through the promotion of NF-κB, ROS generated during Huh7.5 cell infection resulted to the activation of LX-2 cells and an increased expression of fibrogenic genes; procollagen α1(I) (ColA) and tissue inhibitor of

metalloproteinases-1 (TIMP1). These results were further supported by, Shi *et al.* (2016), utilising the same strategy, demonstrated HCV infection of Huh7.5 cells infected by J6/JFH-1 drives the expression of epimorphin in LX-2 cells via the extracellular signal-regulated kinase (ERK) pathway. The ERK pathway allows fast communication between the surface membrane and the nucleus, allowing a genomic response to environmental signals (Wang et al., 2004).

1.9.3. 3D spheroids

The majority of *in vitro* assays, drug screening, toxicity, metabolism and studying of infectious agents, utilises the bidimensional (2D) cell culture models. To mimic the tissue microenvironment, particularly cell-cell and cell-extracellular matrix interactions, there has been an emergence of 3D cell culture models. 3D models are believed to contribute a greater understanding of cell and molecular mechanisms due to imitating the environment of human tissue physiology closer than that of 2D models. For example, recapitulation of hepatocytes polarised state using Huh7 cells in a 3D model has been explored by various groups, notably Sainz *et al*. (2009) utilising a rotating wall vessel and Molina-Jimenez *et al.* (2012) utilising Matrigel-embedded Huh7 cell culture system. Both adopted a hepatocyte polarised stated and supported HCV infection. Spheroids may be formed by various methods (Figure 1.13), depending on the technique used there may be variation in size variability that may impact the concentration and gradient of waste products oxygen and nutrient exchange.

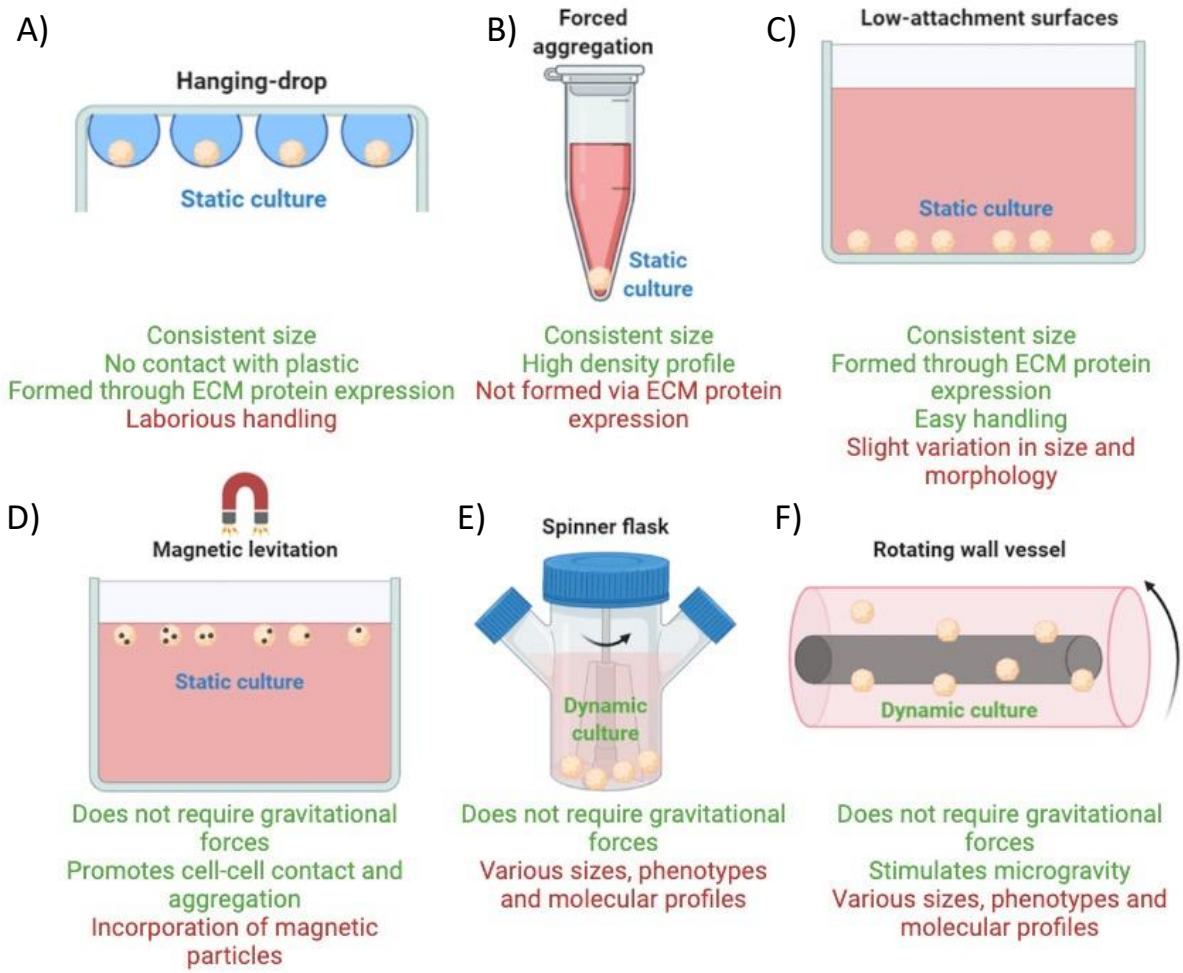

Figure 1.13 Methods of scaffold-free spheroid formation.

Both A) and B) require gravitational forces for the formation of cell aggregates; A) cells hanging within a droplet and B) pellet culturing via centrifugation. C) Relies on self-organisation of suspended cells on a low attachment surface ensuring cells cannot bind to the bottom. D), E) and F) Removes the requirement of gravitational force promoting cell-cell contact and cell aggregation. D) Magnetic forces facilitated by the incorporation of magnetic particles. E) and F) are examples of bioreactor systems promoting dynamic cultures producing spheroids of various sizes as cells are continuously mixed. Adapted from Kouroupis *et al.* (2021).

The method of spheroid formation may alter the characteristics of the spheroids formed which may be crucial to understand experiment results or limit the spheroid formation method used. For example, the hanging droplet technique removes all cell contact with solid surfaces ensuring the spontaneously secreted ECM proteins is the main factor regulating the spheroid formation, however, large scale formation of spheroids is limited by the careful burdensome

handling of the spheroids (Foty, 2011). The use of primary hepatocytes which undergo rapid differentiation when in contact with plastic will benefit from spheroid formation using the hanging droplet method. The size of spheroids may be regulated by the seeding of cells per droplet, tube or well, present within aggregated tube and low-attachment surface spheroid formation. Unlike dynamic formation of spheroids, continuous movement of cell cultures, failing to produce spheroid populations of the same size, phenotype and molecular profiles. Forced aggregation is particularly useful for the formation of high-density spheroids allowing rapid aggregation of many cells (Mackay et al., 1998). Despite magnetic levitation also allows rapid aggregation of cells, an abnormal gravity pull is believed to induce apoptotic pathways resulting in a reduction in cell size, membrane blebbing, reduction of cell viability, alteration to nuclear chromatin and increased caspase-3/7, a signature of mitochondria apoptosis induction (Meng et al., 2011). Microgravity also has negative effects on spheroid formation; disrupting F-actin stress fibres and increasing accumulation of lipids (Meyers et al., 2004). This is particularly important when studying liver fibrosis as F-actin is believed to promote HSC activation (Cui et al., 2014) and dysregulation of lipids homeostasis results to the generation of a toxic lipid environment, also promoting downstream HSC activation and fibrosis promotion (Ekstedt et al., 2015).

1.10. Utilising *ex vivo* models to exploit HCV pathogenesis.

1.10.1. Precision cut liver slices; gold standard for studying liver pathophysiology

Despite mono-, co-, sandwich, organoid and spheroid cultures being used to study a range of liver tissue characteristics and pathophysiology mechanisms, they fail to recapitulate cellular interactions which are physiologically relevant. In particular, mono- and co-cultures are very limited to cell types present and cell:cell interactions specifically lacking the ECM which

plays a critical role in fibrosis progression. Furthermore, cells cultured directly on plastic suffer excess levels of mechanical stress resulting in increased alteration to cellular behaviour (Paish et al., 2019). To combat this, sandwich cultures were developed. This system allows the interaction of primary hepatocytes as the cells are sandwiched between two layers of ECM scaffolds. These interactions have shown to slow the de-differentiation of hepatocytes (Gijbels et al., 2019). De-differentiation of hepatocytes is an important biological phenomenon as removal of cells from human tissue results to a loss of phenotype and specialised function *in vitro*, such as albumin secretion, toxicity assessment and drug disposition (Heslop et al., 2017). In addition to the dedifferentiation of hepatocytes in cell culture, other cell types can become dedifferentiated or transdifferentiated (conversion of one cell type to another). For example, when cultured on plastic stellate cells convert to α-smooth muscle actin resulting in the release of profibrotic genes and secretion of ECM (Olsen et al., 2011).

Three-dimensional (3D) free-floating spheroids cultures, derived from cell lines or tumour biopsies, and organoid cultures, derived from stem cells embedded in ECM soft matrix hydrogels, may contain multiple cell types and provide an alternative to growing hepatocytes and mixed cell cultures (Paish et al., 2019). However, as well as both failing to fully mimic complete cell structural organisation and all cell:cell interactions, the soft matrix hydrogels within organoid cultures result to hepatocyte de-differentiation, supresses profibrotic genes and downgrades albumin synthesis among other factors such metabolic enzymes (Elaut et al., 2006; Paish et al., 2019). Cell metabolism and profibrotic gene expression may also be altered by Matrigel; another substrate used for culturing cells (Novin & Nouri, 2007; Olsen et al., 2011). As such, it becomes evident that PCLS are the gold-standard to exploring pathophysiological mechanisms as the liver 3D structure is maintained containing all cell:cell interactions and the physiological ECM composition (Olinga & Schuppan, 2013; Paish et al., 2019; Starokozhko et al., 2017; Westra et al., 2013). Especially as cell cultures have emphasised the sensitivity of liver cells to different culture environments.

1.10.1.1. Advancement in bioreactor technology to studying fibrosis in PCLS

A major hurdle to overcome in respect to maintaining PCLS to gain reliable results realistic of the native tissue is optimisation of the culture conditions to restrict alterations to cell functions and tissue artefacts. These include cell death, disruption of tissue organisation, significant reduction in albumin secretion, accumulation of cellular waste and spontaneous fibrosis (Koch et al., 2014; Lagaye et al., 2016; Olinga & Schuppan, 2013; Paish et al., 2019; Westra et al., 2013; Wu et al., 2018). As such, various aspects of culturing the PCLS were altered. Examples include advancements in the maintenance of the PCLS via the bioreactor controlling the movement of media either by rocking, shaking and rotating the media. These aid the removal of cellular waste and prevents PCLS experiencing deprivation of oxygen, known as a hypoxic state. Hypoxic states were also prevented by oxygen carriers such as perfluorodecalin (Koch et al., 2014), and by perfusion circuits (Kollmann & Selzner, 2017). Perfusion circuits, in particular normothermic perfusion circuits, have been used readily to rescue steatotic livers by introduction of pharmacological reagents (Aoudjehane et al., 2020; Nagrath et al., 2009). Wu *et al* (2018) explored the introduction of an air-liquid interface whereby PCLS have contact with both the atmosphere and media through the use of Transwells and media movement by a rocking platform. This resulted to PCLS being viable for as long as 15 days. However, PCLS were still susceptible to acceleration of fibrosis and cell death.

As such, it has become evident that a major setback to researching fibrosis in PCLS is the spontaneous fibrogenesis which establishes due to the culturing conditions of PCLS. Paish *et al.* (2019) describes a novel bioreactor which takes into account all the previous advancements in culturing PCLS to maintain viable PCLS to at least 6 days without tissue artefacts occurring, and elongation of normal metabolic activity. This has been accomplished by the creation of a bidirectional flow of media which mimics the sinusoidal flow within an intact liver and semi-

permeable Transwell membranes which restrict PCLS direct contact to plastic and allows movement of media for an air-liquid interface. Lastly, the PCLS are maintained in an oxygen concentration relevant to the organ (Figure 1.14). Additionally, research by Paish *et al.* outlines how the PCLS and the novel bioreactor aids fibrosis research. For example, daily sampling of media can track fibrogenesis by monitoring hyaluronic acid, TIMP1 and MMPs. All of which have been monitored within HCV patients for either fibrosis grades or cirrhosis identification (Lichtinghagen et al., 2001; McHutchison et al., 2000). Measurement of these markers are an addition to an array of other experimental outputs which can be used to exploit the mechanisms of liver fibrosis.

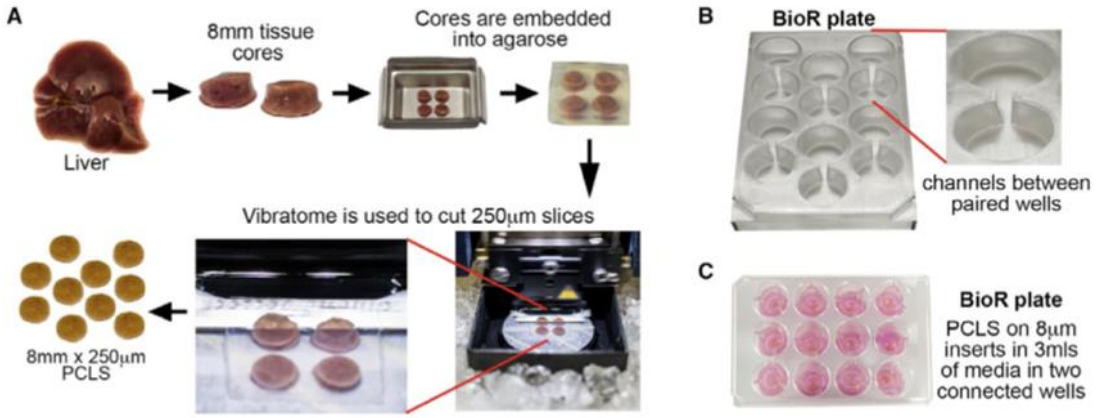

Figure 1.14 Step-to-step production of precision cut liver slices.

Outlines the size and protocol for cutting the PCLS after receiving the healthy tissue from liver biopsies. (B) Illustrates the BioR plate. This plate has been specifically designed for optimal PCLS incubation. The plate contains six bioreactor chambers which constitutes two wells joined by a channel allowing the flow of media on a motor plate at a flow rate of 18.136 μl/sec. (C) PCLS in the BioR plates cultured in 8 μm transwells. Figure was taken from Paish *et al.* (2019).

Fibrogenesis is a result of many etiologies, as such it displays many distinct patterns of development. As all the cells and tissue architecture are maintained in PCLS, fibrosis mechanisms can be investigated. In particular, Kupffer cells maintain the ability to induce an inflammatory response, stellate and myofibroblast cells are still susceptible to activation and

hepatocytes maintain metabolic functioning (Palma et al., 2019). Therefore, fibrosis can be induced in cells by fibrogenic chemicals such as ethanol (Schaffert et al., 2010), TGFβ1 (Paish et al., 2019), lipopolysaccharides and palmitate (Sadasivan et al., 2015). Consequently, antifibrotic activity and pathways can be investigated (Huang et al., 2019). For example, Westra *et al*. (2014) investigated compounds inhibiting the TGFβ1 pathway after activation of fibrosis by bile duct ligation. Additionally, PCLS can be used to depict the mechanisms of viral infections such as adenoviruses, adeno-associated viruses and, importantly to this project, viral hepatitis.

1.10.2. The use of PCLS to address HCV pathogenesis

Studying the mechanism of HCV pathogenesis, specifically promoting fibrosis, was previously limited to cell-culture models. PCLS are a key model to understanding HCV pathogenesis as infection; viral replication, dynamics of viral propagation and testing of antiviral treatments can be conducted with all relevant cell interactions and functions present. Infection of PCLS by HCV has been accomplished by both cell cultured virus (HCV cc) and from HCV infected patient serum (HCV pc). Both HCV cc and HCV pc infections of PCLS were compared by Lagaye *et al.* (2012), where HCV pc was noted as having a higher infectivity due to the conformation of lipoprotein complexes ensuring they remain competent to VLDL. This is believed to be lost in HCV cc as the assembly and maturation of triglyceride-rich VLDL in Huh7.5 cells is not processed the same (Lindenbach et al., 2006; Podevin et al., 2010). However, both HCV cc and HCV pc can infect PCLS with infectious particles being successfully produced. Additionally, Lagaye *et al.* demonstrates the use of PCLS as a tool to analyse HCV antivirals. However, to our knowledge there has been little use of PCLS to exploit the mechanisms of HCV pathogenesis.

To depict HCV pathogenesis, many experimental approaches can be utilised. Many of these experiment outputs have been conducted while researching fibrosis with PCLS. Such as daily media sampling for fibrosis markers (as mentioned in 1.7.2), histological and

immunohistochemistry assessment, RNA isolation, cDNA synthesis and PCR. In respect to PCLS infected with HCV, Lagaye *et al.* (2012) determined expression of core and NS3 proteins by immunofluorescence (IF) *in situ* and co-localisation with mouse antibodies. Furthermore, internalised lipids droplets were visualised by BODIPY dye. Confirmation of the core and NS3 proteins was accomplished by western blot analysis of PCLS cell lysates. To quantify the intracellular presence of HCV, used as a method to quantify the infection of PCLS, strand specific quantitative reverse transcription PCR was conducted. Additional experimental techniques have been outlined by Wu *et al.* (2018) as the use of PCLS was investigated as a tool to study the human innate immunity. As such, PCLS underwent; MTS cell viability assays, isolation of live hepatocytes and non-parenchymal cells prior to flow cytometry and cell sorting analysing detecting for various cluster of differentiation cell markers. These techniques can be used alongside chemical inhibitors targeting specific pathways such as the activin receptor-like kinase 5 inhibitor which inhibits the TGFβ1 pathway. This experimental approach can be used to investigate HCV pathogenesis as expression of TGFβ1 has been observed in HCV-infected hepatocytes (Lin et al., 2010).

1.11. Thesis Aims

This thesis aims to greater understand the mechanisms of HCV pathogenesis by comparing GT2 and GT3. Two approaches were conducted to accomplish this. Firstly, differences between GT2 and GT3 were investigated by comparing infection efficiencies prior to exploring NS5A specific differences; the insertion of an epitope tag in corresponding amino acid sites and comparison of NS5A protein interactions. Secondly, exploration and comparison of different tissue culture models ranging in complexity from monolayer to mixed cell spheroids and finally, human precision cut liver slices, to greater understand the progression of fibrosis during HCV infection.

The genome specific approach is investigated utilising both the SGR and infectious virus (Chapter 3). Differences in infection efficiencies suggest altered abilities to manipulate the host cell, this may be due to differences in NS5A which is crucial for viral genome replication and host protein interactions. The plasticity of NS5A, exploring susceptible sites of insertion using an epitope tag within domain III, may allude to differences in protein function and interaction of GT2 and GT3. Introduction of an epitope tag allows further interrogation of GT2 and GT3 differences by comparing NS5A interactomes through mass tandem tag protein analysis (Chapter 4).

The secondary aim of this thesis was explored using a range of *in vitro* cell models, investigating the requirements of different cell types to greater understand the progression of fibrosis and changes to HCV infection efficiency (Chapter 5). This was explored by completing monolayer infection of Huh7 cells and mixed co-cultures combining Huh7, LX-2 and THP1 cell types during virus infection. Comparisons of cell models, including monolayer, 3D spheroids and PCLS, allows recapitulation of the native liver at differing degrees. This exposes different cell model requirements for researching HCV pathology *in vitro*.

Chapter 2. Methods and Materials

2.1. General materials

2.1.1. Cell culture

2.1.1.1. Eukaryotic cell lines

Mammalian cell lines include Huh7, Huh7.5 and LX-2 cells. Huh7 cells were generated from human liver carcinoma cells (Nakabayashi et al., 1982). Huh7.5 cells are a derivative of Huh7 cells with a defective innate immune response; Huh7 cells grown in the presence of IFN-α, acquiring an advantageous mutation within RIG-I believed to improve HCV replication in comparison to Huh7 cells (Blight et al., 2002). LX-2 cells, gifted from Prof. Scott Freidman and sourced from the Oakley lab, are a highly transfectable human hepatic stellate cell line generated by spontaneous immortalisation under low serum conditions (Xu et al., 2005). THP1 is a human leukaemia monocytic cell line used to investigate monocyte and macrophage modulation and functions (Chanput et al., 2014).

2.1.1.2. Competent bacteria

Cloning was conducted using *Escherichia coli* (E. coli) DH5α genotype; F-ϕ80lacZΔM15 Δ(lacZYA-argF) U169 recA1 endA1 hsdR17(rk-, mk+) phoA supE44 thi-1 gyrA96 relA1 λ- (Invitrogen).

2.1.1.3. Virus strains

DNA constructs contained either the pJFH-1 (Wakita et al., 2005) or pDBN3a (Ramirez et al., 2016), full-length infectious clones, or the SGR containing a firefly luciferase or neomycin phosphotransferase reporter. Wild-type (WT) plasmids, virus and SGR, were modified to contain containing the twin streptavidin tag (TST) or fluorescent proteins. pJc1-JFH-1 chimera

(representative of GT2, structural genes from Jc1 and non-structural genes from JFH-1 infectious clones), containing a RFP or GFP tag fusion was gifted by Ralf Bartenschlager (Schaller et al., 2007).

Virus	Genotype	Accession number
JFH-1	2a	AB047639
Jc1-JFH-1 Chimera	2a	AF177036 and AB047639 (Pietschmann *et al*.)
DBN3a	3a	KX280712-14

Table 2.1 Details of HCV infectious clone DNA constructs.

2.1.1.4. Antibodies

Target	Target (species)	Source	Dilution
NS5A (sheep)	Polyclonal serum	(Macdonald et al., 2003)	WB: 1 in 1000 IF: 1 in 2000
β-Actin	Rabbit polyclonal	Abcam; cat. No.: ab8227	WB: 1 in 2000
	Mouse monoclonal	Abcam; cat. No.: ab6276	WB: 1 in 20,000
Streptavidin	Mouse monoclonal	IBA: 2-1507-001-IBA	WB: 1 in 2000
NAP1L1	Mouse monoclonal	Santa Cruz; cat. No.: sc-81328	WB: 1 in 500
GRP78	Rabbit polyclonal	ThermoFisher Scientific; cat. No.: PA585169	WB: 1 in 500
Phospho-S225	Rabbit polyclonal	Goonawardane *et al.* 2018	WB: 1 in 500
Anti-Actin, α-Smooth Muscle – FITC antibody	Mouse	Sigma; cat. no.: F3777-2ML	IHC: 1 in 1000

Table 2.2 Primary antibodies.

Target (species)	Target	Source	Dilution
Alexa Fluor 594 nm conjugated	Goat	Sigma-Aldrich	IF: 1 in 650
Biotinylated fluorescence	Goat	Vector Laboratories; cat. no.: BA-0601	IHC: 1 in 300

Table 2.3 Secondary antibodies

2.1.1.5. Cell viability

Target	Dye	Source	Dilution	Comments
DNA	Hoechst 33342	Thermo Fisher cat. no.: H1399	1 in 1000	Detection of live cells
DNA	Propidium iodide (PI)	Invitrogen™ cat. no.: P1304MP	1 in 1000	Detection of dead cells

Table 2.4 Cell viability markers.

2.1.2. Molecular biology

2.1.2.1. Oligonucleotides

A list of all oligonucleotides used throughout this project is provided in the supplementary material. Supplied by Integrated DNA Technologies resuspended in dH_2O to 10 μM concentration. Stored at -20°C.

2.1.2.2. Plasmids

Plasmid	Description	Reference
pSGR JFH-1 – WT	Plasmid encoding cell culture adapted derivative of HCV GT2a SGR driven by a T7 promoter containing firefly luciferase as a reporter gene. Plasmid used as a backbone for NS5A cloning.	Wakita *et al.* (2005).
pSGR JFH-1 - GND	Plasmid encoding for cell culture adapted HCV GT2 non-structural proteins under a T7 promoter. Contains a GND amino acid point-specific mutation to GNN within the active site. As such, inactivating the polymerase. Firefly luciferase used as a reporter gene.	Wakita *et al.* (2005).
pVir JFH-1 – WT	Full length viral HCV genome encoding for cell culture adapted derivative of HCV GT2a.	Wakita *et al.* (2005).
pVir JFH-1 - GND	Full length viral HCV genome encoding cell culture adapted HCV GT2. Contains a GND - GNN inactivating mutation within the RNA-dependent RNA polymerase.	Wakita *et al.* (2005).
pVir JFH-1 – TST NS5A amino acid insertion site (Isn) **Isn418** **Isn426** **Isn431** **Isn463**	Full infectious virus genome JFH-1 – WT plasmid encoding twin streptavidin tag within NS5A.	Generated during this project.
pSGR JFH-1 – NS5A eGFP flanked by linkers amino acid insertion site (Isn) **Isn463**	SGR JFH-1 – WT plasmid encoding enhanced green fluorescent protein flanked by linkers within NS5A.	Generated during this project.
pVir JFH-1 – NS5A eGFP flanked by linkers **Isn463**	Full infectious virus genome JFH-1 encoding enhanced green fluorescent protein within NS5A.	Generated during this project.
pVir JFH-1 – eGFP FMDV 2A	Full infectious virus genome JFH-1 – WT plasmid downstream of the 5'UTR delta core region encoding enhanced green fluorescent protein flanked by unique restrictions sites, *MluI* and *BsiWI,* followed by insertion of the foot	Generated during this project.

	and mouth disease 2A protein prior to encoding the core protein.	
pVir JFH-1 NS5A mCherry **Isn418**	Full infectious virus genome JFH-1 encoding mCherry fluorescent protein within NS5A.	Produced by previous lab member, Douglas Ross-Thriepland.
pVir JFH-1 NS5A eGFP **Isn418**	Full infectious virus genome JFH-1 encoding enhanced green fluorescent protein within NS5A.	Produced by previous lab member, Douglas Ross-Thriepland.
pVir Jcl NS5A RFP **Isn396**	Full infectious virus genome Jcl encoding red fluorescent protein within NS5A.	Schaller *et al.* (2007)
pVir Jcl NS5A GFP **Isn396**	Full infectious virus genome Jcl encoding green fluorescent protein within NS5A.	Schaller *et al.* (2007)
pSGR DBN3a – WT	Plasmid encoding for cell culture adapted HCV GT3 non-structural proteins under a T7 promoter. Contains a CPG low luciferase whereby, firefly luciferase was inserted as a reporter gene. Plasmid used as a backbone for NS5A cloning.	Provided by Ward *et al*. (2020)
pSGR DBN3a - GNN	Plasmid encoding for cell culture adapted HCV GT3 as described by DBN3a – WT non-structural proteins under a T7 promoter. Contains a GDD amino acid point-specific mutation to GNN within the active site. As such, inactivating the polymerase. Contains a CPG low luciferase whereby, firefly luciferase was inserted as a reporter gene.	Provided by Ward *et al*. (2020).
pVir DBN3a – WT	Full length viral HCV genome.	Constructed be Ramirez (2016).
pSGR DBN3a – TST NS5A amino acid insertion site (Isn) **Isn423** **Isn431** **Isn436** **Isn449**	SGR DBN3a – WT plasmid encoding twin streptavidin tag within NS5A.	Generated during this project.
pVir DBN3a – TST NS5A amino acid insertion site (Isn) **Isn423** **Isn431** **Isn436** **Isn449**	Full infectious virus genome DBN3a – WT plasmid encoding twin streptavidin tag within NS5A.	Generated during this project.

pSGR DBN3a– NS5A eGFP amino acid insertion site (Isn) **Isn423** **Isn431** **Isn436** **Isn449**	SGR DBN3a – WT plasmid encoding enhanced green fluorescent protein within NS5A.	Generated during this project.
pSGR DBN3a – NS5A eGFP flanked by linkers amino acid insertion site (Isn) **Isn423** **Isn431** **Isn436** **Isn449**	SGR DBN3a – WT plasmid encoding enhanced green fluorescent protein flanked by linkers within NS5A.	Generated during this project.
pSGR DBN3a – NS5A methionine at the start of eGFP **Isn449**	SGR DBN3a – WT plasmid encoding methionine upstream of enhanced green fluorescent protein within NS5A.	Generated during this project.
pSGR DBN3a – NS5A hrGFP **Isn449**	SGR DBN3a – WT plasmid encoding humanised green fluorescent protein within NS5A.	Generated during this project.
pVir DBN3a – eGFP FMDV 2A	Full infectious virus genome DBN3a – WT plasmid downstream of the 5'UTR delta core region encoding enhanced green fluorescent protein flanked by unique restrictions sites, *SpeI* and *SnaBI,* followed by insertion of the foot and mouth disease 2A protein prior to encoding the core protein.	Generated during this project.
pMK0.1-Ac5Ps-hrGFP-du6	Used as a template for the amplification of humanised *renilla* (hr) GFP.	

Table 2.5 Description of plasmids.

2.1.2.3. Enzymes

2.1.2.3.1. Modifying enzymes

Polymerase chain reaction (PCR) was conducted using Phusion® High-Fidelity DNA Polymerase (New England BioLabs, cat. No.: M0530).

2.1.2.3.2. Restriction enzymes

- Restriction enzymes were purchased from New England BioLabs.
- Quick CIP for stable storage of dephosphorylated DNA post enzyme digestion (New England BioLabs, cat. No: M0525S).

2.1.2.3.3. Quantitative PCR

Reverse transcriptase was conducted using LunaScript® RT SuperMix (New England BioLabs, cat. No.: M3010). For quantitative PCR (qPCR), GoTaq® qPCR (Promega; cat. No: A6001) was used.

2.1.2.4. Gel extraction

Conducted following manufacturer's instructions outlined within the Gel Extraction Kit (New England Biolabs; cat. no.: T1020L).

2.1.2.5. DNA purification

Conducted following manufacturer's instructions outlined within Monarch Genomic DNA Purification Kit (New England Biolabs; cat. no.: T3010L).

2.1.2.6. In vitro T7 transcription

- RNAsecure (Invitrogen, cat. No.: AM7005).
- RiboMAX Express T7 transcription (Promega, cat. No.: P1320).
- To purify transcribed RNA the RNA Clean and Concentrator (Zymo; cat. No.: R1014) was used.

2.1.3. Cell culture reagents

2.1.3.1. Huh7 and Huh7.5 cell lines

Maintained in complete DMEM (Dulbecco's Modified Eagle Medium, Gibco™, cat. No.: 41965039); DMEM supplemented with 10 % heat-inactivated fetal bovine serum (FBS) (Gibco™, cat. No.: 16000044), non-essential amino acids 100 X (Gibco™, cat. No.: 11140035), HEPES 1M (Gibco™, cat. No.: 15630056) and 1 % penicillin and streptomycin 5000 units/mL (Gibco™, cat. No.: 15070063).

2.1.3.2. LX-2 cell line

Maintained in complete DMEM; DMEM supplemented with 2% heat-inactivated FBS and penicillin and streptomycin 5000 units/mL.

2.1.3.3. THP1 cell line

Maintained in RPMI (Roswell Park Memorial Institute, Gibco™, cat. No: 61870010), 1640 Medium GlutaMAX™ supplement, with 10 % FBS, 1 % heat-inactivated FBS 1 % penicillin and streptomycin 5000 units/mL (Gibco™, cat. No.: 15070063).

2.1.3.4. PCLS

Maintained in completed Williams E media (Sigma-Aldrich, cat. No: W4128), 2 % heat-inactivated FBS (Gibco™, cat. No.: 16000044), 1% l-glutamine (Thermo Fisher Scientific, cat. No.: 25030024), 1 % pyruvate (Sigma-Aldrich, cat. No: S8636) and 1 % penicillin and streptomycin 5000 units/mL (Gibco™, cat. No.: 15070063).

2.1.3.4.1. Fibrosis stimulant

Stimulant	Concentration	Source
TGF- β	PCLS: 3 ng/mL Monolayer and Spheroids: 10 ng/mL	Thermo Fisher cat. no.: H1399
Platelet-derived growth factor (PDGF)	PCLS: 50 ng/mL	PeproTech cat. no: 100-14B

Table 2.6 Fibrosis stimulant reagents.

2.1.3.5. Stable cell line antibiotic treatment

- Neomycin phosphotransferase - Geneticin™ Selective Antibiotic (G418 Sulfate), Powder (Gibco™; cat. no.: 11811031) used at 400 ng/mL.
- Puromycin N-acetyl transferase - Puromycin Dihydrochloride (Thermo Fisher Scientific; cat. no. A1113802) used at 1 μg/mL.

2.1.3.6. Electroporation

- Cells washed in DEPC-PBS v/v 0.01 % DEPC (BioBasic; cat. No.: DB0154) diluted in 1X PBS.
- Cells were electroporated in SLS Flowgen Electroporation Cuvettes 4mm Long (Scientific Laboratory Supplies; cat. no.: FBR-204).

2.1.3.7. Virus concentration

- Polyethylene glycol (PEG) 8,000 (Thermo Scientific Chemicals; cat. no.: 043443.36) was diluted to 40 % (v/v) using 1X PBS. PEG solution was filtered using 0.45 μm MCE membranes (MF-Millipore™; cat. no.: HAWP04700) using the VPS-200 Air Admiral Vacuum Pump Station (Cole-Parmer).

- Supernatant containing virus was filtered using 20 mL syringes (Thermo Scientific ™; cat. no.: S7510-20) and 0.20 μm syringe filter (Fisher Scientific; cat. no.: 10015301)

2.1.3.8. Transfection reagents

- Lipofectamine™ 2000 (Invitrogen™; cat. no. 11668030).
- Lipofectamine RNA iMax ™ (Invitrogen™; cat. no. 13778100).
- Transfections performed in Gibco™ Opti-MEM™ Reduced Serum Medium (Fisher Scientific; cat. no.: 15392402) or complete DMEM media.

2.1.4. Bacterial cell culture

- Ampicillin sodium salt (Amp) purchased from Fisher (cat. No.: 69-52-3). Ampicillin was reconstituted to 100 mg/mL concentration in dH_2O and filtered through a 0.22 μm filter and stored in -20 °C. Was used at a working concentration 100 μg/mL.
- Luria-Bertani (LB) broth in 1 L constituted of 10 g tryptone (Millipore; cat. No.: T7293), 5 g yeast extract (Millipore; cat. No.: 70161) and 0.1 M sodium chloride (Fisher Scientific; cat. No.: 10598630).
- LB agar in 1 L constituted of 10 g tryptone, 5 g yeast extract, 0.1 M sodium chloride and 0.045 M agar (Millipore; cat. No.: 05040).

2.1.5. DNA/RNA analysis

- Plasmid isolation from bacterial culture carried out using a Miniprep kit (Monarch®; cat. No.: T1010).
- Agarose gel used in DNA gels: 1% (w/v) agarose (Sigma-Aldrich; cat. No: A9539) submerged in Tris-Acetate- EDTA (TAE) buffer; 10X TAE – 0.4 M Tris (Santa Cruz; cat.

No.: 77-86-1), 0.1 % (v/v) glacial acetic acid (Santa Cruz; cat. No.: 64-19-7), 0.013 M EDTA (Millipore; cat. No.: 324503) and dH_2O).

- 1 kb ladder used in DNA gels; DNA HyperLadder™ (Meridian Bioscience; cat. No.: BIO-33053).
- DNA samples visualised in gels by 6X gel loading dye (New England BioLabs, cat. No: B7024).
- Agarose gel used in RNA gels; 1 % (w/v) agarose, 0.07 % (v/v) 10X MOPS (0.2 M MOPS (Sigma Aldrich; cat. No.: M1254), 0.5 M EDTA, 1 M sodium acetate (Sigma Aldrich; cat. No.: 127-09-3), 0.04% (v/v) formaldehyde (Sigma-Aldrich; cat. Non: F8775) and dH_2O) submerged in DEPC- dH_2O (0.001 % DEPC (BioBasic; cat. No.: DB0154)).
- 500 bp used in RNA gels; ss RNA Ladder (New England BioLabs, cat. No: N0362S).
- RNA samples visualised with 2X RNA Gel Loading Dye (New England BioLabs, cat. No: B0363S).
- 10,000X SYBR Safe (Thermo Fisher Scientific, cat. No: S33102) used as gel stain.
- Purification and extraction of DNA from agarose gels was performed using a Gel Extraction kit (Monarch®; cat. No.: T1020).

2.1.6. RNA extraction

- Samples lysed by TRIzol™ Reagent (Invitrogen™; cat. no.: 15596026).
- RNA isolated using chloroform (Thermo Scientific Chemicals; cat. no.: 67-66-3).
- RNA precipitation conducted using 100% isopropanol and glycogen (Thermo Scientific™; cat. no.: 11873933).
- Wash competed using 75 % ethanol (v/v).
- DNAase treatment: TURBO DNA-free™ Kit (Invitrogen™; cat. no.: AM1907).
- Reaction conducted with the BIO-RAD CFX Connect™ Real-Time System.

2.1.7. Western blotting

- Colour Prestained Protein Standard purchased form New England BioLabs (cat. No.: P7719).
- Running buffer constituted of 5X SDS-PAGE: 0.25M Tris, 1.92 M glycine (Sigma-Aldrich; cat. No.: G8790) and 0.5 % (w/v) SDS (Sigma-Aldrich; cat. No.: 75746) .
- Sample loading dye constituted 5x reducing SDS-PAGE Laemmli buffer; (5 mL) 2 mL 10 % SDS, 2 mL glycerol (Sigma-Aldrich; cat. No.: 56-81-5), 0.5 mL β-mercaptoethanol (Sigma-Aldrich; cat. No.: 60-24-2), 0.6 mL 1 M Tris-HCl (Promega; cat. No.: H5123) pH 6.8, trace of bromophenol blue to colour (Sigma-Aldrich; cat. No.: 115-39-9).
- SDS resolving gel was produced with 30 % acrylamide (Thistle Scientific; cat. No.: SBL-20-2100-10), 1.5 M Tris-HCl, 10 % SDS, 10 % ammonium persulfate (APS) and Tetramethylethylenediamine (TEMED). SDS stacking gel was produced with 30 % acrylamide, 1 M Tris-HCl, 10 % SDS, 10 % ammonium persulfate (APS, Sigma-Aldrich, cat. no.: A3678) and TEMED.
- PVDF membrane was purchased from Amersham™ Hybond® Western blotting membranes (Cat. No.: GE10600023) and activated in methanol (Sigma-Aldrich; cat. No.: 67-56-1)
- SDS-gels were transferred to PVDF membranes using thick filter paper (Thermo Scientific™; cat. No.: 88620).
- Towbin transfer buffer constituted of 25 mM Tris, 192 mM glycine, 20 % (v/v) methanol.
- TBS-T wash buffer constituted of 10X buffer (250 mM Tris, 1.37 M NaCl (Fisher Scientific; cat. No.: 10326390), 1 % Tween-20 (Sigma-Aldrich; cat. No.: 9005-64-5), pH to 7.5 with concentrated HCl (Sigma-Aldrich; cat. No.: 7647-01-0).

- Blocking buffer contained 50 % Intercept® (TBS) Blocking Buffer (LI-COR; cat. no.: 927-60001) diluted in 1X TBS.
- Protein transferred to membranes via the Trans-Blot Turbo (Bio-Rad).
- Western blots visualised on the LICOR Odyssey Sa.

2.1.8. Immunofluorescence

- Fixed in 4 % paraformaldehyde (v/v, Sigma Aldrich; cat. no.: 47608).
- Blocking with 3 % bovine serum albumin (BSA, Roche: cat. no.: 3117057001) diluted in 1X PBS.

2.1.8.1. Focus forming assay quantification

- Permeabilisation solution: 0.1 % (v/v) Triton X-100 (Sigma-Aldrich; cat. no.: 9036-19-5) in 1X PBS.
- Washing in 1X PBS.
- Microscope: Sartorius IncuCyte S3

2.1.8.2. Spheroids

- Positioned onto glass slides using GeneFrames (Thermo Scientific™; cat. no.: AB0576).
- VECTASHIELD® Antifade Mounting Medium (Vector Laboratories; cat. no.: H-1000-10).
- Visualised using the Ziess LSM880 inverted confocal microscope.

2.1.8.3. Precision cut liver slices

- Antigen retrieval performed using 10 mM Tris (1.21 g), 1 mM EDTA (0.37 g), Tween 20 (0.5 mL), 1000 mL dH20, pH 9.
- Washing in 1X TBS with 0.1 % Triton X-100 (v/v).

- Prolong Gold Antifade mountant (Thermo Fisher: cat. no.: P36934).
- Hoechst solution diluted in TBS-Triton.
- Microscope: Ziess LSM880 inverted confocal and Carl Zeiss LSM980 MP AiryScan 2 and multiphoton.

2.1.9. Histology staining

- Dehydrate in alcohol 100 % and Alcohol 70 %.
- Counterstain in Mayer's Hematoxylin Solution (Sigma- Aldrich; cat. no.: MHS32).

2.1.9.1. αSMA

- To block endogenous peroxides used methanol and 2 % Hydrogen peroxide (Sigma-Aldrich; cat. no.: H1009).
- Antigen unmasking solution, sodium citrate buffer (Vector Laboratories; cat. no.: H3300) and Vector ABC tertiary (Vector Laboratories; cat. no.: PK-7100); (4.96mL vector solution and 500 mL water.
- Washes completed in 1X PBS.
- Avidin/Biotin Blocking kit (Vector Laboratories; cat. no.: SP-2001).
- Antibody blocking completed in 20% pig serum (Serotec; cat. no.: C15SB) diluted in PBS.
- Monoclonal Anti-Actin, α-Smooth Muscle – FITC antibody produced in mouse, 100 μL per slide.
- Biotinylated anti-fluorescein made in goat (Vector Laboratories; cat. no.: BA-0601) diluted in 1 % pig serum.
- DAB mix (Vector Laboratories; cat. no.: SK-410,) Mix 2 drops buffer, 4 drops DAB, 2 drops hydrogen peroxide to 5 mL of dH_2O.

- Scott's Tap water solution (Leica; cat. no.: 3802900) wash after counterstain.
- Clearing conducted using Clearene Solvent – (Leica; cat. no.: REF: 3803620e).
- Mounted using Pertex (Leica; cat. no.: 08709E).

2.1.9.2. Picro-Sirius Red

- Wash in dH_2O.
- Hydrate treated with 0.2 % phospho molybdic acid (Supelco.; cat. no.: 79560).
- Stained with Picro-Sirius Red (Abcam; cat. no.: ab246832) and rinsed in 0.01% HCl.
- Wash in running tap water after counterstain.
- Clearing conducted in Xylene (Thermo Scientific Chemicals; cat. no.: L13317.AP)
- Mounted using DXP (Merck; cat. no.: 06522).

2.1.10. Lactate Dehydrogenase (LDH)

- CyQUANT LDH Cytotoxicity Assay as per manufactures instructions (Invitrogen; cat. no.: C20300).
- Absorbance was read on the Filter Max F5 Multi Mode Micro plate reader, measured at 490 + 680 nm wavelength.

2.1.11. Aspartate Aminotransferase (AST)

- AST Activity Assay Kit as per manufactures instructions (Merck; cat. no.: MAK055).
- Absorbance was read on the Filter Max F5 Multi Mode Micro plate reader, measured at 450 nm wavelength.

2.1.12. Enzyme-linked immunosorbent assay (ELISA)

- Completed as per manufactures instructions R&D Systems.

- Wash solution; 1X PBS with 0.05 % Tween.
- Stop solution; 26.7 mL of H2SO4 and 473.3 mL dH_2O.
- Reagent diluent; 1 % BSA in PBS.
- Human Albumin detection (R&D Systems; cat. no.: DY1455).
- Human Col1A1 detection (R&D Systems; cat. no.: DY6220-05).
- Tecan Infinite 200 Pro plate reader between wavelengths of 450 nm – 570 nm.

2.1.13. Resazurin cell viability

- Completed as per manufacturers instructions (Abcam; cat. no.: ab145513).

2.1.14. Immunoprecipitation and protein purification

- Cell lysed using Glasgow Lysis Buffer (GLB) prepared from 2X concentration; 20 mM PIPES (Sigma Aldrich; cat. no.: P6757), 240 mM KCl (Sigma Aldrich; cat. no: P9541), 60 mM NaCl, 10 mM $MgCl_2$ (Sigma Aldrich; cat. no.: M2670), 2% Triton X-100 (v/v) and 20% glycerol (v/v), pH 7.2. Protease inhibitors include 1 μg/mL leupeptin (Sigma Aldrich; cat. no.: 62070), 1 μg/mL pepstain A (Roche; cat. no.: 10253286001), 2 μg/mL Aprotinin (Roche; cat. no.: 10236624001) and 0.2 mM Pefabloc® SC 9Roche; cat. no.: 11429868001). Phosphatase inhibitors include 1 mM EDTA, 2 mM Na_3VO_4 (Sigma-Aldrich; cat. no.: S6508) and 5 mM sodium pyrophosphate (Supelco.; cat. no.: PHR2205).
- Wash buffer 10X Buffer W produced by IBA Lifesciences (cat. no.: 2-1003-100) containing 100 mM Tris-Cl, 150 mM NaCl and 1 mM EDTA diluted in dH_2O.
- High salt wash consisting of 10X Buffer W diluted in dH_2O with 1 M NaCl and 2 % Triton X-100 (v/v).
- Sepharose suspension beads: Strep-Tactin™ Sepharose™ Resin (IBA Lifesciences; cat. no.: 2-1201-010).

- Magnetic beads: MagStrep "type 3" XT (IBA Lifesciences; cat. no.: 2-4090-002).
- Eluted in 10 % SDS.

2.1.15. Luciferase assay

- Firefly and Renilla Luciferase Single Tube Assay Kit (Biotium, cat. No.: 30081).
- 5X Passive Lysis Buffer (Promega; cat. no.: E19410 diluted in dH_2O.
- FLUORstar Omega microplate reader (BMG LABTECH).

2.1.16. Software

- Benchling used for sequence analysis.
- Figures were created using BioRender.com
- ImageStudio (LI-COR, 2017) were used for image processing of western blots.
- GraphPad Prism (Version 10.1.0) used for graphic design and statistical analysis.
- Sartorius Incucyte® S3 Live Cell Analysis System (v2018B) used for IncuCyte S3 image analysis.
- ZEN software (Zeiss) was used for the analysis of immunofluorescence images.
- ImageJ (Fiji) used to analysis spheroid segmentation using the SpheroidJ plug-in (Lacalle et al., 2021).
- Proteome Discover (Version 2.4) was used to integrate all the data for quantitative analysis of LC-MS/MS results. Data was searched using Mascot against the *human* database (download from UniProt 05/03/23).
- Tecan i-control to analyse ELISA results.
- OPTIMA Software was used to perform luciferase assay readings.
- SoftMax Pro 6.5.1 was used to perform AST assay readings.

2.2. Methods

2.2.1. Molecular cloning

2.2.1.1. Restriction cloning

Restriction cloning was accomplished using restriction enzyme sites within the JFH-1 and DBN3a WT SGR and virus plasmids. Oligonucleotide sequences are listed in the Appendix. For insertion into the C terminus of NS5A, restriction sites *BsiW*I and *BspE*I were used for DBN3a and, *BamHI* and *AfeI* was used for JFH-1 plasmids. Primers were produced by Integrated DNA Technologies.

2.2.1.2. DNA amplification

Polymerase chain reaction (PCR) was conducted using Phusion High-Fidelity (HF) DNA Polymerase and performed as per manufacturers instructions. PCR components and PCR cycling conditions are outlined for a 2-step and 3-step PCR primer amplification (Table 2.7, 2.8, 2.9, 2.10). Successful PCR reactions were confirmed by visualising products by agarose gel electrophoresis and underwent gel extraction prior to restriction digestion and bacterial transformation. Restriction digest was performed using restriction enzymes flanking the region being cloned into the vector, outlined below. Quick CIP treatment was conducted on the DNA of the vector to inhibit self-ligation.

Component	Volume (μl)
Forward Primer	2.5 (10 μM)
Reverse Primer	2.5 (10 μM)
5X High Fidelity Buffer	10
dNTPs (deoxyribonucleotide triphosphate)	1 (10μM)
Phusion	0.5
Template DNA	1 (10 ng/μl)
dH_2O	32.5
Total	50

Table 2.7 Round 1 of 2-step PCR amplification.

Forward PCR reaction; forward primer of oligonucleotides containing the upstream restriction site and the beginning of the twin streptavidin tag (TST) sequence and reverse primer being the oligonucleotides from the SGR containing the complementary restriction site sequence. Reverse PCR reaction; reverse primer of oligonucleotides containing the downstream restriction site and end of the TST sequence and the forward primer sequence being the oligonucleotides from the SGR containing the complementary restriction site sequence. In both cases the template DNA would be the TST sequence.

Component	Volume (μl)
Forward Primer	2.5 (10 μM)
Reverse Primer	2.5 (10 μM)
Forward Template	1 (10 ng/μl)
Reverse Template	1 (10 ng/μl)
5X High Fidelity Buffer	10
dNTPs (deoxyribonucleotide triphosphate)	1 (10μM)
Phusion	0.5
dH_2O	31.5
Total	50

Table 2.8 Round 2 of 2-step PCR amplification.

Forward and reverse primers refer to the SGR oligonucleotides. Forward and reverse template refer to the PCR products from round 1.

Component	Volume (μl)
Forward Primer	2.5 (10 μM)
Reverse Primer	2.5 (10 μM)
Forward Template	1 (10 ng/μl)
Reverse Template	1 (10 ng/μl)
5X High Fidelity Buffer	10
dNTPs (deoxyribonucleotide triphosphate)	1 (10μM)
Phusion	0.5
dH_2O	31.5
Total	50

Table 2.9 Round 3 of 3-step PCR amplification.

Forward and reverse primers refer to the SGR oligonucleotides. Forward and reverse template refer to the PCR products from round 2 and the last individual product of step 1.

	Step	Temp	Time
	Denature	98 °C	30 secs
Touchdown PCR 5 cycles	Denature	98 °C	10 secs
	Anneal	72 °C – 62 °C	30 secs
	Extend	72 °C	1 minute per kb
30 cycles	Denature	98 °C	10 secs
	Anneal	62 °C	30 secs
	Extend	72 °C	1 minute per kb
	Anneal	Primer dependent	30 secs
	Extend	72 °C	1 minute per kb

Table 2.10 PCR cycle conditions.

2.2.1.3. Insertion of twin streptavidin tag

2-Step PCR was completed for the insertion of TST, amplifying the regions downstream of the *BsiW*I through the TST tag, and upstream of the *BspE*I through the TST tag. This created an overlapping region with the TST nucleotide sequence allowing both PCR fragments to be combined (Figure 2.1). All PCR amplification concerning the cloning within NS5A was conducted using the WT SGR plasmids. Once a construct was successfully produced, NS5A from the SGR was cut out of the SGR and inserted into the viral plasmid due to the presence of the same restriction sites.

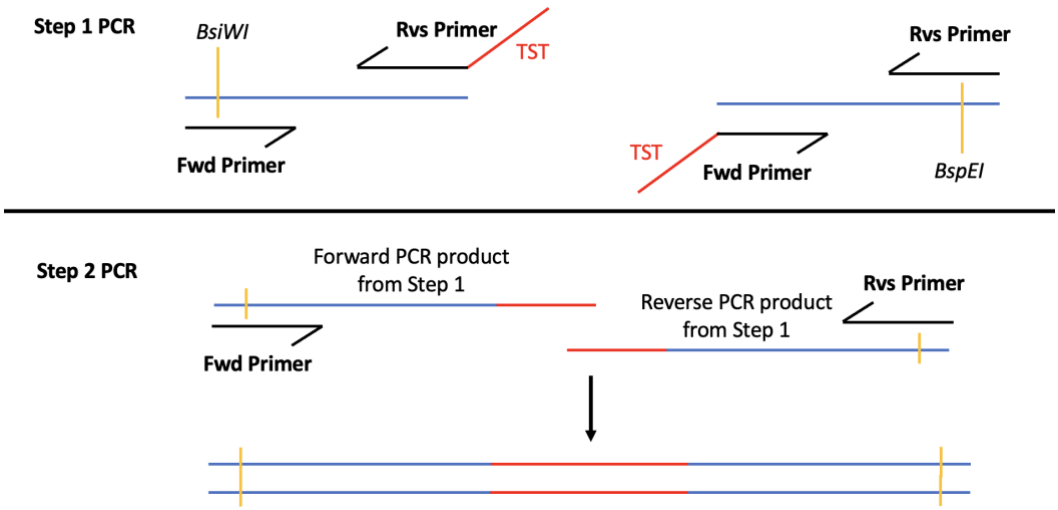

Figure 2.1 2-step PCR amplification.

Diagram outlining the requirements of two different PCR amplifications in step 1; individual amplifications required for the forward and reverse primers. Step 2 outlining the combining of two PCR products from step-1 to one product due to the overlapping twin streptavidin sequences.

2.2.1.4. Insertion of fluorescent protein tags

A 3-step PCR amplification was conducted when inserting larger genes such as green fluorescent protein (GFP).

2.2.1.5. Insertion into NS5A

The primary PCR reactions created fragments amplifying the regions downstream of the *BsiW*I through to the start of GFP, a second fragment amplified the region upstream of the *BspE*I through to the end of GFP. A third fragment amplified the complete GFP ORF. Overlapping regions were created flanking GFP and allowing PCR fragments to be combined (Figure 2.2). PCR amplification step 1 and 2 are the same as PCR amplification of the TST.

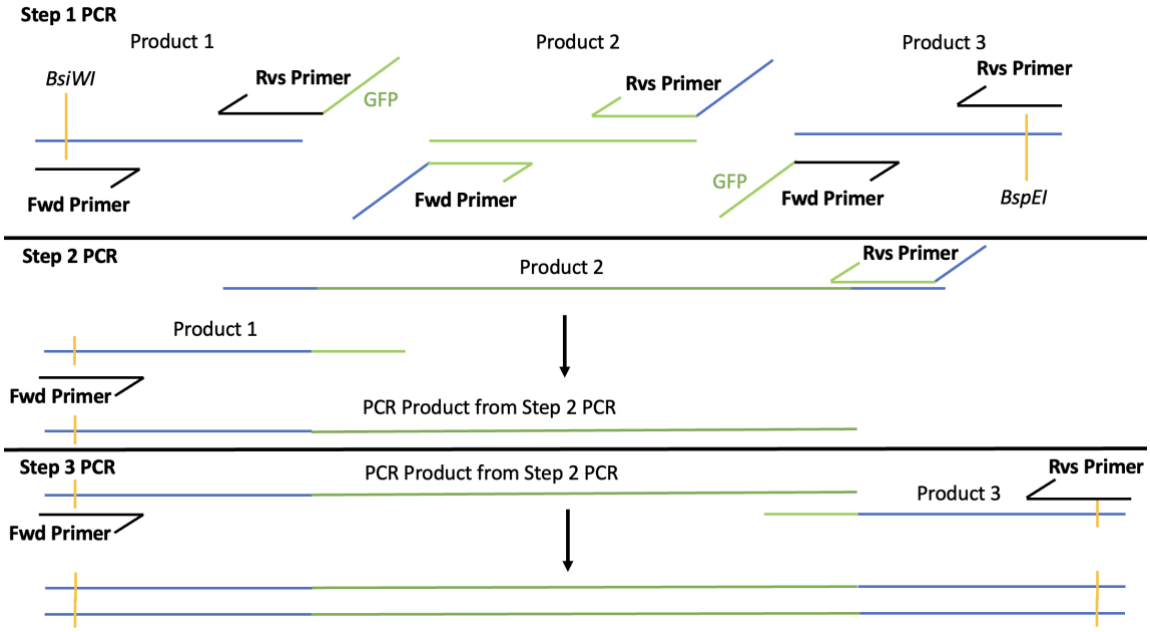

Figure 2.2 3-step PCR amplification.

Diagram outlining the requirements of three different PCR amplifications in step 1; individual amplifications of three products required for the forward and reverse primers. Step 2 outlining the combining of two PCR products from step-1 to one product due to the overlapping green fluorescent protein (GFP) sequences. Step 3 outlining the combining of three PCR products from Step 1 and Step 2 to one product due to the overlapping GFP sequences.

2.2.1.6. Insertion of upstream of viral polyprotein translation

The primary PCR reactions created fragments amplifying the 5'UTR containing the delta core region (amplified from the SGR containing the luciferase reporter gene upstream of the non-structural proteins), enhanced GFP (eGFP) with flanking unique restriction sites between nucleotides from the 5'UTR delta core and start of the FMDV 2A sequence, and a third fragment of the FMDV 2A with the unique restriction site before the core protein region (Figure 2.3). Restriction sites introduced varied dependent on the HCV GT; JFH-1 *MluI* and *BglII* and, DBN3a *SpeI* and *BglII*. PCR amplification step 1 and 2 are the same as PCR amplification of the TST and, step 3 PCR amplification was the same as the step 3 amplification of GFP however, viral oligonucleotides sequences were used.

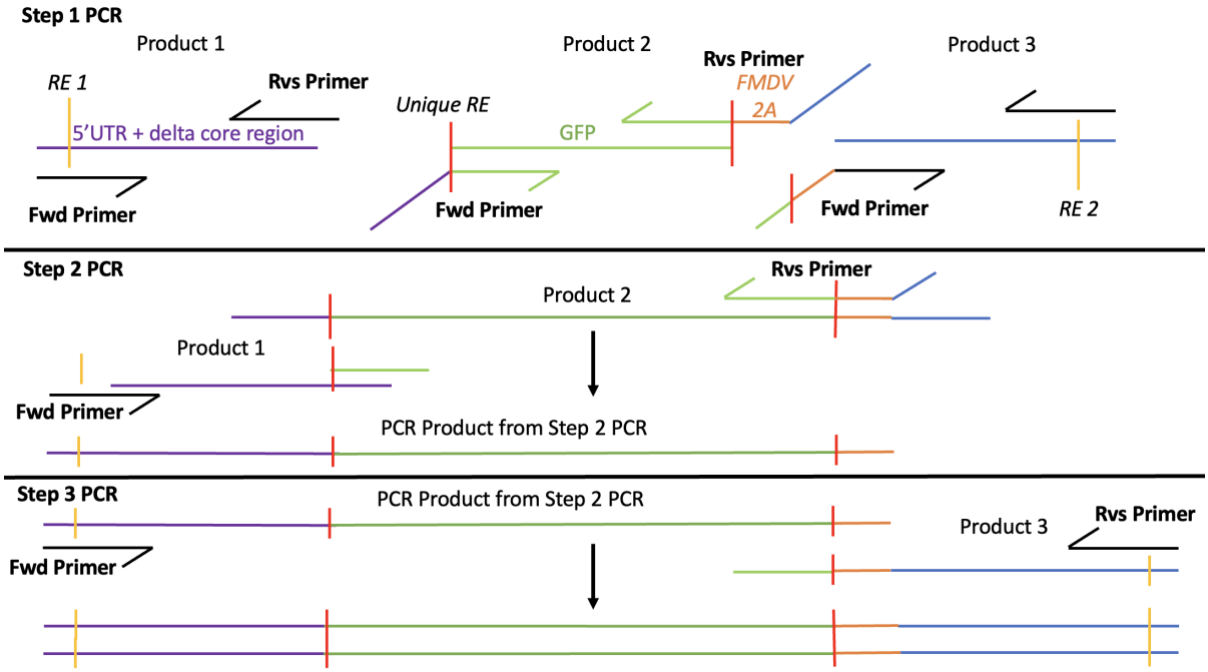

Figure 2.3 3-step PCR amplification to insert GFP and FMDV 2A sequences.

Diagram outlining the requirements of two different PCR amplifications in step 1; individual amplifications of three products required for the forward and reverse primers. Product 2 introduced unique restriction sites flanking green fluorescent protein (GFP) and the foot and mouth disease virus (FMDV) 2A sequence at the 3' end. Step 2 outlining the combining of two PCR products from step-1 to one product due to the overlapping GFP sequences. Step 3 outlining the combining of three PCR products from Step 1 and Step 2 to one product due to the overlapping GFP and FMDV 2A sequences.

2.2.2. DNA digest

DNA was digested based on the existence of restriction sites and the use of restriction enzymes. When producing DNA to perform *in vitro* transcription, 5 – 8 μg of DNA was digested utilising the restriction site *XbaI* to linearise the plasmid. The reaction was incubated at 37 °C for 3 h. When digesting PCR products, all DNA harvested from the PCR reaction was digested. Digested DNA products were visualised by agarose gel electrophoresis prior to DNA gel extraction.

2.2.2.1. Agarose gel electrophoresis

PCR products and digested DNA were visualised on gels consisting of 1 – 2 % (w/v) agarose, 10,000X SYBR Safe gel stain in 1X TAE. Samples were mixed with 6X gel loading dye and loaded into a gel submerged in 1X TAE. An additional well was loaded with GeneRule 1 kb DNA Ladder. Electrophoresis was performed at 80 V to allow appropriate separation of desired fragments. If required, gel extraction was completed using Monarch Gel Extraction Kit.

In vitro transcribed RNA quality was assessed and visualised on gels consisting of 1 – 2 % (w/v) agarose. Once components were dissolved 0.04 % (v/v) formaldehyde and 10,000X SYBR Safe gel stain were added. Ss RNA Ladder and 1μg of sample was mixed with 2X RNA Gel Loading Dye prior to denaturation at 85 °C for 5 minutes. All samples and ladder were loaded into a gel submerged in DEPC-dH_2O and 0.1 % (v/v) 10X MOPS. Electrophoresis was performed at 60 V to allow appropriate separation.

2.2.3. Insert and vector ligation

The PCR products (insert) and plasmids (vector) was digested by flanking restriction, sites *BsiW*I and *BspE*I with the restriction enzyme buffer 3.1 (NEB). After the digest incubation was complete, Quick CIP was added as per manufacturer instructions, for stable storage of dephosphorylated DNA. Ligation reaction requires a 3-fold molar excess of the insert with total DNA not exceeding 100 ng (Table 2.11). Reaction was pipetted 10-20 times prior to the addition of DH5α (50 μl) and completion of the bacterial transformation protocol.

Component	Volume (μl)
Instant Sticky-end Ligase Master Mix (New England BioLabs, cat. No.: M0370S)	5
Vector	*x*
Insert	*y*
dH_2O	*z*
Total	10

Table 2.11 Components of ligation reaction.

2.2.4. Bacterial transformation

50 μl of Endura Competent or DH5α cells were incubated on ice for 30 minutes with a maximum 10 ng of DNA prior to heat shocking at 42 °C for 1 minute. Bacteria returned to ice for 2 minutes prior to the addition of 360 μl of LB broth and 1 h recovery incubation at 37 ° C with agitation at 180 revolutions per minute (rpm). Cells were plated on LB agar plates containing the appropriate antibiotic for a final incubation at 37 °C overnight. However, if transforming the HCV plasmids post ligation, 950 μl of LB broth was added after heat shocking, recovery incubation was extended to 3 h and the final incubation was 30 °C for 16 h.

2.2.5. *In vitro* transcription and RNA preparation

Prior to *in vitro* transcription, linearized DNA was purified using the Monarch Genomic DNA Purification Kit. To inactivate RNases prior to *in vitro* T7 transcription, 1 μg of purified DNA (DNA template) was treated with RNAsecure. Once all components of the RNAsecure reaction were added, DNA templates were placed on a 60 °C heat block for 10 minutes and then cooled on ice before completion of RiboMAX Express T7 transcription as per manufacturer instructions (Table 2.12). Note; an exception to the manufacturer instructions, the incubation at 37 °C was increased to 2 h instead of 30 minutes. The DNA template was digested via DNase (also included in the kit) whereby, 1 μl of DNase was added followed by a second incubation at 37 °C for 15 minutes. RNA was further purified using the Zymo RNA Clean and Concentrator kit as per

manufacturer instructions. RNA concentration was determined by NanoDrop and were stored at – 80 °C.

Component	Volume (µl)
RNAsecure	1
RNase free water	*x*
DNA Template	*y*
Total	8

Table 2.12 RNAsecure reaction components.

2.2.6. Plasmid isolation

Single colonies were selected from LB agar plates using a pipette tip and placed directly into 10 mL LB broth containing 100 µg/mL of the appropriate antibiotic and incubated overnight at 37 °C (or 30 °C if HCV plasmid) and agitated at 180 RPM. Small-scale isolation of the plasmid was completed using the Monarch Plasmid Miniprep Kit (cat. No.: T1010S) as per manufacturer instructions. Successful cloning was confirmed by Sanger sequencing provided by Genewiz. Plasmid DNA concentration was determined by NanoDrop.

2.2.7. Maintenance of eukaryotic cell lines

2.2.7.1. Adherent cell lines

All adherent cell lines (Huh7/Huh7.5/LX-2) were maintained in either T25, T75 or T175 flasks at 37 °C with 5 % CO_2. Cells were grown to 80 % confluency prior to splitting. To detach cells from the flask, cells were washed with 10 mL PBS (Phosphate Buffered Saline) before incubating with 1 X trypsin (Gibco™, cat. No.: 25200072) for 5 minutes at 37 °C. Subsequently, cells were transferred into a falcon and pelleted by centrifuging at 1200 x RPM for 3 minutes. Cells were resuspended in fresh cell culture media.

2.2.7.2. Establishment of bi- monolayer cultures

Bi- monolayer co-cultures were conducted with Huh7 and LX-2 cells only. All cultures were performed as a 1:1 ratio when seeding cells with cells cultured within LX-2 complete DMEM media. LX-2 completed DMEM media was used due to reduced presence of FBS (2%) in comparison to the Huh7 complete DMEM media (10% FBS). Number of cells was determined by the well size (Table 3), cells were mixed within the well prior to incubation for 4 h allowing adherence of cells (or 70-80% confluency) prior to performing experiments.

2.2.7.3. Suspension cell lines

Suspension cell line (THP1) were maintained in either T75 (maximum volume of 20 mL) or T175 (maximum volume of 35 mL) flasks at 37 °C with 5 % CO_2 until roughly 1.5 x 10^6 cells/mL. Volume was monitored to ensure maximum gas exchange. Cells were transferred into a falcon and pelleted by centrifuging at 500 x RPM for 3 minutes. Cells were resuspended in fresh cell culture media (Table 2.13).

2.2.8. Cell seeding densities

Culture plate size	Seeding Density
96 well plate	0.5 x 10^4
48 well plate	0.03 x 10^6
24 well plate	0.05 x 10^6
12 well plate	0.1 x 10^6
6 well plate	0.3 x 10^6

Table 2.13 Monolayer seeding cell densities.

Numbers of cells seeded dependent on the size of well used, unless otherwise stated.

2.2.9. Precision cut liver slices (PCLS)

2.2.9.1. Obtaining human liver tissue

Obtained normal resection margin surrounding colorectal metastasis, surplus to pathology requirements, from adult patients undergoing surgical resection at the Freeman Hospital (Newcastle-upon-Tyne, UK). Ethics approval: Human liver tissue was obtained under full ethical approval from the NovoPath Biobank Newcastle, (REC reference: 22/NE/0054, approved 12/04/2022) and used subject to patients' written consent. PCLS was generated within 2 h post-hepatectomy.

2.2.9.2. Generating PCLS

Conducted by Dr Hannah Paish as described within Paish *et al.* (2019). Liver tissue was cut into 8 mm cores embedded into low melting agarose allowing the cutting of tissue into 250 μm slices. Slices were selected for further culturing if no tears were present.

2.2.9.3. Maintaining PCLS

Maintained within 8-μm-pore Transwell inserts, in a modified tissue culture plate (BioR plate) and rocked on the bioreactor platform (patent PCT/GB2016/053310) at a flow rate of 18.136 μL/sec. Media was changed daily.

2.2.10. Production of spheroids

Spheroids were produced using the low-attachment surface and static culture method (Kouroupis & Correa, 2021), in correspondence to the protocol conducted within Prof. Oakley research group. Prior to cell seeding, U-bottom 96 well plates were coated with low melting agarose by aliquoting 100 μl of agarose per well and knocking the agarose out of the 96 well plate within the tissue culture hood. Plates were left to dry within the hood for a minimum of

10 minutes prior to seeding cells. Spheroids were produced using 1 x 10^5 cells per well using LX-2 preferred DMEM media. When producing mixed cell cultures, a 1:1 ratio of cells was seeded; 5 x 10^4 cells of each cell type. All wells contained a final volume of 100 μl media.

2.2.11. Electroporation of eukaryotic cell lines

Performed for the insertion of the viral genome; SGR to measure genome replication or, the full viral genome to propagate virus. Cells were trypsinised and resuspended in complete media prior to counting cells. Cells were washed twice by centrifugation at 1200 RPM for 3 mins using cold DEPC-PBS. After the final wash step, cells were resuspended to achieve 0.5 x 10^7 cells/mL concentration. Utilising a cold electroporation cuvette, 400 μl of cells was added with RNA. Cells were electroporated using square wave 260V/25ms/1Pulse and immediately resuspended in 11.6 mL of warm complete media.

2.2.11.1. Sub-genomic replicon

Per electroporation, 2 μg of RNA was used. After resuspension, cells were seeded dependent on the downstream analysis. Luciferase assays and fluorescent protein observations were conducted within flat bottom 96 well plates with 100 μl per well. SGR stable cell lines were initially established in 6 well plates with 2 mL per well.

2.2.11.2. Virus propagation

Per electroporation, 5 μg of RNA was used. After resuspension cells from two electroporations were pooled and placed in a T175 flask before being immediately transferred to the BSL-3 facility. Media was replaced 72 h post electroporation and cells were further cultured to 144 h post electroporation. All media collected was stored at 4°C and titre analysed by focus forming assay (FFA) or was concentrated using PEG centrifugation.

2.2.12. Transfection of eukaryotic cell lines

Comparison of transfection reagents, Lipofectamine 2000 or RNA iMax, efficiency was compared for the siRNA knockdown experiments. At approximately 12 h post seeding 1 x 10^5 cells per well of a 12 well plate (or 60-70% confluency), transfection was performed. Lipofectamine 2000 or RNA iMax lipofection, was performed as per manufacturers instructions. Volumes of Opti-MEM and transfection reagent was calculated for a 12 well-plate. If changing media 4 h post transfection, transfection reagent was performed in Opti-MEM. If media was not to be changed post-transfection, transfection reagent was performed in complete Huh7 cell DMEM media.

2.2.13. Luciferase reporter assays

Cells were lysed using 1X Passive Lysis Buffer for a minimum of 10 minutes, long term storage of lysed cells at -20 °C. 50 μl of cells lysed in passive lysis buffer were transferred to a white 96 well plate prior to the addition of the luciferase reagent (50 μl) directly before insertion into the FLUORstar Omega microplate reader at room temperature. Plates were read for a total of 3.5 seconds with 0.5 second intervals.

2.2.14. Fluorescent reporter assays

Fluorescent assays were observed using the IncuCyte S3. Analysing the expression of protein fluoresce overtime, monolayer cells were visualised from 4 h post cell seeding and images acquired at 4-hour intervals maintained within the IncuCyte S3. If observing protein fluorescence at 24 hour intervals and collecting cell lysates to analyse the expression of luciferase, cells were imaged directly before lysing cells. Analysis of images was performed using

the Sartorius IncuCyte® S3 Live Cell Analysis System. Across different biological repeats the same software analysis parameters was used; IncuCyte parameters outlined in the Appendix.

2.2.15. Establishment of stable cell lines

Cells were treated with antibiotic for 2 weeks to selectively grow cells containing the antibiotic resistance gene. If cells reached confluency, they were placed in a larger flask or split. Completion of siRNA transfections and cell harvests are conducted at least one week after initial antibiotic treatment not to interfere with siRNA transfection efficiency as per manufacturer's instructions.

2.2.16. Concentration of virus stocks

Performed adapting the protocol outlined by Baktash *et al.* (2019). PEG 8000 was resuspended to a 40% concentration with 1X PBS (v:v) prior to filtration and storage of the solution at 4°C. Within BSL-3, virus supernatant was filtered using 0.2 μm filters and syringes. Using 50 mL falcons and a maximum concentration of 40 mL, virus was concentrated using a final concentration of 8% PEG (v:v), which was mixed and stored at 4°C overnight prior to pellet formation the following day at 5000 RPM for 25 minutes at 4°C. If pooling multiple virus pellets, 10 mL of supernatant remained, and pellet was resuspended prior to pooling multiple pellets into one falcon. A final centrifugation was completed at 5000 RPM for 15 minutes at 4°C. Final pellets were resuspended in 1 mL 1X PBS and stored at -80°C. Virus titre was determined by FFA.

2.2.17. Determining virus titre by focus forming assay

FFAs were performed on monolayers of Huh7.5 cells seeded into 96 well plates. Serial dilutions of virus inoculum was performed in complete DMEM media for Huh7.5 cells. If performing a FFA using virus supernatant not concentrated, 100% of virus inoculum was added

as the highest titre. If performing a FFA on concentrated virus stocks resuspended in PBS, the highest virus titre was diluted to 25% (v:v) with complete DMEM prior to performing serial dilutions. The assay was incubated for 48 h, after which cells were washed with 1X PBS and formaldehyde fixed for 30 minutes. Detection of virus infected cells was conducted by immunofluorescence staining of cells, described below in section 2.2.5.1. Virus titres were calculated using the following equation:

2.2.18. Virus infections

All completed in the biological safety level 3 laboratory (BSL-3).

2.2.18.1. Mono- and bi- monolayer cultures

Cells were seeded into the appropriate well size and incubated for 4 h allowing cell adherence. Virus (MOI 0.2) and TGF-β (10 ng/mL) treatment dilutions were performed in complete DMEM, dependent to the cell types present, to an MOI 0.2. Treatment of cells with TGF-β acted as a positive control to stimulate fibrosis pathways. When comparing HCV infection in the presence of LX-2 cells, all infections were conducted using LX-2 complete DMEM media. Virus inoculum was aliquoted into 100 μl (96 well plate), 200 μl (24 well plate) or 500 μl (12 well plate). If analysing the cell growth of the adherent monolayer, cells were incubated within the IncuCyte S3 and images were acquired at 4 hour intervals. Virus infected cells were incubated for 72 h. p. i prior to cell washing cells in 1X PBS and cell harvest via formaldehyde fixation or cell lysis methods for 30 minutes.

When comparing differences between HCV GT infection efficiency, Huh7 cells were seeded into 24 well plates using Huh7 cell complete DMEM media. Prior to inoculation, media was removed and placed with 100 μl media per well. Virus (MOI 0.2) and TGF-β (10 ng/mL) treatment dilutions were performed in complete DMEM for Huh7 cells and 200 μl aliquots were

placed in the relevant wells. Virus was adsorbed onto cells at 37 °C for 4 h prior to removal of virus inoculating media, replaced with fresh complete DMEM media. At each timepoint (4 h/ 8 h/ 24 h/ 48 h/ and 72 h post infection). Supernatant was collected and stored at 4 °C to perform FFAs and cells were washed with 1X PBS prior to formaldehyde fixation or cell lysis methods for 30 minutes.

2.2.18.2. Tri- culture of mixed monolayer and suspension cultures

All cells were cultured at a 1:1:1 ratio, within a 12 well plate, each cell type was seeded at a 0.5 x 10^6 cell density per well. To ensure all cells were cultured in the THP1 RPMI complete media, Huh7 and LX-2 cells were pelleted and resuspended in complete RPMI media. Adherent monolayer cells were directly placed into the 12 well plate, THP1 suspension cells were placed in a 24 well plate, all cells were incubated at 37 °C for 4 h allowing cell adhesion of monolayer cultures. Prior to cell infection, THP1 cells were combined to the monolayer culture and the total volume per well 1 mL. Virus (MOI 0.2) and TGF-β (10 ng/mL) dilutions were performed in complete RPMI media and virus inoculum was aliquoted into 200 μl per well. If analysing the cell growth of the adherent monolayer, cells were incubated within the IncuCyte S3 and images were acquired at 4 hour intervals. Virus infected cells were incubated for 72 hpi prior to removal of media and THP1 cells. Adherent cells were in 1X PBS and cells harvested via formaldehyde fixation or cell lysis methods.

2.2.18.3. Spheroid

Post seeding, cells were directly taken to BSL-3. Virus (MOI 0.2) and TGF-β (10 ng/mL) dilutions were performed in complete RPMI media and inoculum was aliquoted into 50 μl per well. Cells directly incubated within the IncuCyte S3 and images were acquired at 4 hour intervals. Post-infection, live cell staining of spheroids was performed or media was removed

and spheroids washed in 1X PBS prior to spheroid harvest via formaldehyde fixation or cell lysis methods.

2.2.18.4. PCLS

Prior to infection of PCLS, the slices were rested for 12 h post slice generation to reduce mechanical stress from cutting the tissue altering results observed within PCLS. Virus (MOI 0.06) dilution was performed in 1X PBS and fibrotic stimulated (Fib. Stim) control treatments (TGF-β (10 ng/mL) and PDGF (3 ng/mL) dilutions were performed in complete Williams E media. To control for the addition of PBS to the infected PCLS, all dual wells of PCLS were cultured in PBS for 4 hour virus inoculation incubation. Concerning infected PCLS, all media was removed and replaced with 2.5 mL media, slices were inoculated with 500 μl virus containing PBS. Fib. Stim PCLS had all media removed and replaced with the TGF- β and PDGF containing media (2.5 mL) and 500 μl 1X PBS. The mock control had complete media replacement of 2.5 mL and the addition of 500 μl 1X PBS. During the inoculation, PCLS returned to the rocker until 4 h.p.i, when all media was replaced on PCLS with 3 mL complete Williams E, except the Fib. Stim sample which was cultured in the presence of TGF- β and PDGF for the reminder of the experiment. Media was changed daily. PCLS were harvested 72 h.p.i. via TriZol for 30 minutes or formaldehyde fixation. PCLS were directly formaldehyde fixed and inactivated for 48 h prior to removal from BSL-3. PCLS fixation was completed by collecting transwells containing the PCLS, dabbing excess media off the bottom of transwells with tissue prior to submerging the full transwell containing PCLS in 1X PBS to wash the slice. Excess PBS was removed by dabbing the transwell on tissue and following by inactivation by submerging the transwell and slice in formaldehyde.

2.2.19. Determining soluble factors by conditioned media experiments

To investigate soluble factors released by Huh7 cells during HCV infection, Huh7 cells were pelleted and resuspended in completed DMEM for LX-2 into a 12 well plate. Huh7 cells were infected with HCV or treated with TGF- β within BSL-3, 4 h post seeding. Supernatant of Huh7 cells was collected 72 h.p.i and cell debris was removed from the supernatant via a syringe and 0.20 μm filter. Media was removed from LX-2 cells, which had been seeded into a 48 well plate 4 h prior, and directly treated with 100 % supernatant collected from Huh7 cells termed as conditioned media. To control for media quality and a direct fibrosis stimulated control sample, LX-2 cells were cultured in fresh DMEM complete media, and TGF- β diluted in DMEM complete media. LX-2 cells were incubated in the IncuCyte S3 allowing cell growth analysis, images acquired at 4 hour intervals.

2.2.20. Immunofluorescence

2.2.20.1. Monolayer

After fixation, cells were washed with PBS three times and permeabilization solution was applied to the monolayer for 7 mins prior to washing cells and incubation of sheep anti-NS5A serum in BSA blocking buffer for 1.5 h. Prior to the addition of the Alexa Fluor 594 nm conjugated secondary antibody, cells were washed three times. After a 40-minute incubation, cells were washed 3 times prior to covering the monolayer in PBS and long-term storage at 4 °C in the dark. The number of virus infected cells was analysed within the IncuCyte S3.

2.2.20.2. Spheroid cell viability

Prior to live cell staining, doxorubicin (200 nM) diluted in complete DMEM media for LX-2 cells was used to treat spheroids as a positive control for cell death, 12 h before spheroid

staining. At 72 h.p.i, media was removed from all spheroids, Hoescht 33342 and propidium iodide (PI) were diluted in complete DMEM for LX-2 cells and 100 μl of stain containing was added to each well containing a spheroid. Spheroids were incubated at 37 °C for 30 mins. Spheroids were harvested by removing all media and washing cells twice in 1X PBS prior to formaldehyde fixation for 30 mins. Prior to mounting spheroids to glass slides within gene frames and glass cover slips, spheroids were washed three times with 1X PBS. Mounted spheroids were stored at 4 °C. Spheroids were visualised using the Zeiss LSM880 inverted confocal microscope.

2.2.20.3. PCLS

Fixed PCLS were washed in 1X PBS three times prior to performing tissue antigen retrieval. PCLS were transferred into histology cassettes lined with sponges to inhibit folding of the tissue slice during the 15 minute antigen retrieval in the microwave (800 W at P80) using 500 mL of antigen retrieval buffer. The solution was cooled at room temperature with the addition of 300 mL tap water prior to removing slices from the histology cassettes and transferring PCLS to a 24 well plate for the remainder of the protocol. All wash steps were conducted as washing PCLS in TBS-Triton three times for 5 mins and all incubations were conducted at room temperature on a rocker. Prior to the addition of the primary antibody, PCLS were blocked in 3% BSA for 1 hour, blocking solution was removed and primary antibody (sheep anti-NS5A serum, 1 in 200 diluted in 3% BSA) was directly added to the PCLS and incubated for 2 h. PCLS were washed prior to incubating PCLS with the secondary antibody (Alex Fluro 594, 1 in 600 diluted in 3% BSA) for 1 hour, from which point PCLS was protected from light. Staining of nuclei was conducted with Hoechst 33342, diluted in TBS-Triton incubated for 30 mins after washing the PCLS to remove all secondary antibody. Before mounting slices to glass slides secured using Geneframes and glass cover slices, a final wash step of PCLS was completed. Slides

were stored at 4 °C for long term storage prior to visualising slices using the Zeiss LSM880 inverted confocal microscope, Carl Zeiss LSM980 MP AiryScan 2 utilising two photons.

2.2.21. Measurement of soluble factors released by PCLS

All longitudinal media samples was collected during the course of PCLS experiments and was stored at -80 °C.

2.2.21.1. AST

All reagents of the AST Activity Assay Kit, except the AST positive control, were thawed at room temperature protected from light. The AST positive control, included within the kit, was thawed on ice. Glutamate standards were performed as outlined (Table 2.14). All samples were diluted 1:4 in assay buffer prior to transferring to a flat bottom 96 well plate and the addition of the master mix solution (Table 2.15). Once the master mix was added to all samples, the standards and AST positive control wells, the plate was wrapped in aluminium and mixed for 30 seconds prior to incubating at 37 °C for 2 minutes and completion of the initial absorbance measurement using the on FilterMax F5 MultiMode Micro using the software SoftMax Pro 6.5.1 measured at 450 nm wavelength. Continue to incubate the plate at 37°C taking absorbance measurements every 5 minutes. Take measurements until the value of the most active sample is greater than the value of the highest standard (10 nmole/well). At this time the most active sample is near or exceeds the end of the linear range of the standard curve.

Standard name	Concentration mM	Volume of Standard (μL)	Volume of Assay Buffer (μL)
A	1	5 uL of standard stock	495
B	0.8	400 of A	100
C	0.6	375 of B	125
D	0.4	333 of C	167
E	0.2	250 of D	250
F	0	0	500

Table 2.14 AST dilution of glutamate standards.

Reagent	Master Reaction Mix (per well (uL))	Master Reaction Mix (per plate (uL))
AST Assay Buffer	20	2000
AST Enzyme Mix	0.5	50
AST Developer	2	200
AST Substrate	2.5	250

Table 2.15 Preparation of AST master mix solution.

2.2.21.2. LDH

All reagents of the CyQUANT LDH Cytotoxicity Assay kit were thawed at room temperature protected from the light. The reaction mixture consisted of 1 vial of substrate dissolved in 11.4 mL dH_2O. The LDH positive control, included in kit, was diluted with 200 μl 10% Triton (v/v) and made up to 1.5 mL with PCLS media. The assay was performed in a flat bottom 96 well plate with 25 μl of either the sample, positive control or blank sample (media only control) and, 25 μl of the reaction mixture per well. All samples were performed in duplicate. The reaction was incubated for a maximum of 30 minutes in the dark prior to the addition of 25 μl of the stop solution. Absorbance was measured between 490 nm - 680nm wavelength measured on the Tecan plate reader.

2.2.21.3. ELISAs

Performed as per the manufacturer's instructions (R&D Systems). Standard solutions were diluted as outlined (Table 2.16). Assay was performed in flat bottom 96 well plates and

read at 450 nm – 570 nm wavelength on the Tecan plate reader. Concentrations were determined by mean OD values via standard curve.

	Alb (pg/mL)	Col1A1 (pg/mL)
Tube 1	**1600**	**2000**
Tube 2	**800**	**1000**
Tube 3	**400**	**500**
Tube 4	**200**	**250**
Tube 5	**100**	**125**
Tube 6	**50**	**62.5**
Tube 7	**25**	**31.25**
Blank	**0**	**0**

Table 2.16 Standard concentration of albumin and collagen 1A1 for ELISA analysis.

2.2.22. PCLS viability

Testing the cell viability of PCLS post a 4 hour incubation with 1X PBS diluted in complete Williams E media to ensure infection of virus resuspended in PBS would not introduce additional cell damage. PCLS rested for 24 hour post generating slices, were incubated with complete Williams E media or 1X PBS 17 % or 33 % (v:v) diluted in complete media. Incubation was completed at 37 °C on a rocker. Post 4 hour incubation, all media was replaced with fresh complete media and changed daily for 3 days. PCLS were harvested and directly used to complete a resazurin assay (completed as per manufacturer's instructions).

2.2.23. Cellular RNA extraction

2.2.23.1. Monolayer cell harvest

At time of harvest, all media was removed and cells were washed with 1X PBS. Cells were scraped into an 1.5 mL Eppendorf and cells were pelleted by centrifugation at 5000 RPM

for 5 minutes. Supernatant was removed and 1 mL TRIzol was used to lyse all cells for 30 minutes prior to long term storage at -80 °C.

2.2.23.2. Spheroids cell harvest

Pooling of 48 spheroids per experimental condition was required to acquire a sufficient amount of extracted RNA. Spheroids were collected into a 15 mL Eppendorf prior to pelleting all spheroids via centrifugation at 5000 RPM for 5 minutes. Supernatant was removed and spheroids were resuspended in 1 mL 1X PBS and transferred into a 1.5 mL Eppendorf. Cells were pelleted by centrifugation at 5000 RPM for 5 minutes prior to the addition of 1 mL TRIzol used to lyse all cells for 30 minutes prior to long term storage at -80 °C.

2.2.23.3. PCLS cell harvest

Slices from adjoined wells were pooled to acquire a sufficient amount of RNA. A transwell containing a PCLS was collected from media and dabbed onto tissue to remove excess media and liquid tension prior to completely submerging the transwell in 1X PBS to wash the PCLS prior to using plastic tweezers to place the slice directly into a 1.5 mL Eppendorf containing 1 mL TRIzol and inactivated for 30 minutes prior to storing in -80°C.

2.2.23.4. RNA extraction protocol

Prior to manual RNA extraction, TRIzol samples were defrosted at room temperature and heat treated at 55 °C shaking at 300 RPM agitation for 10 minutes. After which, 200 µl chloroform/mL was added to TRIzol, samples were vortexed to ensure completing mixing of solutions and incubated for 2 minutes at room temperature prior to centrifugation for 15 minutes at 12,000 x G at 4 °C. The upper aqueous phase was transferred to a clean Eppendorf in addition to 500 µl isopropanol and 1 µl RNAse free glycogen (10 mg/µl). The sample was vortexed briefly and incubated at room temperature for 10 minutes before centrifugation for

10 minutes at 12,000 x G at 4 °C. The supernatant was removed and the RNA pellet was washed with 75% ethanol (v:v) and centrifuged for 7 minutes at 7,500 x G at 4 °C. The ethanol wash was removed and the RNA pellet air dried before resuspending in 20 μl nuclease free dH_2O and heating the sample for 10 minutes at 60 °C. DNAse treatment was performed as per manufacturers instructions utilising the TURBO DNAse kit. Long term storage of RNA at -80 °C.

2.2.24. cDNA synthesis

Reverse transcription of cDNA from cellular RNA extraction was used for Real-time qPCR analysis. LunaScript Supermix was used to synthesis cDNA as per manufacturers instructions.

2.2.25. mRNA gene expression

Completion of qRT-PCR was conducted following GoTaq® qPCR Master Mix (2X) Promega manufacturer's instructions completed on a Bio-Rad CFX Connect Real-Time PCR Detection System including a melt curve cycle analysis post detection for 35 cycles.

2.2.26. RT-qPCR calculating virus titre

To quantify all virus particles released during virus propagation compared to viable virus particles produced and quantified by FFA, the number of viral genome copies released into the supernatant 72 h.p.e was quantified by qRT-PCR. Supernatant was collected virus inactivated by TRIzol LS reagent prior to removal of samples from BSL-3. RNA was extracted as per previously outlined protocol (LINK) however the full RNA extract was used for downstream cDNA synthesis; 16 μl of RNA was used for all samples within the LunaScript Supermix reaction. The number of virus genomes released was calculated via a standard curve created by DNA of JFH-1 and DBN3a extracted from WT viral plasmids, the number of DNA copies accounting for double stranded

DNA was calculated creating a standard curve used to quantify the number of viral genome copies per mL of supernatant.

2.2.27. Protein analysis

Proteomic analysis conducted utilising SGR stable cell lines or infectious virus; SGR; 72 h post seeding 2.2 x 10^6 cells in a 10 cm dish, in the presence of infectious HCV virus; either 72 h post-electroporation or post-infection. Virus infection was conducted after seeding 0.3 x 10^6 cells into a 6 well plate. At time of harvest, cells were washed with 1X PBS prior to scraping cells into a 1.5 mL Eppendorf and pelleting cells by centrifugation at 5000 RPM for 5 minutes. Cells were lysed with Glasgow Lysis buffer and long termed stored at -80 °C. Prior to conducting protein analysis, samples were centrifuged at 13,000 x G for 5 minutes to pellet cell debris and transferred to a clean Eppendorf.

2.2.27.1. Co-immunoprecipitation

Streptavidin sepharose suspension beads were primarily used to pulldown NS5A containing a twin streptavidin tag (TST). Beads were prepared by taking 100 µl of 50% Streptactin resin suspension (in sepharose), resuspended by inverting the vial 10 times. Beads were separated from resin via centrifugation for 5 minutes at 3000 x G in 4 °C (conditions of all centrifugation steps) and supernatant was removed. Beads were further washed in 500 µl wash buffer incubated on a rotator wheel for 5 minutes (all incubation steps completed on rotator wheel at 4 °C) prior to centrifugation. Beads were incubated with 500 µl lysis buffer and centrifuged prior to the addition of 500 µl cell lysate samples. Beads were incubated with samples overnight at 4 °C prior to removal of unbound protein via centrifugation. Beads were primarily washed with a high salt wash buffer prior to completing the wash steps another four times using the standard wash buffer. The beads were transferred to a fresh tube prior to centrifugation of the last wash step to remove the presence of unbound protein coating the

Eppendorf potentially contaminating the samples. The sample was eluted in 10% SDS prior to heating at 95 °C for 10 minutes to denature the proteins. A final centrifugation step was completed prior to transferring supernatant to a fresh 1.5 mL Eppendorf.

Co-immunoprecipitation utilising MagStrep "type 3" XT magnetic beads was initially conducted as per the manufacturers instructions. Optimisation of the protocol to reduce unbound protein was conducted following steps outlined within the protocol of sepharose suspension beads, in particular the addition of beads washed with lysis buffer prior to the addition of cell lysates, the addition of a high salt wash after incubation of cell lysates with the beads, and transferring beads to a fresh Eppendorf during the final wash step. All wash steps were conducted using the same volumes outlined in the sepharose suspension bead protocol. All samples were stored at -80 °C.

2.2.27.2. Western blotting analysis

5X Laemmli buffer was diluted into samples and protein was denatured by heating samples at 95 °C for 10 minutes prior to loading into a 12 % SDS- polyacrylamide gels prepared with 5 % stacking gel. Gels were assembled in a gel tank filled with running buffer. Polyacrylamide gel electrophoresis (PAGE) was conducted at 180 V until required protein resolution was achieved. Using a Trans-Blot Turbo (Bio-Rad) semi-dry trans-blotter, proteins were transferred on to a PVDF membrane by soaking thick filter paper in Towbin transfer solution and subjected to a constant voltage of 15 V for 30 minutes. Following transfer, membranes were blocked in LI-COR-TBS blocking buffer for a minimum of 40 minutes, rocking at room temperature. Primary antibody was diluted in LICOR-TBS blocking buffer diluted in TBS overnight at 4 °C. Prior to the addition of secondary antibody, membranes were washed in TBS-T for 5 minutes on a rocker at room temperature, three times. Secondary antibody was diluted in LICOR-TBS blocking buffer diluted in TBS for 40 minutes protected from the light at room

temperature on a rocker. Membranes were washed three times prior to drying membranes on clean filter before visualisation on the LICOR Odyssey Sa.

2.2.27.3. Mass-spectrometry analysis

Huh7 cells were electroporated as previously described and seeded into T175 flasks in addition to 100 μl of pooled electroporations seeded onto a 96 well plate. To reduce changes in host protein expression as a result of the presence of dead cells, media was changed 24 h post electroporation. To reduce changes in host protein expression if Huh7 cells overgrown, once cells reached 80% confluency all cells were harvested. Supernatant was collected from all flasks and cell lysates were collected as previously described. Cells within the 96 well plate were fixed and stained to confirm the presence of NS5A. Supernatant was collected and virus was titred by FFA to confirm the production of virus particles. Co-immunoprecipitation was conducted via MagStrep "type 3" XT magnetic beads using the optimised protocol as described.

Mass tandem tag proteomics was conducted by the Centre for Proteome Research (CPR) with the University of Liverpool. As per instructions sent by the CPR, all samples were eluted in 40 μl and quality checked for the presence of tagged protein, using 10 μl of eluted sample, prior to conduction of LC-MS/MS. Four technical repeats were performed for each experimental group (WT virus not containing a TST within NS5A, JFH-1 WT and DBN3a WT, and samples containing a TST within NS5A JFH-1 TST and DBN3a TST). TMT labelling of samples was conducted with the CPR facility prior to completion of the LC-MS/MS analysis conducted using the Ultimate 3000 RSLC™ nano-system (Thermo Scientific, Hemel Hempstead) coupled to a Q Exactive HF Quadrupole-Orbitrap™ mass spectrometer (Thermo Scientific). The sample was loaded onto the trapping column (Thermo Scientific, PepMap100, C18, 300 μm X 5 mm), using partial loop injection, for seven minutes at a flow rate of 4 μL/min with 0.1% (v/v) FA. The sample was resolved on the analytical column (Easy-Spray C18 75 μm x 500 mm 2 μm column) using a gradient of 96.2% A (0.1% formic acid) 3.8% B (79.95% acetonitrile, 19.95% water, 0.1% formic

acid) to 50% A 50% B over 90 minutes, in the 2-hour program at a flow rate of 300 nL min-1. The data-dependent program used for data acquisition consisted of a 60,000-resolution full-scan MS scan in the orbitrap (AGC set to 3e6 ions with a maximum fill time of 100ms). The 12 most abundant peaks per full scan were selected for HCD MS/MS (60,000 resolution, AGC set to 1e5 ions with a maximum fill time of 100 ms) with an ion selection window of 2 m/z and normalised collision energy of 30 %. Ion selection excluded singularly charged ions and ions with a greater than +6 charge state. To avoid repeated selection of peptides for fragmentation the program used a 60-second dynamic exclusion window.

Analysis of the LC-MS/MS data was initially performed using Proteome Discover 2.4 to ascertain labelling efficiency. Data were searched using Mascot against the human database (download from UniProt 05/03/23). Data were searched with dynamic modifications of Oxidation (M) and TMT label (N-term and K) and with the static modification of carbamidomethylation (C). The labelling of samples was assessed and recorded at 87% fully labelled. A further 10% of peptides have at least one site labelled. Therefore 97% of peptides have a TMT label. Proteome Discover 2.4.was used to integrate all the data for quantitative analysis. Data were searched using Mascot against the human database (download from UniProt 05/03/23) and the supplied fasta file containing proteins of interest. Data were searched with dynamic modifications of Oxidation (M) and TMT label (N-term and K) and with the static modification of carbamidomethylation (C).

Chapter 3. Utilising molecular tools to expose different HCV NS5A plasticity and functions in comparison to other HCV genotypes

3.1. Introduction

In a clinical setting, it has been well researched and practised for patients to receive different treatment depending on the HCV GT they have been infected with (Keikha et al., 2020; NHS, 2021). As discussed previously, this is due to different clinical manifestations and disease outcomes presented by each genotype. It is therefore important to study the molecular differences between the HCV GTs to better inform these treatments. It is believed NS5A may play a crucial role in driving disease pathology due to its multi-functional role. To investigate this further, and in direct relation to the primary aim of this thesis, insertion of a protein tag into the NS5A of both JFH-1 and DBN3a was performed. By directly comparing JFH-1 and DBN3a, clear distinctions can be drawn between the GTs due to the comparable virus propagation characteristics previously described by Ramirez *et al.* (2016) and an extensive amount of literature available based on JFH-1 research.

Domain III of NS5A is uncharacterised and removal of domain III or insertion by GFP has no significant effect on RNA replication (Appel et al., 2005; Moradpour et al., 2004). However, some functions have been ascribed to this domain. For example, Hughes *et al.* (2009) demonstrated that an insertion of 19 amino acid sequence near the C-terminus in all GT2 isolates enhances the rate of RNA replication and virus production. Contributing to the functional role of domain III, Appel *et al.* (2008) demonstrated that the C-terminus of domain III was a determinant for NS5A particle formation. By deleting various regions of domain III in the GT2a clone, NS5A co-localisation with the core protein can be disrupted, stopping particle formation and resulting in an accumulation of the core protein on the surface of lipid droplets (Figure 3.1). Therefore, as different regions of the domain play a role in the production of virions,

levels of virion fitness may vary depending on which part of the domain is disrupted which may impact pathogenesis, particularly as domain III is one of the more variable regions of the HCV genome (Appel et al., 2008).

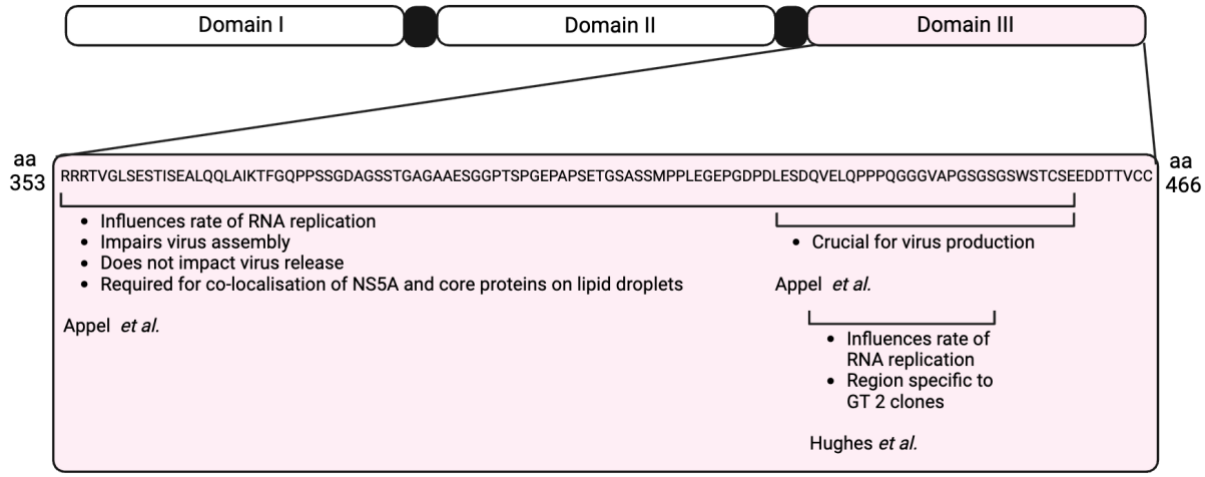

Figure 3.1 Summary of known NS5A domain III functions.

A diagram compiling the regions of domain III important for RNA replication, virus assembly and production, and co-localisation of NS5A and core protein on the surface of lipid droplets. Annotations; amino acid number of JFH-1 NS5A; aa. Information compiled from (Appel et al., 2008) and (Hughes et al., 2009).

Protein tags can have a multitude of applications. Depending on the tag inserted, they may confer increased stability and solubility characteristics to the protein; glutathione S-transferase (GST) can be used for one-step purification with glutathione protecting against proteolysis, small ubiquitin-related modifier (SUMO) helps the stability and folding of a protein, as does maltose-binding protein (MBP) that can also be inserted to help protein solubility (Butt et al., 2005; Freitas et al., 2022). As NS5A, in particular domain III is uncharacterised, fusing an affinity tag to the C terminus of domain III was determined to be least disruptive. Affinity tags tend to be small sequences of amino acids allowing detection, immunoprecipitation and purification of the fused protein. Such tags include FLAG, hemagglutinin antigen (HA) and streptavidin tags (ST). By inserting multiple copies of epitope tags, affinity can be increased which may optimise downstream analysis of the protein (Freitas et al., 2022; Keeble et al., 2019).

Fluorescence tags may be inserted as a direct method of subcellular localisation experiments however, are considerably larger than epitope tags. Regardless of the tag inserted, each tag also presents disadvantages; they may disrupt the function and structure of the protein, may need to be removed depending on downstream application, possible instability of the protein after tag removal, and larger tags may impose a heavy metabolic burden within the host cell (Bell et al., 2013).

This chapter introduces the differences between HCV GT2 and GT3, at both a genome replication and a virus propagation level using both the SGR and cell culture virus systems, JFH-1 and DBN3a, due to their ability to replicate well in cell culture. Protein plasticity is a general characterisation of a protein; the ability to alter the structural arrangement of a protein and potential protein interactions determined through the identification of tolerable insertion sites (Atwell et al., 1997). For example, by comparing the insertion of an epitope tag at corresponding aa sites within JFH-1 and DBN3a, it is possible to determine if NS5A plasticity is the same between HCV GTs. To explore possible differences of NS5A plasticity and function between GT2 and GT3, the insertion of an epitope tag and fluorescent tag into multiple sites of the C-terminus of domain III was conducted.

3.2. Results

3.2.1. Limitations of using the IncuCyte S3 to analyse fluorescent cells

Throughout this project, the IncuCyte S3 was used to visualise and quantify cell growth assays as well as to define HCV positive cells via fluorescence; direct live cell imaging or in-direct staining of cells with sheep anti-NS5A. It is important to note that, depending on the number of positive cells in a well or the entire plate, the IncuCyte may "over-expose" images to find fluorescent objects (Figure 3.2). This can occur predominantly when there is little to no fluorescence within the plate. Therefore, depending on the analysis parameters set by the user, false positives may obscure experiment results. As such, throughout this thesis only three analysis parameters are used for the counting of fluorescent cells (Table 3.1). In conjunction with using different parameters, when calculating the number of fluorescent positive cells, the number of objects counted in "mock" is subtracted, as they are deemed to be false positives or auto-fluorescent cells (a side effect of cell death). When quantifying cell growth, phase is calculated by defining the space free with no cells present. As no fluorescence is detected, over-exposure and risk of false positives is eliminated. Therefore, the same confluency parameter is used regardless of the number of fluorescent objects counted or well size used.

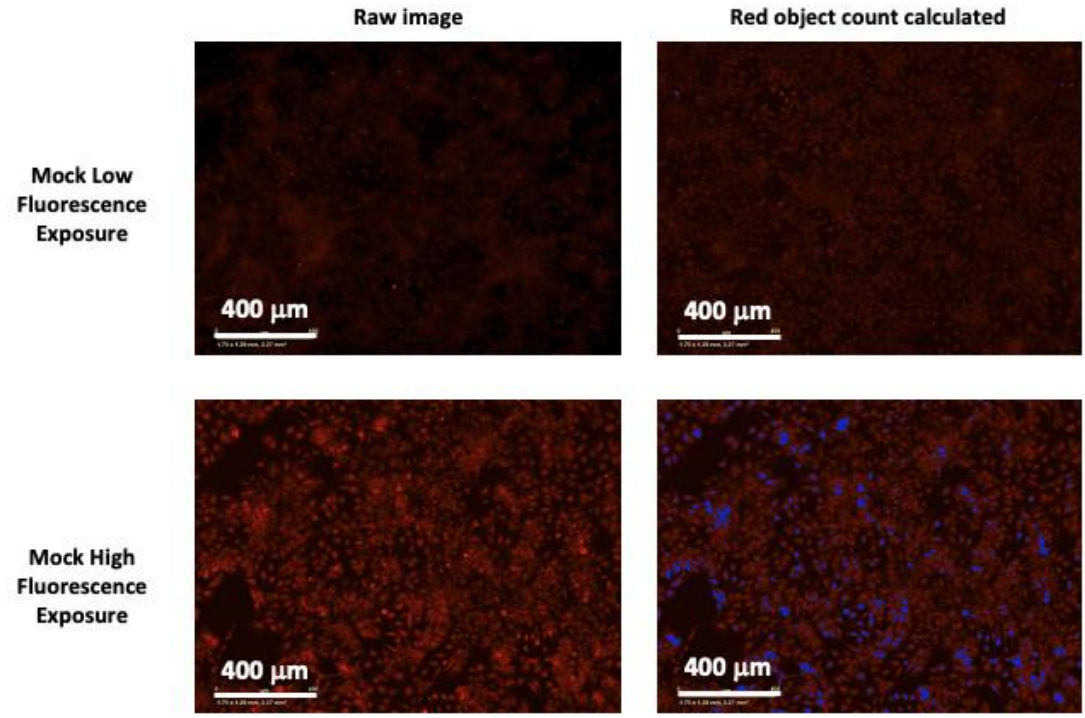

Figure 3.2 Autofluorescence of cells.

Shown is an example of mock images taken from an experiment using a 96 well plate with a low amount of surrounding fluorescence (NS5A not present in any well on plate) compared to an experiment with an adequate to high amount of surrounding fluorescence (NS5A present in multiple wells on plate). Red objects were determined using the general HCV analysis – refer to methods. Images were taken at 10 x magnification and scale bars = 400 microns.

Analysis Type	When analysis is used
General	Experiment contained lots of positive cells therefore fluorescent objects easily defined. Most used analysis type.
High background	There are not many or no fluorescent cells observed. Cells looked over-exposed defined by lots of positive cells within the mock control.
Large area	There are not many or no fluorescent cells observed in a larger well (>24 well in size). Parameters differ slightly from "high background" analysis.

Table 3.1 Rational of using different IncuCyte analysis parameters.

Refer to "Appendices: IncuCyte Parameters" for a breakdown of each analysis parameter.

3.2.2. Differences between JFH-1 and DBN3a virus production

An in depth, direct comparison of JFH-1 and DBN3a virus production has yet to be conducted. Deciphering key differences between JFH-1 and DBN3a cell culture propagated virus is important prior to conducting proteomic analysis and comparing virus infection in different cell culture models. The HCV cell culture infectious clones JFH-1 and DBN3a were used for the completion of *in vitro* experiments. Ramirez *et al.* (2018) states that JFH-1 and DBN3a have comparable replication and propagation characteristics. To confirm these characteristics with our own virus production protocol, either Huh7 cells or Huh7.5 cells were electroporated with RNA derived from each respective infectious clone. Supernatant was collected 72 and 144 h post electroporation (h.p.e). Virus titration via focus forming assay (FFA) was performed on Huh7.5 cells to calculate the number of infectious particles per millilitre (focus forming units (FFU)/mL) by staining cells with sheep anti-NS5A 48 h post infection (h.p.i). Virus titre was quantified using the IncuCyte S3 and red objects count from mock infection was subtracted from experiment group results (Figure 3.3 A). No significant differences were noted between the virus titre produced from Huh7 cells and Huh7.5 cells for both JFH-1 and DBN3a (Figure 3.3 B). However, when Huh7.5 cell supernatant was collected at both 72 and 144 h.p.e, DBN3a virus titres increased significantly at 144 h.p.e. (Figure 3.3 C). A trend of increasing virus titre was noted for JFH-1 however, was not statistically significant. This suggests that virus propagation of both JFH-1 and DBN3a is comparable when analysing the derivatives of Huh7 cell lines however, DBN3a is producing more infectious virus particles than JFH-1 at 144 h.p.e.

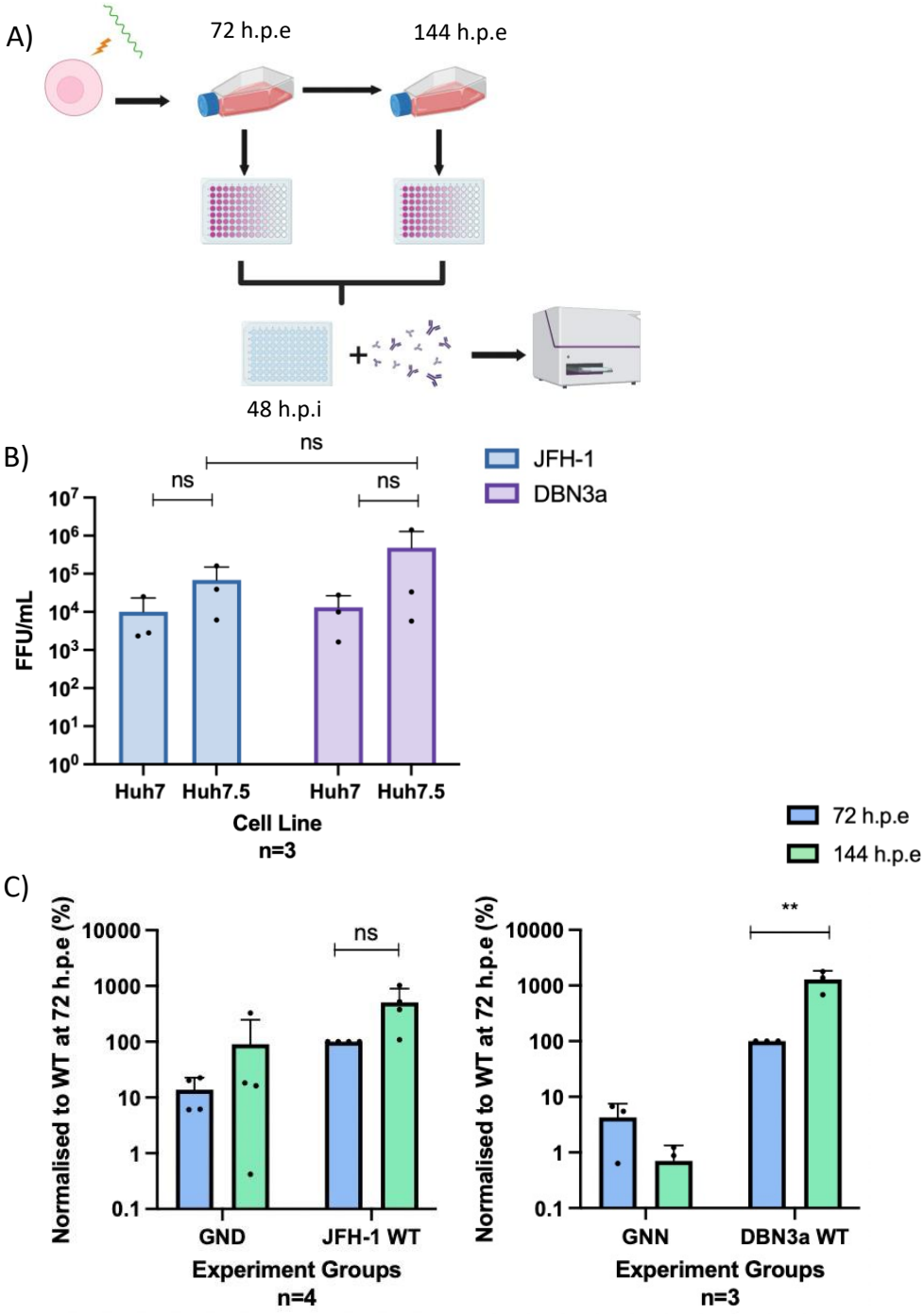

Figure 3.3 Characteristics of JFH-1 and DBN3a virus production.

A) Schematic of the virus production protocol. B) Both Huh7 cells and Huh7.5 cells were electroporated with either JFH-1 or DBN3a. C) Supernatants were harvested 72 h.p.e and the virus titre was calculated. Only Huh7.5 cells were used to produce virus. Supernatant was collected at 72 and 144 h.p.e and normalised to the FFU/mL calculated at 72 h.p.e. A mutation in the GDD amino acid sequence active site inactivation polymerase acts a replication negative control; JFH-1 – GND, DBN3a – GNN. Virus titre was normalised to the WT at 72 h.p.e. Data are presented as mean with standard deviation. Statistical significance was tested using one-way ANOVA with the Bonferroni's multiple comparison test, with a single pooled variance. P values; ns, P ≥0.05; **, P <0.005.

3.2.3. Differences between JFH-1 and DBN3a virus infection.

To further compare JFH-1 and DBN3a, infection efficiency of the two viruses was investigated. Huh7 cells were infected with either JFH-1 or DBN3a at an MOI of 0.2. At 72 h.p.i, cells were stained with sheep anti-NS5A and visualised using the IncuCyte S3 (Figure 3.4 A). Visualisation of infected Huh7 cells suggests possible differences between the two infectious clones by the localisation of NS5A. JFH-1 appears to flood the cytoplasm of the Huh7 cell. Contrary to DBN3a, which appears to be less universal in the cytoplasm with a speckled effect. This observation has previously been described in Ward *et. al.* (2020). In addition, the number of cells infected by JFH-1 appears less than the number of cells infected by DBN3a at 72 h.p.i despite using the same MOI. Quantitative analysis of the infection was performed (Figure 3.4 B), revealing a significant difference in the number of cells infected by DBN3a. The amount of NS5A within a cell can be quantified by averaging the red intensity of all infected cells, noted as the red calibrated unit (RCU). Results suggest that despite JFH-1 not infecting as many cells as DBN3a, there appears to be a greater accumulation of NS5A within JFH-1 infected cells (Figure 3.4 C), corroborating the differences seen in Figure 3.4 A. These results suggest that there is a possible difference in NS5A localisation and accumulation in Huh7 cells during JFH-1 and DBN3a infection. Despite JFH-1 not infecting as many cells during the 72 h time course, there is a greater accumulation of NS5A resulting in a higher RCU per infected cell.

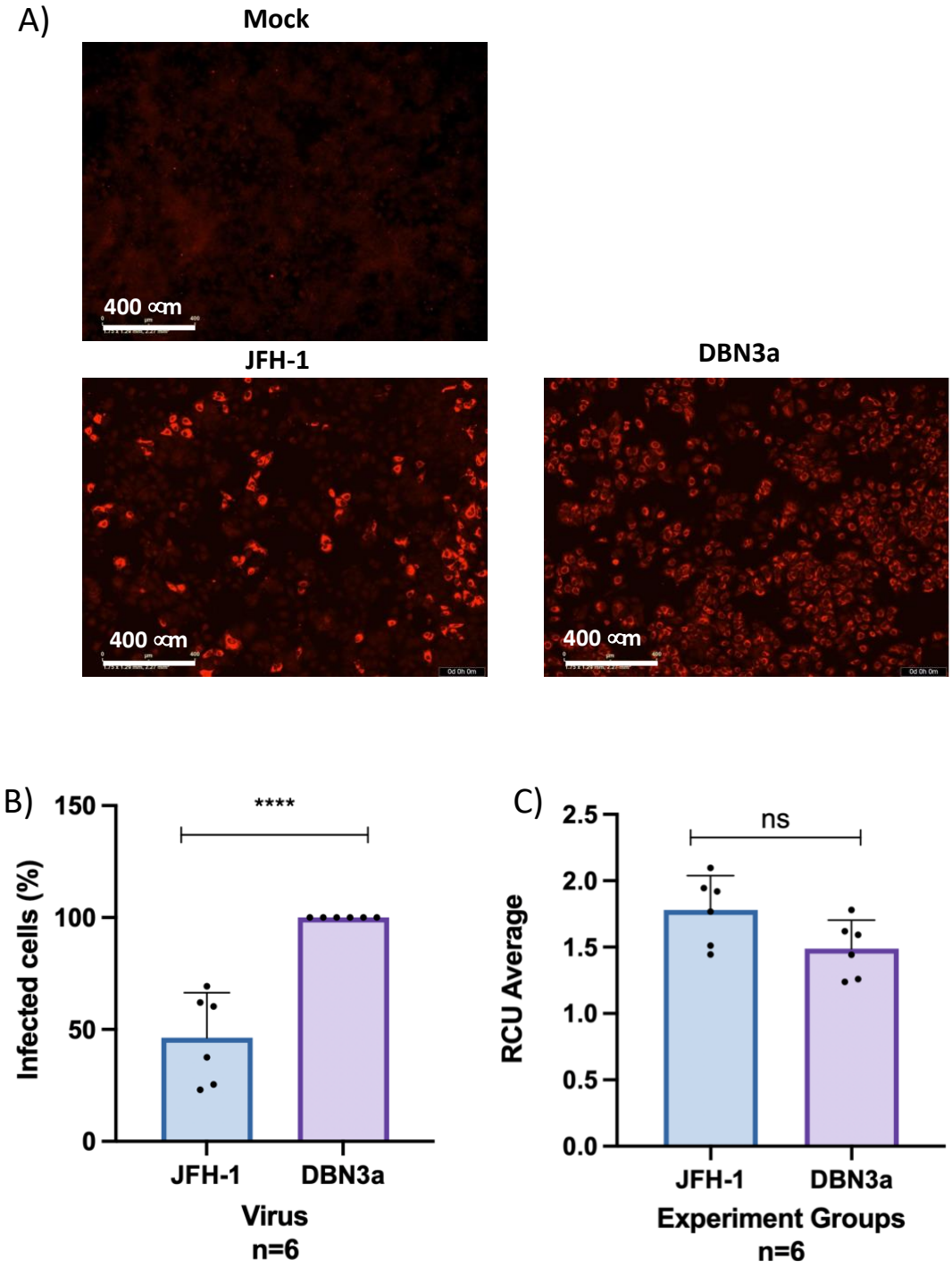

Figure 3.4 Comparison of JFH-1 and DBN3a virus infection.

A) Representative images of sheep anti-NS5A staining 72 h.p.i. Images acquired on the IncuCyte S3, taken at 10 x magnification and scale bars = 400 microns. B) Percentage of infected cells. Quantification of the numbers of Huh7 cells infected by either JFH-1 or DBN3a normalised to the number of cells infected by DBN3a. C) Quantification of the mean object intensity red calibrated unit (RCU) of each NS5A positive cell. Data are presented as mean with standard deviation. Statistical significance was tested using unpaired t test assuming both populations have the same standard deviation. P values; ns, P ≥0.05; ****, P <0.00005.

3.2.4. Evaluation of particle: infectivity ratios for JFH-1 and DBN3a

To investigate the discrepancy between the number of Huh7 cells infected by JFH-1 and DBN3a, despite infecting using the same MOI, two virus quantification methods were evaluated for JFH-1 and DBN3a virus produced in Huh7 and Huh7.5 cells. Both cell lines were electroporated with the respective full infectious virus genome. Supernatant was collected 72 h.p.e. The specific infectivity of each virus was calculated; defined as the ratio between the number of infectious viruses, measured in FFAs, and the total amount of viral RNA, determined by quantitative RT-PCR (Figure 3.5 A). FFA provides quantification of the number of infectious virions produced; the number of virions deemed to be successful at infecting naïve cells, described as the "functional titre". RT-qPCR was performed after extraction of RNA in the supernatant using a primer set specific for the virus 5'UTR. By calculating the number of virus genomes in the supernatant by RT-qPCR, the total number of virions produced by either the Huh7 or Huh7.5 cells can be calculated, described as the "physical titre". Results suggest there is a significant difference between the number of JFH-1 virions released into the supernatant when produced in Huh7.5 cells, this difference is a greater during the production of DBN3a (Figure 3 B). However, despite a comparable trend, there is no significance between the number of virus particles produced and infectious virions when virus is produced in Huh7 cells (Figure 3.5 C). A ratio between the number of virus particles released and infectious virions during virus production shows no significance between JFH-1 and DBN3a for both Huh7.5 cells (Figure 3.5 D) and Huh7 cells (Figure 3.5 E) producing virus. For both viruses, there is roughly 1 viable virion for every 10,000 virus particles produced. Results suggest that despite DBN3a releasing a larger amount of virus particles than JFH-1, both viruses produce a large amount of non-infectious virions. Results demonstrate no differences in the ratio of physical and functional virus titres of JFH-1 and DBN3a.

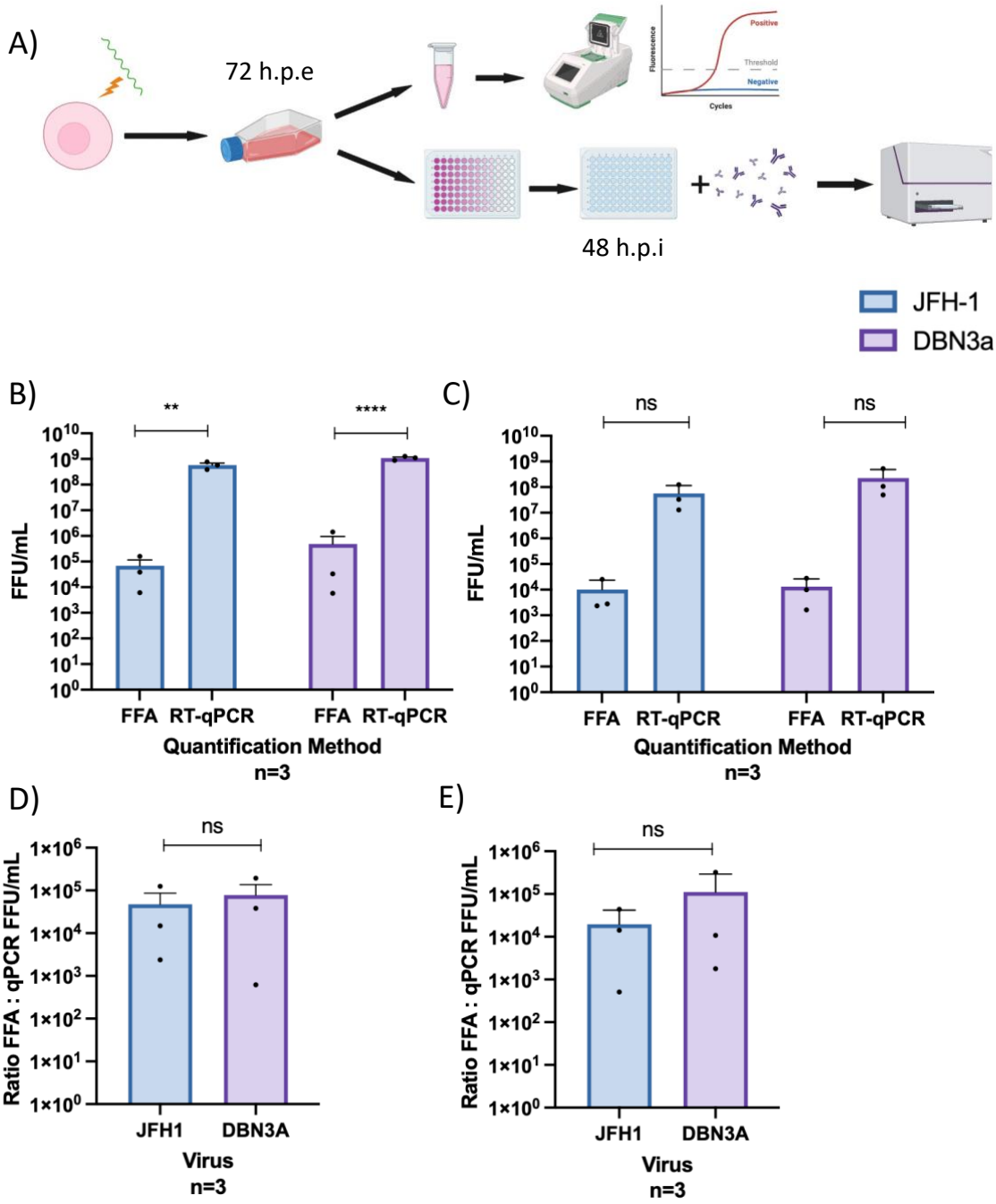

Figure 3.5 Quantification of the production of viable virus particles.

A) Schematic of virus quantification methods. The concentration of virus produced by B) Huh7.5 cells or C) Huh7 cells determined by RT-qPCR or by FFA. Ratio determined between the number of virus particles detected by RT-qPCR and by FFA D) Huh7.5 cells and E) Huh7 cells. Data are presented as mean with standard deviation. Statistical significance was tested using unpaired t test, assuming both populations have the same standard deviation, if only one condition was compared. If multiple conditions were compared statistical significance was tested by one-way ANOVA with the Bonferroni's multiple comparison test, with a single pooled variance. P values; ns, P ≥0.05; **, P <0.005; ****, P <0.00005.

3.2.5. Temporal analysis of DBN3a and JFH-1 infection kinetics

One explanation for the more efficient infection exhibited by DBN3a could be that this virus established a productive infection more rapidly than JFH-1. To test this, a time course evaluating the number of cells infected and the number of virions produced was conducted. Huh7 cells were infected with either JFH-1 or DBN3a (MOI=0.2). Media was changed 4 h.p.i to remove the inoculum. At each timepoint, Huh7 cells were directly stained with sheep anti-NS5A and visualised by the IncuCyte S3 to determine the number of virus infected cells and supernatant was collected to perform a virus titration via FFA on Huh7.5 cells to detect the number of virus particles produced during each time point. Red objects count from mock infection was subtracted from experiment group results (Figure 3.6 A). Results suggest that the first round of virus replication, 4 h.p.i, the number of cells infected is not significantly different between JFH-1 and DBN3a virus. There is a general trend of the number of DBN3a infected cells increasing between 8, 24 and 48 h.p.i in comparison to JFH-1 infected cells. The number of cells infected by JFH-1 compared to DBN3a only becomes significantly different at 72 h.p.i. The significant increase in the number of DBN3a virus positive cells between 48 and 72 h.p.i is not comparable to JFH-1 infection and was found to be non-significant (Figure 3.6 B). Despite the difference in the number of cells infected by JFH-1 and DBN3a at 72 h.p.i, the amount of NS5A present within an infected cell, calculated by the average RCU of all positive cells, suggests a larger amount of NS5A in JFH-1 infected cells than DBN3a at the later timepoints; 48 and 72 h.p.i (Figure 3.6 B). To determine if the possible accumulation of NS5A by JFH-1 is linked to the number of virions released, the virus titre produced at each time point was calculated (Figure 3.6 C). Results suggest that the amount of DBN3a virus produced at 72 h.p.i is higher than the amount of virus produced by JFH-1. This data further supports the hypothesis that differences between the number of cells infected by JFH-1 and DBN3a at 72 h.p.i are not due to a significantly higher number of cells infected by DBN3a during the first round of virus infection. These results suggest DBN3a has greater efficiency producing virus particles than JFH-1,

resulting in a greater number of cells infected at 72 h.p.i for DBN3a than JFH-1. Virus production efficiency between the two cell culture virus clones has not been previously defined. Investigating the difference of HCV genome replication dependent on HCV GTs may have clinical implications altering treatment outcome during human infection.

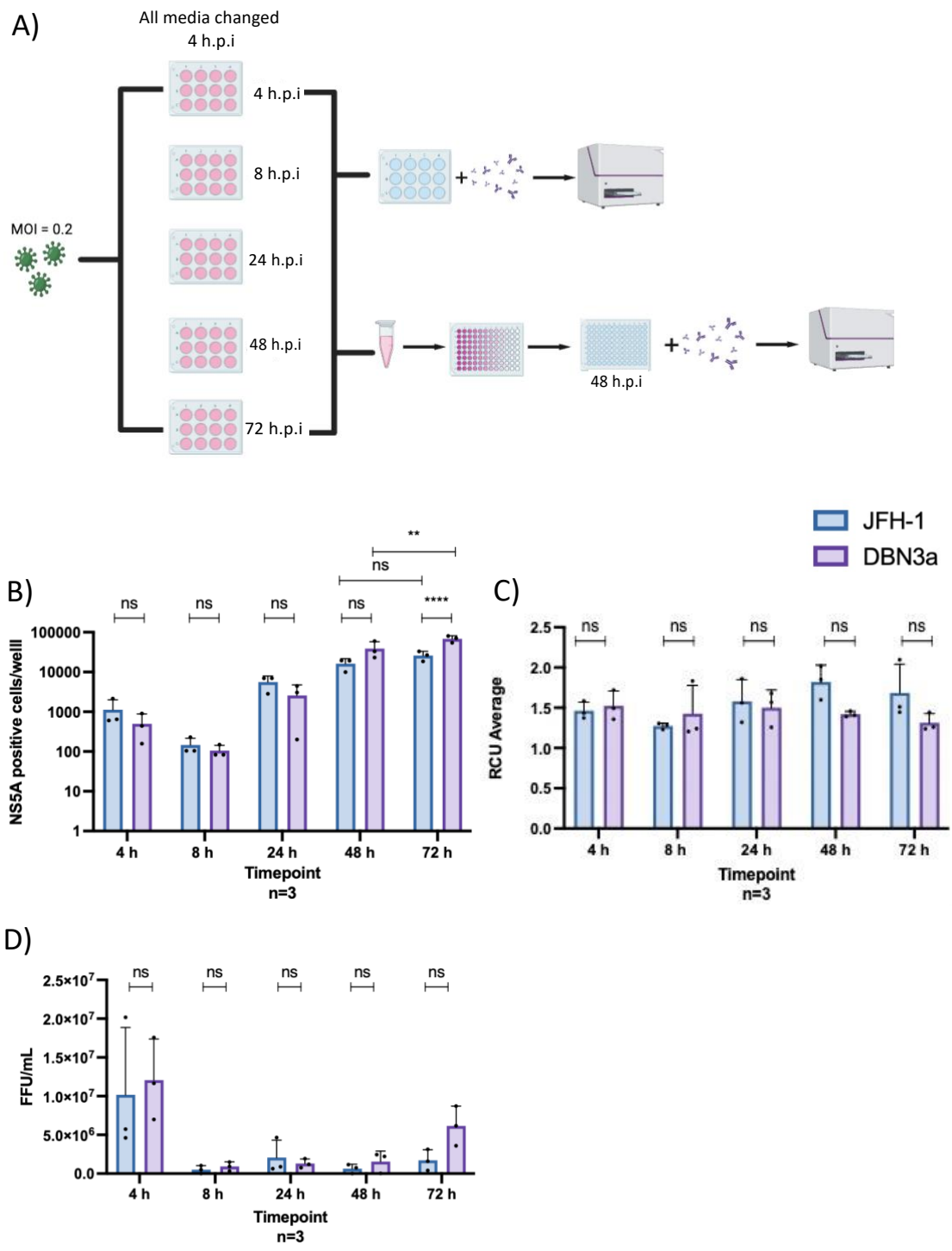

Figure 3.6 Assessing HCV monolayer infection.

A) Schematic of virus infection and sample collection. B) The number of Huh7 cells infected by JFH-1 or DBN3a. C) Quantification of the mean object intensity red calibrated unit (RCU) of each NS5A positive cell. D) FFU/mL calculated for the supernatant collected at each timepoint. Data are presented as mean with standard deviation. Statistical significance was tested by one-way ANOVA with the Bonferroni's multiple comparison test, with a single pooled variance. P values; ns, P ≥0.05; **, P <0.005; ****, P <0.00005.

3.2.6. Comparison of the genetic plasticity of NS5A domain III between JFH and DBN3a

The second objective of this chapter was to facilitate future research into GT3 NS5A function through the insertion of a TST epitope tag. This was conducted by assessing various insertion sites to give a greater understanding of permissive and flexible cloning sites which can be utilised for further genetic modification of NS5A. Furthermore, it was intended to use the TST to facilitate the identification of potential NS5A binding partners through an immunoprecipitation and mass spectrometry approach, as previously performed for GT2a (Goonawardane et al., 2017). Furthermore, the TST tag was chosen as the presence of two epitopes increases the affinity of antibody binding and has previously been inserted into a range of viruses; such as RNA virus; SARS-CoV-2 (Demone et al., 2022), DNA virus; varicella zoster virus (González-Motos et al., 2017)and, retrovirus; HIV (Ananthaswamy et al., 2019). NS5A protein tags already exist in other HCV GT for both SGRs and cell culture infectious clones (Goonawardane et al., 2017; McCormick et al., 2006; Ross-Thriepland et al., 2015) (Figure 3.7 B).To directly compare between GT3 and other HCV GTs, three sites tested in DBN3a directly correlate to these previously used sites within other GTS. In addition, a novel site is located at the furthest possible point of domain III within the C terminus, without interfering with the proteolytic cleavage site between NS5A and NS5B, to further reduce the risk of altering protein function (Figure 3.7).

A)

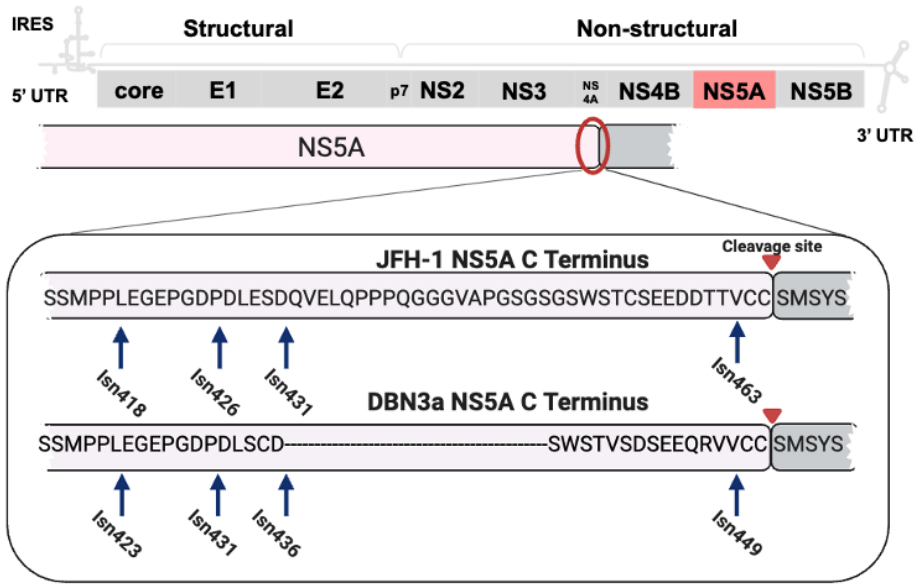

B)

Genotype	Author	Tag	Site in JFH1 (NS5A AA)	Site in DBN3A (NS5A AA)
FK5.1 (GT1)	McCormick *et al.* (2006)	PSTCD	Isn418	Isn423
JFH1 (GT2)	Goonawardane *et al.* (2017)	TST	Isn426	Isn431
JFH1 (GT2)	Ross-Thriepland *et al.* (2015)	SNAP	Isn431	Isn436
DBN3A (GT3)	Novel	TST	Isn463	Isn449

Figure 3.7 JFH-1 and DBN3a susceptible insertion sites.

A) Diagram representing the corresponding insertion sites (Isn) of JFH-1 and DBN3a NS5A insertion sites B) Table depicting insertion sites used to tag NS5A in other HCV GTs. Insertion sites are noted by the amino acid location in reference to the synthetic construct clones of JFH-1 (GenBank: KY427259.1) and DBN3a (GenBank: KX280714.2).

All of the sites tested in DBN3a were also tested in JFH-1. Initially, the insertion of the TST sites were tested in the SGR system (SGR), a system used to isolate and assess RNA replication in a containment level 2 environment. Huh 7.5 cells were transfected with 2 ug of in vitro transcribed SGR RNA for JFH-1 or DBN3a containing a luciferase reporter. Replication was measured by the firefly luciferase reporter by relative light units (RLU) at various time points post electroporation; 4, 24 48 and 72 h.p.e (Figure 3.8 A). As expected, all sites tested in JFH-1 were tolerable to the insertion of TST with no significant changes to RNA replication when compared to the wild-type (WT) clone (Figure 3.8 B). However, the C terminal site within DBN3a appeared to be the site of highest tolerance, allowing efficient RNA replication with a 1.6-fold increase of RNA replication in comparison to WT at 72 h.p.e. Sites further upstream performed poorly, with RLU at 72 h.p.e accounting for less than 12% of WT RNA replication (Isn423 – 7%, Isn431 – 1% and Isn436- 12%) (Figure 3.8 C). If the function and plasticity of NS5A in DBN3a is the same as JFH-1, the sites which tolerated in JFH-1 should also be tolerated in in DBN3a. However, only the C terminus insertion site within DBN3a allowed RNA replication. Therefore, results suggest the plasticity of NS5A domain III differs between HCV infectious cell culture clones, JFH-1 and DBN3a.

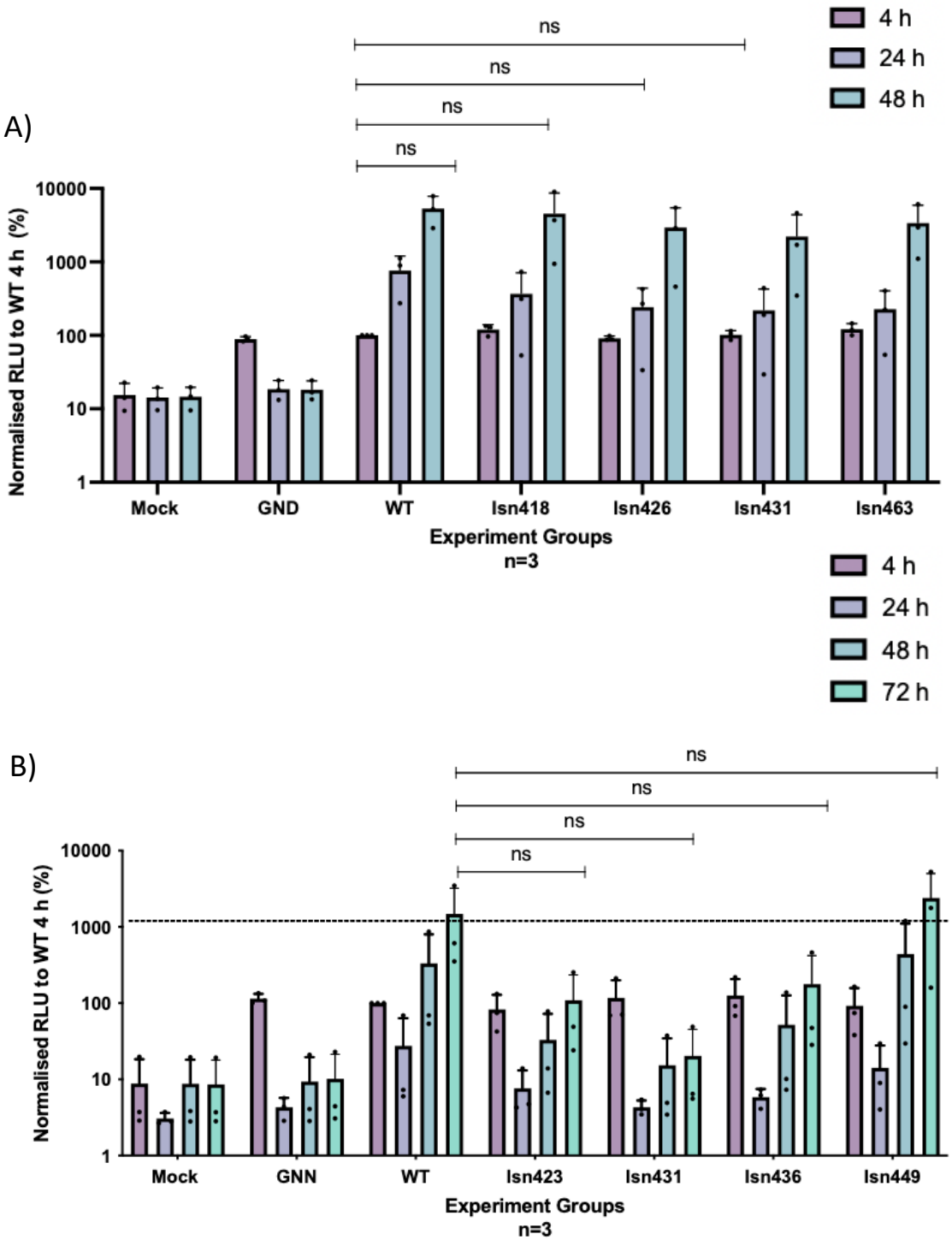

Figure 3.8 Testing tolerable insertion sites of TST in the SGR of JFH-1 and DBN3a.

SGR replication of A) JFH-1 and B) DBN3a analysed by luciferase assay. Data presented as mean with standard deviation. Statistical significance was tested by one-way ANOVA with the Bonferroni's multiple comparison test, with a single pooled variance. P values; ns, P ≥0.05.

RNA replication results suggest that all insertion sites in JFH-1 should be tolerated in the virus clone and furthest downstream insertion site will allow the production of viable virus for DBN3a. The ultimate aim of this approach was to develop infectious DBN3a clones containing TST tags. To this end, the TST tag was inserted into all four sites within NS5A domain III for both the JFH-1 and DBN3a infectious clones. After electroporation of *in vitro* transcribed RNA into Huh7.5 cells, virus titration via FFA was performed on naïve Huh7.5 cells to calculate the virus titre (FFU/mL) as described previously (Figure 3.9 A). An insertion site was deemed tolerable if infectious virions were produced. Despite all insertion sites being tolerated within the SGR of JFH-1, only the upstream insertion sites were tolerated with a general decline in virus titres as the TST was inserted closer to the C terminus in comparison to WT; Isn418 – 37%, Isn426 – 32%, Isn431 – 16% and Isn436 – 1% (Figure 3.9 B). Interestingly, the opposite results was observed for DBN3a, the sites inserted closer to the C terminus of NS5A are most tolerable to the presence of the TST in comparison to WT virus titre; Isn423 - <1%, Isn431 - <1%, Isn436 – 20%, Isn449 – 60% (Figure 3.9 C). Results suggest that the tolerated sites for the insertion of an epitope tag within the SGR can be suggestive of potential tolerable sites in the infectious virus however, not fully representative. In addition, the tolerated sites vary between JFH-1 and DBN3a, alluding to the idea that NS5A, in particular domain III, plasticity and potential the function varies between the GTs.

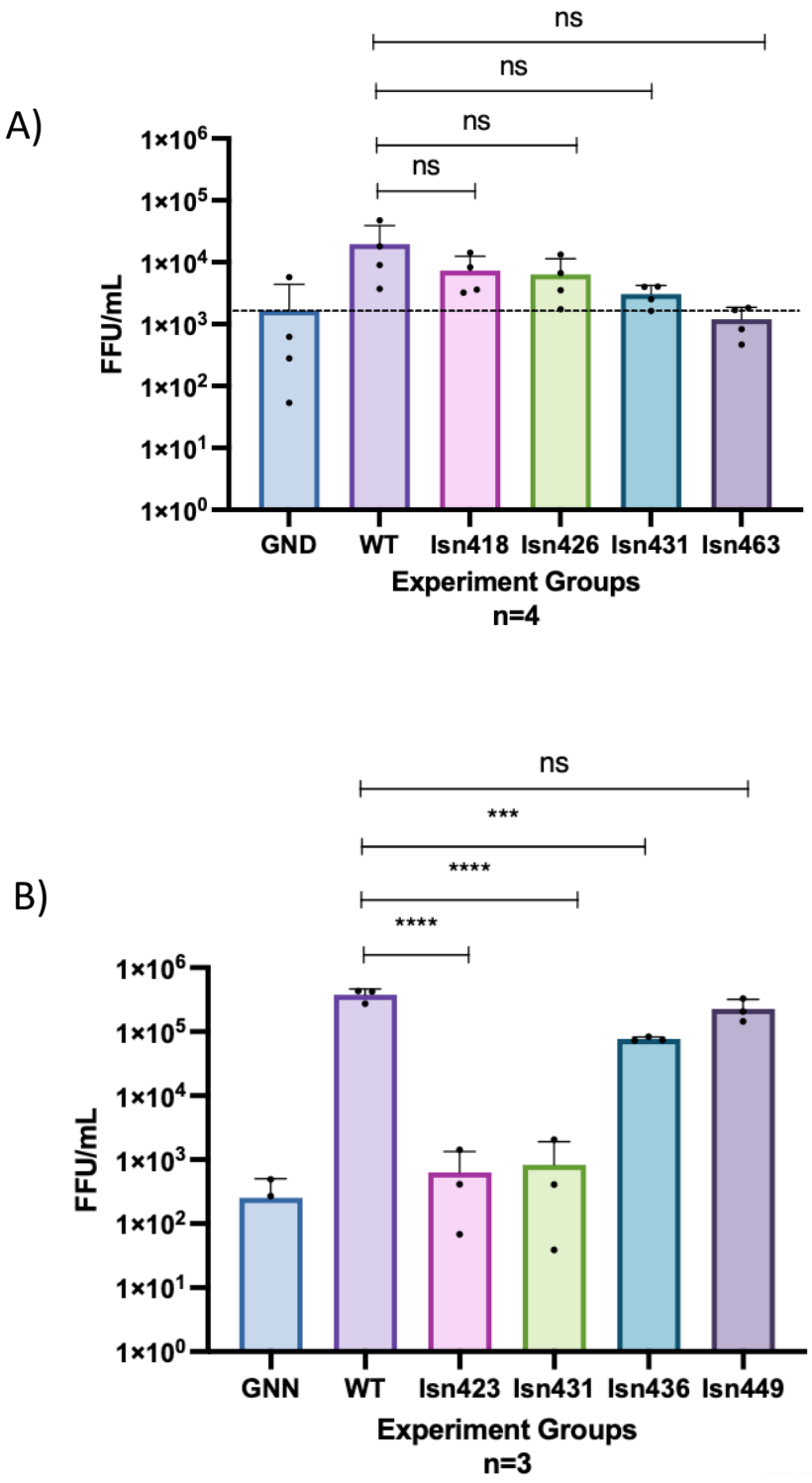

Figure 3.9 Testing tolerable insertion sites of TST in the C terminus of NS5A domain III for JFH-1 and DBN3a.

Virus titre of A) JFH-1 and B) DBN3a collected at 144 h.p.e. Data are presented as mean with standard deviation. Statistical significance was tested by one-way ANOVA with the Bonferroni's multiple comparison test, with a single pooled variance. P values; ns, P ≥0.05; ***, P <0.0005; ****, P <0.00005.

To further analyse potential differences in the functions of NS5A between JFH-1 and DBN3a, cell lines stably expressing SGRs were established. The SGR of both JFH-1 and DBN3a containing the TST inserted into the most tolerated sites were chosen to be maintained in Huh7 cells (Figure 3.10 A). To allow for selection and maintenance of SGR harbouring cells, a neomycin phosphotransferase (NPT) gene was cloned in place of the luciferase reporter. In order to provide a functional HCV internal ribosome entry site (IRES), the coding sequence for the first 12 amino acids of the Core protein (Δ-Core) (Shimoike et al., 2006) was cloned in frame at the 5' end of NPT (Figure 3.10 B). Confirmation of the established stable cell line was completed by western blot analysis. Presence of the TST fused to NS5A can be confirmed by the molecular weight of the protein, 56-58 kDa depending on the phosphorylation status of NS5A. Additionally, scanning the membrane at 700 nm and 800 nm wavelength, displays the NS5A (green) and TST (red) at the same apparent molecular weight (Figure 3.10 C). Further confirmation that the stable cell line containing the TST can be used for NS5A purification, performed by co-immunoprecipitation using streptavidin sepharose suspension beads and analysed by western blot (Figure 3.10 D). A weak NS5A band is present in the elution of the JFH-1 pull down, suggesting a low amount of NS5A is present in the final elution in comparison to DBN3a where a strong NS5A band is present.

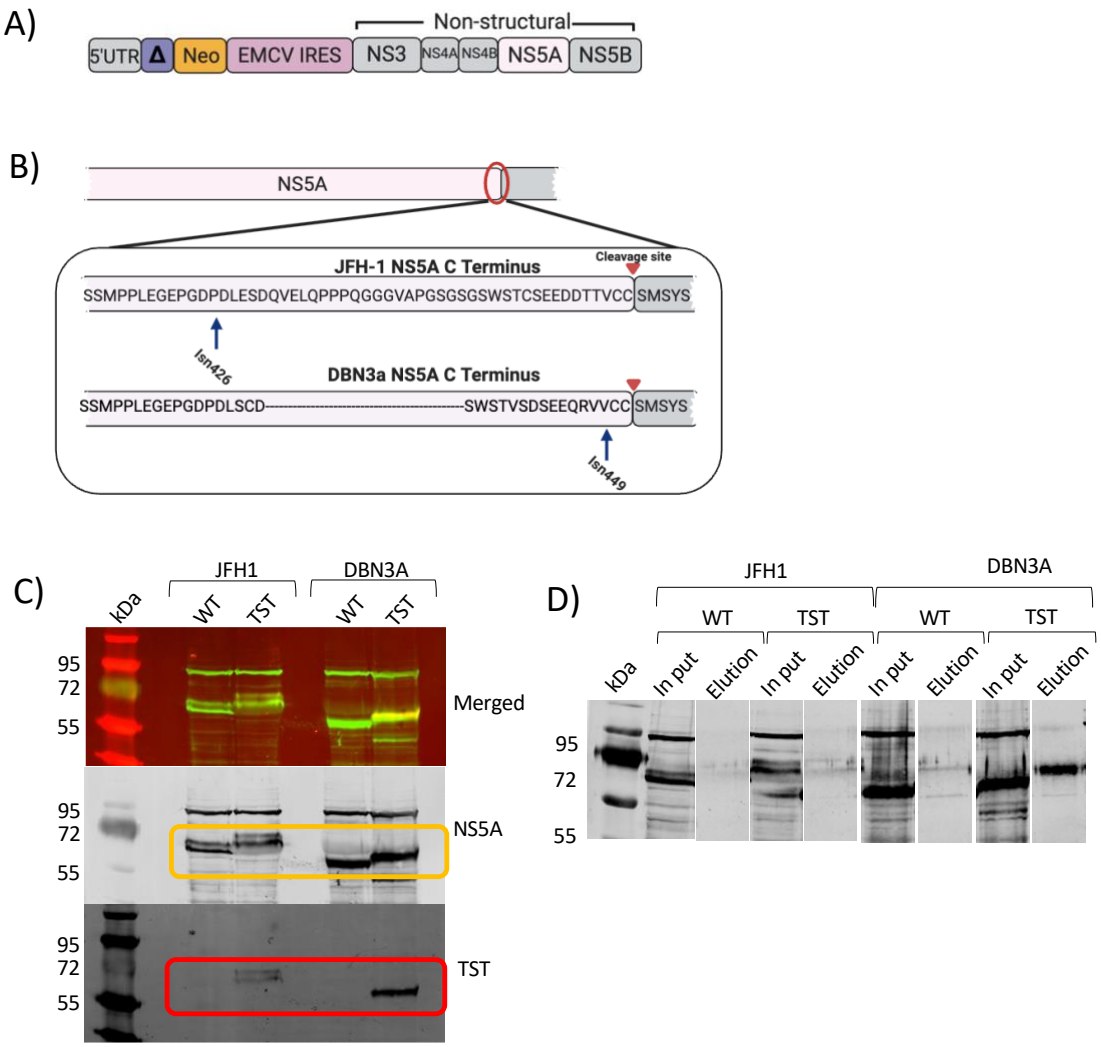

Figure 3.10 Establishment of TST SGR stable cell line.

A) Diagram outlining the SGR structure containing the neomycin resistance gene. B) Diagram representing the corresponding twin streptavidin tag (TST) insertion sites in the NS5A C terminus of JFH-1 and DBN3a. Insertion sites are noted by the amino acid location in reference to the synthetic construct clones of JFH-1 (GenBank: KY427259.1) and DBN3a (GenBank: KX280714.2). C) Confirmation western blot of HCV NS5A and TST fusion. D) Confirmation blot of HCV NS5A pull down by presence of TST using streptavidin sepharose suspension beads.

3.2.7. Insertion of eGFP into the novel C terminal site of NS5A within the DBN3a SGR

As the insertion of the TST within DBN3a at insertion site Isn449 was tolerated allowing RNA replication and the production of infectious virus progeny, the insertion of eGFP was investigated. eGFP constructs would be useful for functional analysis of NS5A by conventional and newly developed super-resolution imaging technologies. As fluorescent proteins have previously been inserted into JFH-1 (Isn418 and Isn426 (Ross-Thriepland et al., 2015; Sahuc et al., 2019)) and have proven to be tolerated allowing efficient RNA replication, this was performed in the SGR as previous data suggests if an insertion is not tolerated within the SGR, it is unlikely to be tolerated in the viral genome. As performed previously, eGFP was inserted into the SGR containing the firefly reporter gene upstream of the non-structural HCV proteins to test RNA replication (Figure 3.11 A). Huh7.5 cells were transfected with 2 μg of *in vitro* transcribed RNA. SGR replication was measured by the firefly luciferase reporter and relative light units (RLU) at various time points post electroporation; 4, 24, 48 and 72 h.p.e (Figure 3.11 B). Both eGFP alone (Figure 3.11 C), and eGFP flanked by linkers (Figure 3.11 D), was inserted into all four previously tested sites. This was investigated to determine if previously deemed "non-tolerated" sites would be more susceptible and experience less disrupted RNA replication when a larger gene is inserted in comparison to insertion at the C terminus site proximal to the NS5A-NS5B cleavage site. Regardless of the presence or absence of linkers, none of the tested sites tolerated the insertion of eGFP. Experiments focussed on the insertion of a fluorescent gene into site Isn449 due to previous toleration shown in the presence of the TST, unlike the other three upstream sites. To increase the stability of the eGFP and potentially increase the translation initiation of the gene, a start codon was placed in front of the eGFP. As such, an eGFP was fused without linkers and a start codon was inserted at the start of eGFP sequence to test the cloning strategy. Regardless of the addition of the start codon, RNA replication was not observed (Figure 3.11 E). To determine if the form of GFP was inhibiting RNA replication, by

eGFP inducing a cytotoxic environment, a humanised renilla (hr) form of GFP was inserted (Figure 3.11 F). HrGFP originated and optimised from sea pansy *Renilla reniformis*, unlike eGFP which was optimised and derived from the jellyfish *Aequorea victoria* (Lengler et al., 2005). Results suggest, independent of the type of GFP inserted, Isn449 cannot tolerate the insertion of eGFP and hrGFP. For all cloning techniques conducted, RLU expression was observed 4 h.p.e. This relates in direct translation of the RNA suggesting all cloning strategies did not introduce a detrimental fault inhibiting translation. As such, these results suggest the insertion site Isn449 cannot tolerate as large an insertion as GFP in comparison to the toleration observed with the insertion of TST.

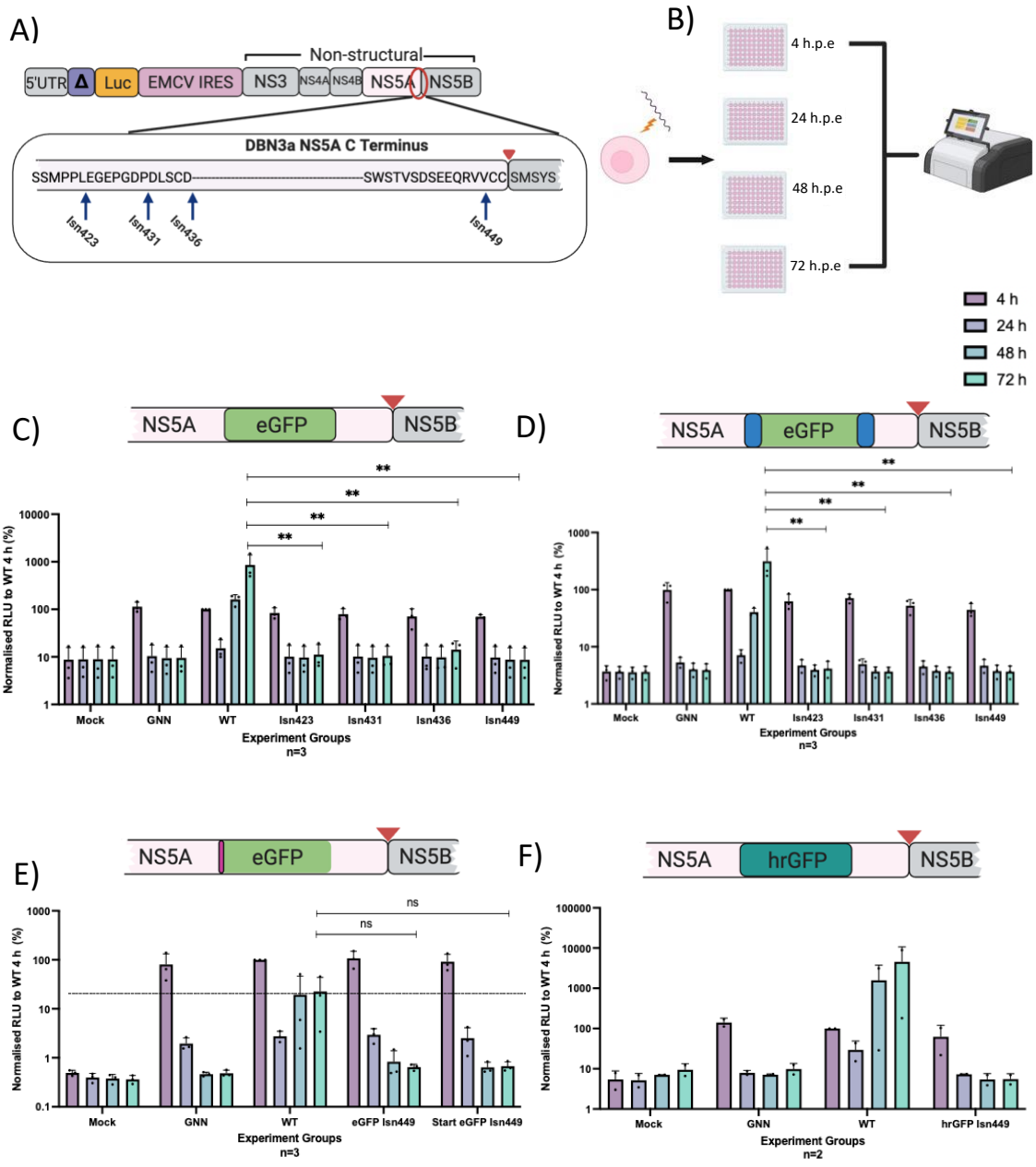

Figure 3.11 Assessing insertion of GFP into the SGR DBN3a.

A) Diagram outlining the SGR genome containing the firefly luciferase gene and fluorescent protein insertion sites. Insertion sites are noted by the amino acid location in reference to the synthetic construct clones of DBN3a (GenBank: KX280714.2). B) Schematic of the SGR replication assay. Luciferase assay was conducted on different SGR constructs; C) eGFP inserted into all four sites of interest, D) eGFP flanked by linkers inserted into all four sites of interest, E) inserted eGFP into site Isn449 either with or without a methionine at the start of eGFP and F) hrGFP inserted only into site Isn449. Data are presented as mean with standard deviation. Statistical significance was tested by one-way ANOVA with the Bonferroni's multiple comparison test, with a single pooled variance. P values; ns, P ≥0.05; **, P <0.005.

3.2.8. Insertion of a large fluorescent protein tag (eGFP) into the novel C terminal site of NS5A within the JFH-1 SGR

As the insertion of the TST was well tolerated in all sites within SGR JFH-1, specifically the furthest downstream site proximal to the C terminus, it was of interest to compare our DBN3a SGR results to determine whether a larger gene insertion was compatible with genome replication and therefore, GT specific. Focus was placed on the insertion of eGFP at amino acid location Isn463. As all previous insertions of fluorescent proteins with JFH-1 were flanked by linkers to provide flexibility (McCormick et al., 2006; Ross-Thriepland et al., 2015; Schaller et al., 2007), eGFP was cloned with flanking linkers into Isn463 of the SGR containing the luciferase reporter upstream of the HCV non-structural proteins. (Figure 3.12 A). To analyse RNA replication, Huh7.5 cells were transfected with 2 ug of *in vitro* transcribed RNA, followed by assessment of luciferase and eGFP expression. SGR replication was measured by the firefly luciferase reporter relative light units (RLU) at various time points post electroporation; 4, 24, 48 and 72 h.p.e, and eGFP expression was analysed for 72 h.p.e by visualisation using the IncuCyte S3 (Figure 3.12 B). Typically, the SGR JFH-1 peak replication is reached at 48 h.p.e however, as I inserted a large gene, I was cautious the RNA replication time may be delayed. Thus, the time course was completed to 72 h.p.e. Initial results suggested the NS5A-eGFP containing SGR was not replicating as no eGFP expression could be detected (Figure 3.12 B). To further confirm these results, the plate visualised for eGFP was stained for NS5A (Figure 3.12 C) as well as performing a luciferase assay to indirectly measure SGR RNA replication (Figure 3.12 D). Luciferase assay was not performed on the eGFP positive control plasmid as it did not contain a luciferase reporter. These results suggest that despite the Isn463 site being tolerant to the presence of TST, the length and structure of the insertion may play a role in amino acid site susceptibility to insertions.

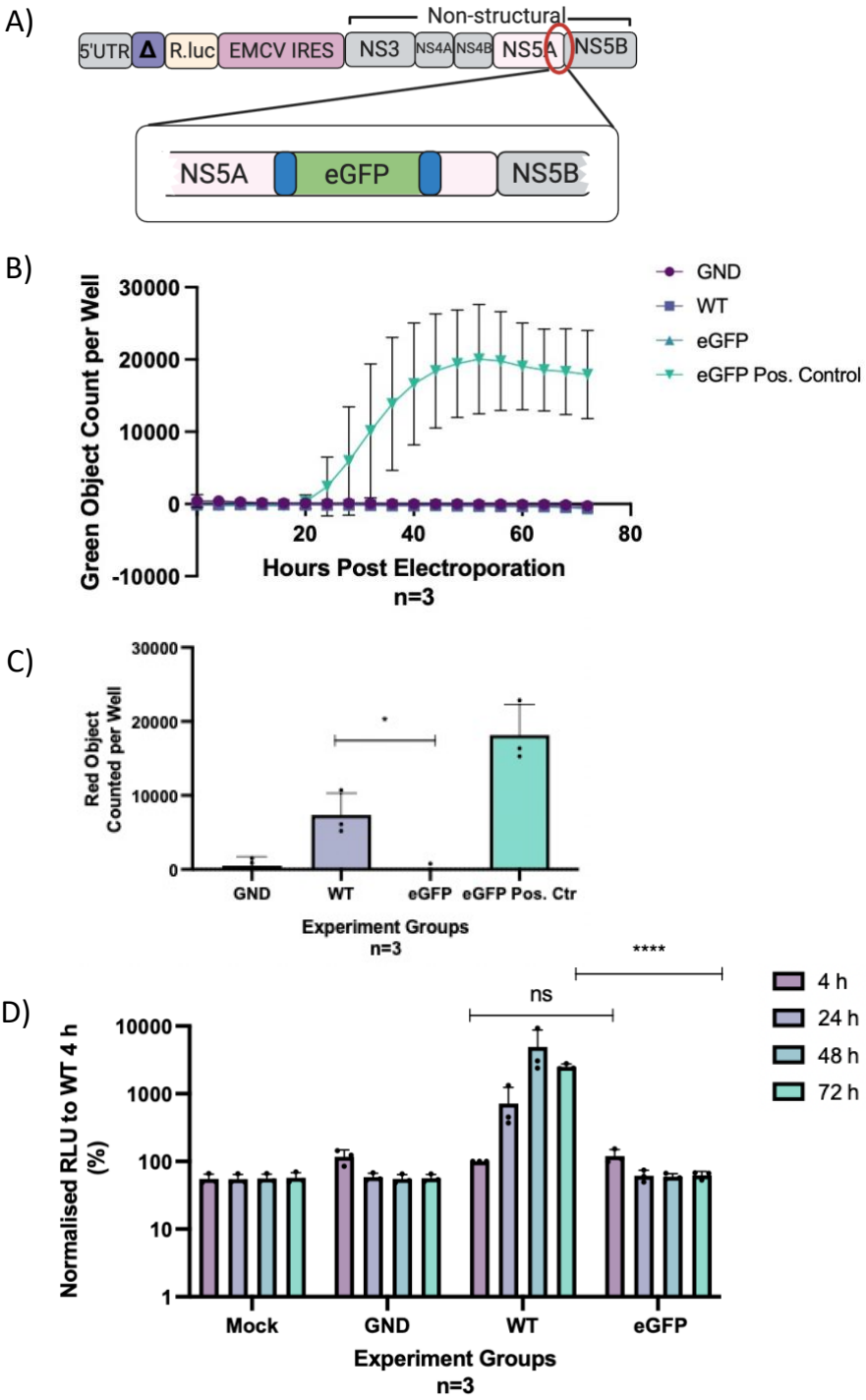

Figure 3.12 Assessing insertion of linker eGFP into the SGR JFH-1.

A) Diagram outlining the SGR genome containing the firefly luciferase gene and eGFP insertion flanked by linkers on either side. B) Time course of eGFP expression after electroporation. C) The cells visualised for eGFP were stained with sheep anti-NS5A to determine the number of cells with successful SGR replication 72 h.p.e. Red object count from mock electroporated cells was subtracted from experiment group results. D) SGR of JFH-1 was analysed by luciferase assay. Data are presented as mean with standard deviation. Statistical significance was tested by one-way ANOVA with the Bonferroni's multiple comparison test, with a single pooled variance. P values; ns, P ≥0.05; *, P <0.05; ****, P <0.00005.

3.2.9. Insertion of eGFP at the novel C terminal site of NS5A within the JFH-1 infectious clone

Although the JFH-1 SGR did not tolerate the larger insertion of eGFP at the C terminal site (Isn463), it was formally possible that this insertion of GFP could be tolerated in the infectious clone. In addition to this, existing GT2 infectious clones containing fluorescent proteins fused to NS5A within domain III were tested (Figure 3.13 A). Schaller *et al.* (2007) demonstrated that the insertion of RFP and GFP flanked by linkers at amino acid site Isn396, was compatible with both genome replication and the production of infectious virions. In addition, JFH-1 infectious clone derivate with the insertion of eGFP or mCherry flanked by linkers at the amino acid site Isn418 were provided by Dr Christopher McCormick (University of Southampton) (Figure 3.13 B). Huh7.5 cells were electroporated with 5 μg RNA of the full infectious virus infectious virus genome. Fluorescent protein expression and cell growth was analysed for 72 h.p.e by visualisation using the IncuCyte S3. Initial results demonstrate cells after electroporation, testing RNA replication only, without the completion of FFA which determines production of infectious virions (Figure 3.13 C). Results suggest the Isn396 and Isn418 insertion sites are susceptible to the expression of both eGFP/GFP and RFP/mCherry. Both insertion sites follow a trend where the number of fluorescent cells increase until 48 h.p.e and then plateau. Interestingly, Isn396 appears to have a greater number of fluorescent positive cells than Isn418; Isn418 only exhibits 35-36% fluorescent cells at 72 h.p.e in comparison to Isn396 (Figure 3.13 D, E). To determine if the number of positive fluorescent cells is limited due to cells reaching confluency, the confluency of cells per well measured 72 h.p.e was measured (Figure 3.13 E). Interestingly, all wells, independent of the expression of fluorescent proteins, become confluent by 40 h.p.e. In addition to this, supporting SGR JFH-1 results, insertion of eGFP at the Isn463 amino acid site does not allow eGFP expression (Figure 3.13 D).

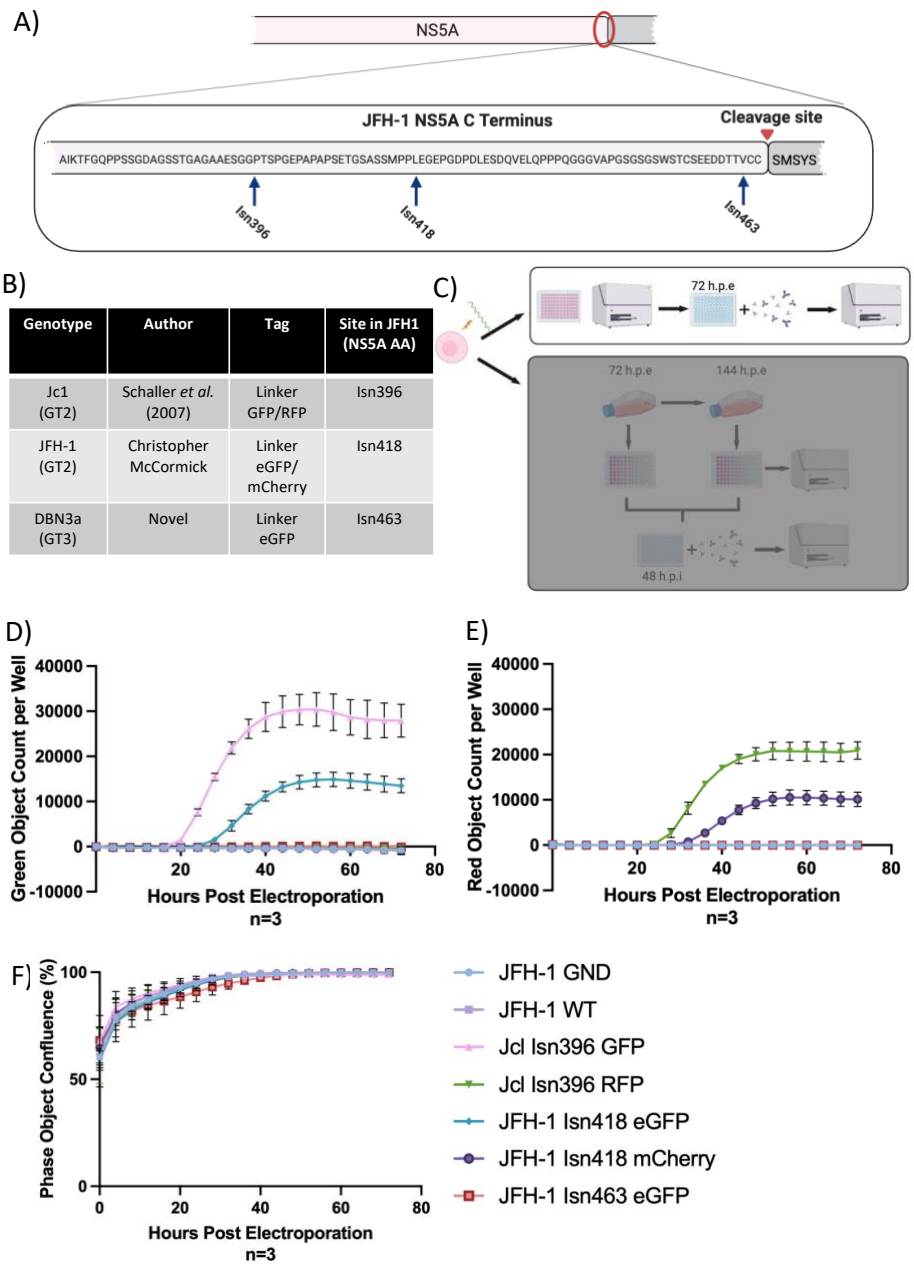

Genotype	Author	Tag	Site in JFH1 (NS5A AA)
Jc1 (GT2)	Schaller *et al.* (2007)	Linker GFP/RFP	Isn396
JFH-1 (GT2)	Christopher McCormick	Linker eGFP/ mCherry	Isn418
DBN3a (GT3)	Novel	Linker eGFP	Isn463

Figure 3.13 Assessing expression of fluorescent proteins in the viral genome of JFH-1.

A) Diagram representing the insertion sites within genotype 2 (GT2) where a fluorescent protein has been inserted. B) A table outlining the amino acid sites that had previously been used for insertion of protein tags in HCV genotypes. Insertion sites are noted by the amino acid location in reference to the synthetic construct clones of JFH-1 (GenBank: KY427259.1). C) Schematic of the protocol to determine virus genome replication and expression of the fluorescent proteins after electroporation. Time course of D) GFP and eGFP expression and E) RFP and mCherry expression 72 h.p.e. F) Cell growth quantified by the phase percentage confluency per well. Data are presented as mean with standard deviation. Statistical significance was tested by one-way ANOVA with the Bonferroni's multiple comparison test, with a single pooled variance. P values; ns, P ≥0.05.

To further quantify the differences in replication between the Isn396 and Isn418 insertion sites, the mean intensity of each fluorescent positive cell after electroporation was investigated; this is indicative of the amount of NS5A present within a fluorescent cell and does not measure the number of fluorescent cells. Due to the inability to subtract background fluorescent cells (using the mock control) without using different software parameters per sample, the number of green, and especially red, calibrated units being averaged for all "positive" cells may obscure results. For example, the GND sample, incapable of expressing fluorescent protein has a RCU average of 0.5 – 1 during the 72 h time course, similar to that of the fluorescent positive control sample; Jcl Isn396 RFP (Figure 3.14 B). However, GND had less than 100 cells identified as positive for RFP expression. The positive control sample, Jcl Isn396 RFP, had approximately 20,000 cells identified as positive for RFP. As such green and red calibrated units are displayed for all samples (Figure 3.14 A, B), as well as displaying only the fluorescent protein inserted samples (Figure 3.14 C, D). Interestingly, when the fluorescent protein is inserted into Isn396, results mirror the number of fluorescent cells counted; a peak fluorescence intensity per object reached by 48 h.p.e. When the fluorescent protein is inserted into Isn418, no peak is reached. These results suggest differences in the expression of fluorescent proteins is dependent on the insertion site.

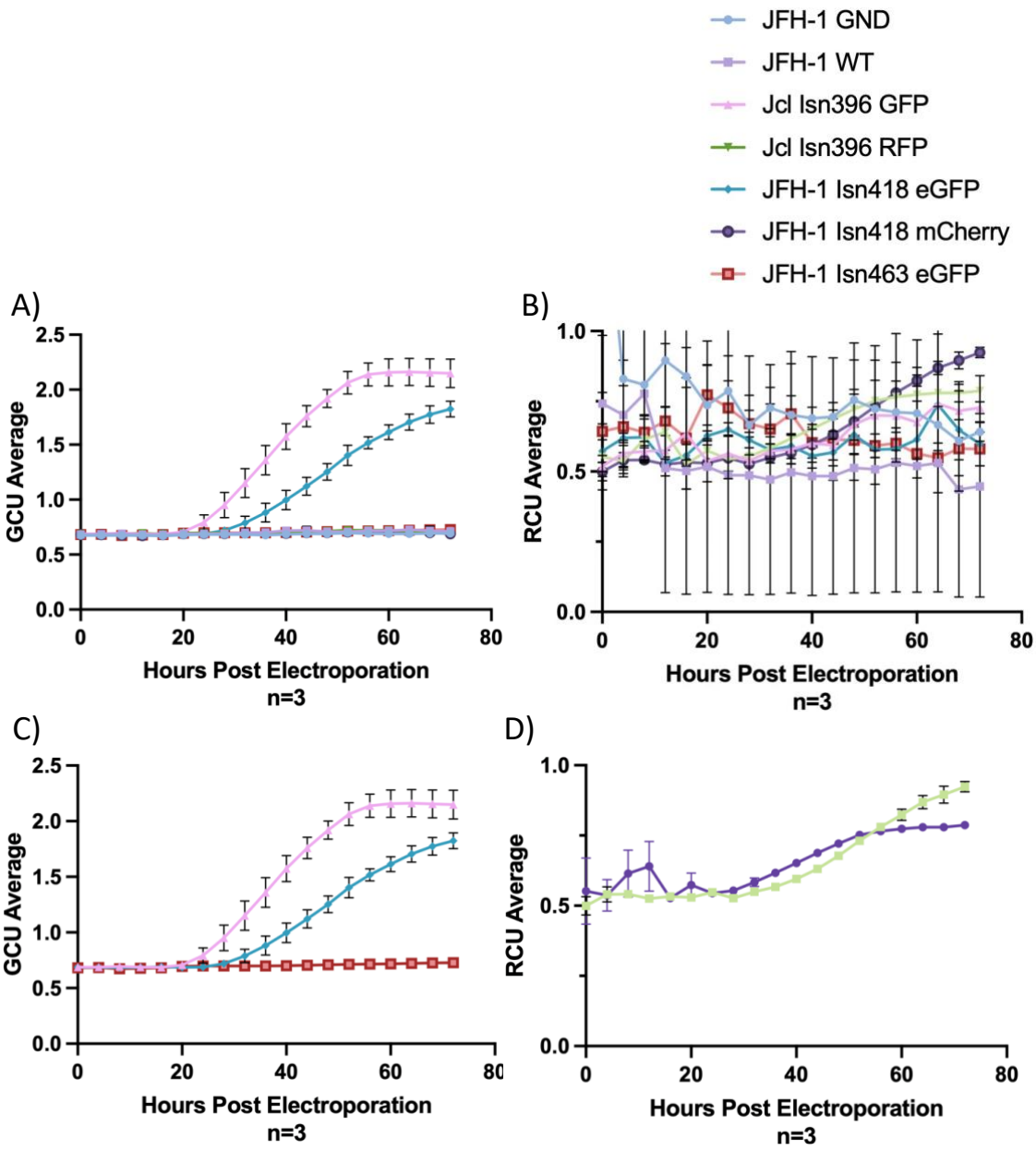

Figure 3.14 Assessing the dependence of NS5A expression based on the insertion site of a fluorescent protein post electroporation.

Quantification of the mean object intensity A) green (GCU) and B) red calibrated unit (RCU) calculated for all samples. C) GCU and D) RCU for samples expressing fluorescent protein. Data are presented as mean with SEM. Statistical significance was tested using one-way ANOVA with the Bonferroni's multiple comparison test, with a single pooled variance comparing the change fold in confluency of cells at 72 hours. P values; ns, P ≥0.05.

Post electroporation results suggests the expression of the fluorescent protein and the number of positive fluorescent cells are dependent on the amino acid insertion site. No fluorescence is detected when RFP or GFP is inserted into Isn463. Additionally, results allude to differences in the expression of NS5A dependent of the insertion site used as Isn396 expresses a greater number of fluorescent cells and calibrated units than Isn418. To confirm NS5A is not expressed when eGFP is inserted into Isn463, the cells used to determine fluorescent protein expression were also stained with sheep anti-NS5A to determine genome replication 72 h.p.e and visualised using the IncuCyte S3. Red object count from mock electroporated cells was subtracted from experiment group results (Figure 3.15). Results confirm NS5A is not expressed in in JFH-1 eGFP Isn463. Therefore, RNA replication was occurring when a fluorescent gene was inserted into Isn396 and Isn418 however, not when a fluorescent gene is inserted into Isn463. These results also highlight that the number of fluorescent/NS5A positive cells are the same regardless of the type of fluorescent protein inserted; if eGFP or mCherry is inserted into the same site, similar rates of RNA replication will occur.

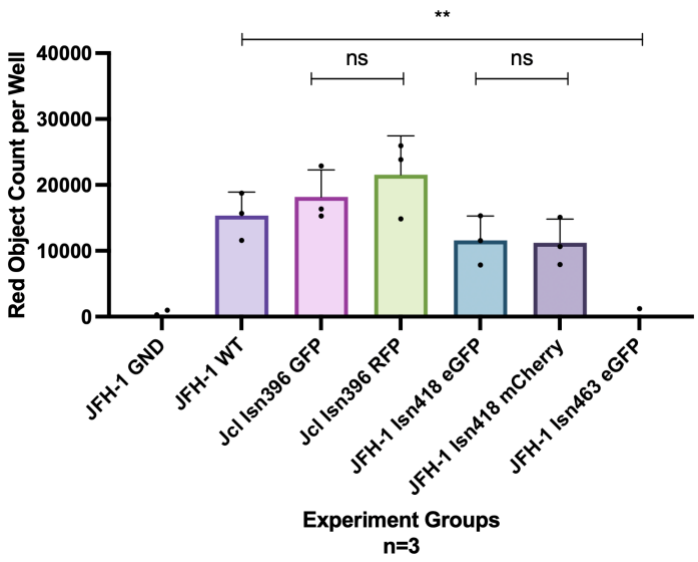

Figure 3.15 Assessing the expression of NS5A when fused to a fluorescent protein post-electroporation.

Data are presented as mean with standard deviation. Statistical significance was tested using one-way ANOVA with the Bonferroni's multiple comparison test, with a single pooled variance. P values; ns, P ≥0.05; **, P <0.005.

Results thus far are limited to investigating RNA replication. To determine the production of viable virus progeny, a FFA was performed. Huh7.5 cells were electroporated with 5 μg RNA of the full infectious virus genome. Supernatant may be collected 72 and 144 h post electroporation (h.p.e). Virus titration was performed via FFA on Huh7.5 cells to calculate number of virus particles per millilitre (FFU/mL) by staining cells with sheep anti-NS5A. Fluorescent protein expression was observed for 48 h.p.i, visualised using the IncuCyte S3, prior to staining cells with sheep anti-NS5A. Red object count from mock infection was subtracted from experiment group results (Figure 3.16 A). By visualising cells prior to the staining for the detection of NS5A, I can confirm all infectious virions contain the fluorescent protein (Figure 3.16 B, C). Virus titres prior to staining with anti-NS5A suggest only the fluorescent genes inserted into the Isn396 site can produce infectious virions expressing a fluorescent protein. To confirm WT virus was produced and fluorescent genes inserted into sites Isn418 and Isn496 are not capable of propagating virus, FFA plates are stained to detect NS5A (Figure 3.16 D). This provides confirmatory results that only Isn396 insertion site can tolerate the insertion of a fluorescent gene allowing both RNA replication and the production of viable infectious virus progeny; confirming the results of GFP/RFP expression in Figure 3.16 B, C. By comparing insertion of fluorescent protein into sites Isn396 and Isn418, I have compared how the IncuCyte S3 may be used to greater understand virus genome replication and virus propagation after electroporation.

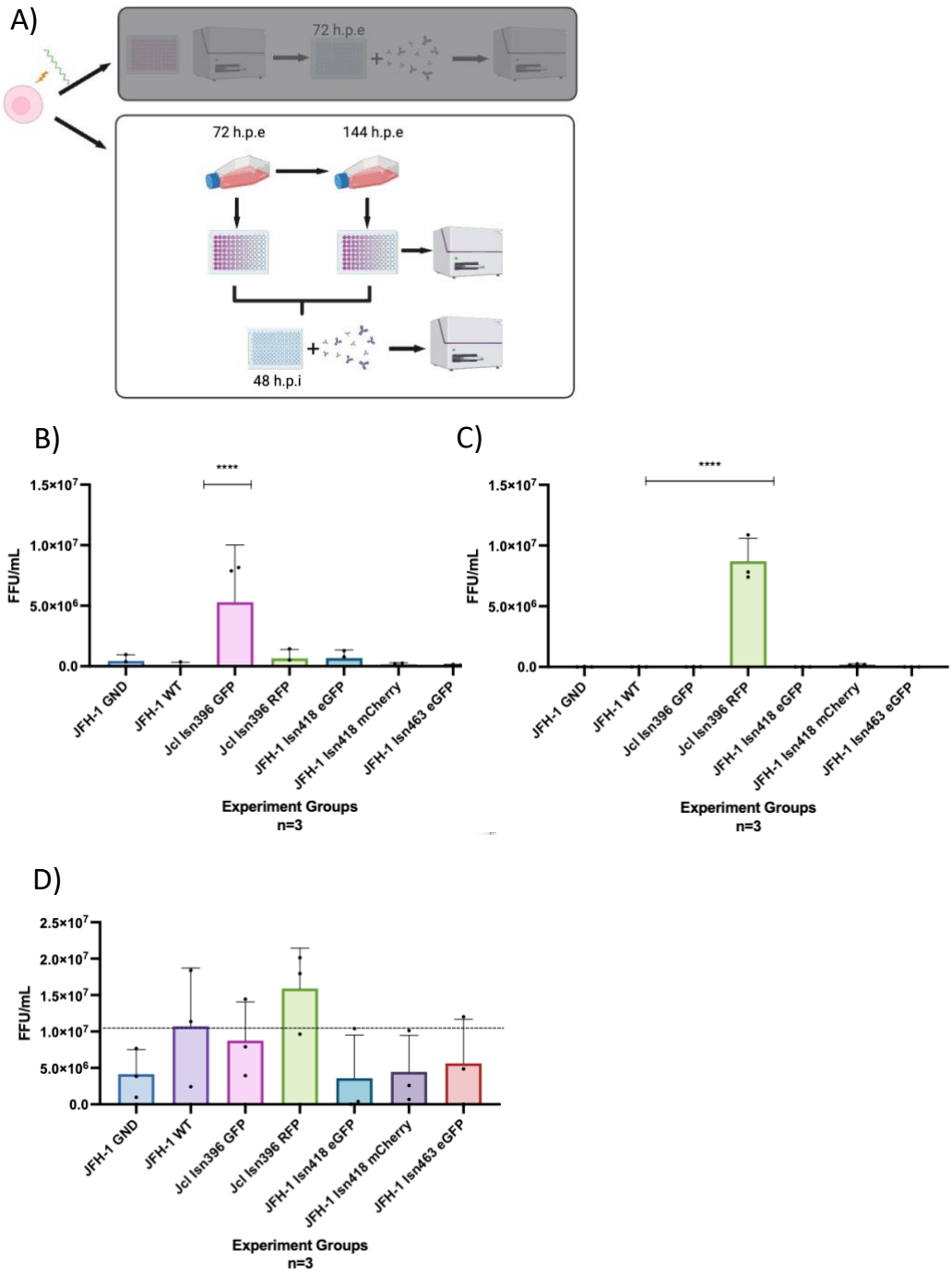

Figure 3.16 Assessing insertion of linker eGFP in the viral genome of JFH-1 by production of virions.

A) Schematic of the protocol to determine virus assembly and release. Prior to staining cells for the detection of NS5A, cells were visualised for the detection of green (B) and Red (C) fluorescent proteins. D) The cells visualised for fluorescent protein expression was stained with sheep anti-NS5A to determine the presence of NS5A 48 h.p.i. Virus titre from supernatant collected 144 h.p.e is shown. Data are presented as mean with standard deviation. Statistical significance was tested by one-way ANOVA with the Bonferroni's multiple comparison test, with a single pooled variance. P values; ns, P ≥0.05; ****, P <0.00005.

3.2.10. Utilising the foot-and-mouth disease virus 2A sequence to co-express eGFP and the HCV polyprotein

The aim of this work was to express NS5A with an eGFP fusion for co-localisation studies; ability to analyse NS5A localisation at a sub-cellular level and in conjunction with live-cell imaging. However, due to the inability to find a tolerated site within the NS5A of DBN3a compatible with RNA replication and production of infectious virions, it was deemed to be advantageous to derive a method by which DBN3a positive cells could be identified by fluorescence methods. As an alternative approach therefore, the 2A sequence, derived from foot-and-mouth disease (FMDV), was utilised in an attempt to express eGFP independently of the HCV polyprotein. This technique has been readily used in a range of different model systems; *in vitro* and *in vivo* (Lewis et al., 2015; Minskaia & Ryan, 2013). eGFP was flanked by the HCV delta core, allowing the correct formation of the IRES, and the 2A sequence results in ribosomal skipping and therefore separation of the eGFP protein from the downstream HCV polyprotein during translation (Figure 3.17 A). Restriction sites flanking eGFP were introduced to aid potential downstream cloning experiments, insertion of RFP for example. This was performed in both JFH-1 and DBN3a, to maintain direct comparison of the two HCV GTs. Huh7.5 cells were electroporated with 5 μg RNA of the full infectious virus genome. eGFP expression was observed at 72 h.p.e, visualisation using the IncuCyte S3, prior to staining cells with sheep anti-NS5A. Supernatant was collected 72 h.p.e. Virus titration via FFA was performed on Huh7.5 cells to calculate the virus titre by staining cells with sheep anti-NS5A 48 h.p.i (Figure 3.17 B). To determine RNA replication post electroporation, cells were visualised for eGFP expression prior to staining for NS5A. Interestingly, eGFP was able to express in JFH-1 and not DBN3a (Figure 3.17 C). This suggests possible differences in HCV protein functions required for RNA replication and virus production upstream of NS5A. However, despite expression of eGFP post-electroporation, JFH-1 FMDV 2A eGFP was not able to propagate virus suggesting the presence of eGFP and the 2A sequence is disrupting virus production.

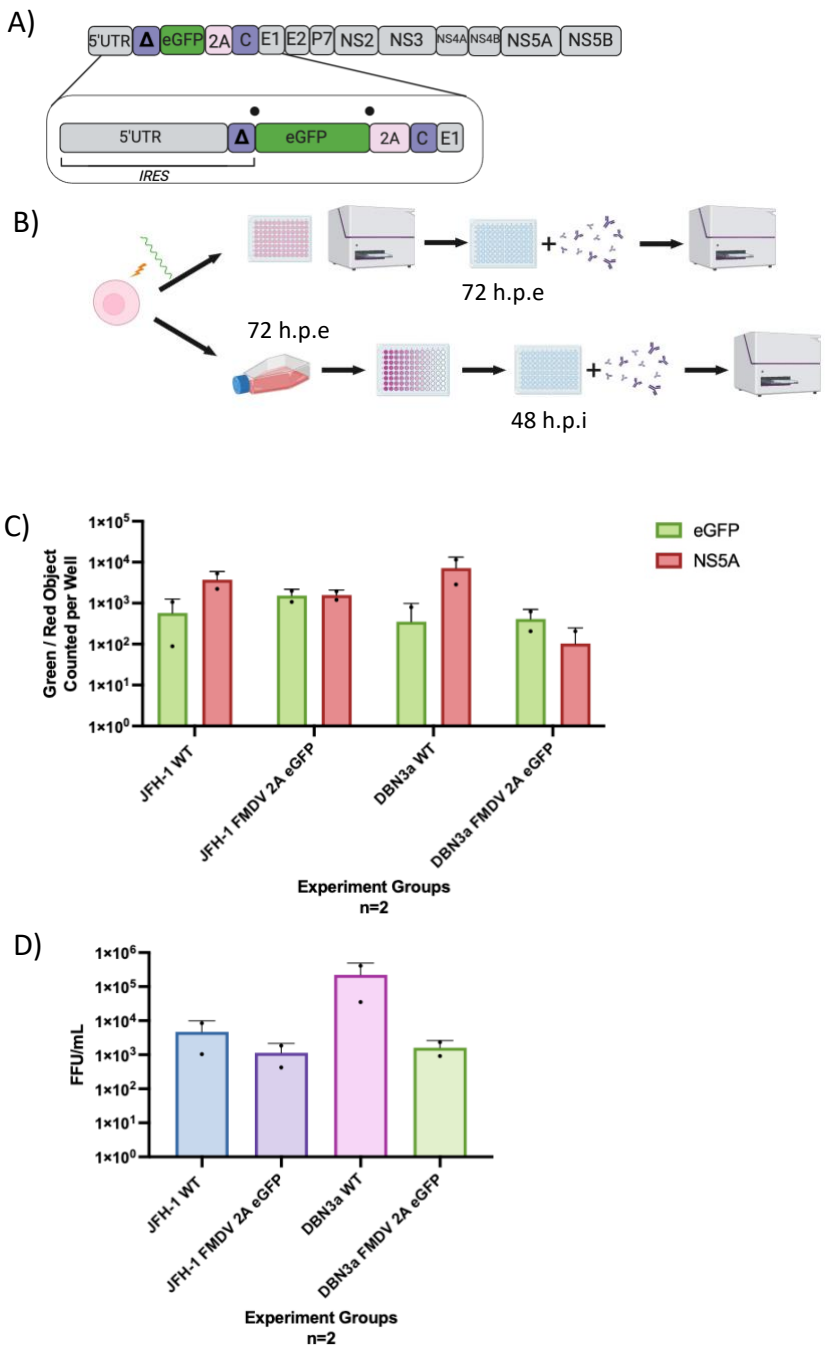

Figure 3.17 Effect of inserting eGFP FMDV 2A upstream of the translation of the viral polyprotein.

A) Diagram depicting the viral genome whereby the eGFP was inserted flanked with unique restrictions as well as the delta core region, at the 5' end, and the foot and mouth disease (FMDV) 2A sequence, at the 3' end. To indicate ribosomal skipping, a line has been inserted between FMDVA 2A and the HCV core protein. B) Schematic of the protocol to determine virus assembly and release. C) To determine genome replication 72 h.p.e, cells were stained and visualised for both NS5A and eGFP expression. D) Calculated virus titre 72 h.p.e. red and green object count from mock infection was subtracted from experiment group results. Data are presented as mean with standard deviation.

3.3. Discussion

The work described in this chapter aimed to discover differences between HCV GT2 and GT3 both related to infection dynamics as well as genetic plasticity of NS5A domain III. Experiments were conducted *in vitro* using both SGR and cell culture infectious clones, JFH-1 and DBN3a, allowing a distinction between RNA replication and virus assembly/release between the two viruses.

3.3.1. Exploring IncuCyte S3 image analysis abilities

As both the SGR and the cell culture virus experiments benefited by the visualisation of cells using the IncuCyte S3, the ability to set-up user defined analysis parameters is highly advantageous. However, absence of fluorescent objects or variation of well sizes may result in the software collecting false positive results. Over-exposed images cannot be controlled by the user, however false positives may be removed by altering the analysis parameters and subtraction of negative control samples (Figure 3.2). By setting three analysis parameter sets used throughout my project, consistency between experiments can be maintained (Table 3.1). Verification of IncuCyte results could be conducted by comparing results to other cell counting methods; manually counting infected cells or the use of flow cytometry. Flow cytometry,in particular, could easily generate the percentage of infected cells and mean fluorescence intensity analysis which would be particularly useful when comparing differences between JFH-1 and DBN3a infected cells. Use of the same the IncuCyte software, or any algorithmic tool reduces user bias and ensures the same experiment parameters are set for all samples and all biological repeats. This is particularly important to note for the analysis of fluorescence objects which is crucial to this project for the quantification of virus titres by FFA.

3.3.2. Efficiency of virus production differs between JFH-1 and DBN3a

As previously mentioned, Ramirez *et al.* (2016) established a cell culture virus clone of HCV GT3a which had comparable RNA replication and virus propagation characteristics to JFH-1. These characteristics were confirmed during the production of both cell culture viruses using the in-house protocol (Figure 3.3). By comparing propagation of virus in both Huh7 cells and Huh7.5 cells (Figure 3.3 B), concludes that both viruses follow a similar trend and respond the same to the presence of RIG-1 that differs between the two cell lines; Huh7.5 cells, a derivative of Huh7 cells, are believed to be more submissive to HCV infection due to a missense mutation in RIG-1, involved in the host intracellular antiviral defence (Sumpter et al., 2005). For both JFH-1 and DBN3a, there is a trend of greater virus propagation in Huh7.5 cells than Huh7 cells. However, DBN3a virus has a significant increase in virus titre between the 72 h.p.e and 144 h.p.e which is not comparable to JFH-1 virus propagation (Figure 3.3 C). Further differences in virus propagation are highlighted when comparing JFH-1 and DBN3a infection of Huh7 cells (Figure 3.4). As both viruses perform in a similar manner under the stresses presented by Huh7 cells (Figure 3.3 B), a significant difference in the number of cells infected by JFH-1 is not due to the infection occurring in Huh7 cells instead of Huh7.5 cells. By using the average intensity of fluorescence as a measure of the level of NS5A expression there is more NS5A within JFH-1 infected cells than DBN3a infected cells. However, as less cells are infected by JFH-1, it is reasonable to suggest that NS5A is accumulating within an infected cell potentially due to an inefficiency of JFH-1 releasing virus progeny (Figure 3.4).

The difference in the number of infected cells might have been explained by differences in specific infectivity of the two viruses. To assess this, two methods of virus quantification were used (Figure 3.5). This allows us to determine the “physical titre”, the genome copies/mL calculated by qRT-PCR, and the “functional titre”, infectious units/mL calculated by FFA (Ojosnegros et al., 2011). Interestingly, these ratios change depending on the virus. Lentivirus

can have a functional to physical ratio of 1 in 100, SARS -CoV2 can range between 1 in 1000 to 1 in 1,000,000 and SARS can be 1 in 360 (Despres et al., 2022; Duke et al., 2020). Despres *et al.* (2022) investigated the changes in functional and physical virus titres for different strains of SARS -CoV2, linking ratio variations between strains as a potential reason for increased spread. This ratio can suggest how efficient an infected cell is at producing infectious virions and concludes that both JFH-1 and DBN3a produce roughly 1 functional unit for every 10,000 physical units produced in Huh7.5 cells (Figure 3.5 D). Critically, the protocol conducted to measure the functional to physical ratio of JFH-1 and DBN3a virus did not include treatment to remove non-capsulated RNA. Thus, qRT-PCR results are not specific to virions produced and include released viral genome that is not capsulated from host cells. Non-capsulated RNA may be removed by completing a pre-treatment of propidium monoazide (PMA) prior to RNA extraction. PMA is an intercalating dye with a photo-inducible azide group that covalently binds to nucleic acids that are non-capsulated, “unprotected”, preventing their amplification during PCR (Purves et al.). Based on qRT-PCR results gathered in this project, I hypothesise that JFH-1 is unable to infect as many cells as DBN3a during a 72 h infection as DBN3a is able to release more virus particles during the course of infection thereby increasing the likelihood of DBN3a releasing more functional units.

To confirm this hypothesis, samples measuring the number of cells infected and the production of virions during the course of a 72 h infection was conducted (Figure 3.6). As there is no difference between the number of cells infected at 4 h.p.i, virus entry does not differ between JFH-1 and DBN3a. The number of cells infected by JFH-1 and DBN3a virus at 4 h.p.i supports our hypothesis that as the infection length increases, there is a greater difference in the number of cells infected as there is a greater length of time for DBN3a to produce more functional unit virions than JFH-1 (Figure 3.6 B). This is supported by the increasing number of virions produced over the course of infection based on the virus titre calculated, in particular 72 h.p.i (Figure 3.6 D). Additionally, these results mimic the initial investigation into JFH-1 and

DBN3a virus propagation; DBN3a producing significantly more virus at 144 h.p.e than JFH-1 when comparing to the 72 h.p.e virus titre (Figure 3.3 C). However, it is important to note, that the virus titre during this infection will increase at 72 h.p.i not only because DBN3a infected cells may be producing more virions, but because more cells are infected at this timepoint. To confirm if there is a greater number of physical units being released by DBN3a at 72 h.p.i, a qRT-PCR detecting the HCV 5'UTR should have been conducted to compare physical and functional titres.

Supporting this theory that JFH-1 is unable to release as many virus particles as DBN3a, the fluorescence intensity is trending higher for JFH-1 infected cells than DBN3a infected cells particularly at the 72 h.p.i (Figure 3.6 C). To gain greater confidence that JFH-1 is maintaining virus particles within cells, intracellular virus titres could be compared between JFH-1 and DBN3a by freeze thawing infected cells allowing release of virus particles within the cytoplasm. Virus titre could be calculated by qRT-PCR and FFA, to determine functional and physical units. The buoyancy of intracellular virus could also be investigated to determine if virus particles have high-density, reflecting an immature precursor, or low-density, reflecting a mature infectious particle due to be released (Gastaminza et al., 2008). If JFH-1 infected cells contain more high-density particles than DBN3a, it could be suggested that JFH-1 ability to release mature particles is restricted. The presence of very low density lipoproteins (VLDL) is associated to lipid droplets, which may be hijacked during HCV infection to promote virus production (Miyanari et al., 2007). The number of lipid droplets present during JFH-1 and DBN3a infection could be compared by confocal microscopy. Fundamentally, if DBN3a can release more virions, the ability of DBN3a to manipulate the host cell may differ from JFH-1.

Multiple virus-host cell factors are involved to ensure successful release of virus particles. For example, Diacylglycerol acyltransferase-1 (DGAT1) and cytosolic phospholipase A2 (PLA2G4A) are crucial to recruiting the core protein to lipid droplets. DGAT1 interacts with both core and NS5A HCV proteins allowing localisation on lipid droplets and ensuring particle assembly (Herker et al., 2010; Li et al., 2021). PLA2G4A is essential to produce virus particles as

it cleaves lipids containing arachidonic acid. Cleaving of arachidonic acid is crucial for establishing a membrane environment that allow efficient incorporation of both host and virus factors for the construction of highly infectious virus particles (Menzel et al., 2012). This is believed to play a role in membrane homeostasis by altering the phospholipid composition and the release of VLDL. This hypothesis is supported by Su *et al.* (2017), demonstrating PLA2G4A increased expression by HCV infection promotes lipid droplet formation. In relation to this project, NS5A plays a crucial role in the assembly and envelopment of HCV however I was interested in the NS5A progressive role in disease pathology linked to GT3. For example, both the VLDL and microsomal triglyceride transfer protein inhibition (MTTP) are involved in HCV assembly through interaction with NS5A and disease pathology pathways in GT3.

During HCV assembly, HCV utilises cell-death-inducing DFFA-like effector B (CIDEB), a key regulator of VLDL, to promote the NS5A:ApoE interaction (H. Cai et al., 2016). This interaction is required for efficient production of HCV particle assembly and release (Benga et al., 2010). The assembly and secretion of hepatic VLDL is regulated by MTTP, which also modulates the production of ApoB and ApoE. Jiang and Lou (2009) performed a knockdown ApoE proving its interaction with NS5A as crucial for the assembly of HCV. ApoB is not involved in HCV assembly however forms the VLDL required to export the triglycerides into the bloodstream. In terms of GT3 pathology, HCV has been reported to inhibit the MTTP pathway during HCV GT3 infection by restricting the transfer of lipid molecules to ApoB resulting in the degradation of ApoB and a decreased reduction in VLDL production (Perlemuter et al., 2002). Research has shown this to be HCV-core protein mediated with all GTs capable of inhibiting the pathway. However, Jhaveri *et al*. (2008) expresses that particular polymorphisms in the core protein of GT3a may be the reason why the MTTP is more greatly affected during GT3 infection. This is suggestive of a link between NS5A interactions required for particle assembly and release within these pathways. The result of this would be disease progression that differs between JFH-1and DBN3a.

As such, it may be suggested that JFH-1 is unable to release virus to the capability of that of DBN3a due to a reduction in infection at 72 h.p.i and an accumulation of NS5A in comparison to DBN3a. This may be because JFH-1 is unable to manipulate host factors affecting virus assembly to the same extent as DBN3a. This warrants further research specifically investigating differentiation of NS5A plasticity, alluding to potential functional differences between JFH-1 and DBN3a.

3.3.3. Insertion of TST demonstrates different plasticity of JFH-1 and DBN3a NS5A domain III

To investigate differences between JFH-1 and DBN3a NS5A, an insertion of an epitope tag would be greatly advantageous. Insertion of the tag in the C terminus was favoured due to the short structural elements present within the N terminus, suggested by Hanoulle *et al.* (2009), as well as an interest in characterising the C terminus domain. Data has been published negating the theory as domain III being dispensable to RNA replication; domain III plays a role in virus assembly and production (Appel et al., 2008). In addition to this, the amino acid locations within the C terminus have been well documented in GT1 and 2 as being susceptible to the insertion of epitope tags as well as fluorescent proteins. To directly compare the plasticity of NS5A in JFH-1 and DBN3a, the same sites were used to insert a TST (Figure 3.7). Despite domain III being characterised as tolerant to large heterologous insertions and deletions with no impact on RNA replication (Foster et al., 2010), this was only true for JFH-1 (Figure 3.8 A). For SGR DBN3a only the C-terminal site (lsn449) was compatible with RNA replication (Figure 3.8 B). This suggests that there are significant differences between the plasticity and function of JFH-1 and DBN3a RNA replication within domain III.

To decipher if Isn449 of DBN3a plays a crucial role in the production of virus particles, the quantification of virus titres of both JFH-1 and DBN3a containing the TST in all four sites was

investigated (Figure 3.9). Within JFH-1, as the TST is inserted closer to the C terminus, there is a decline in virus titre, notably with site Isn431. This could be linked to the crucial area required for virus production, amino acid location 427 – 458, due to interaction of NS5A with the core protein of HCV (Appel et al., 2008). Failure to produce virus particles with the TST inserted at site Isn463 is not surprising as this site is proximal to the cleavage of NS5A to NS5B and the amino acid area 427 – 458, as such the area between these two important areas may be less tolerant to the insertion of even a small epitope tag. These insertions within the SGR of JFH-1 can allow predictions of insertion sites within the virus genome that will successfully produce virus particles. However, as the insertion of the TST only worked at the furthest downstream point of NS5A in DBN3a, Isn449, and no other insertion sites produced virus particles, there is the suggestion that the areas of function discovered in JFH-1 NS5A domain III cannot be extrapolated to GT3.

To summarise, by inserting the TST into all four sites in both the SGR and virus genomes, I can conclude that the plasticity and functional areas of domain III NS5A of DBN3a does not mirror that of JFH-1. As insertion site Isn418 in JFH-1 and Isn423 in DBN3a has been cited as a tolerable site in GT1 via the FK5.1 SGR clone, domain III in GT1 and GT2 may retain similar functions. To test this fully, all four insertions should be tested in GT1 *in vitro* cell culture systems. This further alludes to the idea of NS5A domain III within DBN3a as having different plasticity and potential functions, yet to be defined. It is important to note, only virus production was tested, the presence of the TST in the virus genome and localisation with NS5A and RNA replication post electroporation was not tested. Further work would allow this assessment by staining the electroporated cells for NS5A as well as a streptavidin antibody for the visualisation of NS5A and TST co-localisation by confocal microscopy.

3.3.4. Potential use of stable cell line expressing TST allowing proteomic analysis

As an alternative approach to understand the differences between JFH-1 and DBN3a stable cell lines harbouring the SGR were produced for potential proteomic analysis by co-immunoprecipitation of NS5A to investigate host protein interactions (Figure 3.10). The TST inserted into amino acid site Isn426 within SGR JFH-1 was used as proteomics analysis had previously been conducted by Goonawardane *et al.* (2017) using this site and epitope tag. This would allow us to directly compare our results, using the results from Goonawardane *et al.* (2017) as a control to our proteomic protocol and JFH-1 results. Insertion site Isn449 was used for the establishment of the DBN3a stable cell line as it maintained the best RNA replication in comparison to wild-type.

Despite confirmation of the established stable cell line by western blot, the elution of the co-immunoprecipitation assay suggests a poor pull down of JFH-1 NS5A-TST. As the stable cell line was a polyclonal population, the TST coding sequence may have been compromised by deletion or point mutation in some cells, resulting in a mixed population. The poor presence of the TST tag present in the western blot may provide evidence for this. To eliminate the risk of knocking-out the TST during the establishment of the stable cell line, a monoclonal cell line could be established after confirmation of the presence of the TST by Sanger sequencing.

3.3.5. Viral genome replication is impacted by large amino acid insertions in previously tolerated TST insertion sites

3.3.5.1. GFP insertion into DBN3a SGR

The tolerance of previously tested insertion sites to fluorescent genes, in particular Isn449, in the SGR clone of DBN3a (Figure 3.11) was investigated. Primarily all four sites were tested, eGFP was inserted with and without linkers, with all sites deemed as non-tolerable

(Figure 3.11 C, D). The linkers used, providing structural flexibility, was the same amino acid sequence as the linkers used when inserting the TST. When a fluorescent gene has been inserted into JFH-1, linkers appear to always be present and the linker type can vary depending on the clone produced (McCormick et al., 2006; Ross-Thriepland et al., 2015; Schaller et al., 2007). As such, I believe the sequence of the linker used is not the determinant allowing RNA replication when a fluorescent gene is inserted, however, I did not test different linkers.

As expected, the three upstream insertion sites that did not tolerate the insertion of TST within the SGR clone did not tolerate the insertion of eGFP, efforts were focussed on the susceptible TST insertion site Isn449 when conducting further attempts to express a NS5A fusion with eGFP (Figure 3.11 E, F). The insertion of a start codon at the start of eGFP was conducted in an attempt to increase the protein structure stability (Aledo, 2019; Valley et al., 2012). Additionally, the stability and potential toxicity of eGFP was explored by replacing eGFP with hrGFP (Figure 3.11 F). hrGFP is codon-optimised, mutant version of GFP from *Renilla reniformis*, specifically designed for mammalian cell expression (Heim et al., 1995). The potential of eGFP inhibiting RNA replication by inducing cellular cytotoxicity during DBN3a expression but not during JFH-1 expression was a premature hypothesis; the expression eGFP is not affected during co-expression of the DBN3a SGR as noted by the eGFP reporter present in the SGR DBN3a established by Ward *et al.* (2020). This suggests the cellular stress of HCV RNA replication in a cell does not exhibit an environment rendering eGFP expression as unstable. I believe the fundamental problem inhibiting eGFP expression and RNA replication may be due to the large amino acid sequence and structure disrupting the cleavage of NS5A to NS5B. By inserting hrGFP instead of eGFP, it could be suggested that hrGFP consists of a slightly different structure than eGFP. However, structural differences in hrGFP and eGFP has not been well documented or suggested as a factor promoting GFP expression in previous plasmids. To test if it is the structure of eGFP inhibits RNA replication, a different fluorescent gene should be inserted. eGFP was not

inserted into the virus genome of DBN3a, however, as RNA replication was not achieved in the SGR, virus particle production is not likely to occur in any of the four insertions sites.

3.3.5.2. eGFP insertion into JFH-1 SGR

As the insertion site Isn463 was tolerated during the insertion of a small epitope tag, I investigated if this site was also tolerable to a larger insertion; eGFP. If the insertion was tolerated, I can conclude that this area of domain III is very susceptible to insertion despite its proximity to the NS5A-NS5B cleavage site (Pawlotsky & Germanidis, 1999). Three methods were used to test RNA replication, confirming that insertion of eGFP was not tolerated in Isn463 (Figure 3.12). This was expected due to the increase in size and structure of eGFP in comparison to the TST. eGFP consists of 249 amino acids and forms a very distinct structure containing a classical β-barrel fold with a helix running through the core of the structure containing the chromophore (Arpino et al., 2012). However, TST consists of only 28 amino acids and contains two binding units each comprising an eight residue helical confirmation. The ninth amino acid, at the C terminus, forms a salt bridge to streptavidin (Schmidt & Skerra, 1993; Wu & Wong, 2013). By initially cloning eGFP into the SGR in site Isn463, disruption of RNA replication was observed. This suggests both RNA replication and virus production will be disrupted by the presence of eGFP in site Isn463 of the JFH-1 virus genome.

3.3.5.3. Fluorescent protein insertion into JFH-1 virus

JFH-1 NS5A fused fluorescent viruses have already been successfully established; Isn396 allows RNA replication and the production of virus particles (Schaller et al., 2007) and Isn418 cloned by Christopher McCormick allows RNA replication however, virus production assays had not been conducted. Initially, RNA replication of the virus genome with fluorescent proteins inserted was tested (Figure 3.13). Corresponding to the literature and suggestive of our previous results, eGFP inserted into Isn463 disrupted RNA replication, fluorescent proteins inserted into

Isn396 and Isn418 allowed successful RNA replication. Interestingly, expression of fluorescent proteins inserted in Isn418, plateaued at a lower number of fluorescent cells per well than Isn396 (Figure 3.13 D, E). I hypothesised that Isn418 had a lower number of fluorescent positive cells per well as the site was tolerable for RNA replication, allowing cells with electroporated RNA to express the viral genome, however, was incapable of producing virus particles and therefore did not spread through the cell population during the 72 h time course. This was confirmed by analysing cell confluency kinetics, suggesting the plateau of fluorescent positive cells for insertion site Isn396 is defined by the number of naïve cells present.

Fluorescence intensity was analysed to confirm RNA replication and accumulation of the viral genome within an electroporated cell. When displaying all samples (Figure 3.14 A, B), a fluorescent negative sample may contain false positives after performing the IncuCyte software analysis. Interestingly, the analysis parameters for green fluorescence appears to better distinguish between positive and negative cells (Figure 3.14 A) than parameters set to identify red fluorescence (Figure 3.14 B) based on the clarity of results presented with all samples present. This may be due to Huh7.5 cells auto-fluorescing more within the red fluorescent channel than green making the distinguishing of false positive objects more difficult.

Replicating similar results to JFH-1 inefficiency of producing virions compared to DBN3a infection, the intensity unit of the fluorescent proteins did not reach a plateau. Contrary to Isn418, the intensity unit plateaus by 60 h.p.e for fluorescent proteins inserted into Isn396. I believe this is due to a saturation of HCR RNA replication within virus producing cells. A longer time course is required to observe peak fluorescence intensity for Isn418 which is not producing virus and therefore, may be less efficient at RNA replication (Figure 3.14 C, D). By confirming the presence of NS5A within electroporated cells, I can confirm fluorescence expression is indicative of RNA replication (Figure 3.15) and Isn463 is definitively not expressing NS5A.

By confirming Isn418 is incapable of producing virions, by expression of protein fluorescence (Figure 3.16 B, C) and expression of NS5A within infected cells (Figure 3.16 D), I can

conclude that the insertion of TST does not confirm an amino acid site as being tolerable to all insertions whether in the SGR or the virus genome. This is probably due to the difference in size and structure of eGFP and TST, as mentioned previously. As such, unlike the insertion of the TST, the Isn418 insertion site not being tolerable to the presence of a fluorescent gene does not deem this amino acid location as crucial to the production of virus particles. However, the production of virus particles was only tested by the number of NS5A expressing cells after FFA. I cannot exclude the possibility that the insertion of eGFP/mCherry into Isn418 produces virions that may be non-infectious; incapable of infecting naive cells. To test this, I would perform qRT-PCR analysis of the supernatant of electroporated cells for the presence of the HCV 5'UTR.

The insertion of a fluorescent gene into the virus genome and RNA replication and virus production assessment may be determined by multiple methods. I suspected site Isn418 was not producing infectious virions prior to the completion of the FFA. This highlights the diverse range of quantitative analysis the IncuCyte can provide, allowing a higher out-put of results and multiple methods of result confirmations.

As I know, by the insertion of a TST, domain III of DBN3a plasticity is not parallel to JFH-1. Insertion of eGFP in the corresponding Schaller *et al.* (2007), amino acid position Isn396 within JFH-1, should be tested in DBN3a to confirm if this site is potentially tolerated in other HCV GTs. It could also allude to further potential differences or similarities of domain III functions in JFH-1 and DBN3a. Our results demonstrate that despite differences in tolerated TST insertion sites, insertion of eGFP into JFH-1 and DBN3a SGRs follows the status-quo that toleration of insertion sites can be dictated by size of the gene inserted.

3.3.6. Differences of tolerated insertion sites of JFH-1 and DBN3a are not limited to NS5A

By being unable to fuse eGFP onto NS5A, other reporter systems were explored to establish a fluorescent reporter within the DBN3a virus genome. Possibilities considered

included the insertion of two NS5A genes; one with a fused eGFP, allowing co-localisation studies, and the second allowing cleavage of NS5A to NS5B, which is possibly the inhibiting factor of RNA replication. This system was not explored, as downstream studies included specific focus of NS5A inducing and promoting HCV disease pathology. Having a system which overexpressed our protein of interest could obscure these results, creating a further divide between *in vitro* and *in vivo* HCV analysis. Producing NS5A fused to a split eGFP system was also discussed, as the full eGFP sequence would not be fused onto NS5A; only 16 amino acids constituting the C terminus of the β strand would be inserted, and the larger N-terminus 10 β strand would be transfected into the cell separately (Dáder et al., 2019). However, downstream experiments include a range of different cell culture models trying to recapitulate the architecture of liver, including 3D models and PCLS, transfection of cells was not desirable as would place more stress on cells and would not mimic a natural HCV infection. As the length of eGFP was deemed as the limiting factor within the genome, inserting eGFP upstream of the HCV genome with independent translation of the genes using the FMDV 2A system was investigated (Figure 3.17).

Minskaia *et al.* (2013) demonstrates the various factors should be considered and adapted when cloning using the FMDVA 2A system, outlining the different sequences of 2A that can be used altering cleavage efficiency. "2A-like" sequences may also be adopted such as that from *Thosea asigna* virus (Liu et al., 2017). In our system, RNA replication, but not virus production, of the JFH-1 virus genome suggests that despite eGFP being expressed before the translation of the HCV polyprotein, there is still disruption to the production of infectious virions. No RNA replication or virus production of DBN3a suggests there could be a more systemic difference between JFH-1 and DBN3a virus genomes not restricted to NS5A. There is also limited output from IncuCyte analysis as there was no visualisation of electroporated cells throughout the 72 h.p.e to detected eGFP expression, in particular average intensity unit of a fluorescent cells which can decipher limited RNA replication and virus production. Virus production was only

assessed 72 h.p.e and not 144 h.p.e despite the possibility of RNA replication and virus production efficiency rate declining and requiring a longer time course.

The identification of differences between JFH-1 and DBN3a at an infection level, by the completion of monolayer experiments and a genomic level, specific to NS5A by the insertion of small epitope tags and larger fluorescent genes, highlights fundamental differences between the two HCV GTs. These differences support future investigation of *in vitro* HCV infection specifically exploring the function of NS5A during DBN3a infection and comparing to JFH-1.

3.4. Summary

- IncuCyte S3 allows the in-depth analysis of RNA replication and HCV infection. User subconscious bias can be eliminated by using the same analysis parameters consistently between biological repeats.
- Despite the same number of Huh7 cells infected by JFH-1 and DBN3a at 4 h.p.i, data suggests DBN3a is more efficient at producing virus particles in comparison to JFH-1 based on a greater number of Huh7 cells infected by DBN3a than JFH-1 at 72 h.p.i.
- Insertion of a small epitope tag, TST, alludes to different plasticity and function of NS5A within DBN3a when directly comparing tolerated insertion sites to JFH-1.
- The size of gene insertions can impact RNA replication and virus particle production of previously discovered tolerable amino acid insertion sites.

Chapter 4. Comparing NS5A host-protein interactions between JFH-1 and DBN3a

4.1. Introduction

Viruses are defined as obligate intracellular pathogens which rely on host cell machinery to successfully complete their life cycle. Upon entry, host cell surface receptors and trafficking factors are required. Virus genome replication and translation relies on host translation factors. Host organelles are required for virus assembly and, virus egress relies on host trafficking factors. However, host cell defences have evolved to combat the threat of viral infection via pathogen-associated molecular patterns (PAMPs) which triggers the innate antiviral response (Shah et al., 2022). During an infection, a virus must combat the antiviral response while exploiting host cellular factors to provide efficient virus replication. By understanding virus-host protein interactions, I can identify novel drug treatment targets. For example, virus-host interactions of influenza virus provide proof-of-concept to targeting host protein interactions for viral therapeutics. Inhibition of protein kinase C (PKC) and the Raf-MEK-ERK signalling cascade resulted in a reduction in virus production. Since then, more than 80 compounds have been identified directly targeting the pathway inhibiting influenza virus replication (de Chassey et al., 2014).

Determining protein interaction networks by proteomic approaches provides a detailed understanding of cellular biology. Proteomics provides direct measurements of cellular states that cannot be determined by genomic and transcriptomic data where alterations may not result to protein changes or reveal post-translational modifications (Wilhelm et al., 2014). A map of molecular systems, networks and pathways can generate and directly link to cellular activities such as cell proliferation, differentiation and apoptosis. This increases the complexity of sample collection as protein expression is altered by time and environmental conditions (Cui et al., 2022). Protein expression may be analysed using conventional methods such as western blot,

immunohistochemistry and enzyme-linked immunosorbent assay (ELISA). High-throughput analysis allows greater accuracy and depth of analysis and includes methods such as tissue microarray and mass spectrometry (Aslam et al., 2017).

Mass spectrometry (MS) outperforms immunoassays due to its ability to detect intact protein or a subset of composite peptides by utilising the ionisation of protein molecules allowing their mass to be calculated based on the mass-to-charge ratio. This allows rapid detection and provides quantitative analysis of proteins involved in a complex. Liquid chromatography uses a liquid mobile phase for continuous separation of all the proteins in a complex and can be combined with mass spectrometry (LC-MS) allowing the separation of a full-length protein and its fragments in addition to peptide identification. MS qualitative and quantitative analysis can be improved by performing LC-MS/MS which uses tandem mass spectrometry to gather information on molecular and fragment ion peaks (W. Cai et al., 2016). MS data is matched to a protein sequence database and peptide scores, protein scores and protein inference results can be provided (Cui et al., 2022; Matthiesen & Bunkenborg, 2013).

Proteomics has been used widely to expand our knowledge of the HCV life cycle, liver pathogenesis, host-altered metabolism, and host immune responses. Expression proteomics identifies changes to protein expression in different conditions. Such an analysis was performed by Vravas *et al*. (2022), utilising a Huh7.5 cell line stably expressing the Core+1/Long isoform of HCV-1a, an Alternative Reading Frame Protein (ARFP), which is conserved in different HCV genotypes. Isoforms of ARFP of the HCV core protein uncovered a molecular signature found to be important for the progression of HCV liver disease to cancer by triggering oncogenesis and metastasis pathways.de Chassey *et al.* (2008) suggests a multi-functional role for HCV NS3 and NS5A proteins. As well as being involved in RNA replication, NS3 and NS5A interactions were found to play a role in the regulation of cellular focal adhesions. This function leads to the hypothesis of NS3 and NS5A involvement in liver pathology; promoting tumorigenesis and cell detachment from extracellular matrix components. Structural proteomics exposes 3D structures

and complexities such as protein interactions with cell organelles, typically using nuclear magnetic resonance spectroscopy and X-ray crystallography. Structural proteomics aided Lussignol *et al.* (2016) discovery of the HCV capsid protein interacting with nucleoporin Nup98 as essential for virion assembly. In addition, HCV mediating replication of the viral genome was discovered by Kim *et al.* (2017) by HCV inducing lipid raft localisation to autophagosomes. Functional proteomics identifies the biological role of a protein through the identification of protein complexes leading to roles in cellular pathways. Exploiting this method, Kumar *et al.* discovered the interaction of NS2 with the ubiquitin proteasome system, specifically MARCH8, a member of the membrane-bound E3 ubiquitin ligases family. MARCH8 mediates K63-linked ubiquitination, a type of post-translational modification that regulates the interaction, translocation, and activation of proteins, of HCV NS2 which promotes recruitment of the host endosomal sorting complex binding to NS2 allowing HCV envelopment.

Specific to NS5A, many protein interactions have been described in the literature. Ross-Thriepland *et al.* (2015), reviewed more than 130 interactions in 2015. Since, then further interactions have been described, such as interaction with the nucleosome assembly protein 1-like protein 1 (NAP1L1) (Goonawardane et al., 2017; Çevik et al., 2017) and apoptosis-stimulating of p53 protein 2 (ASPP2) (Smirnov et al., 2023). A high number of NS5A to host protein interactions supports the hypothesis of NS5A acting as a multi-functional protein. As a phosphoprotein, NS5A may be present in two forms, a hyperphosphorylated form, molecular weight of 58 kDa, or a hypophosphorylated form, molecular weight at 56 kDa. It is suggested that NS5A is able to facilitate a large number of host protein interactions by presenting itself in these different forms, acting at spatially and temporally distinct patterns in a host cell, with functionally different roles and protein interactions. As such, proteomic analysis of NS5A interactions may focus on the phosphorylation status of NS5A. Multiple groups have shown phosphorylation sites of NS5A to be crucial for genome replication (Chong et al., 2016; Cordek et al., 2014; Lee et al., 2016). Cordek et al. (2014) proposed that phosphorylation and other post-

translational modifications allow expansion of the viral proteome under limited coding capacity. Chon *et al.* (2016) demonstrated that serine-235 phosphorylated by casein kinase 1α (CK1α) promotes HCV replication by increasing NS5A interaction with vesicle-associated membrane protein-associated protein A (VAP-A). Goonawardane *et al.* (2017), demonstrated that the phosphorylation status of NS5A, specifically serine 225, plays a crucial role in NS5A to host protein interactions within the SGR; NAP1L1, bridging integrator 1 (Bin1), and VAP-A. Based on the phosphorylation status of the protein, genome replication and the subcellular localisation of replication complexes were altered.

Smirnov et al. (2023) performed similar proteomic analysis, a streptavidin tag inserted into the C terminus of NS5A within the infectious JFH-1 clone, unlike the use of the SGR by Goonwardane *et al.* (2017). Similar to Goonawardane *et al.*, proteomic analysis identified previously described interactors of NS5A, Bin1 and NAP1L1, identifying protein interactions as occurring in both the SGR and infectious clone. Smirnov *et al.* (2023) characterises the interaction of ASPP2 to NS5A, an interaction not previously identified in SGR proteomic analysis, however previously identified in a yeast two-hybrid assay (de Chassey et al., 2008). During HCV infection, ASPP2 is described as binding to NS5A via its SH3 domain promoting HCV RNA replication and spread of HCV transmission. Unlike research by Goonwardane *et al.* (2017), there was no association of NS5A-ASPP2 interaction being specific to the phosphorylation state of NS5A. As ASPP2 binds to the polyproline motif of NS5A, Smirnov *et al.* (2023) describe the interest in understanding the influence NS5A-ASPP2 complex influencing the serine/threonine NS5A phosphorylation status, which requires interaction of the proline rich region to the SH3 domain.

To date, proteomic analysis of HCV has only used patient samples, HCV SGR or the JFH-1 infectious clone. As I hypothesise NS5A in GT3 promotes liver pathogenesis, allowing a more rapid progression of liver disease and increased severity, I utilised the insertion of a TST within NS5A of JFH-1 and DBN3a to directly compare NS5A virus to host proteins interactions. This was

utilised to directly analyse functional differences between GT2 and GT3 NS5A which have not been accomplished to date.

4.2. Results

4.2.1. Evaluating NS5A immunoprecipitation by sepharose suspension beads

As I have established cell culture infectious clones of JFH-1 and DBN3a containing a TST in domain III of NS5A, amino acid insertion site JFH-1 Isn426 and DBN3a Isn449, I evaluated the immunoprecipitation of NS5A with any interacting proteins from these infectious clones. To confirm efficient immunoprecipitation of HCV NS5A, visualisation of NS5A from infectious clones via SDS-PAGE and western blotting was performed. At 72 h.p.e, cell lysates of Huh7 cells electroporated with HCV infectious clones were harvested (Figure 4.1 A). The control immunoprecipitation was performed on Huh7 cells electroporated with the WT HCV infectious clones without the TST tag. Following pulldown, 10 μL of the elution was visualised by SDS-PAGE and western blot analysis (Figure 4.1 B). Presence of NS5A can be confirmed by the apparent molecular mass of protein, NS5A at 56-58 kDa. Input samples confirm the presence of NS5A in cell lysates (WT and TST). NS5A for both the control pulldown (WT) and TST containing infectious clones is absent in the elution samples. This suggests the pulldown does not contain sufficient enrichment of NS5A for proteomic analysis. To further evaluate the presence of NS5A in pulldown elution samples, the remaining 30 μL of elution was analysed by western blot (Figure 4.1 C). Results suggest the protocol is capable of JFH-1 NS5A-TST pulldown however, not in a sufficient quantity to be visualised by using 10 μL of elution. Pulldown of DBN3a NS5A-TST was unsuccessful, as evidenced by a lack of NS5A within the elution of the immunoprecipitation despite presence of NS5A within input sample. All pulldown controls did not contain NS5A in elution samples. Results suggest efficiency of TST pulldown is low thus requiring optimisation of the protocol either through increased concentration of input virus to ensure sufficient pulldown or altering the stringency of wash/elution conditions.

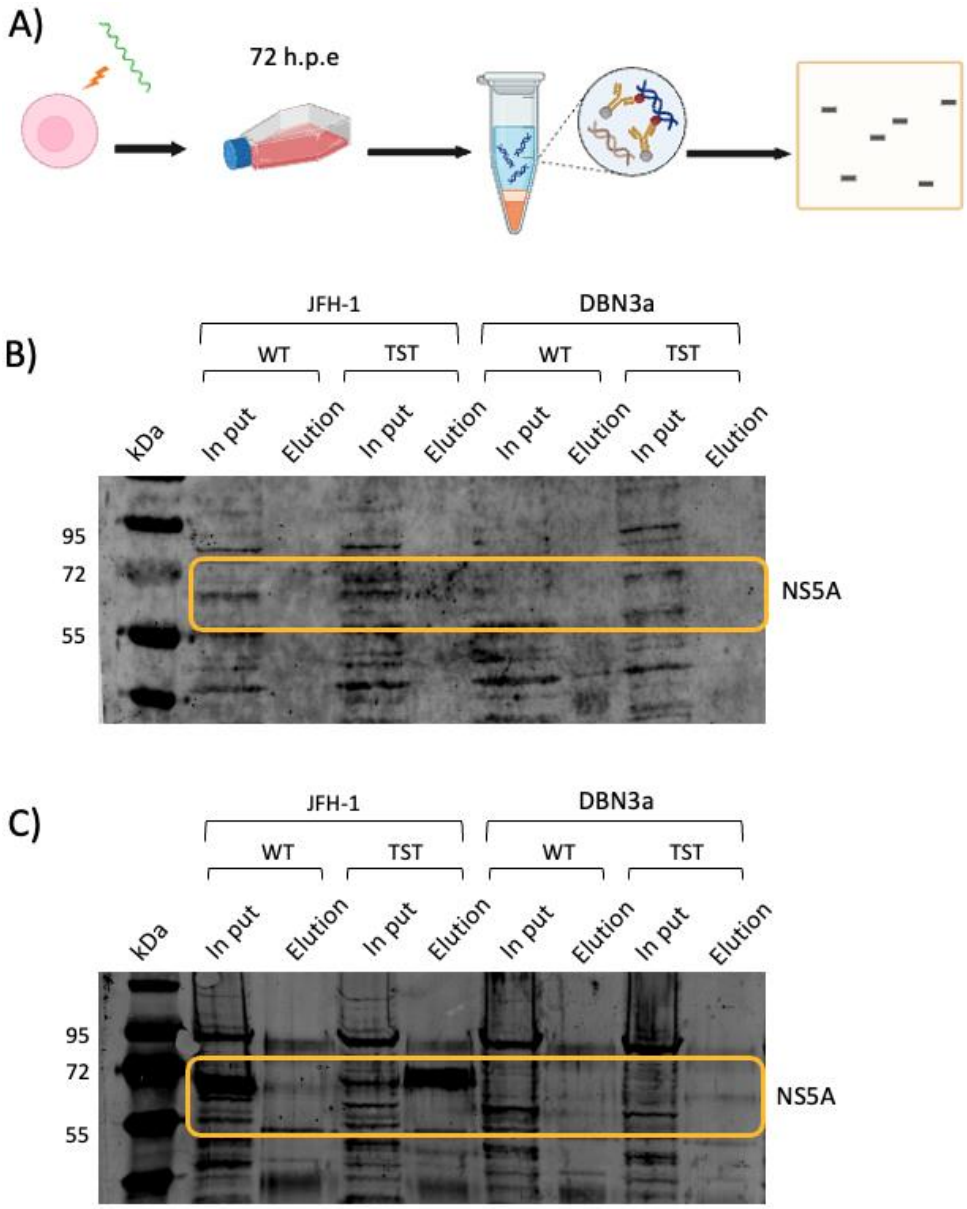

Figure 4.1 HCV TST virus immunoprecipitation utilising sepharose suspension beads.

A) Schematic of cell lysate production protocol. Immunoprecipitation was completed using streptavidin sepharose suspension beads and visualised by western blot. Western blot visualised by the LI-COR Sa Odyssey. Inputs show cell lysate controls. Elution samples were collected after immunoprecipitation B) 10 μL of sample. C) 30 μL of sample.

4.2.2. Optimisation of NS5A immunoprecipitation by sepharose suspension beads

To gain a more concentrated sample of NS5A in the elution from immunoprecipitation by sepharose suspension beads, I attempted to increase the concentration of NS5A within the input cell lysate. I hypothesised that by increasing the amount of RNA electroporated into Huh7 cells this would increase NS5A expression. Thus, to increase the presence of NS5A within cell lysates either 5, 7.5 or 10 μg of *in vitro* transcribed JFH-1 or DBN3a WT RNA was electroporated into Huh7 cells. Cell lysates were collected 72 h.p.e to investigate the relative amounts of NS5A via western blot and densitometry analysis (Figure 4.2 A). Western blot confirms the presence of NS5A and housekeeper control actin for all cell lysates collected. Despite increasing the amount of RNA electroporated into Huh7 cells, there was no significant difference in the expression levels of NS5A present in cell lysates for both JFH-1 and DBN3a. Virus titres were calculated from supernatant collected at 72 h.p.e (Figure 4.2 B C). Virus titre was normalised to the titre calculated from Huh7 cells electroporated with 5 μg HCV RNA at 72 h.p.e, as this was the standard amount of RNA electroporated into cells. There was no significant difference in the virus titres when increasing the amount of RNA electroporated into Huh7 cells. Reflecting western blot analysis, the amount of virus produced does not increase in a linear trend to the increasing amount of RNA electroporated into Huh7 cells. These results suggest immunoprecipitation via sepharose suspension beads cannot be optimised by increasing the presence of NS5A present in cell lysates through the amount of RNA electroporated into Huh7 cells.

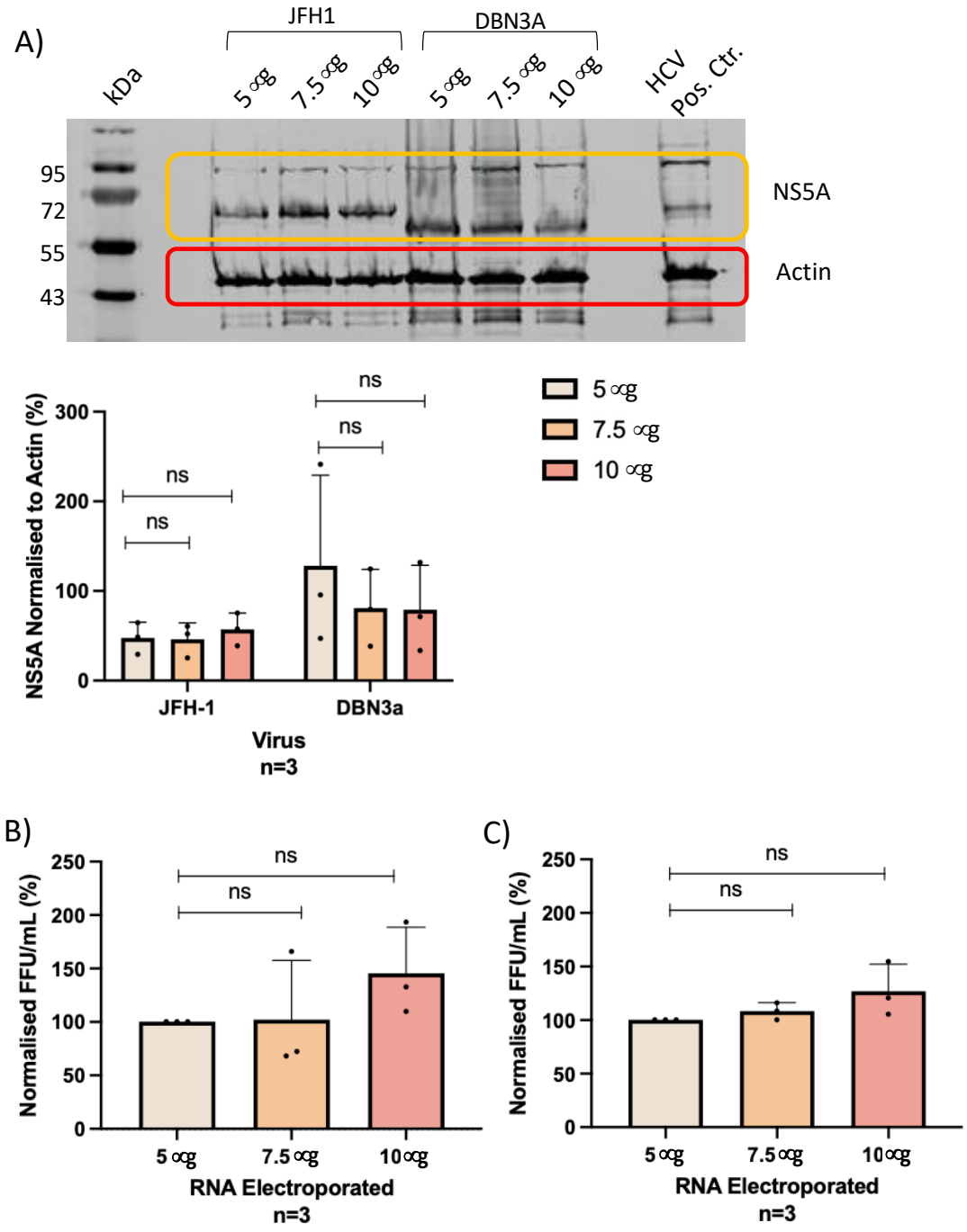

Figure 4.2 Detection of NS5A in Huh7 cell lysates.

Huh7 cells were electroporated with either 5, 7.5, or 10 μg RNA of the infectious virus clones. Supernatant and cell lysates was collected 72 h.p.e. A) Cell lysates were visualised by western blot allowing densitometry analysis of NS5A to actin. Representative western blot visualised by the LI-COR Sa Odyssey and densitometry results normalising NS5A expression to actin housekeeper control. Virus titre at 72 h.p.e B) JFH-1 and C) DBN3a. Data presented as mean with standard deviation. Statistical significance was tested by one-way ANOVA with the Bonferroni's multiple comparison test, with a single pooled variance. P values; ns, P ≥0.05.

4.2.3. Immunoprecipitation of NS5A via MagStrep magnetic beads

As I was unable to increase the expression of NS5A within cell lysate samples, it was deemed sepharose suspension beads were not able to provide the adequate amount of NS5A required to perform proteomic analysis. I hypothesised magnetic beads may provide a higher binding capacity to the streptavidin and reduce sample loss during wash steps, providing higher specificity and thus would provide an adequate pulldown of NS5A. To investigate this, Huh7 cells were electroporated with 5 μg *in vitro* transcribed HCV RNA (WT and TST infectious clones). Cell lysates were collected 72 h.p.e and immunoprecipitation was conducted by MagStrep "type 3" XT beads. All elution samples were visualised with 10 μL of the total 40 μL elution collected. Immunoprecipitation was conducted following the protocol outlined by manufacturers protocol. The presence of NS5A for both WT and TST clones was visualised by western blot (Figure 4.3 A). The control immunoprecipitation, WT JFH-1 infectious clone, suggests inadequate wash steps as NS5A is present in the elution sample, which would not be acceptable for proteomic analysis. Therefore, the iba Ltd. protocol was optimised by introducing a primary high salt concentration wash after the incubation of cell lysates with magnetic beads and changing of Eppendorfs prior to the final wash step to remove unbound protein presence on the walls of the Eppendorfs (Figure 4.3 B). As control samples, JFH-1 and DBN3a WT, contain NS5A in the eluted samples, results suggest the optimised protocol is sufficient to remove non-specific protein contamination. This provides confidence MagStrep "type 3" XT beads may be used for the immunoprecipitation of samples required for proteomic analysis without further optimisation.

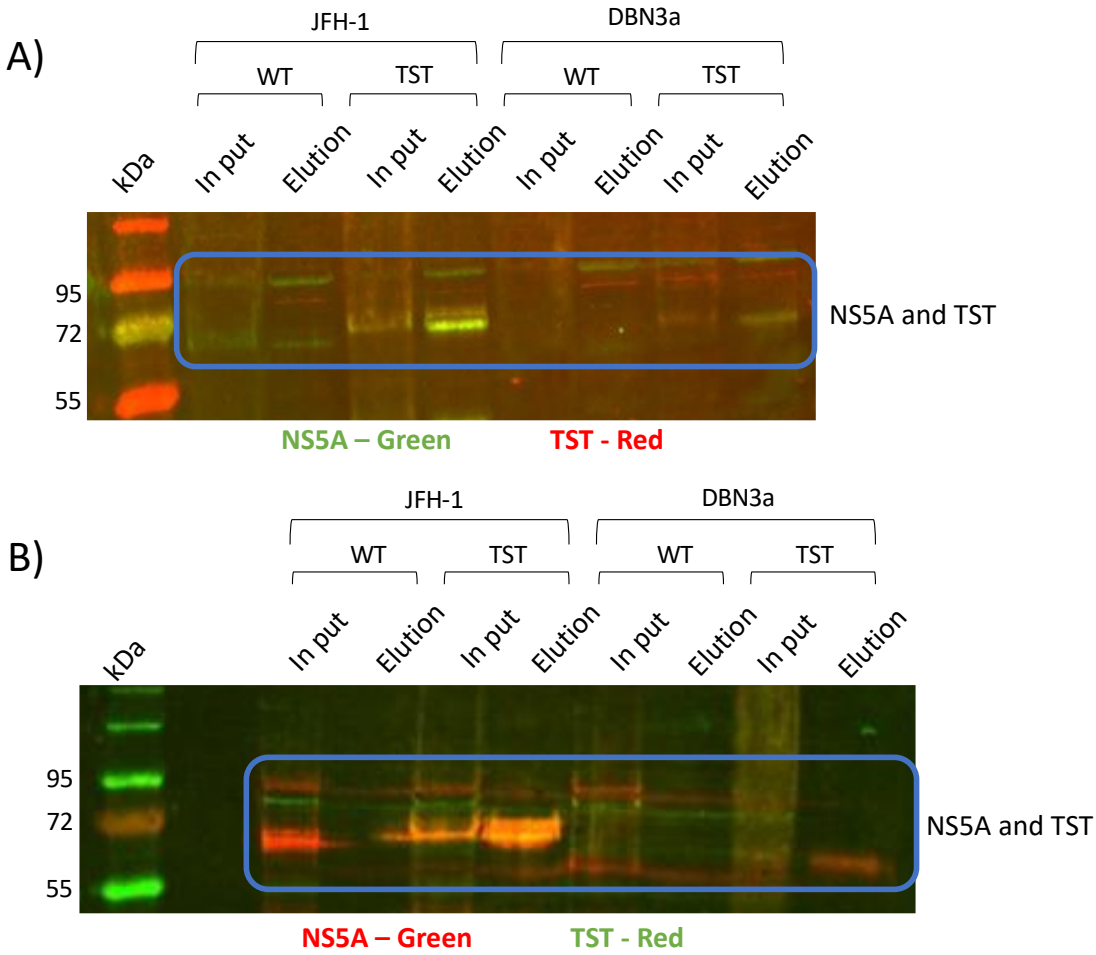

Figure 4.3 Optimisation of immunoprecipitation utilising magnetic beads.

Input refers to cell lysate prior to immunoprecipitation. Elution refers to samples collected after immunoprecipitation. Samples were analysed by western blot and visualised by the LI-COR Sa Odyssey. Two immunoprecipitation protocols were completed. A) As outlined by the manufacturers protocol. The presence of NS5A and TST was visualised, scanning the membrane at 700 nm and 800 nm wavelength, displays the NS5A (green) and TST (red). B) Optimised protocol using a high salt concentration wash and changing of Eppendorfs. The presence of NS5A and TST was visualised, scanning the membrane at 700 nm and 800 nm wavelength, displays the NS5A (red) and TST (green).

4.2.4. HCV proteomic analysis reveals similar NS5A interactions of JFH-1 and DBN3a

To investigate the interaction partners of HCV NS5A, a immunoprecipitation of NS5A-TST was performed at 72 h.p.e in Huh7 cells. To confirm the presence of NS5A in eluted samples all technical repeats were analysed by western blot to confirm the presence of NS5A (Figure 4.4). Following pulldown and western blot confirmation, technical samples were analysed by LC-MS/MS to identify proteins captured by HCV NS5A. Using a tandem mass tag quantification approach, protein abundance was analysed by Proteome Discover 2.4 (Figure 4.5). Proteome Discover defines a protein as present within an experimental group if 3 of the 4 technical repeats express that a particular protein. Overall, a total of 330 proteins were identified with high confidence (false discovery rate 1%). Protein abundances were normalised to the median across each channel and scaled to the control (pooled) samples. Many protein interactions are unchanged and therefore it is hypothesised that there would be an even distribution of protein intensities across all the channels. Normalisation and scaling are more challenging in pull-down experiments because the background proteome has been depleted. The median of each channel should be the same post-normalisation. Therefore, the pre-normalised data has been exported out of the Proteome Discover and further analysis was conducted in Perseus. Presented in this data, strict analysis parameters were set by logging the P values, the analysis may be relaxed by removing the log which may allow more proteins being identified as significantly different. I identified 4 potential interactors of HCV NS5A as being significantly altered in their abundance between JFH-1 and DBN3a. Volcano plots distinguish between significantly different protein abundances, P value of 0.5 or lower, as well as variable mean change between technical repeats, -log P. Volcano plots outlines the comparisons of protein abundance between each experimental group (JFH-1 WT/JFH-1 TST/DBN3a WT/DBN3a TST) (Figure 4.6). Comparing WT - TST samples, suggests NAP1L1 is the only host protein interactor of NS5A in JFH-1 that was significantly enriched as the protein is present in the TST sample and not the WT

(immunoprecipitation negative control). Comparison of the WT-TST of DBN3a suggests there are no potential protein interactions of the host proteins to HCV NS5A of DBN3a. Comparison of WT – WT samples (JFH-1 and DBN3a virus without TST tagged NS5A) suggests the expression of the 40S Ribosomal Protein S7 and S24 may be defined as background binding and not specific to NS5A (Figure 4.6 A B C). Comparison of the TST only samples (Figure 4.6 D), suggests NAP1L1 interacts with the NS5A of JFH-1 but not NS5A of DBN3a. A list of the potential top 9 different protein interactors of NS5A between JFH-1 TST and DBN3a TST (Table 4.1) provides further insight into other protein interactions that may differ between JFH-1 and DBN3a NS5A, however, were not deemed as significantly different using the strict metric analysis. These proteins include endoplasmic reticulum chaperone protein (GRP78) and aldo-keto reductase family 1 member C2 (AKR1C2). Interestingly, JFH-1 NS4A protein interaction is not noted as significant when comparing JFH-1 TST and DBN3a TST. In addition to this, the presence of other HCV poly protein products interacting with NS5A of either JFH-1 or DBN3a have not been noted.

When comparing our results to Goonwardane et al.(2017), 12 out of the 29 significantly different proteins between WT to TST JFH-1 samples were found in our proteomic results. When comparing our identified proteins to Smirnov *et al.* (2023) hits, only 7 out of 268 proteins were identified. Of all the proteins identified in both the Goonwardane *et al.* (2017) and Smirnov *et al.* (2023) data, only one was significantly different between WT and TST in our analysis (for both relaxed and strict analysed data parameters); NAP1L1. GRP78 and AKR1C2 were not identified in either protein interactome results. Our results suggest few differences between potential interactors of NS5A JFH-1 and DBN3a and inability to identify previously noted NS5A interacting partners in our model.

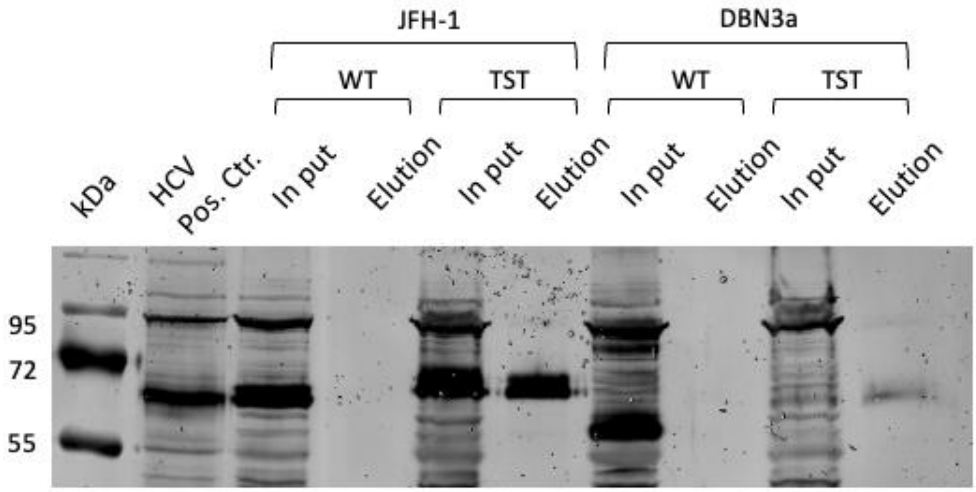

Figure 4.4 Representative image of immunoprecipitation samples sent for proteomic analysis. Input refers to cell lysate prior to immunoprecipitation. Using 10 μL of the 40 μL eluted volume, elution refers to samples collected after immunoprecipitation using MagStrep "type 3" XT beads. Samples were analysed by western blot and visualised by the LI-COR Sa Odyssey.

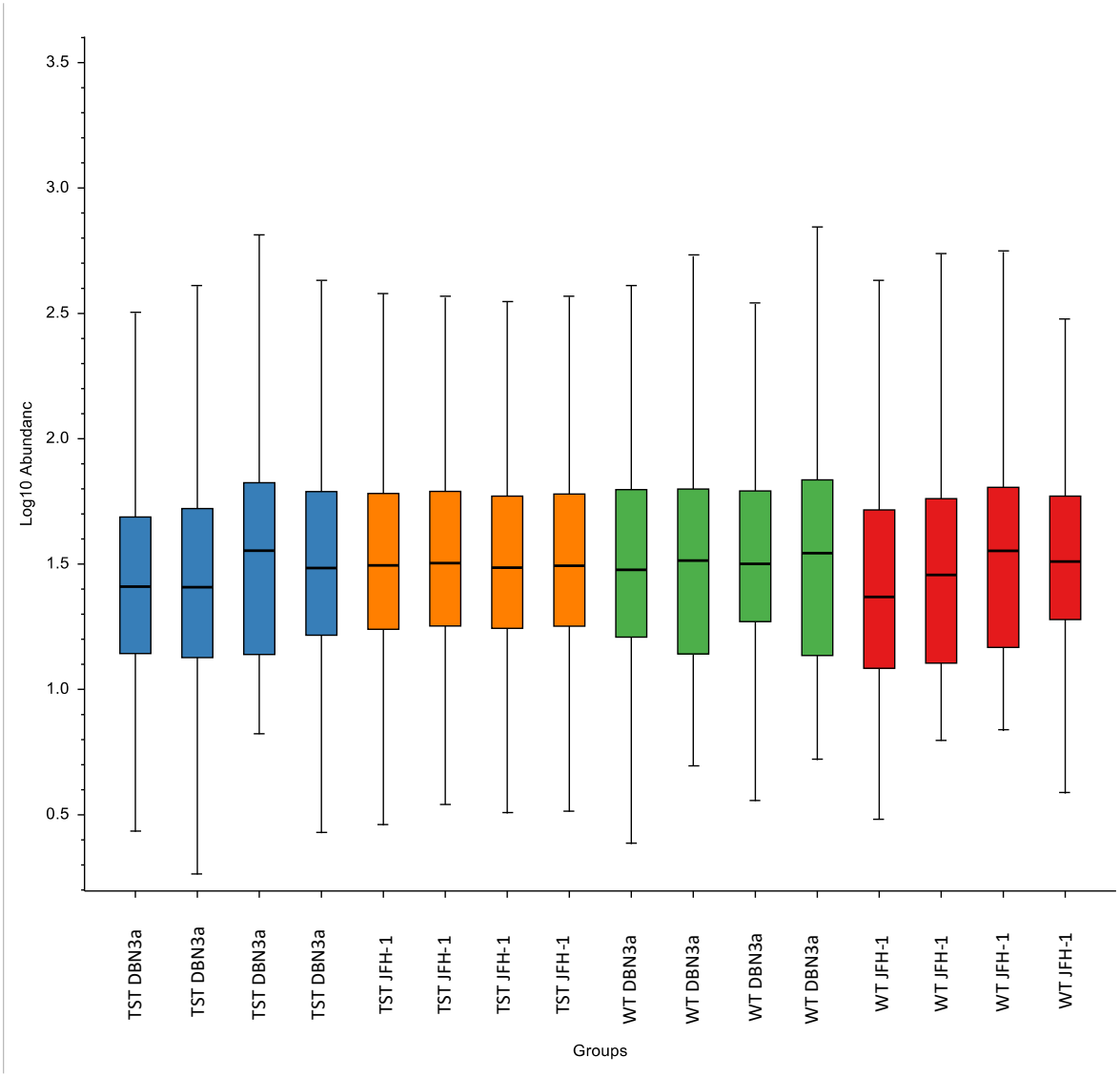

Figure 4.5 Proteomic samples protein abundances.

Protein abundances were calculated in PD and then imported into Perseus. Entries were filtered on having a minimum of 3 valid values in at least one condition. Channels were normalised by dividing by the median of the channel. Missing values were imputed based on a normal distribution with a downward shift of 1.2 and a width of 0.5. Results were log2 transformed.

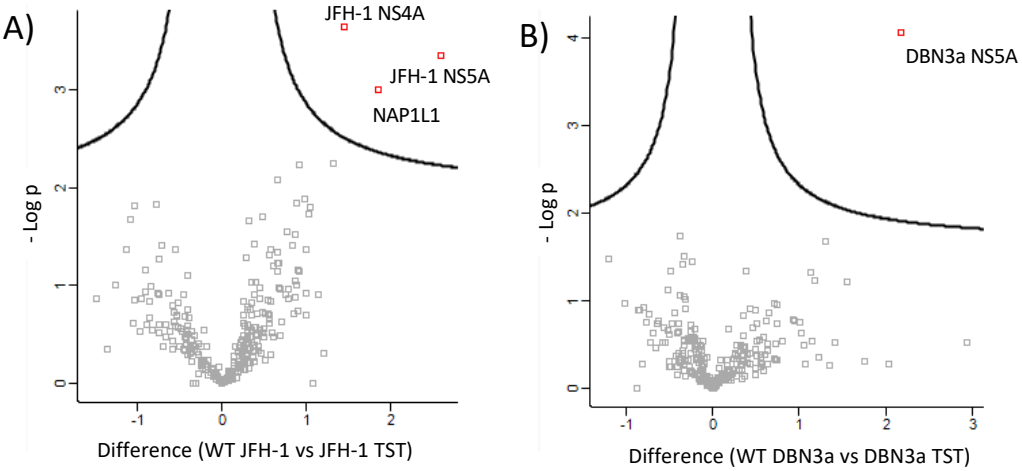

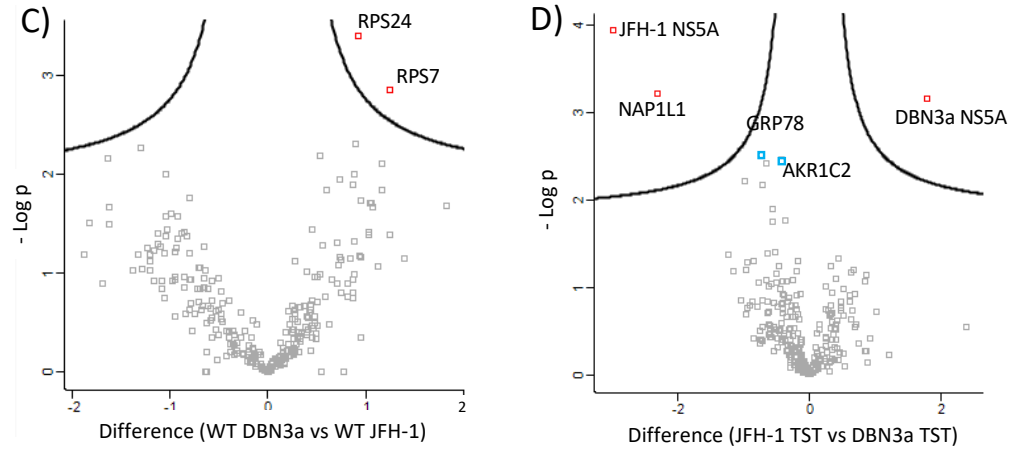

E)

Significant proteins	(A) JFH-1 TST– WT JFH-1	(B) DBN3a TST– WT DBN3a	(C) DBN3a TST – JFH-1 TST	(D) WT DBN3a – WT JFH-1
JFH-1 NS5A	X		X	
JFH-1 NS4A	X			
DBN3a NS5A		X	X	
Nucleosome Assembly Protein	X		X	
40S Ribosomal Protein S24				X
40S Ribosomal Protein S7				X

Figure 4.6 Volcano plot of NS5A interactions between JFH-1 and DBN3a.

Potential protein interactors were determined by LC-MS-MS analysis. To confirm protein interactions are specific, multiple samples were compared A) JFH-1 TST vs JFH-1 WT, B) DBN3a TST vs DBN3a WT, C) DBN3a TST vs JFH-1 TST D) WT DBN3a vs WT JFH-1. The x-axis represents the difference of protein expression between experimental groups. The y-axis outlines the abundance of the protein in the sample. Red signifies a protein in significance abundance. E) A summary table of protein defined as significantly different in abundance between samples. Black lines indicate q-value significances; p-value <0.05 defined as significant and -Log P defining variance between technical repeats.

Significant	-LOG(P-value)	Difference	Accession	Description	JFH-1 Average Abundance	DBN3a Average Abundance
++	3.949859	-2.9733228	JFH-1 Cleaved NS5A Tagged	JFH1_Cleaved_NS5A_Tagged	4.95380378	1.980481
++	3.214686	-2.3028491	P55209	Nucleosome assembly protein 1-like 1 OS=Homo sapiens OX=9606 GN=NAP1L1 PE=1 SV=1	1.97407952	-0.3287696
++	3.159318	1.79535182	DBN3a Cleaved NS5A Tagged	DBN3A_Cleaved_NS5A_Tagged	1.47461371	3.26996553
+	2.506537	-0.713574	P11021	Endoplasmic reticulum chaperone BiP OS=Homo sapiens OX=9606 GN=HSPA5 PE=1 SV=2	2.25136679	1.53779277
+	2.470161	-0.4068907	P52895	Aldo-keto reductase family 1 member C2 OS=Homo sapiens OX=9606 GN=AKR1C2 PE=1 SV=3	0.46005125	0.0531605
+	2.418328	-0.6454394	P11142	Heat shock cognate 71 kDa protein OS=Homo sapiens OX=9606 GN=HSPA8 PE=1 SV=1	4.51557267	3.87013322
+	2.220295	-0.9666161	P0DMV8	Heat shock 70 kDa protein 1A OS=Homo sapiens OX=9606 GN=HSPA1A PE=1 SV=1	-0.9983589	-1.964975
	2.172311	-0.703172	P30101	Protein disulfide-isomerase A3 OS=Homo sapiens OX=9606 GN=PDIA3 PE=1 SV=4	-0.1715905	-0.8747625
	1.899176	-0.5523272	P14618	Pyruvate kinase PKM OS=Homo sapiens OX=9606 GN=PKM PE=1 SV=4	1.87283948	1.32051232

Table 4.1 Differences between JFH-1 TST and DBN3a TST NS5A protein interactions.

NS5A protein interactions identified by LC-MS/MS. Protein abundance was calculated in Proteome Discover, the average of four experimental repeats is shown. Protein analysis was completed in Perseus where entries were filtered by having a minimum of 3 valid values in at least one condition. ++ signifies significance calculated by strict matrix analysis. + signifies significance calculated by relaxed matrix analysis.

4.2.5. Confirmation of NS5A proteomic analysis

To confirm the results of the proteomic analysis, the presence of NAP1L1 and GRP78 within our eluted samples was investigated. Primarily, expression levels of NAP1L1 and GRP78 were investigated in samples sent for proteomic analysis by utilising western blots confirming NS5A presence prior to sending samples (Figure 4.7 A). The membrane was re-probed with antibodies to the two proteins, NAP1L1 (dual band detected 52 and 60kDa) and GRP78 (78 kDa) both visualised in green. NS5A was previously probed and shown in red. Neither NAP1L1 nor GRP78 were detected in any elution samples, however, both were detected in all input samples. To determine if the presence of NAP1L1 and GRP78 was below the limit of western blot detection in the 10μl sample analysed, the remainder of the sample (30 μl) was also analysed by western blot (Figure 4.7 B) however, there was no detection of NAP1L1 or GRP78 in elution samples. As the positive control failed to indicate efficient antibody binding, it was undetermined whether NAP1L1 or GRP78 had a specific interaction with NS5A.

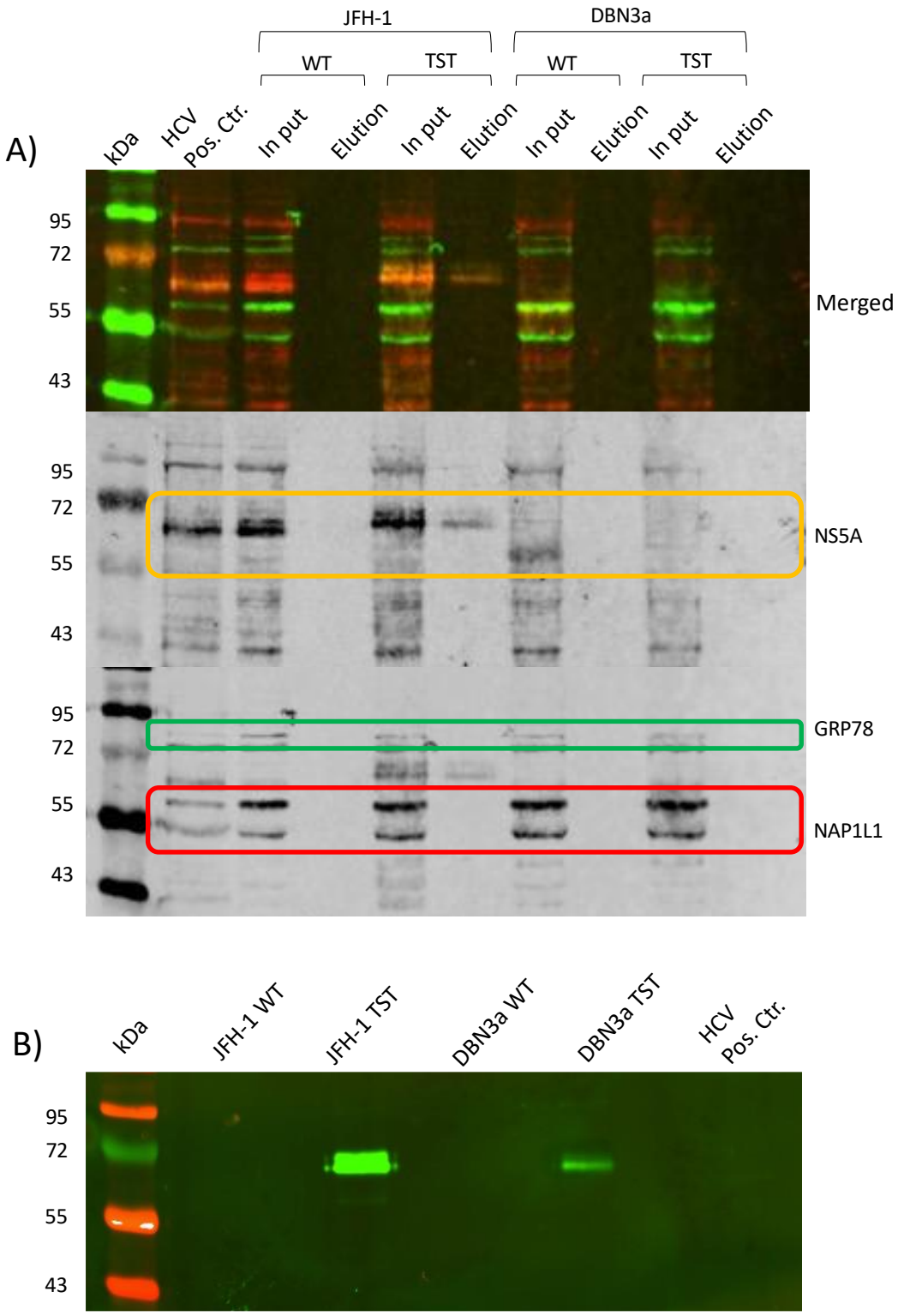

Figure 4.7 Confirmation of NAP1L1 interacting with HCV NS5A.

A) Western blot originally used to confirm protein samples prior to running LC-MS/MS analysis. Western was re-probed for NAP1L1 and GRP78. Input refers cell lysate that did not undergo immunoprecipitation. Elution refers to samples collected after immunoprecipitation. 10 µL of sample was visualised. B) Eluted samples for proteomics analysis was visualised on a western blot containing 30 µL elution.

As I was unable to detect NAP1L1 and GRP78 in elution samples of infectious virus, I hypothesised the potential interaction of NS5A JFH-1 to these host proteins may be dynamic during the virus life cycle. To test our hypothesis, immunoprecipitation of NS5A in JFH-1 and DBN3a was conducted in Huh7 cells stably expressing the SGR HCV (WT and TST clones). Huh7 cells expressing the WT and TST clones of JFH-1 and DBN3a were harvested and underwent immunoprecipitation via MagStrep “type 3” XT beads. All elution were analysed by western blot for the detection of NS5A, NAP1L1 and actin (Figure 4.8 A). Results are consistent with immunoprecipitations containing infectious virus. The elution of SGR HCV containing TST successfully immunoprecipitated NS5A however, did not contain NAP1L1, and all input samples contained NS5A and NAP1L1. These results suggest proteomic analysis is more sensitive in detecting protein expression in comparison to western blot analysis.

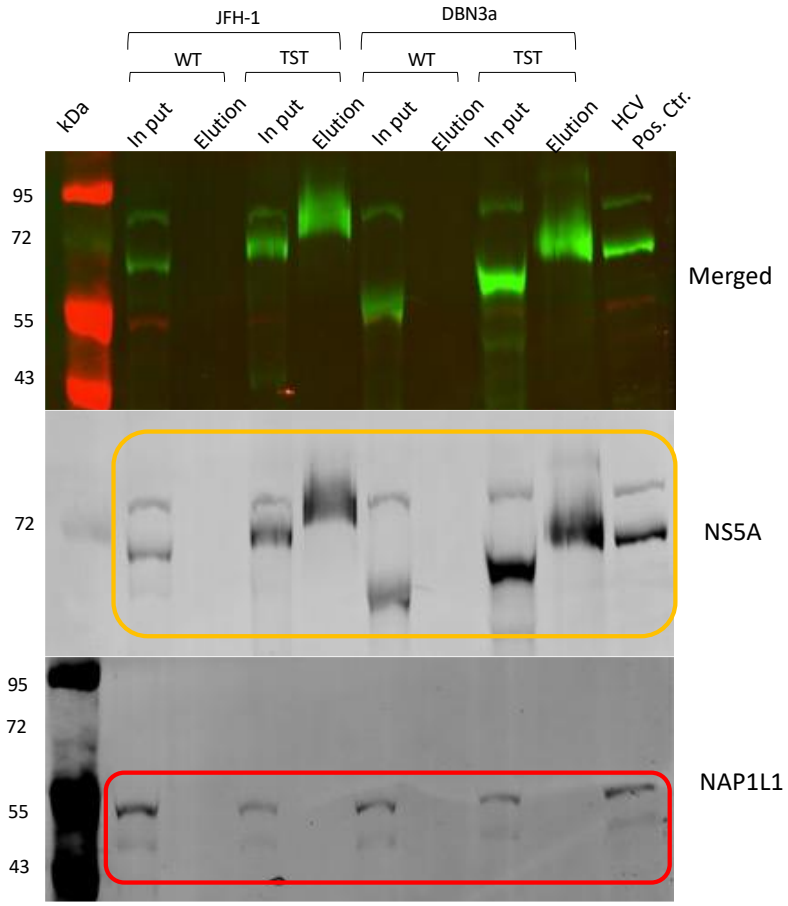

Figure 4.8 Comparing HCV NS5A NAP1L1 interaction in HCV SGR.

A) Huh7 cells stably expressing the HCV SGR. Cell lysates underwent immunoprecipitation completed using MagStrep “type 3” XT beads. Input refers cell lysate that did not undergo immunoprecipitation. Elution refers to samples collected after immunoprecipitation NS5A interactions were analysed by western blot and expression of NS5A and NAP1L1 visualised by the LI-COR Sa Odyssey.

4.2.6. Optimisation of siRNA silencing of NAP1L1 gene expression

As the interaction of NAP1L1 with NS5A of JFH-1 has been previously described (Goonawardane et al., 2017; Çevik et al., 2017), to further investigate the importance of NAP1L1, I initially used an siRNA approach to ablate NAP1L1 expression and determine the effect on replication of the two isolates. I expected a reduction of JFH-1 genome replication and infection of cells in the presence of reduced NAP1L1 expression. Contrary to JFH-1, I expected to see no change in DBN3a genome replication or infection in the presence of reduced NAP1L1 presence. Primarily, I focused on the optimisation of NAP1L1 siRNA silencing. Huh7 cells were transfected with a pool of siRNA targeting NAP1L1; transfection was completed using Lipofectamine 2000 or RNA iMax containing either 10 nM or 40 nM of siRNA in addition to varying the change in media 6 h post transfection. A negative control scrambled (Scr) RNA, comprising of a human non-targeting nucleotide sequence, distinguishes sequence-specific RNA silencing from non-specific effects. At 48 h post transfection, cells were visualised by IncuCyte S3 determining cell growth and harvested for western blot analysis to detect protein expression (Figure 4.9 A). Protein expression visualised by western blots detecting for NAP1L1 (52-60 kDa) and actin (45 kDa), were analysed by densitometry (Figure 4.9 B). NAP1L1 protein expression was normalised to the housekeeper control, actin, and compared to the NAP1L1 expression in the scrambled control of the same performed under the same transfection method. Results suggest adequate silencing of NAP1L1 when using Lipofectamine 2000. When changing media 6 h post transfection there was a 67% silencing of NAP1L1 using 10 nM siRNA, and there is suggestion of a greater silencing effect (72%) when transfecting 40 nM siRNA. The optimal condition of siRNA silencing was determined to be transfection of 10 nM siRNA without a media change (95% silencing). RNA iMax may provide greater silencing efficiency than Lipofectamine 2000 as both the 10 nM transfection and 40 nM transfection provides a greater silencing in comparison to Lipofectamine 2000 (10 nM – 89%, 40 nM – 87%. Contrary to Lipofectamine 2000, not changing the media post-transfection using RNA iMax appears to negatively impact siRNA expression as there was an 8%

reduction of gene expression in comparison to the scrambled control. To determine the health of the cells post-transfection, the confluency of cells was analysed by imaging the wells using the IncuCyte S3. For both Lipofectamine 2000 (Figure 4.9 C) and RNA iMax (Figure 4.9 D), there is suggestion the confluency of cells decrease when a higher amount of siRNA is transfected (10 nM vs 40 nM) and cell confluency appears to be greatly negatively affected when media is not changed post-transfection regardless of the transfection reagent used. In addition to this, the confluency of cells does not appear to be dependent on the siRNA or scrambled control groups suggesting changes in cell confluency is not dependent on the siRNA target. By using cell confluency as an indication of cell health in addition to protein expression analysis by densitometry, results suggest RNA iMax can silence cells more efficiently than Lipofectamine 2000 while maintaining healthy cell division.

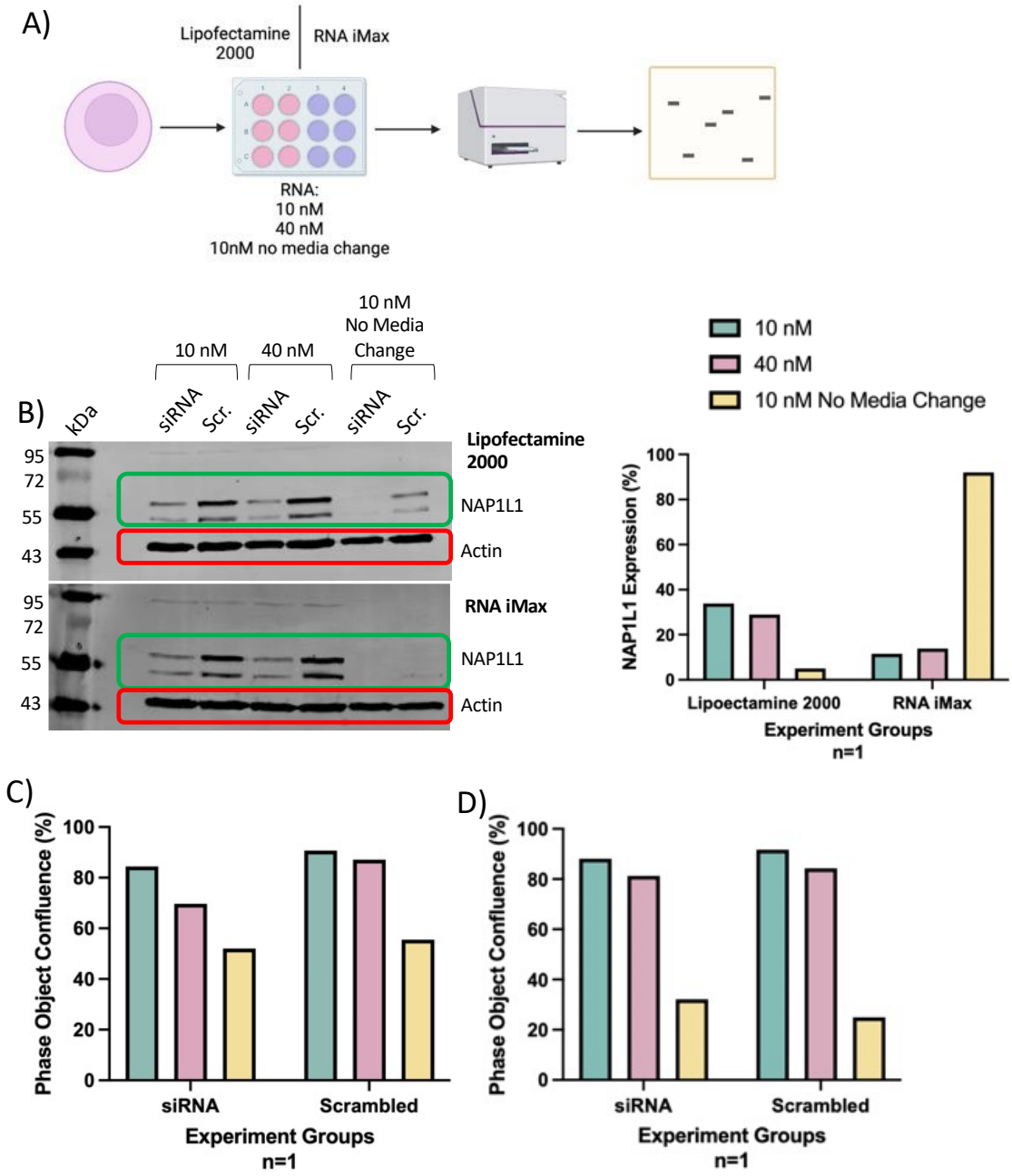

Figure 4.9 Optimisation of NAP1L1 siRNA silencing.

A) Schematic of siRNA silencing evaluation experiment. Cell lysates were collected for western blot analysis. B) Protein expression was visualised by western blot allowing densitometry analysis. Representative western blot visualised by the LI-COR Sa Odyssey and densitometry results normalising NAP1L1 (highlighted in green box of western blot) expression to actin (highlighted in red box of western blot), housekeeper control and compared to the corresponding scramble control of that experiment condition. Cell growth was analysed for the different transfection reagents used, C) Lipofectamine 2000 and D) RNA iMax.

4.2.7. NAP1L1 impact on HCV genome replication

Evaluation of previous literature suggests contradictory requirements of NAP1L1 for efficient HCV genome replication (Goonawardane et al., 2017; Çevik et al., 2017). To investigate the requirement of NAP1L1 interacting with HCV proteins for genome replication, Huh7 cells stably harbouring the SGR of JFH-1 or DBN3a were transfected with siRNA targeting NAP1L1 mRNA. 48 h post transfection, cells were harvested (Figure 4.10 A), and RNA expression was analysed via qRT-PCR (Figure 4.10) and protein expression analysed via western blot (Figure 4.11). RNA levels of NAP1L1 and HCV 5'UTR suggests marginal silencing of NAP1L1 in all cell types 48 h post transfection (mock – 35%, SGR JFH-1 – 25%, SGR DBN3a – 32%). To account for the normalisation of gene expression by the housekeeper gene, HPRT1, HCV 5'UTR abundance of mock was normalised to JFH-1 (Figure 4.10 C) and DBN3a (Figure 4.10 D), demonstrating mock Huh7 cells were not contaminated with the HCV genome. Despite NAP1L1 mRNA showing moderate silencing, there was no change in HCV genome replication, based on the presence of the HCV 5'UTR RNA (SGR JFH-1 – 97% and SGR DBN3a – 111%).

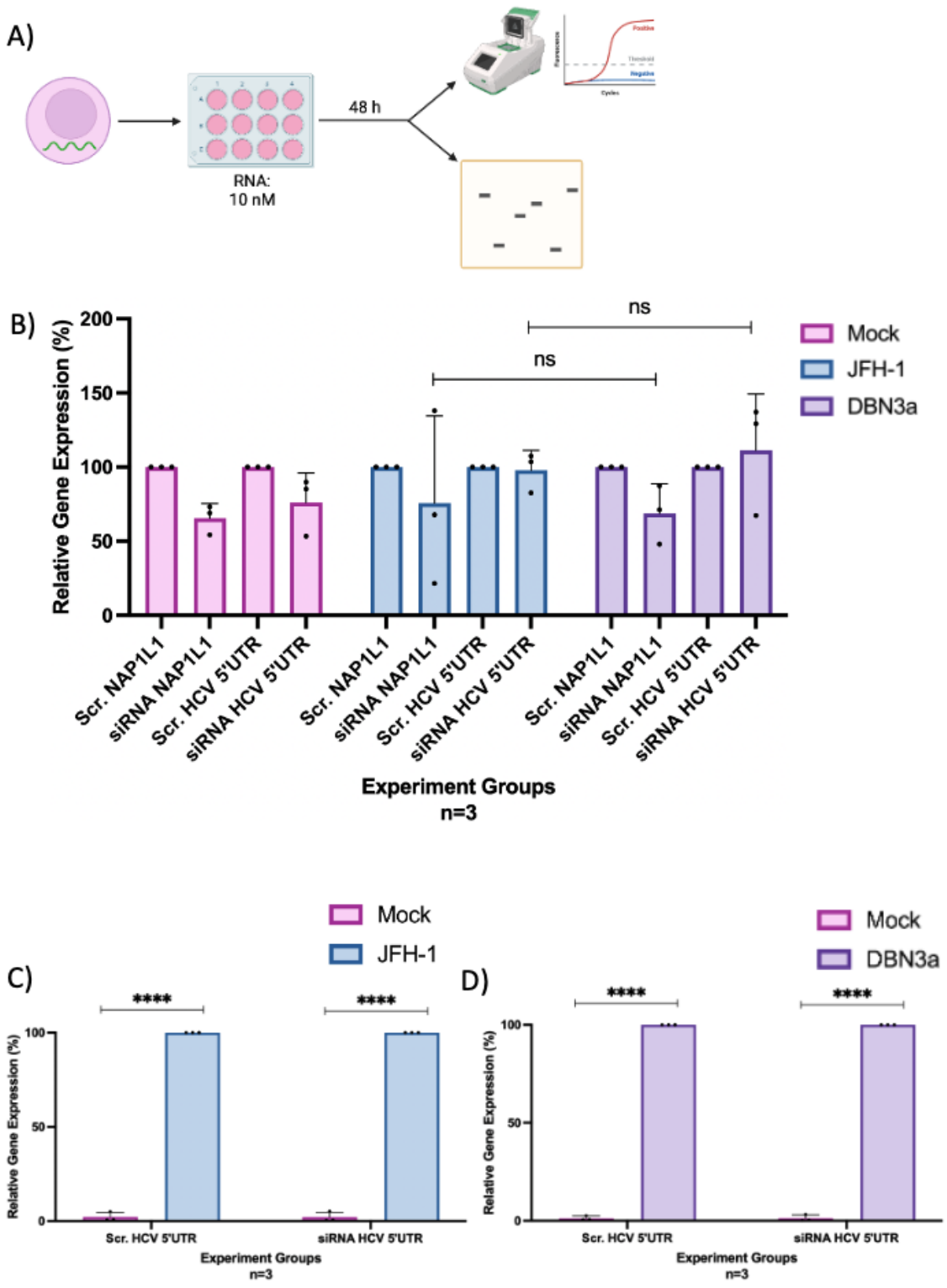

Figure 4.10 SiRNA silencing of NAP1L1 effect on HCV SGR NS5A RNA expression.

A) Schematic of sample collection. B) Relative gene expression of NAP1L1 and HCV 5'UTR normalised to the housekeeper control gene, HPRT1. Gene expression of mock HCV 5'UTR normalised to C) JFH-1 and D) DBN3a. Data presented as mean with standard deviation. Statistical significance was tested by one-way ANOVA with the Bonferroni's multiple comparison test, with a single pooled variance. P values; ns, P ≥0.05; ****, P <0.00005.

To determine if the mRNA silencing of NAP1L1 alters the expression of the functional unit, protein levels were analysed. Western blots detecting NS5A, NAP1L1 and actin were visualised, and densitometry analysis was performed normalising the expression of both NS5A and NAP1L1 to housekeeper control protein, actin (Figure 4.11 A). Comparison of NAP1L1 silencing demonstrates a reduction of NAP1L1 in mock (61%), SGR JFH-1 (78%) and SGR DBN3a (87%). Despite a reduction of NAP1L1 protein expression, there is a reduction of NS5A expression in SGR JFH-1, an average of 15%, however this is not significant. There appears to be no reduction of NS5A expression within SGR DBN3a, maintaining 103% NS5A expression level in comparison to the scramble control. To determine if NAP1L1 is silenced in the HCV SGR stable cell line, relative expression of NAP1L1 was analysed by western blot and densitometry analysis of the scramble controls (Figure 4.11 B). There is no significant difference in NAP1L1 expression between cell lines during siRNA scrambled transfection. These results suggest the possible interaction of NAP1L1 with the SGR JFH-1 and SGR DBN3a does not significantly contribute to efficient HCV genome replication within GT2 and 3.

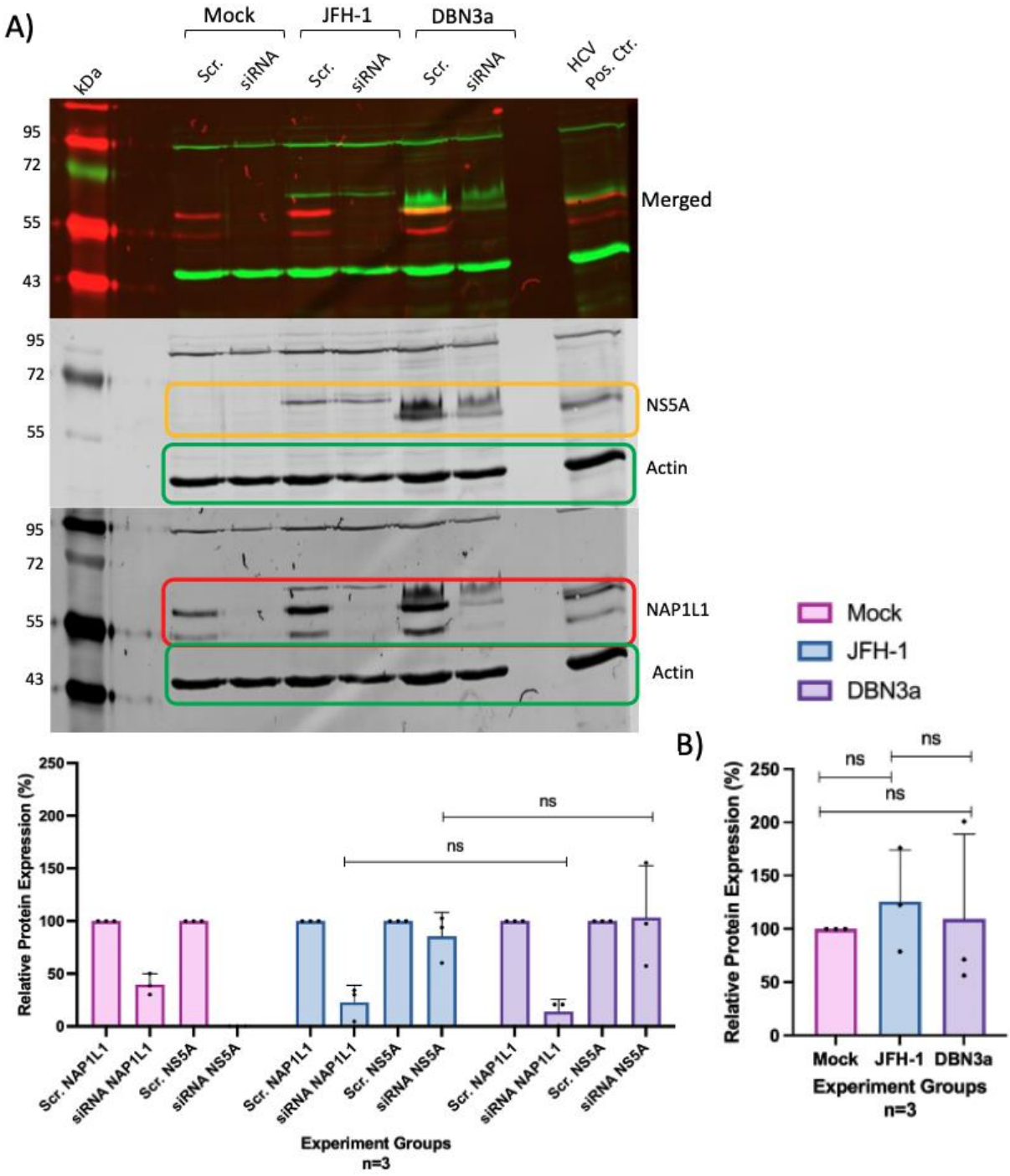

Figure 4.11 SiRNA of NAP1L1 effect on HCV SGR NS5A protein expression.

A) Representative image of western blot and densitometry results normalising NAP1L1 and NS5A expression to housekeeper control, actin and scrambled control samples. B) Expression of NAP1L1 within scrambled controls normalised to Huh7 mock cell line. Data presented as mean with standard deviation. Statistical significance was tested by one-way ANOVA with the Bonferroni's multiple comparison test, with a single pooled variance. P values; ns, P ≥0.05.

4.2.8. NAP1L1 expression may be required for efficient HCV infection

As the expression of NAP1L1 was not required for HCV SGR genome replication, the requirement for NAP1L1 expression during HCV infection was investigated. Huh7 cells were transfected with siRNA specifically targeting the mRNA of NAP1L1, 48 h post transfection, Huh7 cells were infected with HCV (MOI 0.2) prior to harvesting cells for RNA and protein expression analysis (Figure 4.12 A). RNA expression suggests NAP1L1 mRNA expression was increased when normalised to the housekeeper control, HPRT1, and scrambled expression; Mock – 47% overexpressed, JFH-1 – 32% overexpressed, DBN3a – 25% overexpressed. The expression of the HCV 5'UTR, used as a marker for viral genome expression, appears not to be affected by the overexpression of NAP1L1 with the average expression of HCV 5'UTR like the scramble control (JFH-1 – 2% over expressed, DBN3a – 0.5% reduced expression (Figure 4.12 B)). To confirm mock cells were not contaminated with HCV, mock HCV 5'UTR gene expression was normalised to the HCV 5'UTR expression of JFH-1 (Figure 4.12 C) and DBN3a (Figure 4.12 D).

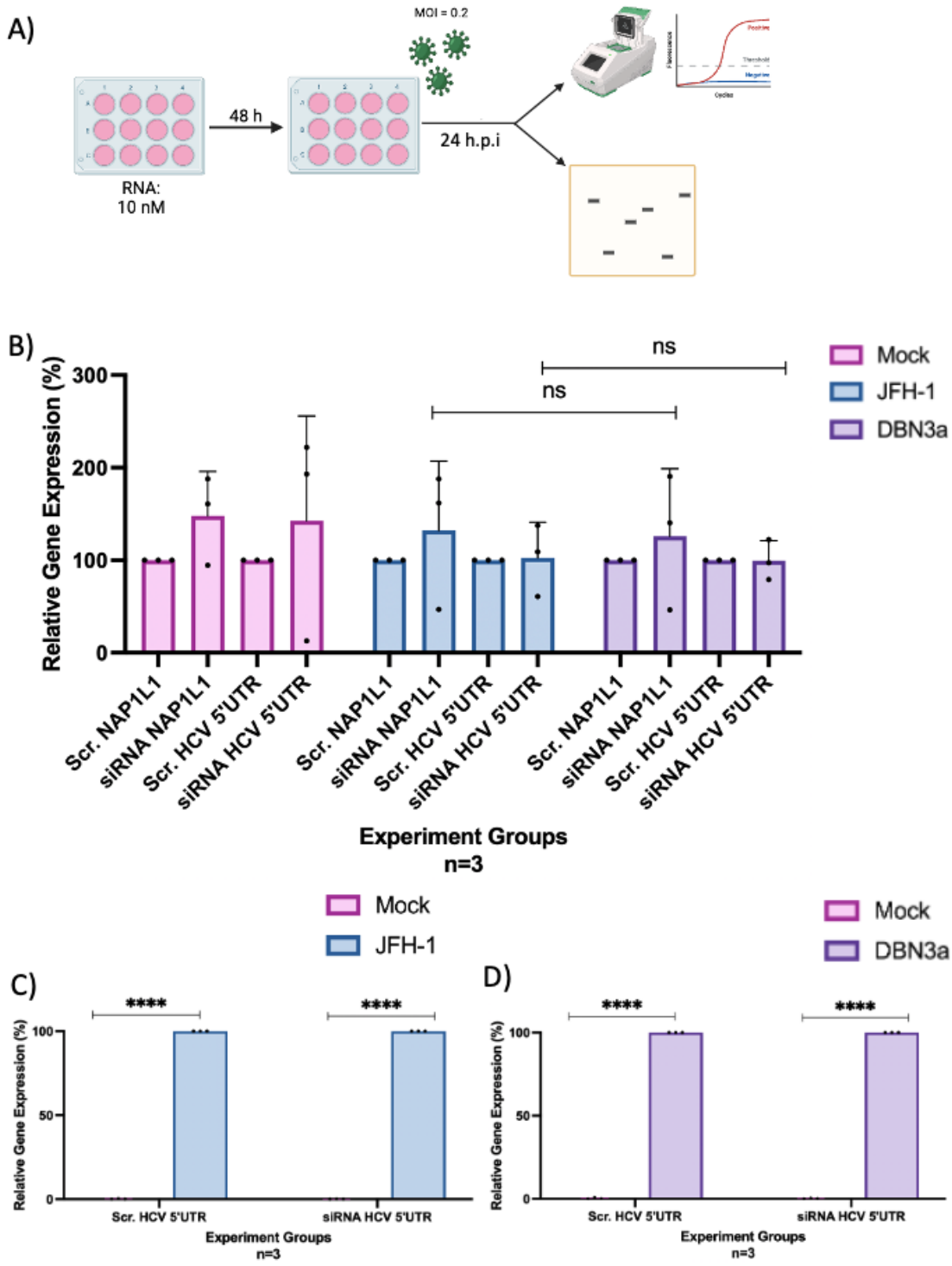

Figure 4.12 SiRNA silencing of NAP1L1 effect on infectious HCV NS5A RNA expression.

A) Schematic of sample collection. B) Relative gene expression of NAP1L1 and HCV 5'UTR normalised to the housekeeper control gene, HPRT1. Gene expression of mock HCV 5'UTR normalised to C) JFH-1 and D) DBN3a. Data presented as mean with standard deviation. Statistical significance was tested by one-way ANOVA with the Bonferroni's multiple comparison test, with a single pooled variance. P values; ns, P ≥0.05; ****, P <0.00005.

As RNA expression levels of NAP1L1 was not silenced 72 h post transfection, it was important to determine if protein expression was reduced. Western blots detecting NS5A, NAP1L1 and actin were visualised, and densitometry analysis was performed normalising the expression of both NS5A and NAP1L1 to housekeeper control protein, actin (Figure 4.13 A). Despite no reduction of NAP1L1 gene expression 72 h post transfection, comparison of NAP1L1 protein expression to the scrambled control demonstrates silencing of NAP1L1 in mock (75%), JFH-1 (44%) and DBN3a (44%). Results also indicate a reduction of HCV NS5A protein expression in both JFH-1 (63%) and DBN3a (57%) when NAP1L1 expression is reduced. To determine if NAP1L1 is expression is reduced during HCV infection, without the use of siRNA, relative expression of NAP1L1 was analysed by western blot and densitometry analysis of the scramble controls (Figure 4.13 B). There is a general trend of NAP1L1 expression being reduced during HCV infection. These results suggest NAP1L1 expression may play a partial role in HCV infection of both JFH-1 and DBN3a.

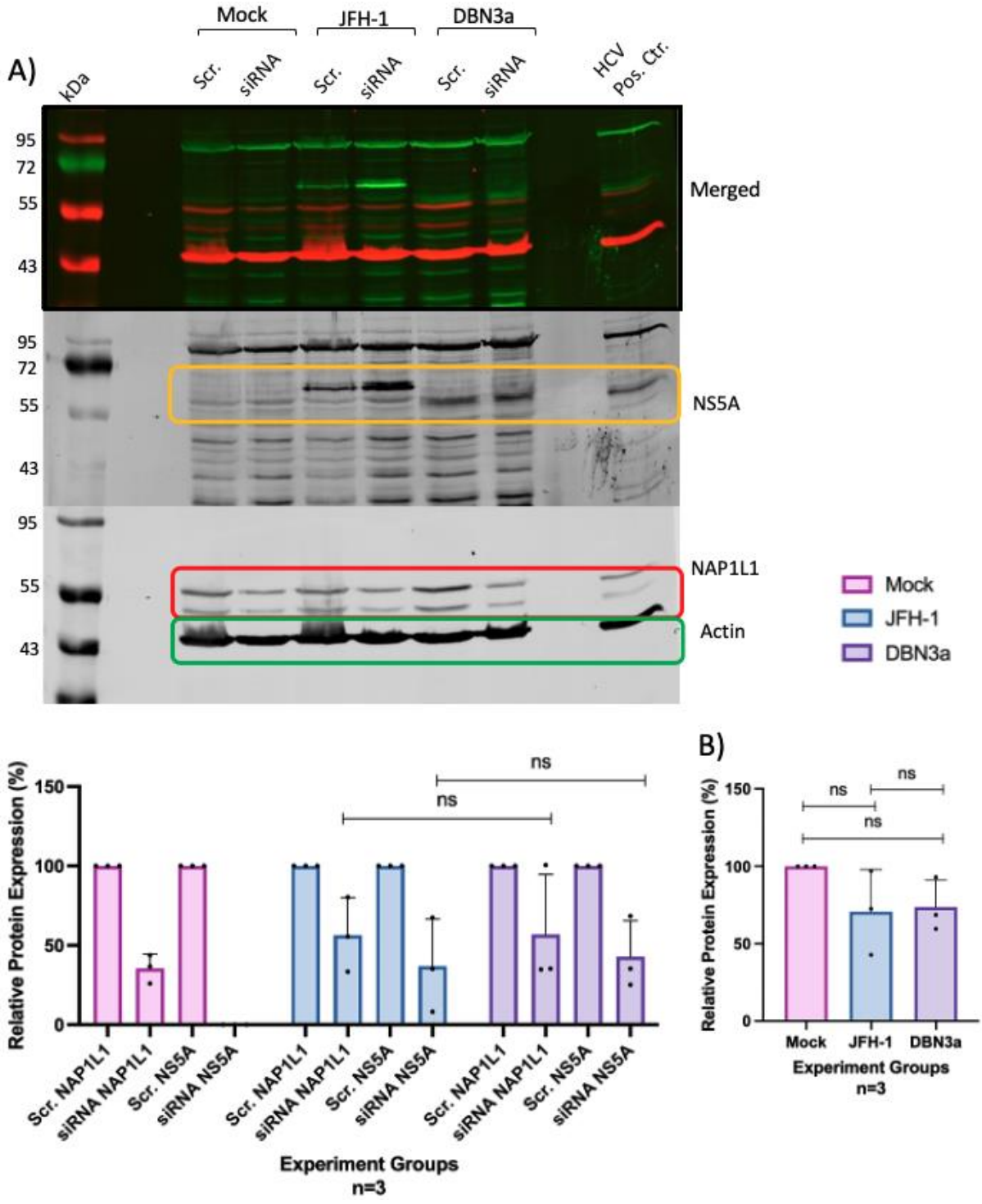

Figure 4.13 SiRNA of NAP1L1 effect on HCV NS5A protein expression by infectious clones.

Representative image of western blot and densitometry results normalising NAP1L1 and NS5A expression to housekeeper control, actin and scrambled control samples. B) Expression of NAP1L1 within scrambled controls normalised to Huh7 mock cell line. Data presented as mean with standard deviation. Data presented as mean with standard deviation. Statistical significance was tested by one-way ANOVA with the Bonferroni's multiple comparison test, with a single pooled variance. P values; ns, P ≥0.05.

4.2.9. SiRNA transfection results to autofluorescence of Huh7 cells

Optimisation of NAP1L1 silencing in Huh7 cells allows greater investigation of NAP1L1s effect on HCV infection and genome replication. As well as analysing HCV genome replication by qRT-PCR detecting HCV 5'UTR and NS5A presence by western blot, it was also possible to quantify the number of NS5A positive cells by staining infected Huh7 cells with sheep anti-NS5A allowing visualisation and analysis via IncuCyte S3. However, post siRNA transfection and HCV infection, quantification of mock and NS5A-positive cells showed increased levels of cell auto-fluorescence (Figure 4.14). Representative images demonstrate the IncuCyte S3 software inability to decipher non-infected cells from NS5A positive cells; almost all cells are identified as positive in both mock and HCV infected samples. As a result of this, a comparison of NS5A positive cells between siRNA and scrambled control groups was not conducted.

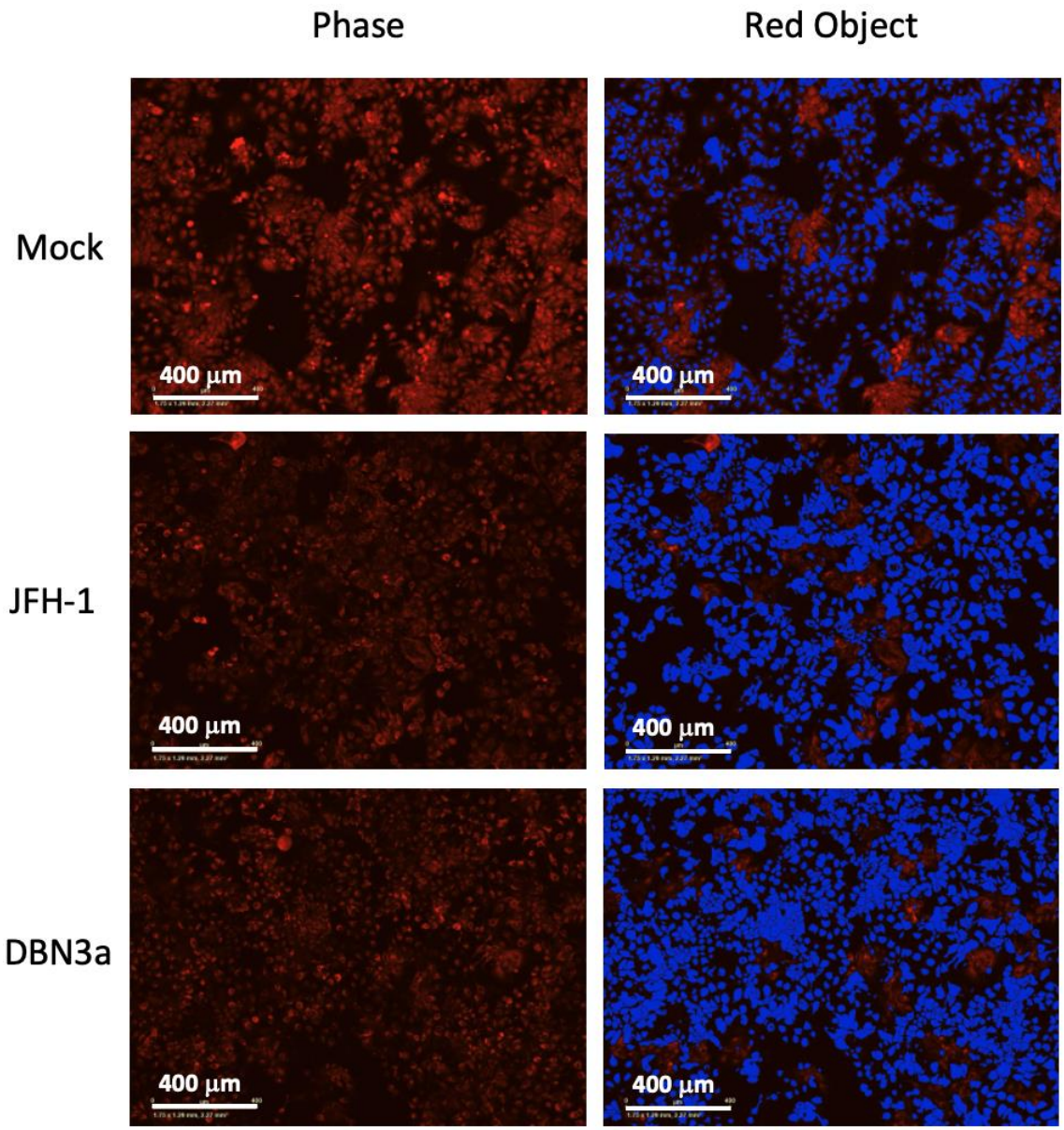

Figure 4.14 Auto-fluorescence of cells post siRNA transfection.

Huh7 cells expressing HCV SGR 48 hours post transfection were stained with sheep anti-NS5A and visualised by IncuCyte S3. Raw images and images depicting red objects counted by "high background" analysis parameters. Images were taken at 10 x magnification and scale bars = 400 microns.

4.2.10. Phosphorylation status of NS5A varies between HCV cell models

These results have suggested NAP1L1 does not contribute to HCV genome replication however, does contribute to the HCV infectious life cycle. This was tested using two different HCV cell models; Huh7 cell line stably expressing HCV SGR and infecting Huh7 cells with infectious clones. It has been previously published the phosphorylation status of NS5A plays a crucial role in NS5A interacting with host proteins, interactions may only occur in the presence of a particular phosphorylated state of NS5A (Chong et al., 2016; Evans et al., 2004; Goonawardane et al., 2017). To investigate if the phosphorylation status of NS5 within JFH-1 and DBN3a differs in different HCV models, NS5A protein expression was analysed by western blot from different HCV cell models; Huh7 harbouring a stable SGR or infected with HCV (MOI 0.2) harvested 72 h.p.i (Figure 4.15). Expression of NS5A within the SGR suggests both JFH-1 and DBN3a present a hyper- and hypo- phosphorylated form of NS5A based on the presence of a 56 kDa and 58 kDa protein band (Figure 4.15 A). Interestingly, in the presence of HCV structural proteins, there appears to be no hyperphosphorylated form of NS5A (58 kDa) in DBN3a, confirmed by probing the western blot with anti-S225. This does not occur during JFH-1 infection which exhibits both phosphorylation forms (Figure 4.15 B). These results suggest there may be a different abundance of host and NS5A protein interactions depending on the HCV cell model investigated.

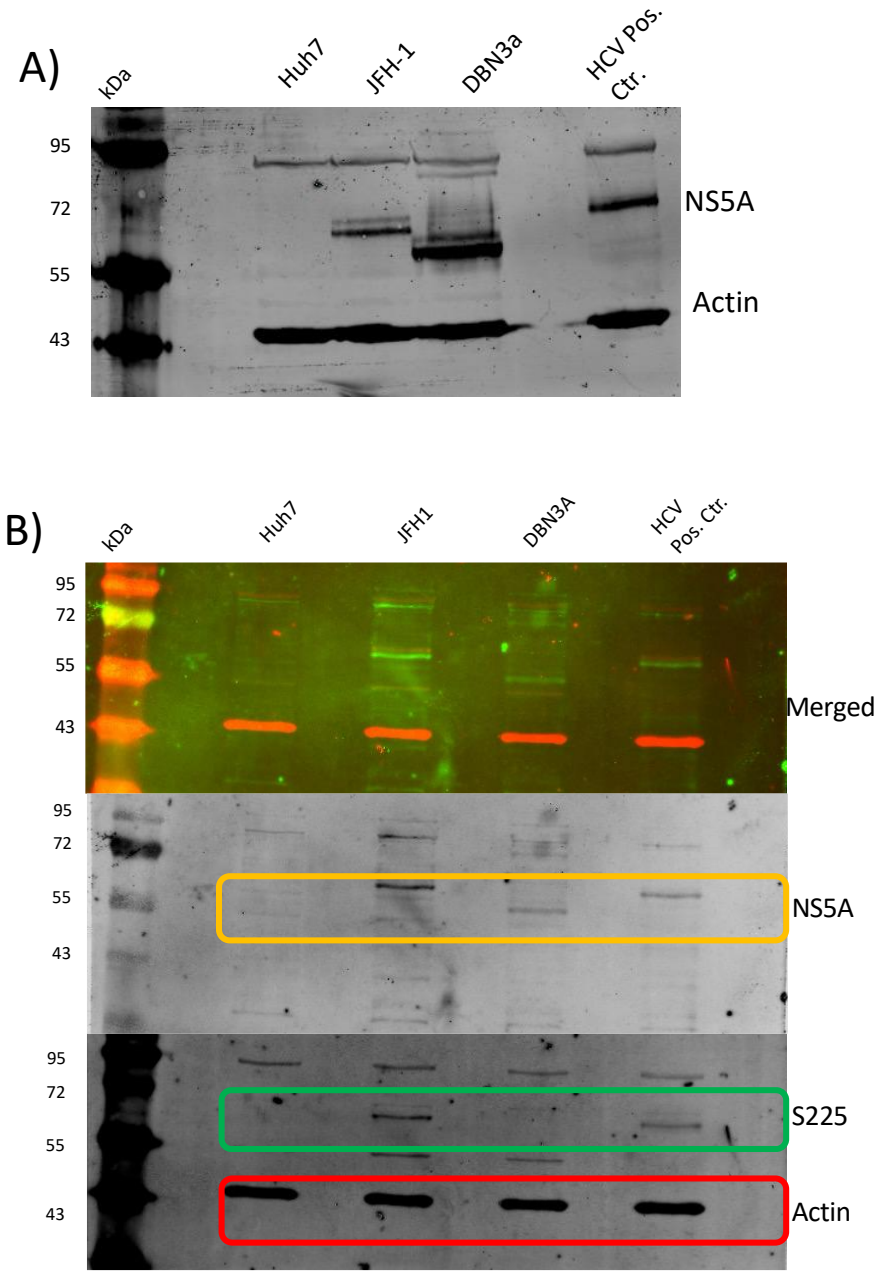

Figure 4.15 NS5A phosphorylation status of HCV in SGR stable cell line and infectious virus models.

A) Huh7 cells either stable expressing the SGR expression of NS5A and actin. B) Huh7 cells were infected with either JFH-1 or DBN3a infectious virus. Cell lysates were collected 72 h.p.i. Cell lysates were analysed by western blot detected for NS5A, S225 and actin. Western blots visualised by the LI-COR Sa Odyssey.

4.3. Discussion

This chapter aimed to describe the optimisation of HCV immunoprecipitation assay to aid downstream proteomic analysis to define differences in HCV JFH-1 and DBN3a NS5A interactions with the host proteome. Experiments investigating the interaction of NAP1L1 to NS5A of JFH-1 and DBN3a in both the SGR and infectious virus clones suggests a role of NAP1L1 required for efficient virus infection. The phosphorylation status of NS5A appears to be dependent on the HCV cell model and GT investigated further alluding to differences between HCV GTs and mechanisms of disease pathology.

4.3.1. Optimisation of immunoprecipitation

To investigate NS5A's interactions with host proteins, immunoprecipitation assays primarily utilising sepharose suspension beads were completed 72 h.p.e (Figure 4.1). Cells were harvested 72 h.p.e to reduce cell culture artefacts introduced once cells become too confluent. Initial pulldown attempts suggested a poor concentration of NS5A in the final elution. To increase the concentration of NS5A collected, higher concentrations of the viral genome were electroporated into Huh7 cells (Figure 4.2). As the concentration of NS5A within cell lysates and virus titre did not increase as a greater amount of viral genome was electroporated, this suggests that 5 μg of *in vitro* transcribed RNA may saturate the Huh7 cells therefore, electroporating more RNA would not be of utility. As the amount of RNA electroporated into the cells increased, the expression of the reporter gene increased as well as a reduction in cell viability measured by Hoechst staining. I was unable to confirm in the results the status of cell viability limiting genome replication and virus production as these outputs were not measured.

As I was unable to increase the expression of NS5A in cell lysates, I could not increase the amount NS5A harvested by sepharose suspension beads. As such, MagStep "type 3" XT

beads were tested (Figure 4.3). I believed this would provide a greater concentration of NS5A in the final elution due to magnetic beads acquiring a higher binding capacity than agarose only beads which have a porous centre and are typically larger (40-150 μm) in diameter. A porous centre results to the possibility of antibody within the structure and not accessible to the target protein. If the agarose bead is not entirely coated there is a greater risk of non-specific binding of lysate binding to unsaturated portions of beads. Magnetic beads do not have a porous centre ensuring antibody binding occurs only on the outer surface and the small diameter (1-4 μm) provides greater surface area allowing a higher binding capacity. Removal of centrifugation during wash steps and reduction of incubation times reduces the risk of losing bound materials, such as different protein complexes, or breaking of weak antibody-antigen binding (Jensen et al., 2021).

Optimisation of the immunoprecipitation using the MagStep ”type 3” XT beads was required as the negative control sample JFH-1 WT was present in the final elution (Figure 4.3 A). This suggested possible contamination of samples or non-specific binding. To reduce non-specific binding, beads were pre-blocked with lysis buffer prior to the addition of the cell lysate and a high salt wash was introduced after the incubation of cell lysate with the beads to remove bound non-specific hydrophilic proteins. However, the introduction of a high salt wash may increase the risk of losing all but the strongest protein interactions. Additionally, beads were transferred to a new Eppendorf during the last wash step to remove unspecific binding of proteins to the tube which may result in carry-over contamination. The optimised protocol removed WT NS5A presence in eluted samples when visualised by western blot (Figure 4.3 B).

It is important to note, electroporation of *in vitro* transcribed RNA was utilised to produce HCV cell lysates instead of virus infection, as Chapter 3 results indicate the ability of JFH-1 to infect cells is significantly less than DBN3a. To harvest an adequate amount of NS5A to allow an efficient pulldown required for proteomic analysis, 1 x 10^7 cells were electroporated per technical repeat. Electroporation ensures the same number of cells express the RNA genome

of JFH-1 and DBN3a, thus is easier to achieve than producing enough virus to infect a large number of Huh7 cells with a high MOI, in particular the production of JFH-1 virus. By 72 h.p.e all newly divided post electroporation cells become naturally infected by HCV mimicking a natural infection cycle however, potential variation in protein expression as a result of stress introduced by electroporating cells was not investigated.

4.3.2. Proteomic analysis suggests little differences between JFH-1 and DBN3a NS5A to host protein interactions

LS-MS/MS proteomic analysis was performed after confirmation of NS5A's presence in only JFH-1/DBN3a TST containing eluted samples (Figure 4.4). Despite the abundance of NS5A differing between the JFH-1 and DBN3a elutions, as shown by varying band intensity (Figure 4.4), the protein abundances do not change significantly between samples, and therefore would expect to see an even distribution of protein intensities (Figure 4.5). Normalisation and scaling are more challenging in pulldown experiments as the background proteome has been depleted. As the median of each sample is the same post-normalisation, the pre-normalised data has been exported out of the proteome discoverer and further analysis was conducted in Perseus.

Six proteins significantly different in abundance via cross-comparison analysis (Figure 4.6). By comparing TST samples to WT, I can confirm protein interactions within the TST samples are not the result of background binding. Strict analysis parameters were presented to highlight the most biologically relevant protein interaction comparisons between JFH-1 and DBN3a. However, it was surprising to see very few protein interactions differing between the two GTs. When I compare our JFH-1 WT and TST results previous proteomic analysis performed by Goonawardane *et al.* (2017) and Smirnov *et al.* (2023), only NAP1L1 is identified as being significantly different across all studies. I believe protein interactions were not identified as significant in our study due to high background noise within the WT control samples by TMT labelling. Contrary to the Smirnov *et al.* (2023), I used the JFH-1 WT sample as a control sample

instead of a TST only sample. It is possible I see more interactors in our control sample as NS5A could be a “sticky” protein with more non-specific interactions.

TMT labelling allows for robust comparisons of protein levels between samples, particularly when comparing multiple samples or conditions as samples are pooled prior to subsequent fractionalisation and LC-MS/MS analysis. This removes run-to-run variation which can be problematic in label-free protein analysis (Zecha et al., 2018). However, I believe results from our proteomic analysis may have resulted in notably few protein interactions as TMT labelling may result in “bleed through” between samples which can result to the inability to detect if a protein is completely absent in one sample and present in another. TMT labelling is not a problem if showing a strong enrichment in the bait protein in comparison to the control (Christoforou & Lilley, 2012). In our case, this is specific to comparing WT samples to TST samples. In our results there are only 1 or 3 proteins noted as being significantly expressed in the TST samples when compared to WT (Figure 4.6 A, B). Despite western blots showing no contamination of NS5A within WT samples, however, LC/MS-MS analysis is much more sensitive to the detection of proteins of low abundance in comparison to western blot. Despite the low amount of significant protein hits in our results, the identification of any significant protein, such as NAP1L1, or close to significant proteins, such as GRP78 and AKR1C2, using stringent analysis parameters provides greater confidence.

NAP1L1 is described as the human homolog of the yeast nucleosome assembly protein, involved in multiple pathways of the host cell as a regulation of transcription, cell cycle progression and a histone-binding factor involved in the nucleosome formation. Playing a role in the promotion of several tumours, such as colorectal cancer (Queiroz et al., 2020), renal cancer (Zhai et al., 2018), ovarian cancer (Xiaohua Zhu et al., 2022) and in particular relation to this project HCC. Zhang *et al.* (2021) describes NAP1L1 functions as a tumour promoter of HCC by recruiting hepatoma-derived growth factor (HDGF) allowing interaction with c-Jun, an oncogenic transcription factor inducing cell cycle factors and promoting cell growth in HCC.

However, how this pathway may be promoted or altered during HCV infection was not described. Specific to the presence of HCV, NAP1L1 has been described as a regulator of HCV entry by regulating the expression of scavenger receptor, class B type 1 (SR-B1) (Yin et al., 2018). Interaction of NAP1L1 to NS3 has been demonstrated by Yin *et al.* (2018) however, the function has not been fully characterised. Contrary to this, the interaction of NAP1L1 to NS5A has been characterised as beneficial to the HCV lifecycle. Goonawardane *et al.* (2017) demonstrates NAP1L1-NS5A is required for the regulation of genome replication and the subcellular localisation of replication complexes. Çevik *et al.* (2017) describes the interaction as a modulatory mechanism of HCV controlling the host cell environment by retaining NAP1L1 in the cytoplasm, inhibiting nuclear chromatin remodelling. Furthermore, depletion of NAP1L1 disrupts the innate immune response leading to inefficient RIG-1 and Toll-like receptor 3 (TLR3) responses which is advantageous to the HCV life cycle. Differences between NAP1L1 interactions with HCV also differs across GTs, Çevik *et al.* (2017) demonstrates only GT2, and not GT1, as capable of targeting NAP1L1 for proteosome-mediated degradation. NAP1L1 interactions to HCV NS5A has been described predominately for JFH-1 using both the SGR and infectious clones, interaction to DBN3a NS5A has not been described or investigated. Yin *et al.* (2018) suggests NAP1L1 is not required once HCV replication has been established. It may be hypothesised DBN3a does not appear to interact with NAP1L1, based on our proteomic data, as the interaction may be dynamic at a particular point of the virus lifecycle, for example at the early stages of virus infection of a host cell.

Glucose regulated protein 78 kDa (GRP78) is an immunoglobin heavy chain binding protein member of the Heat Shock Protein 70 (HSP70). Expression is directly linked to cell stress primarily by the unfolded protein response (UPR) within the endoplasmic reticulum that may be exploited by pathogens (fungal, bacterial or viral) to enter the cell and trigger pathways contributing to pathogenesis (Ibrahim et al., 2019). Overexpression of GRP78 is associated with increased aggressiveness of cancer; playing a role in proliferation, invasion and metastasis

(Wang et al., 2009). Entry of HCV utilising GRP78 has been supported by Elshemey *et al.* (2023), through mathematical modelling demonstrating the possible binding mode of HCV E2 via the cyclic peptide Pep42, thought to target GRP74. GRP78 intracellular action within a host cells as also been described during HCV infection, Wei *et al* (2016) describes how GRP78 contributes to the regulation of TLR3, triggering the interferon regulatory factor-3 (IRF3) innate immune response to HCV through expression mass spectrometry and gene silencing experiments of Huh7.5 cells infected by JFH-1. Further manipulation of the host cell environment and immune response is supported by Sir *et al.* (2008), Sekine-Osajima *et al.* (2008) and Jiang *et al.* (2014), GRP78 expression is enhanced during HCV JFH-1 infection. This was described as a mechanism, regulated by NS5A, to inhibit the triggering of apoptosis pathways to promote HCV-infected cell survival to establish a persistent infection.

Interaction of JFH-1 NS5A to AKR1C2 is particularly interesting as the interaction has not previously been directly linked to HCV infection, only increased during HCC. AKR1C2 is part of a family of enzymes utilised in steroid metabolism. Changes to expression levels has been associated with several human tumours. Increased expression has been observed in many cancers associated with favourable prognostic factors partially due to AKR1C2 role in drug metabolism and toxin detoxification; esophageal squamous cell carcinoma, breast cancer and prostate cancer (Ji et al., 2003; W. Li et al., 2016; Mindnich & Penning, 2009). However, increased expression of AKR1C2 during HCC has been proved as a regulator promoting metastasis contributing to AKR1C2 role as a biomarker for the disease (Li et al., 2014; C. Li et al., 2016; Zhao et al., 2019). Publications focus on database mining, comparing protein and gene expressions of different cancer types, with no evidence suggesting the role of AKR1C2 during HCV infection of any GT. Walker *et al.* (2018) conducted a comprehensive literature search with specific focus for HCC patients infected with HCV. AKR1C2 increased expression was described as an association with HCC of HCV infected patients, however, genotypes classification of patient samples was not noted. As such, this is a crucial area to be explored. Our data demonstrates

JFH-1 NS5A interacts with AKR1C2 suggesting upregulation of AKR1C2 of HCC patients infected by HCV may not be a signature of HCC but as a direct implication of HCV infection.

4.3.2.1. Confirmation of proteomic results

To confirm the results of the proteomic analysis, the presence of NAP1L1 and GRP78 were investigated in immunoprecipitation samples (Figure 4.7). Confirmation of NAP1L1 and GRP78 presence on western blots used to confirm NS5A prior to LC-MS/MS analysis, would allow direct confirmatory results on proteomic analysis. All input samples confirmed the presence of both GRP78 and NAP1L1 proteins in the cell lysates, however, not present in the eluted sample. As the western blot was re-probed 4 months after initial analysis for NS5A detection and produced with a quarter of the elute sample, this may suggest non-optimal conditions for detecting a possibly low abundant protein interaction (Figure 4.7 A). To continue the direct confirmation of cell lysates to proteomic results, a technical repeat of the eluted samples not sent for LC-MS/MS analysis was analysed by western blot with 30 μL of sample loaded onto the SDS-PAGE (Figure 4.7 B). I hypothesised by loading a greater amount of sample, there would be a greater abundance of low interacting proteins and optimal conditions for antibody binding to a freshly produced western blot. Eluted TST samples confirmed the presence of NS5A on the western blot, despite a larger volume of elute loaded, NAP1L1 nor GRP78 was not detected. Unfortunately, the positive control for this western did not confirm the presence of NS5A, NAP1L1 or GRP78. This may be due to protein degradation by poor sample storage or continual freeze thaw cycles. A phenomenon known as “freeze concentration” can cause significant stress on the stability of a protein (Bhatnagar et al., 2007).

To determine if the presence of NAP1L1 and GRP78 in immunoprecipitation elutes was limited by the abundance of protein interactions, a pulldown of NS5A was conducted using the established HCV SGR stable cell line (Figure 4.8). I believed there would be a greater abundance of NAP1L1 and GRP78 interactions as all Huh7 cells are simultaneously expressing the HCV

genome. However, results mimicked that of the virus re-probed western blot; detection of NAP1L1 in the cell lysate (input) but not in the eluted sample. Our data suggests the interaction of NAP1L1 to NS5A JFH-1 may be a weak or transient interaction. Transient and weak protein interactions may be investigated by crosslinking which results to the stabilisation of protein interactions. A membrane permeable crosslinker, such as disuccinimidyl suberate (Pilch & Czech, 1979), may be used to stabilise intracellular protein interactions which can then be analysed by immunoprecipitation and western blot. As HCV is an obligate intracellular pathogen hijacking the host cell machinery, transient interactions with vital host proteins may be more advantageous than a permanent interaction which could result to host cell death via the activation of the innate immunity, for example.

4.3.3. Optimisation of siRNA protocol specific to Huh7 cells

Primary investigation comparing of JFH-1 and DBN3a protein interactions of NS5A focussed on NAP1L1 as the interaction of NAP1L1 to HCV NS5A has previously been characterised for JFH-1, providing further evidence for results I gathered in the biological systems. Firstly, optimisation of NAP1L1 siRNA silencing was performed (Figure 4.9). Cell health was measured by the percentage of cell confluency 48 h post transfection. As the same number of cells were seeded per experimental condition, differences in cell confluency between experimental conditions acts as a generic measure of cell health. A more accurate representation of cell health and viability may be accomplished by cell proliferation measured throughout the 48 hour time course. Cell viability may be further quantified by staining cells for Trypan Blue (indicating cell death) or the completion of a MTT assay. Measurement of cell health is crucial while optimising siRNA assays to characterise changes specific to the silencing of the target protein or as the result of the transfection protocol. This is demonstrated by not removing Lipofectamine 2000 6 h after transfection; despite depicting the greatest reduction efficacy, cell confluency was the lowest in comparison to all other Lipofectamine 2000 transfections

suggesting a negative impact to cell proliferation and non-specific regulation of target genes expression (Figure 4.9 B).

Our results suggests that transfection efficacy of Lipofectamine 2000 showed a negative correlation to cell health, a higher transfection efficacy results in higher level of potential cell stress indicated by a lower percentage of cell confluency, whereas RNA iMax demonstrated a high efficacy with less impact to cell confluency (Figure 4.9). Our results are supported by the findings of Wang *et al.* (2018). Regardless of the transfection reagent used, prolonged exposure of the transfection reagent to cells resulted in the greatest reduction in cell confluency. Interestingly, increasing the amount of siRNA transfected results in only marginal changes to transfection efficacy. I believe this is due to an excessive amount of siRNA contributing to a negative effect on cell health as cell confluency is reduced in comparison to transfection of only 10 nM for both Lipofectamine 2000 and RNA iMax, suggesting the results are independent of the reagent used.

4.3.4. siRNA reduction of NAP1L1 suggests both JFH-1 and DBN3a require NAP1L1 for efficient genome replication

I hypothesised the expression of NAP1L1 is crucial for the replication of JFH-1 but not DBN3a. To investigate the requirement of NAP1L1 presence during HCV genome replication Huh7 cells stably harbouring the JFH-1 or DBN3a SGR were transfected with siRNA and compared (Figure 4.10). Relative gene expression confirms successful reduction of NAP1L1 expression, however, no changes to the levels of the HCV 5'UTR RNA were observed (Figure 4.10 B). Confirmation of the mRNA results are provided by protein expression analysis, the expression of NS5A does not significantly change compared to the scrambled control (Figure 4.11). Interestingly, the percentage of NAP1L1 varies between mock, JFH-1 and DBN3a cell lines. I believe this may be due to NAP1L1 expression changing due to the presence of the HCV genome (Figure 4.10 C). Yin *et al.* (2018) describes the requirement of NAP1L1 as redundant to HCV

genome replication once replication has been established. This could suggest the proteosome-mediated degradation of NAP1L1 after HCV genome replication is not specific to JFH-1 but also occurs in DBN3a genome replication. To investigate this, and other protein interactions occurring during the initial replication of the viral genome, Huh7 cells could be electroporated with infectious virus RNA and cells harvested 4 h after electroporation to capture protein interactions required for primary HCV genome replication. Overall, these results suggest NAP1L1 does not play a role in HCV genome replication of either JFH-1 or DBN3a as reduction of the protein expression does not result in a depletion of HCV genome or NS5A presence. In relation to our proteomic results, depletion of NAP1L1 not impacting DBN3a genome replication is not surprising as no interaction was detected. However, our results is contradictory to data published by Goonawardane *et al.* (2017) and Çevik *et al.* (2017), suggesting JFH-1 utilising the interaction to NAP1L1 to deter the host innate immune response and promote HCV genome replication.

Furthermore, I hypothesised the expression of NAP1L1 is crucial for efficient virus infection of JFH-1 but not DBN3a, particularly as LC-MS/MS proteomic analysis was conducted utilising infectious virus clones. Infection efficacy was measured by infection of Huh7 cells with infectious virus clones 48 h post transfection (Figure 4.12). Relative expression of RNA levels suggests silencing of NAP1L1 was not accomplished as RNA levels for the siRNA samples and scramble controls are not significantly different (Figure 4.12 B) however, protein expression levels demonstrate reduction of NAP1L1 was successfully maintained in comparison to the scrambled control (Figure 4.13 A). It may be suggested discrepancies concerning RNA and protein expression is a result of siRNA depletion post transfection, protein translation and turnover time (Han, 2018). To increase the stability and duration of siRNA gene silencing enoxacin may be added or cells may be re-transfected with siRNA (Han, 2018). Enoxacin is a small molecule which enhances siRNA-mediated mRNA degradation by promoting the loading of siRNA duplexes onto the RNA-induced silencing complex (RISC) (Shan et al., 2008). Protein

expression results suggest NAP1L1 expression is required for efficient infection of both JFH-1 and DBN3a. Mimicking SGR HCV genome expression, the expression of NAP1L1 in the scrambled controls suggest NAP1L1 may be depleted during infection however, results are variable across biological repeats (Figure 4.13 B). Similarly to SGR genome expression, it may be suggested NAP1L1 expression is depleted intracellularly within a host cell during HCV infection. However, reduction of NAP1L1 expression prior to establishing HCV genome replication impacts HCV infection efficiency.

To investigate the downregulation of NAP1L1 affecting infection efficiency of JFH-1 and DBN3a in greater detail, quantification of NS5A positive cells 72 h post transfection and 24 h.p.i was analysed (Figure 4.14). The representative images highlights cell auto-fluorescence resulting in the inability to produce an adequate analysis parameter allowing the identification of HCV infected cells and non-infected cells in the scrambled control. Transfection reagents contributing to cell autofluorescence is not a new phenomenon and has been described previously in the literature (Gharaati-Far et al., 2018; Hunt et al., 2010; Zhao et al., 2019) however, has not been specifically described using RNA iMax transfection reagent. I believe the Huh7 cells are under a considerable amount of stress because of the RNA iMax transfection and not the addition of virus infection as the mock scrambled control also exhibits cell auto-fluorescence. As a result of this, it was not possible to quantify HCV positive cells via IncuCyte S3 analysis.

Investigation of infection efficiency during NAP1L1 silencing suggests NAP1L1 may play an important role in regulating HCV of both JFH-1 and DBN3a infection, however the specific function is not known. Yin *et al.* suggests SR-B1 expression is reduced during NAP1L1 downregulation. Expression of SR-B1 could be investigated in our model via western blot or confocal microscopy to confirm and quantify the expression of SR-B1 during NAP1L1 silencing. Further analysis of the effect of NAP1L1 silencing could be investigated by performing a FFA of virus produced after infection to determine if viable virus progeny are produced in the absence of NAP1L1. It would be desirable to compare the number of virus particles produced between

scrambled and siRNA transfections at a later timepoint than 24 h.p.i to see a greater number of virus particles produced by the scrambled control in particular. Additionally, due to the autofluorescence exhibited post RNA iMax transfection, it would be desirable to establish a stable reduction of NAP1L1 expression within Huh7 cells.

For both genome replication and virus infection assays, I hypothesised silencing of NAP1L1 would not impact the expression of DBN3a as no interaction of NAP1L1 to DBN3a NS5A was discovered in our proteomic analysis. As I was unable to confirm the proteomic results via western blot detection, I expected a reduction of JFH-1 genome replication in correspondence to published data when NAP1L1 expression is knocked down. I can confirm JFH-1 interaction of NAP1L1 is specific to NS5A, and not pulled down in a complex of NS5A interacting with other HCV proteins that may be the true interactor to NAP1L1, as published data has detailed the interaction to C terminal of domain III NS5A (Çevik et al., 2017). It is possible the interaction of NAP1L1 is inhibited in DBN3a TST infectious clone due to the C terminus insertion site of the TST and proximity to the proposed NAP1L1 binding region. However, I believe this binding site is not required for all NS5A interactions to host proteins, as such cannot be the reason for not identifying other DBN3a NS5A interactions in our interactome analysis.

As siRNA transfections are time sensitive and may increase cell stress in addition to silencing a gene which may be a crucial role in cellular activities, a stable reduction of potential protein interactors should be investigated. I hypothesis by establishing a stably silenced expression cell line, further downstream analysis of proteins highlighted in our proteomic data may be investigated due to reduction of cell autofluorescence introduced by transfection reagents and removal of siRNA time limitations particularly when conducting virus infections. To establish a stable host gene silencing, advanced clustered regularly interspaced short palindromic repeats (CRISPR) technology has been developed to allow the manipulation of the cellular genome.

4.3.5. Phosphorylation abundance of HCV NS5A varies depending on GT and cell culture model

Phosphorylation status of HCV cell models was investigated to explore the changes in HCV NS5A protein interactions for JFH-1 and DBN3a. It became evident NS5A DBN3a is phosphorylated in the Huh7 SGR stable cell line however, the presence or abundance of a hyperphosphorylated state is absent during HCV infection (Figure 4.15). To confirm these results, an antibody specific to NS5A phosphorylated on serine-225 was used to help identify a second NS5A band on the western blot and to confirm the singular NS5A band as the hypo-phosphorylated form. As the phosphorylation status of DBN3a differs depending on the system used, protein interactors of NS5A may also change. This is important to note for NS5A proteomic analysis, specifically DBN3a, however should be investigated for potential changes to other HCV GTs. Our research corroborates data from other groups who studied the function of NS5A phosphorylation in JFH-1 and Con1, results suggesting that mutations to the phosphorylation sites within JFH-1 do not result to the same loss of function in Con1 suggesting phosphorylation function is specific to each GT (Appel et al., 2005). Interestingly, hyperphosphorylation may be linked to culture adaption, the most robust culture adaptive mutation resulting in a 20,000 fold increase in replicative efficiency. Noted as S2204I, the mutation was first identified in GT1, S232I, and present in all available SGR apart from JFH-1 (Kim et al., 2014; Ross-Thriepland & Harris, 2015; Saeed et al., 2012; Wose Kinge et al., 2014; Yu et al., 2014), which removes the hyperphosphorylated form of NS5A (Blight et al., 2000).

Differences in the presence of DBN3a phosphorylation status of infectious virus and SGR may be due to a variation in abundance; the hyperphosphorylated form may be present during virus infection however at a low abundance not exhibited by western blot analysis. To confirm total absence of a hyperphosphorylated form of NS5A, a more sensitive assay could be performed such as an ELISA, using S225 antibody as a capture antibody, performed using cells infected by HCV. As different cell models may be a contributing to factor NS5A phosphorylation

status, it is important to explore the phosphorylation state of NS5A in clinical samples. This would ensure observations within cell culture models are clinically relevant to characterising HCV GTs and not an artefact of cell culture mutations. HCV phosphorylation experiments have been predominantly performed in cell culture infectious virus clones, to define clinical relevance to HCV phosphorylation status utilisation of phosphoprotein specific antibodies for phosphoprotein enrichment by immunoprecipitation and downstream proteomic analysis. Furthermore, the status of NS5A phosphorylation differing between cell culture models highlights the importance of investigating HCV infection and disease progression in cell models which more closely mimic the native human liver, such as including different cell lines our than the transformed Huh7 cells.

4.4. Summary

- There is not a linear relationship between amount of *in vitro* transcribed RNA electroporated into a cell and viral genome output.
- Immunoprecipitation methods, for example changing agarose beads suspension beads to magnetic beads, may be altered to optimise pull down efficiency when input products cannot be upscaled.
- Proteomic analysis via TMT labelling is desirably for comparing multiple experiment conditions to LC-MS/MS run-to-run variation, however, may result to indistinguishable background noise between samples. Therefore, unless there is a strong enrichment between bait and negative control samples, analysis of significant protein interactions may be poor.
- NAP1L1 interaction to JFH-1 and DBN3a is required for efficient virus infection but not required for genome replication.
- Phosphorylation status and abundance of NS5A varies depending on the HCV cell model used.
- Stable cell line of gene silencing will allow greater investigation of protein interactions due to redundancy of siRNA that are time sensitive and less physical stress on cells exhibited during lipid-controlled transfection.

Chapter 5. Exploration of tissue culture models to investigate HCV mechanisms driving fibrosis

5.1. Introduction

To investigate the role of HCV in driving fibrosis, it is necessary to recapitulate some of the key characteristics of the liver architecture *in vitro*, namely crosstalk between hepatocytes and the ECM producing activated HSC. Individual analysis of hepatocyte gene expression during HCV infection can allude to cellular stress levels, which may suggest the potential activation of pathways resulting in the release of soluble factors that can activate HSCs. To gain a general overview of hepatocyte status during HCV infection, the expression of stress markers Snail-1, zinc finger E-box-binding homeobox 1 (ZEB-1), fibronectin and TGF-β was analysed.

The expression of Snail-1 and ZEB-1 were previously defined to periods of embryonic development and are associated with epithelial-mesenchymal cell transition (EMT) markers (Serrano-Gomez et al., 2016). However, pathological states, such as fibrosis and cancer, have been shown to cause reactivation of these genes, allowing their gene expression to be used as a marker of cell stress and as well as predictor of fibrosis progression. Snail-1 is part of a "superfamily" of zinc-finger transcription factors, including Slug and Scratch proteins. The Snail subfamily has been implicated in a range of biological processes such as cell differentiation and survival. Relevant to this project, Snail-1 plays an important role in the activation of HSCs; the overexpression of Snail-1 is associated with the accumulation of the ECM and its expression has been observed in fibrotic livers and cholangiocytes, the epithelial cells lining the bile duct (Dooley et al., 2008; Rowe et al., 2011; Scarpa et al., 2011). In addition to this, Snail-1 expression may be altered by the presence of HCV NS5A, as phosphorylation and nuclear localisation of Snail-1 is regulated by PI3K (Katoh & Katoh, 2006), which is further upregulated by the binding of NS5A, as previously described in "1.6.1.3 Hepatocellular carcinoma".

ZEB-1 has demonstrated a role in the progression of many liver diseases such as chronic viral hepatitis and HCC (Kim et al., 2016; L. Li et al., 2019; Sinigaglia et al., 2015). The expression of ZEB-1, as well as Col1A2, Col4A1 and TGF-β has been associated with the expression of microRNA-192 (miR-192). During HCV infection, Kim *et al.* (2016) describes the HCV core proteins ability to increase TGF-β expression through downregulation of ZEB-1 mediated by miR-192 stimulation. ZEB-1 expression has also been associated with the mediation of secreted inflammatory cytokines, IL-6 and TNF-α, driving fibrosis in the liver through activation of the Wnt/β-catenin signalling pathway (L. Y. Li et al., 2019; Rong et al., 2019). Within HSCs induced by TGF-β, ZEB-1 expression is increased and is crucial for LX-2 cell expression of αSMA and Col1A1 (L. Y. Li et al., 2019).

Fibronectin is expressed by fibroblasts, endothelial cells, macrophages, and hepatocytes *in vivo*. It plays an integral role in cell adhesion, growth, differentiation and wound healing thus, differential expression of fibronectin is closely associated with cellular damage and the development of hepatic fibrosis and cancer (Pankov & Yamada, 2002). Despite fibrosis occurring in chronic HCV years after infection, Liu *et al.* (2016) describes the levels of fibronectin as variable depending on the state of liver hepatitis (acute vs chronic). During acute infection, fibronectin increased expression relates to liver injury conversely to chronic hepatitis where fibronectin expression increases due to fibrous hyperplasia.

TGF-β expression is used as a marker of hepatocyte stress and cell repair. TGF-β induces differentiation of HSCs resulting in an increased production of the ECM. This promotes wound healing at early stages of liver injury and contributes to the progression of fibrosis over a long time period. Expression of the cytokine is associated with a large variety of genes, through the action of SMADs acting as transcriptional regulators of TGF-β, transmitting TGF-β signal in the nucleus and performing downstream effects by regulating target-gene transcription (Feng & Derynck, 2005). HCV may promote TGF-β expression through multiple pathways, for example, ROS, endoplasmic reticulum stress, unfolded protein response, activation of NF-κB-dependent

pathways (Chusri et al., 2016; Lin et al., 2013; Smirnova et al., 2016). Independent of HCV infection, and alcohol, the presence of TGF-β alone is sufficient to induce fibrosis, acting as a robust positive control for fibrosis progression both *in vitro* and *in vivo* (Kanzler et al., 2001; Meindl-Beinker & Dooley, 2008).

Collectively within this thesis, the expression of Snail-1, ZEB-1, fibronectin and TGF-β by Huh7 cells may be described as inflammatory markers, known as alarmins, with expression associated to adapting cell stress. Expression of TGF-β may be described as a direct stimulant of LX-2 cells as an independent fibrosis stimulant (Carson et al., 2021).

Fibrosis markers, αSMA, Col1A1 and tissue inhibitor of metalloproteinases 1 (TIMP1), are collectively associated to the activation of HSCs and accumulation of the ECM. Expressed as an intermediate filament protein, αSMA is directly linked to the presence of activated myofibroblast-like cells with a proliferative characterisation driving the deposition of the ECM (such as collagen type I and III) (Lemon & Tjian, 2000) and the expression of TIMPs. Additionally, αSMA is believed to be incorporated into stress fibres resulting in high contractile activity of HSCs and tissue hardening (Schon et al., 2016; W. Zhang et al., 2021). Matrix stiffness as a result of the change to the ECM composition can further promote a pro-fibrotic state as HSCs can become activated through surface receptors, known as integrins (Caliari et al., 2016; Wells, 2013). A major component of the liver ECM are collagens, in particular type I collagen which is implicated as the most abundant ECM protein in disease and the primary matrix protein in hepatic fibrosis (Geerts et al., 1989). Degradation of Col1A1 is controlled by MMPs maintaining a level of homeostasis, however inhibition of MMPs enzymatic function is controlled by TIMPs (Craig et al., 2015). TIMP1 mediating the remodelling of the ECM by MMP, also inhibits apoptosis of HSC (Hemmann et al., 2007; Murphy et al., 2002). Increased expression of TIMP1 is directly related to the stage of hepatic fibrosis with some literature suggesting that in overexpression and MMP mutant mice studies, TIMP1 directly supports hepatic fibrosis development (Hemmann et al., 2007; Roderfeld et al., 2006; Yoshiji et al., 2000) and persistence of HM

(Murphy et al., 2002). Expression of TIMP1 may also be driven by matrix stiffness, upregulating TIMP1 and downregulating MMP-9, a matrix metalloproteinase when uninhibited breaks down the ECM (Lachowski et al., 2019). TIMP1 expression is a consequence of communication between activated HSC and liver macrophages, highlighting that changes in gene expression is impacted by the presence of different cell types *in vitro* (De Minicis et al., 2007). During HCV infection, TIMP1 expression has been suggested as a possible marker of liver fibrosis in HCV infected patients due to a significantly increased expression in comparison to healthy donors (Latronico et al., 2016).

Collectively, the increased expression of these fibrosis markers may be directly impacted by the presence of the HCV core protein. It has been described by multiple groups that the core protein is capable of driving the activation of HSCs via the TLR2-dependent signalling pathway and promotion of an inflammatory state (Coenen et al., 2011; Dolganiuc et al., 2004; Düesberg et al., 2002; Feldmann et al., 2006). This highlights the importance of conducting *in vitro* fibrosis mechanistic experiments in a hierarchy of complexity to gain a greater depth of HCV mechanisms driving fibrosis (Figure 5.1).

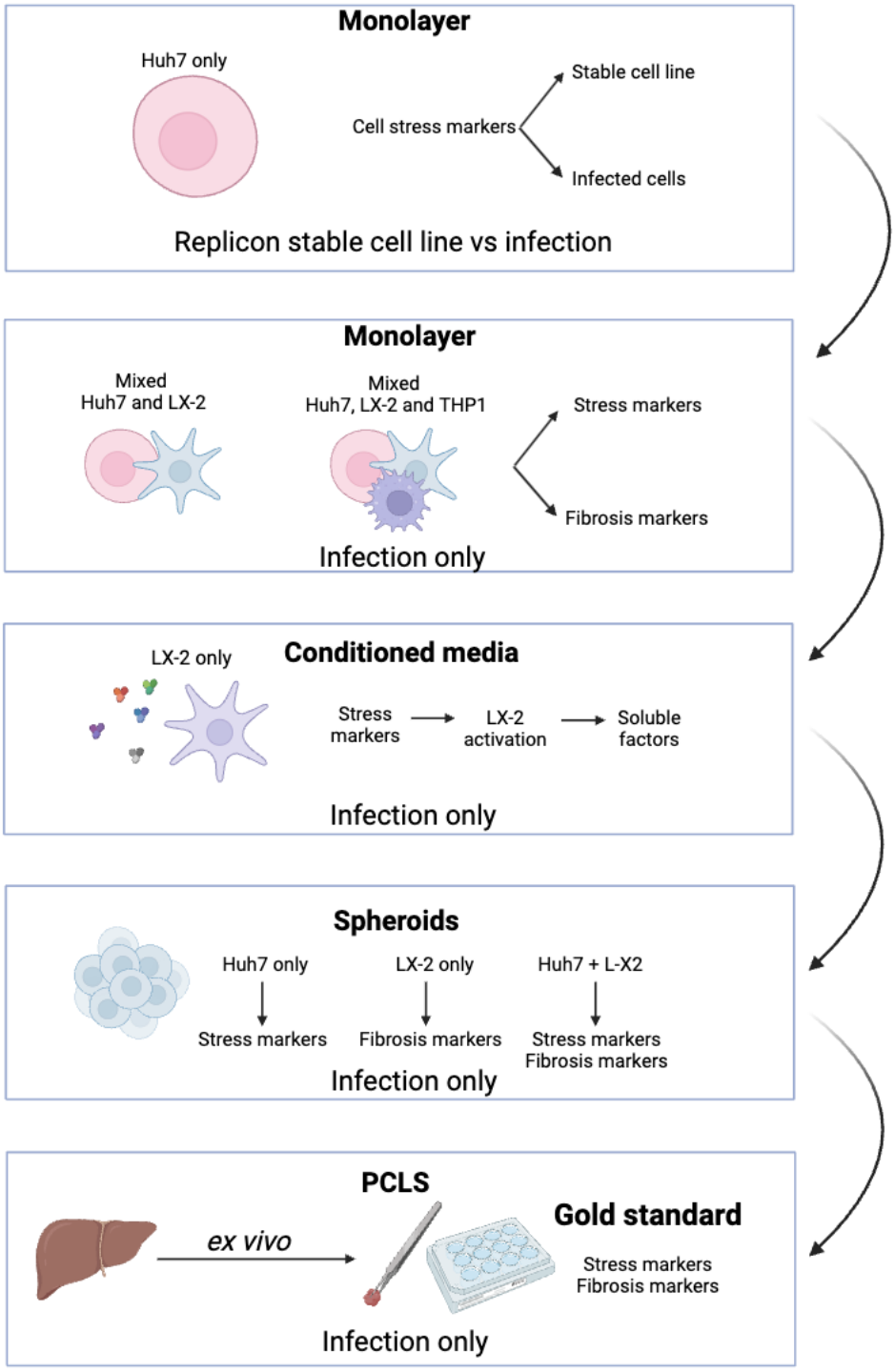

Figure 5.1 Complexity hierarchy of experiments.

Breakdown of cell culture techniques used to exploit potential HCV mechanisms driving fibrosis.

Classically, HCV mechanisms of disease pathology is confined to exploring a specific pathway, typically using monocultured cells, however, this fails to recapitulate the cross-talk between different hepatic cell types. Bility *et al.* (2016) utilised a three-cell-co-culture system

allowing communication of cells types with critical roles in the progression of hepatic fibrosis; hepatocytes, stellate cells and macrophages. The cross-talk of macrophages, activated in the presence of HCV soluble factors from hepatocytes *in vitro,* promoted stellate cell like activation and a suggestive role of macrophage dysregulation promoting chronic HCV infection and liver fibrosis. Akil *et al.* (2019), using a similar three-cell-co-culture system however utilised primary macrophages, demonstrated the upregulation of fibrogenic genes 1.9x greater than the mono- and bi- cell culture experiments and observed morphological changes to LX-2 cells. Morphological and proliferative changes in LX-2 cells from a quiescent to myofibroblast-like morphology has been described in other model systems, such as parasite-induced liver fibrosis (Anthony et al., 2010).

Exploiting the crosstalk of cell types during pathogenesis studies allows partial recapitulation of a native organ however, can lack the recapitulation of cell:cell contact. To mimic this, spheroid cultures have been developed. It was previously described how spheroids can allow cell contact in such a way that hepatocyte *in vitro* cell lines can differentiate into a polarised state (Sainz, TenCate, et al., 2009). This is advantageous to HCV research, as it can maintain liver-specific functions. Additionally, HCV has shown to replicate more efficiently in these models in comparison to monolayer cultures (Ananthanarayanan et al., 2014). This may be due to a hypoxic core in the centre of spheroids promoting HCV replication. This was demonstrated by Vassilaki *et al.* (2013), comparing HCV replication levels in atmospheric oxygen levels and in a hypoxic environment mimicking that of the liver tissue microenvironment (3% oxygen) demonstrating greater HCV replication in the hypoxic environment. Spheroids have been used predominantly in cancer research to assess the migration and invasion of cancer cells and mimicking solid tumours, evaluating ability of drugs efficacy based on spheroid growth and reprisal of a hypoxic and necrotic core (Barisam et al., 2018; Browning et al., 2021; Mark et al., 2020). A limitation of using spheroids in infection biology studies is the formation of a necrotic core which does not mimic the environment of a healthy organ, in addition to changes in the

diffusion of nutrients and waste products (Browning et al., 2021). The formation of a spheroid is different from organoids, which maintains components of the structural architecture of an organ. In the field of organoid models for the brain, kidney, lung and intestine, models are predominantly developed using induced pluripotent stem cells in an organotypic system (Harrison et al., 2021). Liver organoids are currently limited to being "constructed" due to the induction of pluripotent stem cells resulting in a mixed phenotype of fetal/adult characteristics (Baxter et al., 2015; Patterson et al., 2012). An example of a constructed liver organoid includes hepatobiliary organoids with the presence of bile canaliculus, hepatocytes and cholangiocytes in the absence of stellate cells, endothelial structure, and mesenchyme (Wu et al., 2019). As such, the gold standard model for studying liver pathology is PCLS.

As described previously, PCLS is an *ex vivo* model for studying liver pathology, particularly fibrosis due to maintenance of the liver architecture that plays a crucial role in the development of the ECM. Maintenance of PCLS may vary, altering the capacity of maintaining slices without introducing tissue culture artefacts however, the *ex vivo* model has been used for a range of disease pathology studies such as metabolic dysfunction–associated steatotic liver disease (MASLD), formerly named non-alcoholic fatty liver disease (NAFLD), liver cancer and alcoholic liver disease. Specific to this project, PCLS have been used to greater understand HCV pathology. Lagaye *et al.* primarily demonstrated the ability of HCV to infect slices allowing successful viral propagation in addition to using the model as a tool to evaluate HCV antiviral agents (Lagaye et al., 2016; Lagaye et al., 2012). Wu *et al*. (2022) utilised the model to observe changes in the innate immune response after HCV infection. PCLS obtained from non-infected and DAA treated patients identified HCV infected PCLS as having an enhanced hepatic innate immunity compared to non-infected controls. Using PCLS to greater understand HCV mechanisms of driving fibrosis has yet to be fully exploited. Kartasheva-Ebertz *et al*. (2021), alludes to PCLS being used as an effective model to study HCV, alcohol and steatosis driven fibrosis in a bioreactor system maintaining slices up to 21 days. Fibrosis progression was

compared between the different stimuli and liver slices representing different phases of fibrosis (F0 to F4 fibrosis stage according to the METAVIR score) in conjunction to testing new anti-fibrotic therapies. However, it is crucial to evaluate the use of differently prepared PCLS, such as varying slice thickness and maintenance in different bioreactor systems to fully understand the advantages and limitations of using PCLS when modelling liver pathogenesis.

This chapter aims to breakdown the mechanisms of HCV driven fibrosis in a hierarchy of different tissue culture models ranging in complexity of cell types present, cell:cell contact and maintenance of the liver architecture.

5.2. Results

5.2.1. Independent of the cell model used, Huh7 cell growth and stress markers are not affected by HCV genome replication

Prior to the investigation of different cell culture models and differences in the progression of HCV driven fibrosis *in vitro*, comparison of Huh7 cells stably harbouring the SGR and use of the infectious virus was evaluated. As *in vitro* HCV infection is limited to 72 h and SGR stable cell lines can be maintained for months, stable expression of the SGR may be viewed as a model of chronic infection whereas direct infection using the wildtype virus may be described as an early HCV infection model. To evaluate changes in Huh7 cell growth in the presence of the SGR or infectious virus, the confluency of Huh7 cells was evaluated for 72 h post seeding. Result suggests the growth kinetics of Huh7 cells do not change regardless of HCV genome replication in the presence of only the non-structural proteins or the full viral genome (Figure 5.2). Additionally, Huh7 cell growth does not vary depending on the HCV GT present (JFH-1 or DBN3a) but there is a slight reduction in cell growth when treated with 10 ng/mL TGF-β. As such, cell growth cannot be used as a defining factor of Huh7 cell activation.

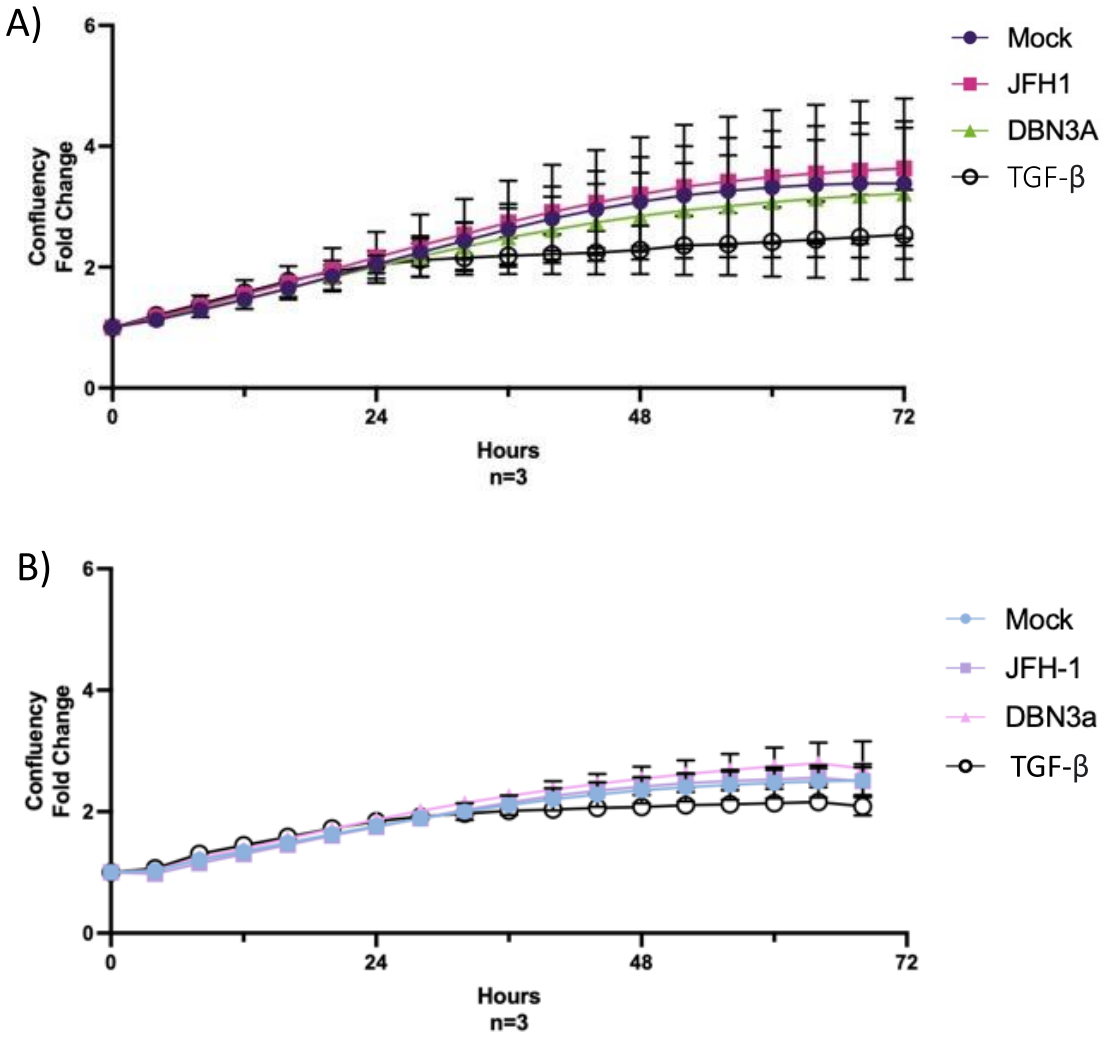

Figure 5.2 Huh7 cell growth does not change in the presence of a stably expressed SGR or virus infection.

A) Huh7 cells stably harbouring the SGR. B) Huh7 cells infected with HCV (MOI 0.2) or in the presence of TGF-β (10 ng/mL). Cell growth analysed by cell confluency fold changes over time and normalised to 4 hour post seeding confluency, analysed by IncuCyte S3. Statistical analysis was completed for fold change confluency values at 72 hours (SGR) or 68 hours (virus) post seeding. Data are presented as mean with standard deviation. Statistical significance was tested using one-way ANOVA with the Bonferroni's multiple comparison test, with a single pooled variance comparing the change fold in confluency of cells at 72 hours. P values; ns, P ≥0.05.

As there are no discrepancies between the cell growth of Huh7 cells in the presence of HCV, stress markers correlating with the potential activation of HSCs was evaluated. Huh7 cells stably harbouring the JFH-1 or DBN3a SGR, and a negative control of parental Huh7 cells without the presence of the SGR, were harvested 72 h post seeding and qRT-PCR analysis of Snail-1, ZEB-1 and fibronectin genes was performed. Expression of all stress markers did not significantly change in the presence of the SGR (Figure 5.3). To decipher whether gene expression of stress markers is biased to the HCV cell model used, stress marker expression was also assessed in the presence of HCV infectious virus. Cells were infected 4 h post seeding and harvested 72 h.p.i. TGF-β treatment was used as a pro-fibrotic stimulus, acting as a positive control and gene expression was normalised to the mock, acting as a negative control. As expected TGF-β treatment induced expression of the fibrogenic genes fibronectin and TGF-β (Figure 5.4). Similar to the presence of the SGR, infection of Huh7 cells does not induce the expression of stress markers regardless of the HCV GT used. As there was little difference between Huh7 cell growth kinetics and stress markers of the stably expressed SGR compared to virus infection, future experiments were conducted using the infectious virus which I believed to be a better model for replicating a natural infection *in vitro*. As such, Huh7 cells infected with HCV or treated with TGF-β were assessed for changes to cell morphology (Figure 5.5). Upon treatment of Huh7 cells with TGF-β, Huh7 cells appeared elongated with spindle-like projections. Similarly, this was observed during HCV infections with both JFH-1 and DBN3a GTs.

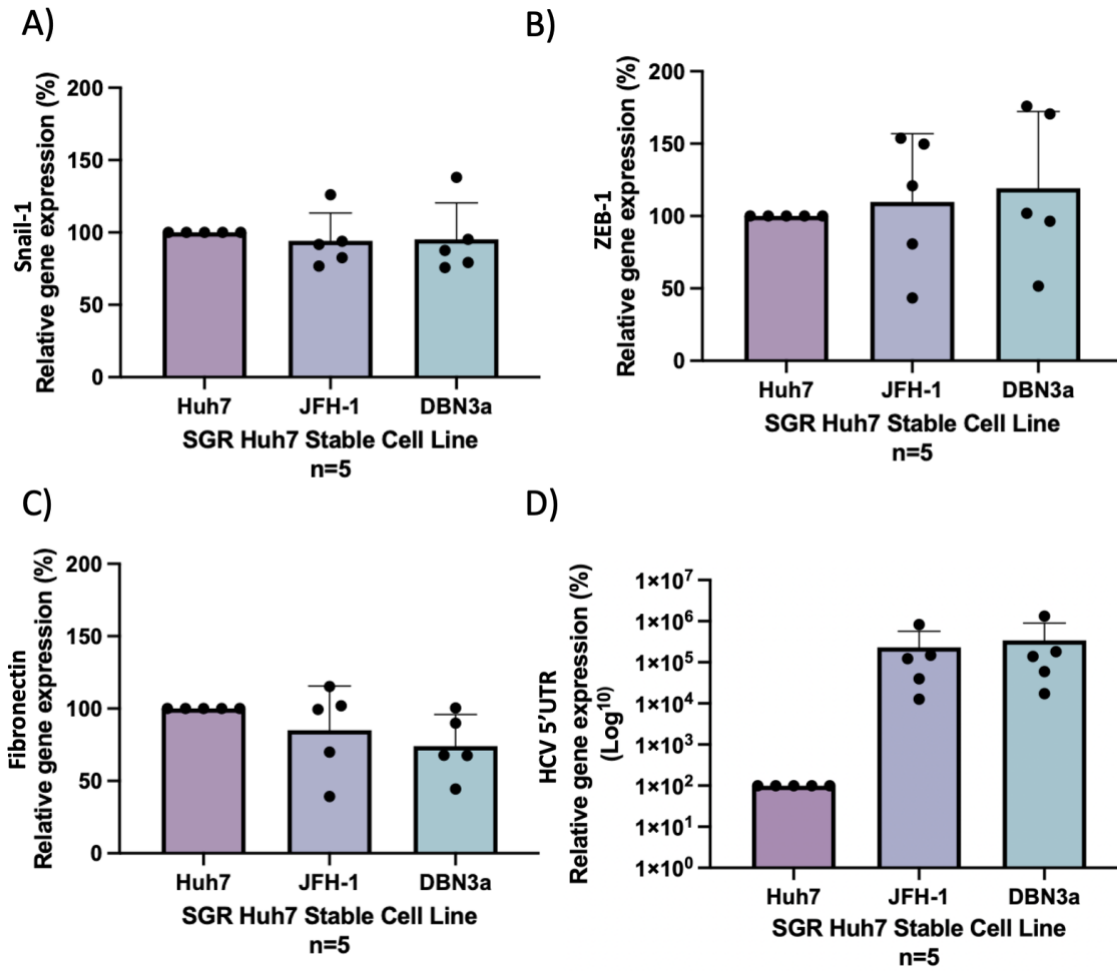

Figure 5.3 Stable expression of HCV SGR does not induce cell stress markers of Huh7 cells.

Huh7 cells stably harbouring the SGR of JFH-1 and DBN3a. mRNA expression of stress markers relative to the housekeeper control HPRT1 A) Snail-1 B) ZEB-1, C) fibronectin and D) HCV 5'UTR. Data are presented as mean with standard deviation. Statistical significance was tested using one-way ANOVA with the Bonferroni's multiple comparison test, with a single pooled variance. P values; ns, P ≥0.05.

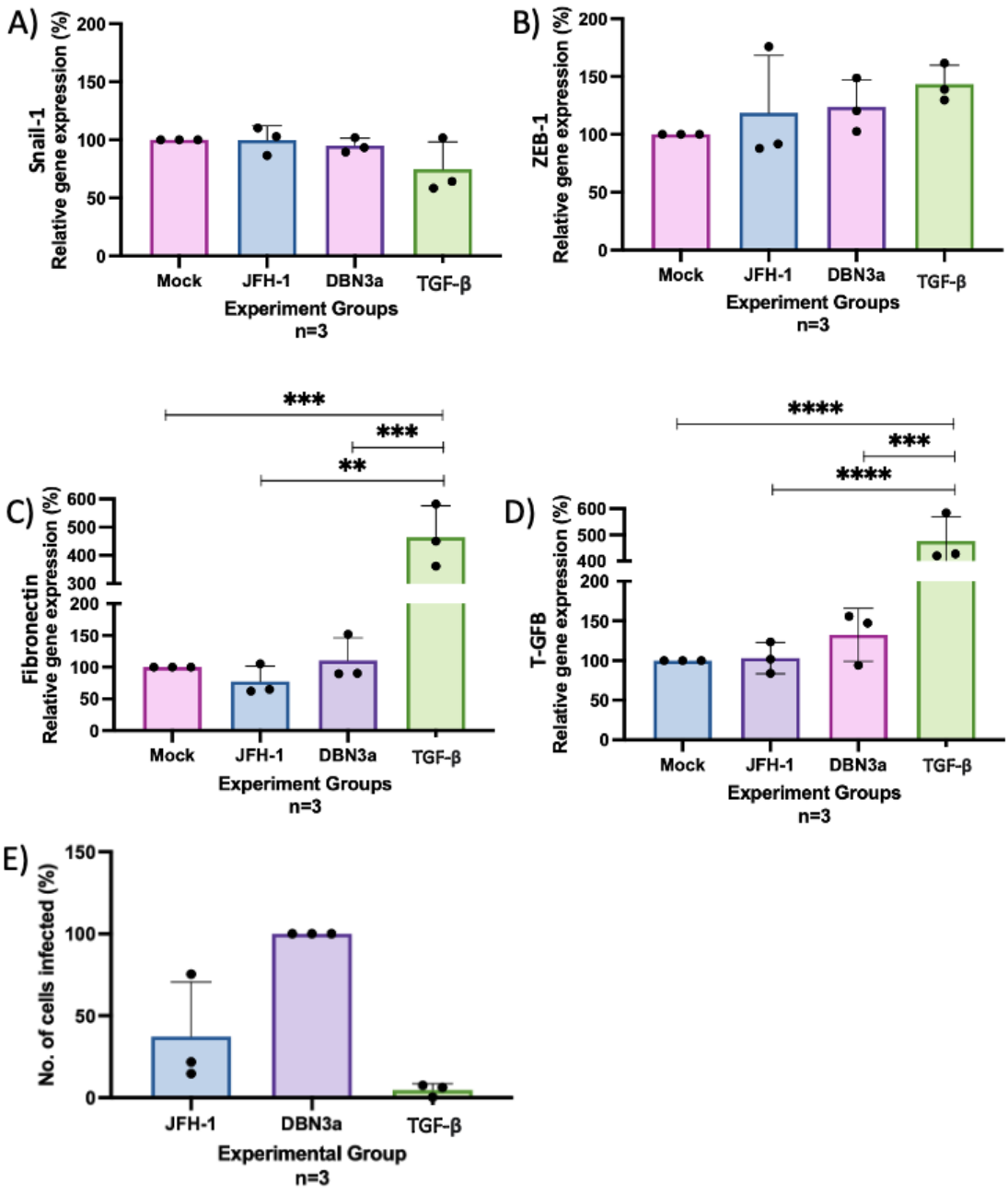

Figure 5.4 HCV infection fails to induce stress markers of Huh7 cells.

Huh7 cells infected with JFH-1 and DBN3a infectious virus (MOI 0.2) or treated with TGF-β (10 ng/mL) were harvested 72 h.p.i. mRNA expression of stress markers A) Snail-1 B) ZEB-1, C) fibronectin and D) TGF-β was analysed. E) The number of cells infected by HCV was calculated via anti-sheep NS5A staining and analysis via the IncuCyte S3. Mock values were removed and the number of infected cells normalised to DBN3a values. Data presented as mean with standard deviation. Statistical significance was tested using one-way ANOVA with the Bonferroni's multiple comparison test, with a single pooled variance. P values; ns, P ≥0.05; **, P <0.005; ***, P <0.0005; ****, P <0.00005.

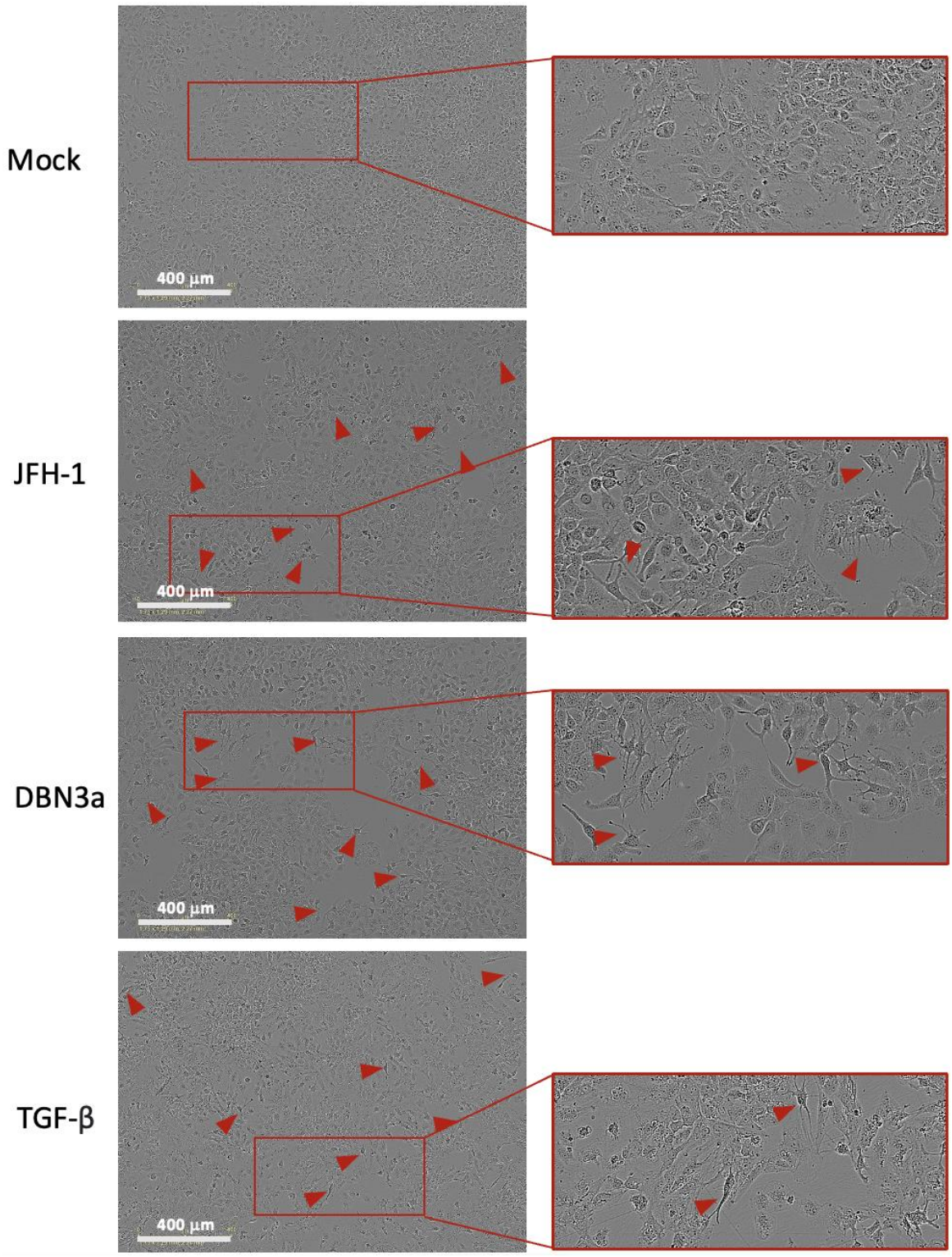

Figure 5.5 Phenotype changes upon activation of Huh7 cells.

Representative images of Huh7 cells infected with HCV JFH-1 or DBN3a (MOI 0.2) or treated with TGF-β (10 ng/mL). Phase images with red arrows highlighting changes in cell morphology. Images acquired by the IncuCyte S3. Images were taken at 10 x magnification and scale bars = 400 microns.

5.2.2. Activation of LX-2 cells results to changes in cell growth and phenotype

To gain a greater understanding of fibrosis progression during HCV infection, LX-2 cells were introduced into the *in vitro* experiments. As an immortalised HSC cell line, I investigated possible changes in phenotype and cell growth upon activation via TGF-β, a direct stimulant of HSC activation. LX-2 cell growth was analysed for 72 h post seeding via the IncuCyte S3. Observations of LX-2 cells 72 h post-stimulation highlights changes to cell morphology; cells appear flat with exaggerated elongated spindle-like features with large open areas spanning between cells in comparison to the mock control (Figure 5.6). Supporting the observation of the formation of large gaps between cells, there is a significant reduction in cell confluency in TGF-β treated cells suggesting cell growth decreases upon stellate cell activation (Figure 5.7). These results suggest analysing the confluency of LX-2 cells may be used as a measurement of LX-2 cell activation.

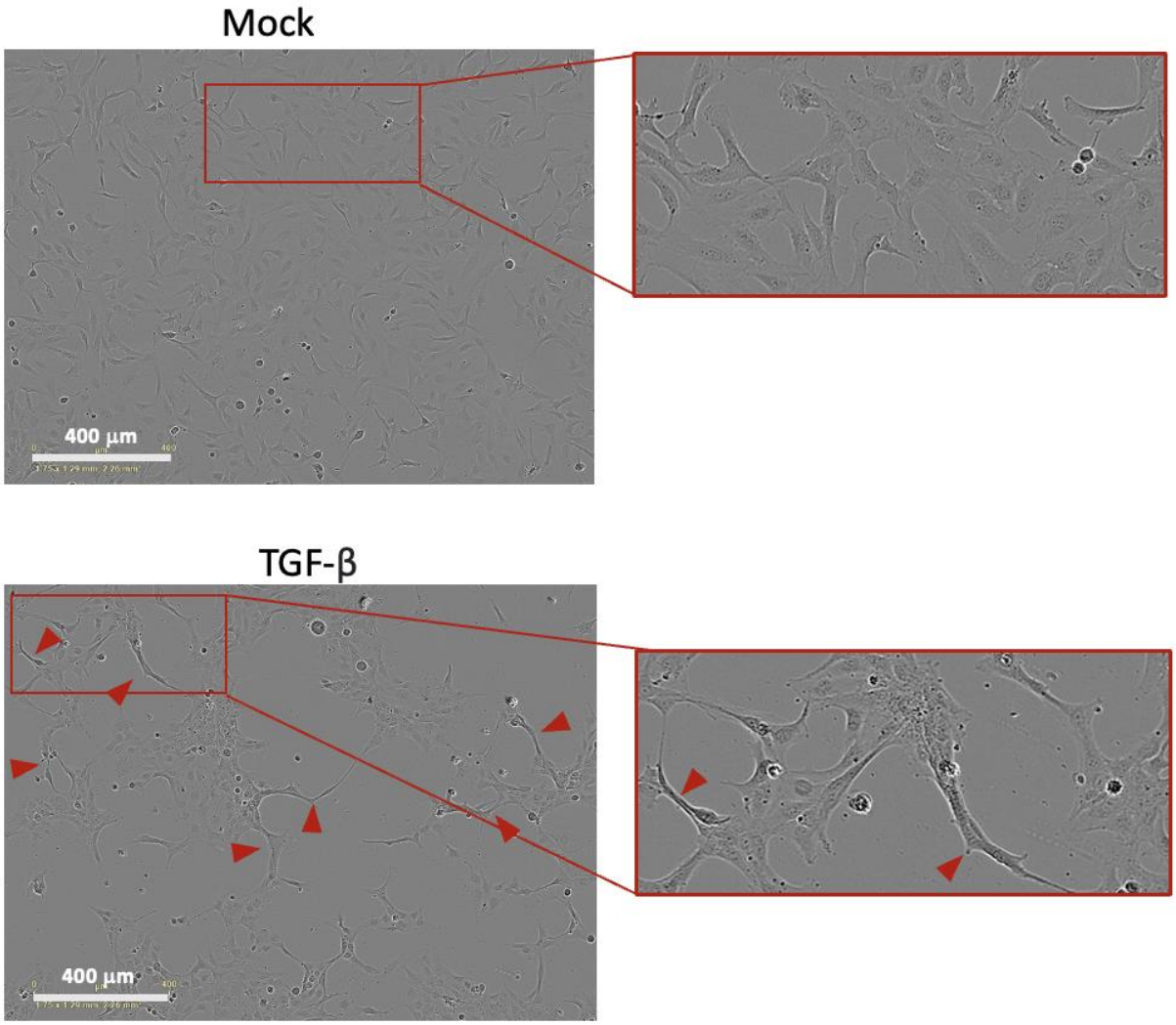

Figure 5.6 Phenotype changes upon activation of LX-2 cells.

Representative images of LX-2 cells treated with and without TGF-β (10 ng/mL). Phase images with red arrows highlighting changes in cell morphology and squares highlighting enlarged area. Images were taken at 10 x magnification and scale bars = 400 microns.

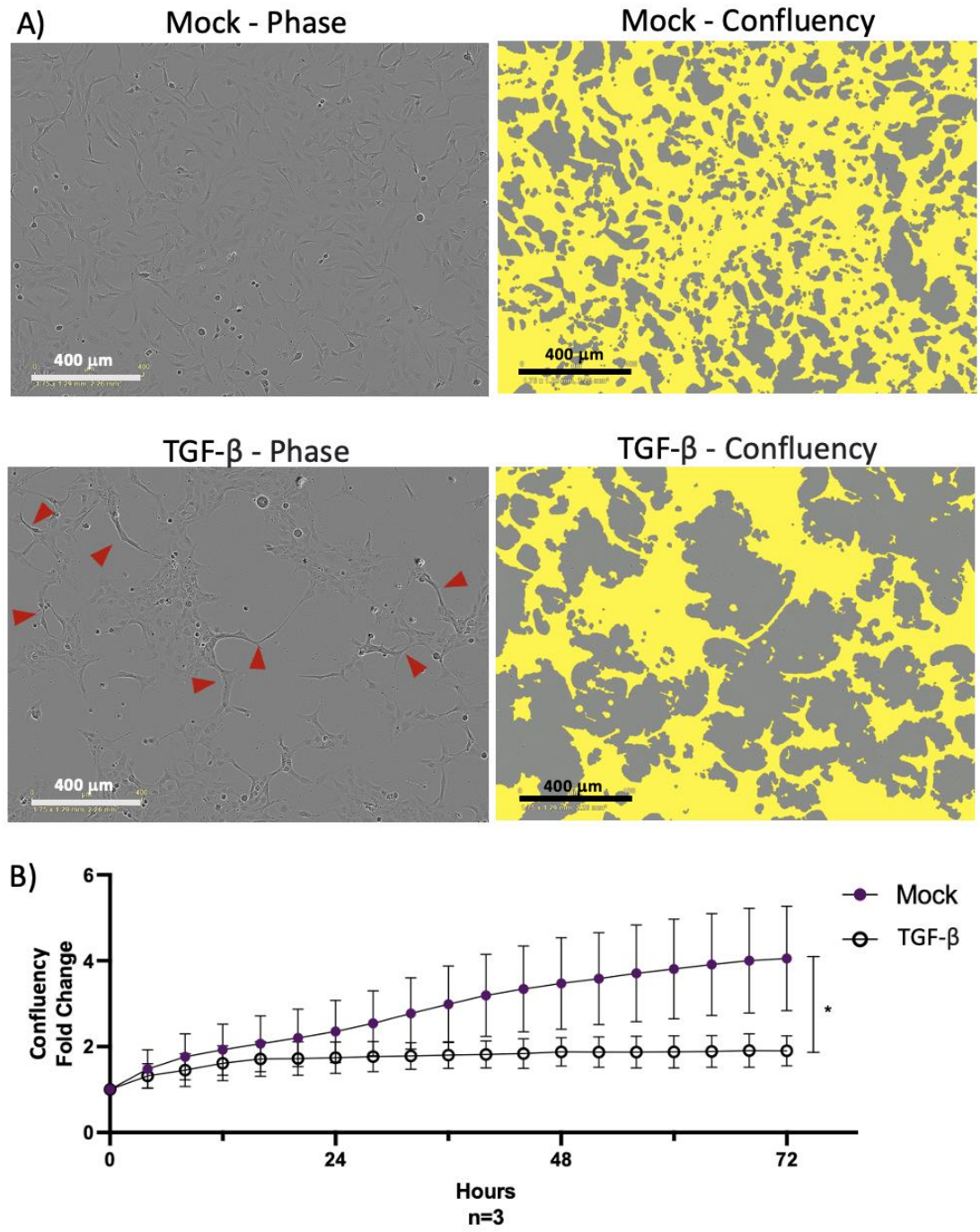

Figure 5.7 Cell growth changes upon activation of LX-2 cells.

A) Representative images of LX-2 cells treated with and without TGF-β (10 ng/mL). Phase images with red arrows highlighting changes in cell morphology. Within the same view as phase images, confluency images highlighting area analysed by the IncuCyte S3 as being occupied by a cell in yellow. B) Cell growth analysed by confluency changes over time and normalised to 4 hour post seeding confluency. Statistical analysis was completed for fold change confluency values at 72 hours post seeding. Data are presented as mean with standard deviation. Statistical significance was tested using unpaired t test assuming both populations have the same standard deviation. P values;*, P <0.05. Images were taken at 10 x magnification and scale bars = 400 microns.

5.2.3. Soluble factors released during HCV infection do not activate LX-2 cells

As I did not see a change in stress markers of Huh7 cells during HCV infection, I investigated the possibility of Huh7 cells releasing soluble factors that may activate LX-2 cells and the initiation of a pro-fibrogenic state. LX-2 cells were cultured with supernatant of Huh7 cells infected with HCV. Activation of LX-2 cells was measured by changes in cell growth, observed with control groups; (1) conditioned media (CM) of mock infected and TGF-β treated Huh7 cells and, (2) LX-2 cells treated with media (mock) or directly treated with TGF-β only. As there is no significant change in cell confluency between CM mock and CM from JFH-1 and DBN3a HCV infected cells results suggest there was no soluble factors released during HCV infection promoting LX-2 cell proliferation. The term "LX-2 proliferation" is associated with LX-2 activation, as the term "activation" is only used when a myofibroblast state has been adopted with expression of myofibroblast markers (Figure 5.8). There were also no changes between mock LX-2 cells and CM mock treated LX-2 cells suggesting media collected from Huh7 cells, regardless of the presence of HCV, maintained sufficient nutrients for normal LX-2 cell growth. Interestingly, there is a potential difference between the confluency of LX-2 cells indirectly activated by CM TGF-β and directly treated TGF-β LX-2 cells. Further investigation is required to assess the activation of LX-2 cells during HCV infection in this model and possible differences between HCV GTs driving the pro-fibrotic state.

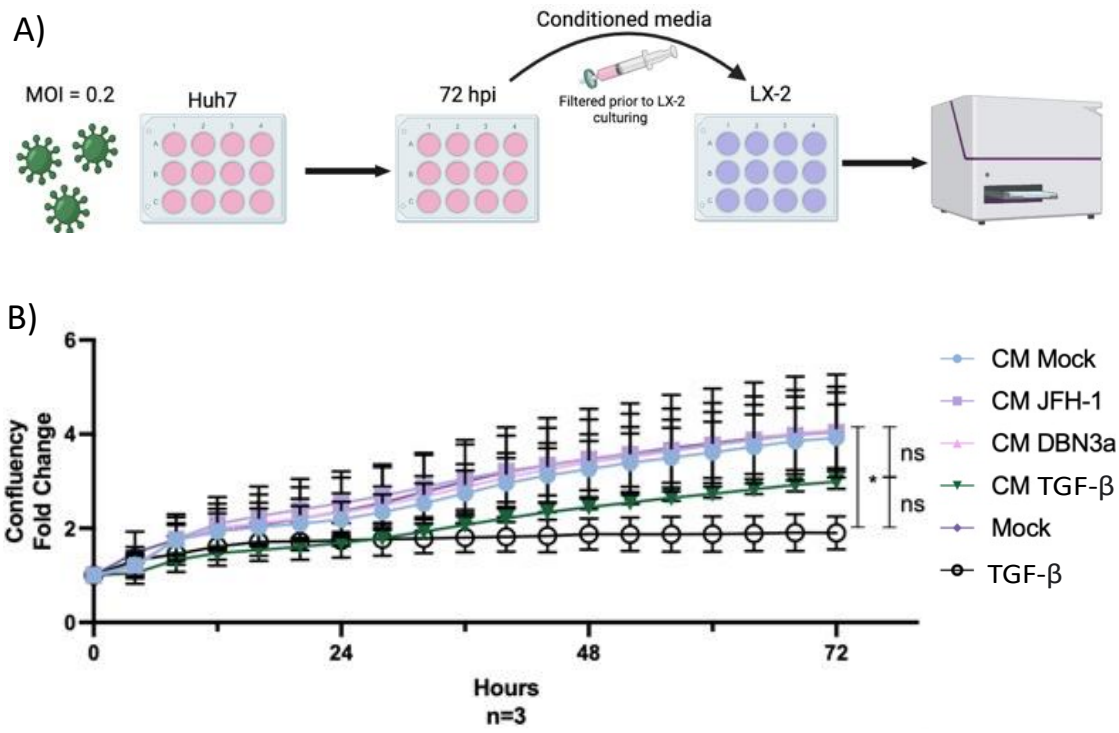

Figure 5.8 Conditioned media from Huh7 cells infected with HCV does not activate LX-2 cells.

A) Schematic of experiment protocol. B) Cell growth of LX-2 cells treated with conditioned media (CM) of infected Huh7 cells, or directly treated with TGF-β (10 ng/mL) analysed by confluency changes over 72 hours and normalised to 4 hour post seeding confluency, analysed by IncuCyte S3. Statistical analysis was completed for fold change confluency values at 72 hours post seeding. Data are presented as mean with standard deviation. Statistical significance was tested using one-way ANOVA with the Bonferroni's multiple comparison test, with a single pooled variance. P values; ns, P ≥0.05; *, P <0.05.

5.2.4. Activated monolayer cell culture of Huh7 and LX-2 cells may not be identified via changes to cell confluency

To decipher if CM of Huh7 cells infected with HCV was incapable of promoting LX-2 activation due to the absence of soluble factors or the requirement of cell:cell contact, mixed monolayer cultures of Huh7 and LX-2 cells were analysed. Primarily, changes to cell growth and morphology upon activation by TGF-β was compared to mock cultures (Figure 5.9). Treatment with TGF-β results in the presence of cells presenting elongated spindle-like features however, without staining cell line specific markers the distinguishing between Huh7 and LX-2 cells is not possible. Contrary to LX-2 cells activated alone, there is a reduction of large open areas spanning between cells in comparison to the mock control (Figure 5.10). This observation is quantified by cell growth analysis via changes in cell confluency, confirming there is no significant differences between Huh7 and LX-2 cell mixed cultures treated with TGF-β compared to the mock control (Figure 5.10 B). Results suggest cell growth analysis cannot be used as an independent factor to signify the promotion of a pro-fibrotic state when Huh7 cells and LX-2 cells are co-cultured together.

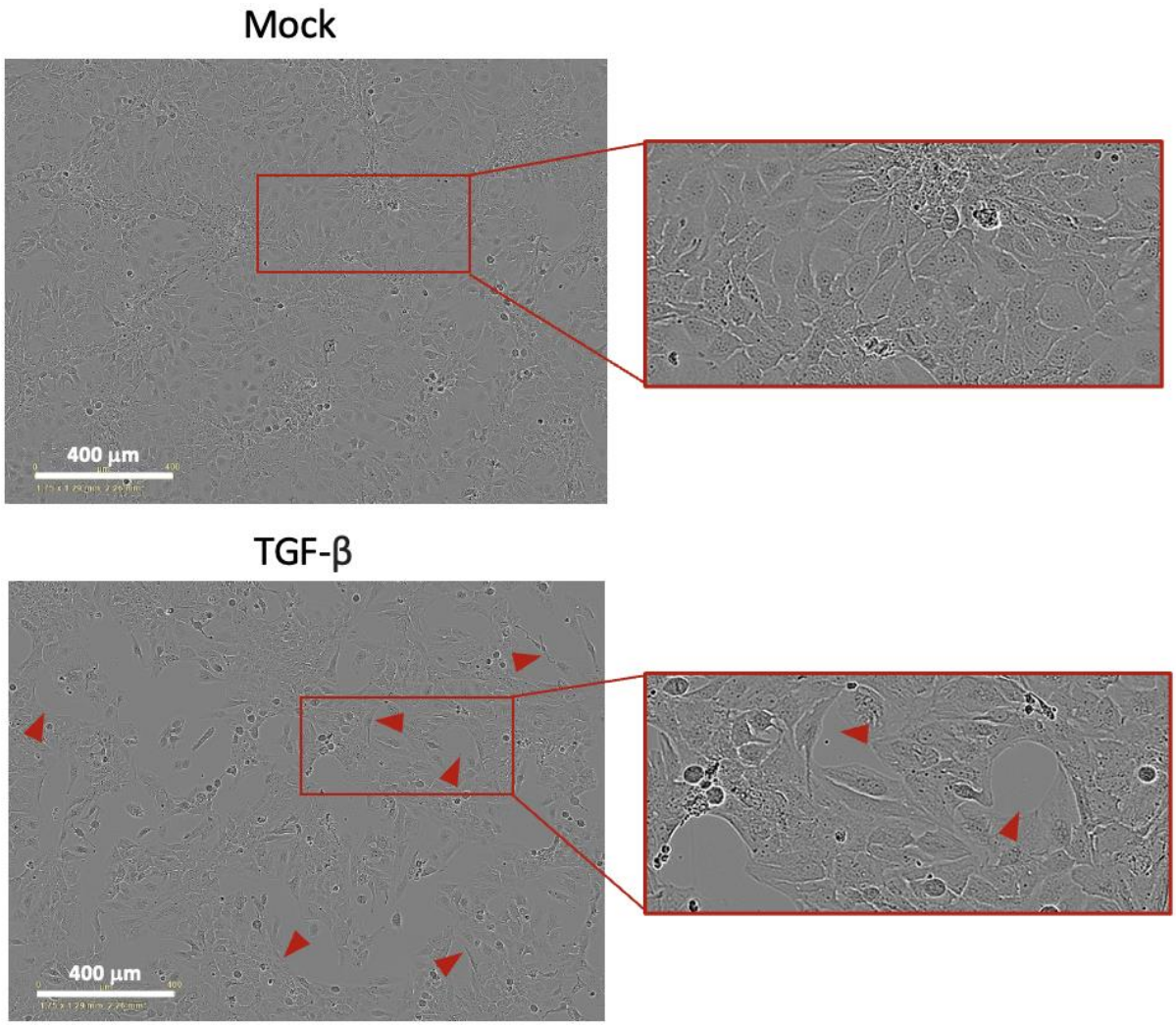

Figure 5.9 Phenotype of co-cultured Huh7 and LX-2 cells in the presence of TGF-β.

A) Representative images of Huh7 and LX-2 cells treated with and without TGF-β (10 ng/mL). Phase images with red arrows highlighting changes in cell morphology and squares highlighting enlarged area. Images were taken at 10 x magnification and scale bars = 400 microns.

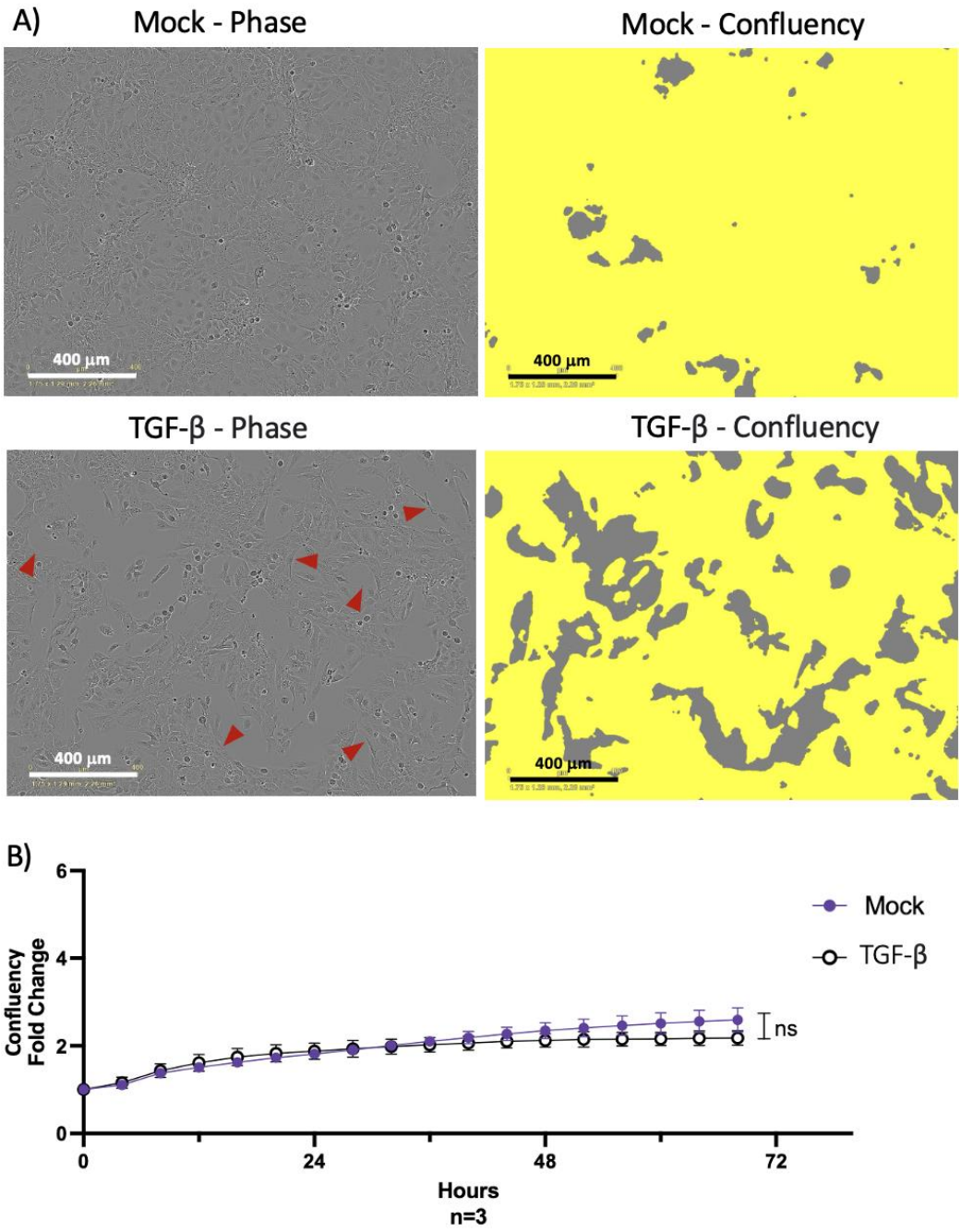

Figure 5.10 Cell growth of co-cultured Huh7 and LX-2 cells in the presence of TGF-β.

A) Representative images of Huh7 and LX-2 cells treated with and without TGF-β (10 ng/mL). Phase images with red arrows highlighting changes in cell morphology. Within the same view as phase images, confluency images highlighting area an analysed by the IncuCyte S3 as being occupied by a cell in yellow. Images acquired by the IncuCyte S3, taken at 10 x magnification and scale bars = 400 microns. B) Cell growth analysed by confluency changes over time and normalised to 4 hour post seeding confluency. Statistical analysis was completed for fold change confluency values at 68 hours post seeding. Data are presented as mean with standard deviation. Statistical significance was tested using unpaired t test assuming both populations have the same standard deviation. P values; ns, P ≥0.05.

5.2.5. Direct cell:cell contact of Huh7 and LX-2 cells does not enhance the expression of a pro-fibrotic state

To investigate the requirement of cell:cell contact of Huh7 cells to LX-2 cells in order to induce a pro-fibrotic state during HCV infection, a mixed monolayer culture of both cell types was established before either infecting with HCV or treatment with TGF-β. To confirm HCV does not induce changes in cell growth, confluency analysis of the mixed monolayer culture was performed (Figure 5.11). Results confirm previous data that LX-2 cell activation or infection of Huh7 cells with HCV or TGF-β treatment in a mixed cell culture cannot determine the progression of a pro-fibrotic state as presence of HCV nor TGF-β alters cell growth (Figure 5.11 A). Further confirmation that the mixed cell culture reflects cell growth characteristics observed with Huh7 cells is confirmed by comparing the cell confluency of Huh7 cells only and the use of the monolayer cell co-culture (Figure 5.11 B). To determine if the presence of LX-2 cells enhances stress markers during HCV infection, qPCR analysis of Snail-1, ZEB-1, fibronectin and TGF-β was performed (Figure 5.12). Overall, there are no significant differences between Huh7 cells cultured alone in comparison to the co-culture suggesting direct interaction of Huh7 cells and LX-2 in the presence of HCV and the treatment of TGF-β does not increase the expression of stress markers. Comparison of JFH-1 and DBN3a infection inducing stress markers replicates previous results that there are no significant differences between HCV GTs inducing stress in the host cell. However, to confirm the activation of LX-2 cells, fibrosis markers of αSMA, Col1A1 and TIMP1 must be analysed by qRT-PCR (Figure 5.13). There are no significant changes in the expression of fibrosis markers in the presence of HCV or TGF-β between the mono- and co-cultures. When comparing mRNA gene expression of HCV GTs, JFH-1 and DBN3a appear to elicit similar expression characteristics with the exception of αSMA. There is a trend of αSMA expression being reduced in the presence of JFH-1, in comparison to mock and DBN3a (Figure 5.13 A). Despite using a range of monolayer cell culture models including mono-, conditioned

media and co- cultures, HCV infection does not induce a pro-fibrogenic state in Huh7 cells nor LX-2 cells, independent of the HCV GT present.

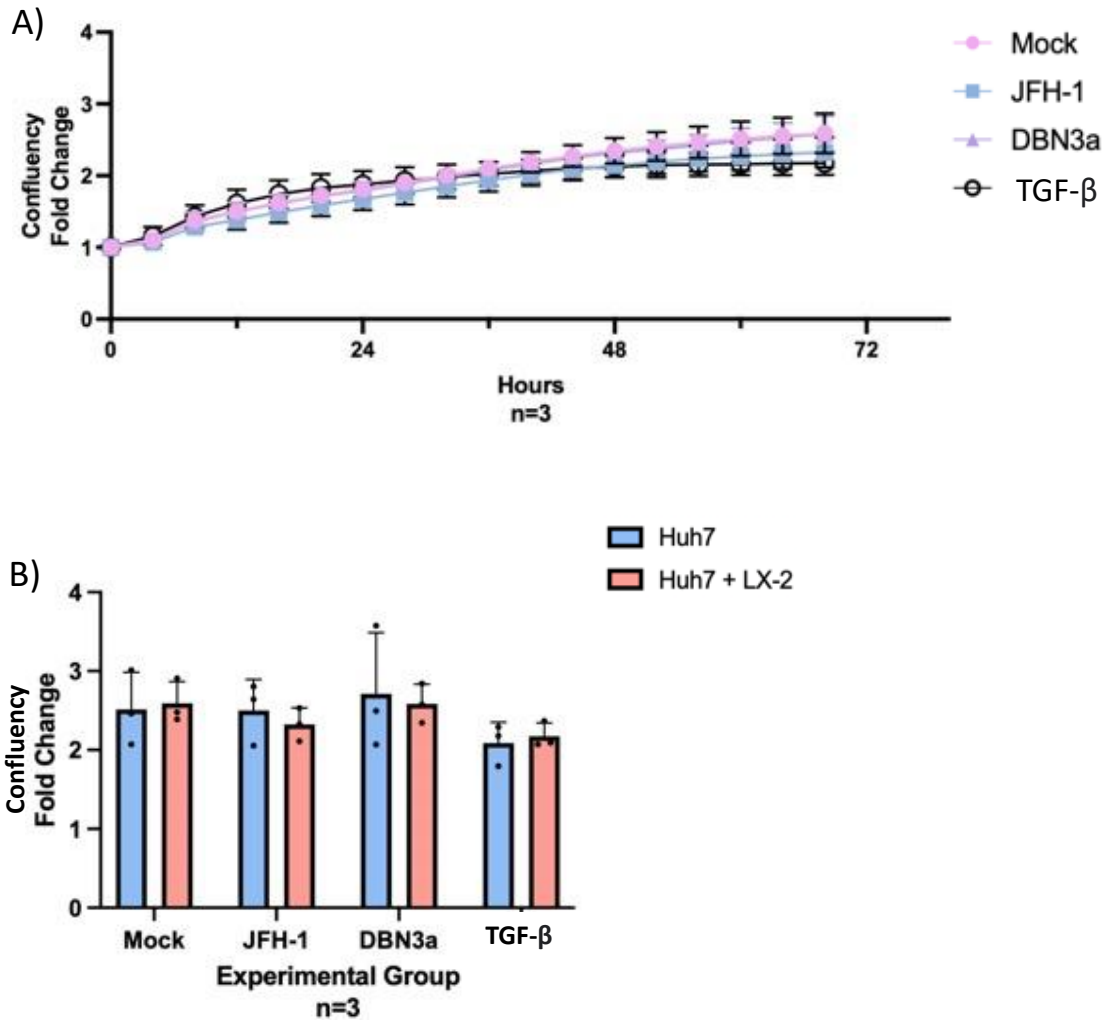

Figure 5.11 Cell growth of co-cultured Huh7 and LX-2 cells is not affected by HCV infection.

A) Cell growth analysed by confluency changes overtime and normalised to 4 hour post seeding confluency and infection with HCV JFH-1 or DBN3a (MOI 0.2) or TGF-β (10 ng/mL) treatment. B) Comparison of monocultured Huh7 cells and co-cultured Huh7 and LX-2 cells infected with HCV. Cell growth analysed by IncuCyte S3. Statistical analysis was completed for fold change confluency values at 68 hours post seeding. Data are presented as mean with standard deviation. Statistical significance was tested using one-way ANOVA with the Bonferroni's multiple comparison test, with a single pooled variance. P values; ns, P ≥0.05.

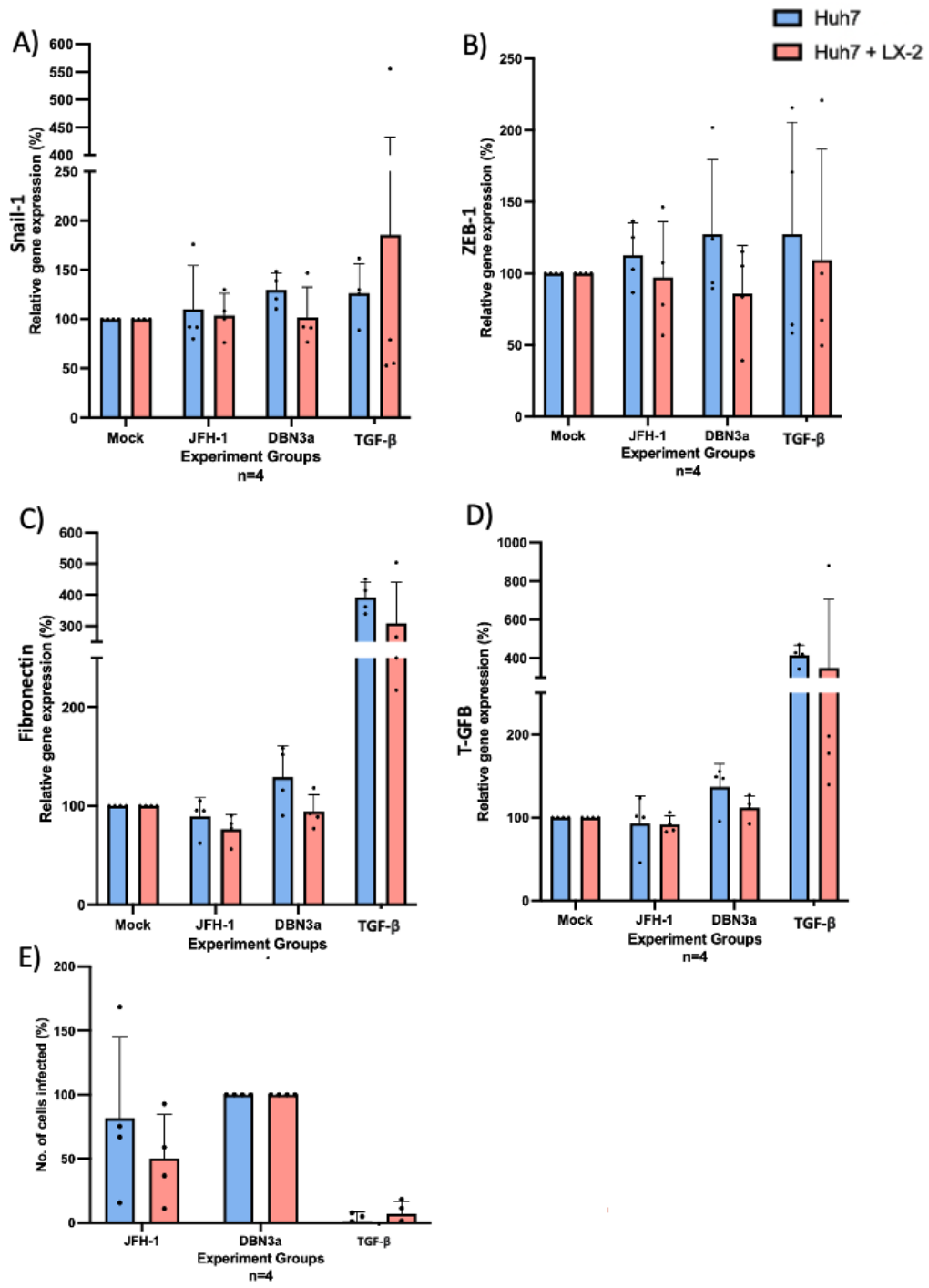

Figure 5.12 Co-culturing of Huh7 cells with LX-2 cells does not induce stress markers during HCV infection.

Co-cultured Huh7 and LX-2 cells infected with JFH-1 and DBN3a (MOI 0.2) infectious virus or treated with TGF-β (10 ng/mL) and harvested 72 h.p.i. mRNA expression of stress markers A) Snail-1 B) ZEB-1, C) fibronectin and D) TGF-β was analysed. E) The number of cells infected by HCV was calculated via anti-sheep NS5A staining and analysis via the IncuCyte S3. Mock values were subtracted, and the number of infected cells normalised to DBN3a values. Data are presented as mean with standard deviation. Statistical significance was tested using one-way ANOVA with the Bonferroni's multiple comparison test, with a single pooled variance. P values; ns, P ≥0.05.

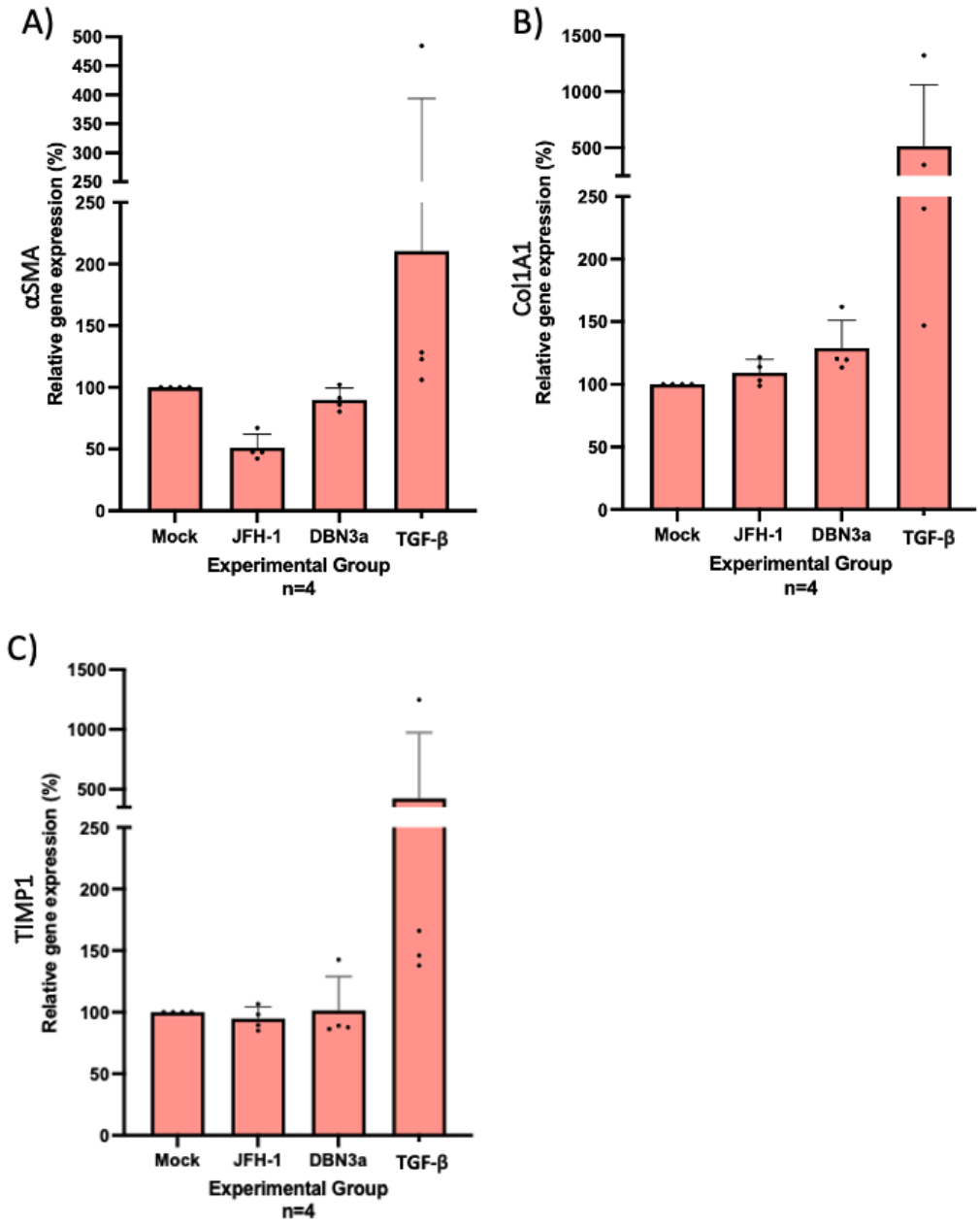

Figure 5.13 LX-2 cells do not become activated when in direct contact with Huh7 cells infected with HCV.

Co-cultured Huh7 and LX-2 cells infected with JFH-1 and DBN3a infectious virus (MOI 0.2) or treated with TGF-β (10 ng/mL) and harvested 72 h.p.i. mRNA expression of fibrosis markers A) αSMA B) Col1A1 and C) TIMP1 was analysed. Data are presented as mean with standard deviation. Statistical significance was tested using one-way ANOVA with the Bonferroni's multiple comparison test, with a single pooled variance. P values; ns, P ≥0.05.

5.2.6. Characteristics of spheroid growth are cell type dependent

To investigate whether the type of cell:cell interaction is important to induce communication promoting pro-fibrogenic pathways and LX-2 cell activation, the formation of Huh7 cell only, LX-2 cell only and, Huh7 and LX-2 mixed cell spheroids was investigated. LX-2 only spheroids were generated as a control to greater understand mixed cell spheroids growth changes as LX-2 cells are not susceptibility to HCV infection and a positive fibrosis control. As the focal point of the IncuCyte S3 image cannot be determined by the user, for ease in producing a high number of spheroids and infecting spheroids in BSL-3, spheroids were formed via the low attachment surface method instead of the hanging droplet method. The IncuCyte S3 allowed regular images to be captured of all spheroid types formed. To ensure the spheroid does not outgrow the field of view imaged, 4X objective lens was used to acquire images for all timepoints (Figure 5.14 A). Analysis of spheroid area may be performed using the IncuCyte S3 by defining of the object via the brightfield view, allowing continual analysis of spheroid formation and growth. The presence of blebbing objects around the circumference of the spheroids, present at 96 h post seeding, are likely due to cells still actively propagating (Figure 5.14 B). Spheroid formation and growth was analysed for 10 days post seeding, using area of spheroids as a measure of spheroid growth (Figure 5.15 A B). Observing the formation of the spheroids immediately post-seeding confirmed the timepoint of complete spheroid formation at 24 h. Complete spheroid formation was classed as the smallest area prior to increasing or stabilisation of spheroid growth, however this was cell type dependent. During the formation of LX-2 cell only spheroids, spheroid size continued to decrease till 96 h post-seeding, followed by stabilisation of the spheroid size. During the 10 day time course, LX-2 only spheroids did not increase in size. Contrary to this, Huh7 cell only spheroids stabilised 24 h post seeding followed by a growth spurt between 72 and 96 h before a second period of stabilised cell growth. A mixed culture of Huh7 cell and LX-2 cell spheroids exhibited both characteristics of the mono-spheroid cell cultures; contracting to a very small size similar to the LX-2 cell only spheroid by 24 h post

seeding but, following a similar trend to Huh7 cell only spheroids, a slight exponential growth phase followed by spheroid stabilisation (Figure 5.15 A). As a possible exponential growth phase was observed in Huh7 only and, Huh7 and LX-2 cell mixed spheroid cultures, 96 h post seeding was deemed as the optimal time of spheroid harvest to minimise the possibility of a necrotic core. Comparison of spheroid volume at 24 and 96 h post seeding confirmed previous spheroid cell line specific characteristics, Huh7 cell only spheroids increase in size however, spheroids containing LX-2 cells do not increase in size (Figure 5.15 B).

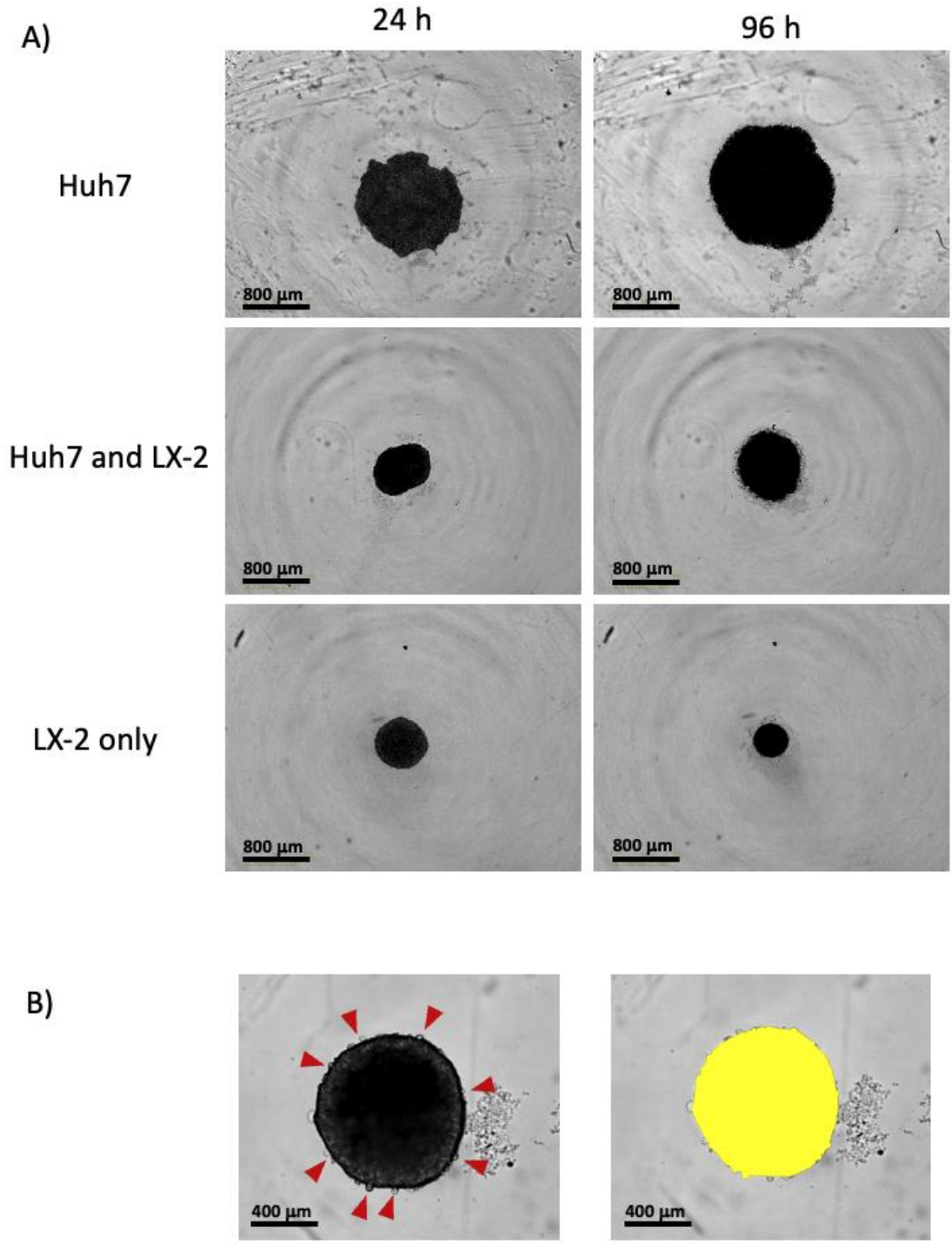

Figure 5.14 Spheroid growth analysed by IncuCyte S3.

A) Representative images of various spheroids formed using mono- and bi- cultures of Huh7 and LX-2 cells formed 24 h and 96 hours post seeding. Images acquired by the IncuCyte S3, taken at 4 x magnification and scale bars = 800 µm. B) Representative image of Huh7 and LX-2 cell spheroids measured by the IncuCyte S3 via brightfield view 96 hours post seeding. Images taken at 10 x magnification and scale bars = 400 microns. Red arrows define single cell growth.

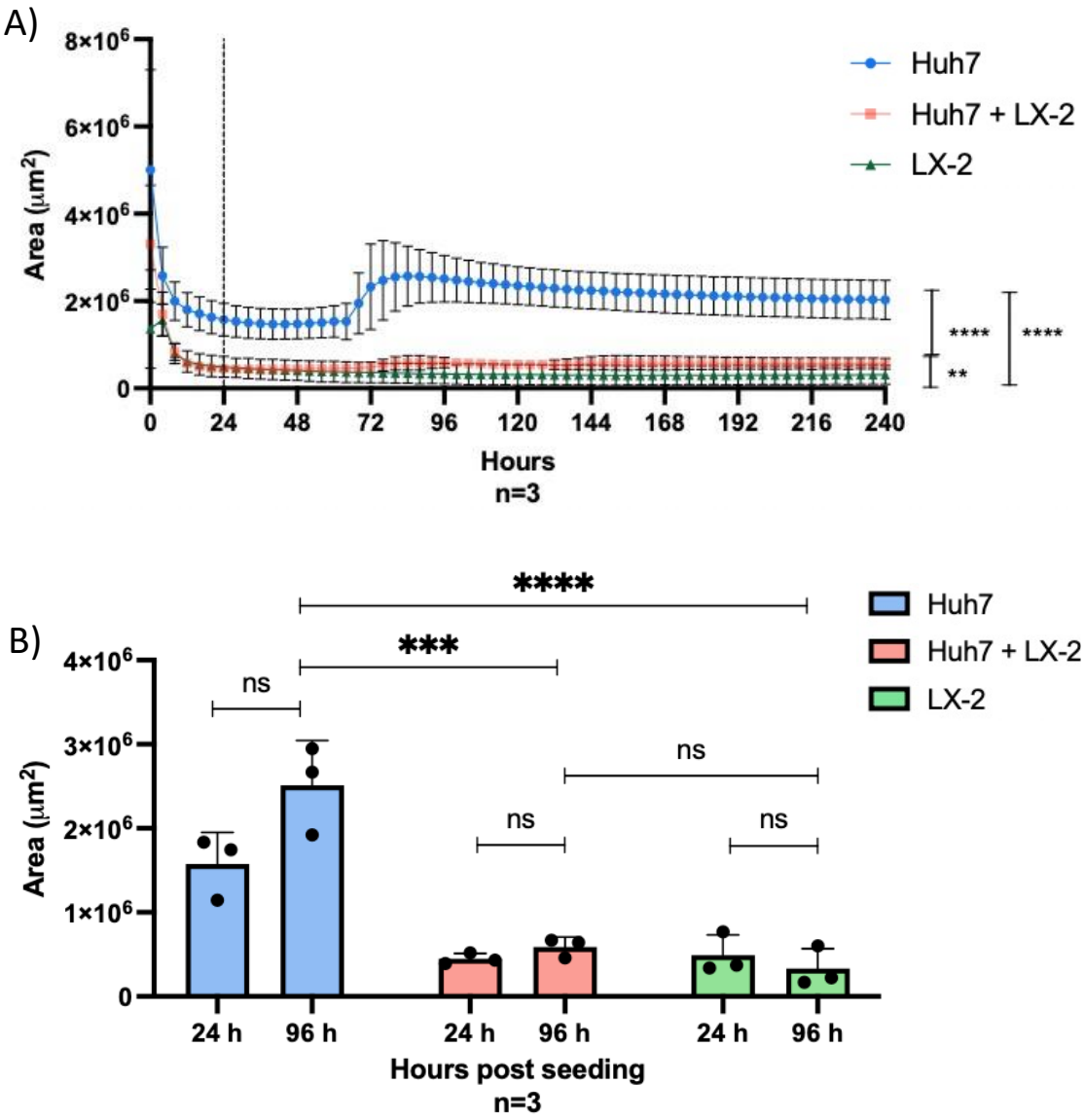

Figure 5.15 Spheroid growth is dependent on the cell type present.

A) Spheroid growth analysed by confluency changes over time. Statistical tests was completed for spheroid area values at 240 hours post seeding. B) Comparison of spheroid growth after spheroid formation at 24 h and 96 hours post seeding. Data are presented as mean with standard deviation. Statistical significance was tested using a one-way ANOVA with the Bonferroni's multiple comparison test, with a single pooled variance. P values; ns, P ≥0.05; **, P <0.005; ***, P <0.0005; ****, P <0.00005.

5.2.7. HCV infection does not change spheroid cell growth

To greater understand the dependence of cell:cell interactions allowing HCV induction of a pro-fibrogenic state, spheroid growth in the presence of infectious HCV, DBN3a, and TGF-

β, acting as a fibrosis induced positive control was analysed. Due to differences in the number of HCV infected cells 72 h.p.i of JFH-1 and DBN3a infection (previously described in Chapter 3), and difficulty in comparing the number of cells infected within a spheroid, only the infection of HCV GT3 assessment of fibrosis induction was performed. HCV infection and treatment of cells with TGF-β was conducted at the time of cell seeding to ensure all cell layers of the spheroid contained DBN3a infected cells or exposed to TGF-β stimuli (Figure 5.16 A). In the presence of HCV, all spheroids regardless of the cell type present grew in the same manner as the mock control (Figure 5.16 B C D). As HCV does not alter a change in spheroid growth of Huh7 containing spheroids, unlike the presence TGF-β resulting in significantly smaller spheroids 96 h.p.i, results suggest pro-fibrotic pathways are not induced. As TGF-β directly stimulates fibrogenic pathways, I believe spheroids containing Huh7 cells only may have reduced growth in response to the activation of fibrogenic pathways. Co-cultured spheroids, containing 1:1 ratio of Huh7 and LX-2 cells, appear to have a delayed reduction to spheroid growth 72 h post seeding in comparison to the Huh7 only cell spheroid with an immediate reduction 24 h.p.i. Interestingly, regardless of the activation of LX-2 cells, LX-2 only cell spheroids do not change in area. To quantify the variation of spheroid formation in the presence of HCV or TGF-β, spheroid size was compared 24 h.p.i (Figure 5.17 A). The area of Huh7 cell only spheroids formed 24 h.p.i is significantly impacted in the presence of TGF-β but not HCV however, regardless of the stimuli present, the area of formed LX-2 cell containing spheroids is not impacted. As LX-2 cell containing spheroids, particularly LX-2 only spheroids, do not vary in spheroid formation or growth in the presence of a pro-fibrotic stimulus, spheroid size of LX-2 containing spheroids cannot be a defining factor of fibrosis pathway activation. Additionally, the circularity of formed spheroids was compared at 24 and 96 h.p.i. Comparison of spheroids formed by different cell types suggests Huh7 cell spheroids form less circular spheroids and more varied spheroid circularity between biological repeats than spheroids containing LX-2 cells. The circularity score is measured on the circularity index between 0 (fully linear) and 1 (fully circular). By 96 h.p.i,

Huh7 cell spheroids show greater circularity than spheroids formed at 24 h.p.i, this trend is reversed when observing spheroids formed containing LX-2 cells, less circular spheroids at 96 h.p.i than 24 h.p.i. Additionally, HCV nor TGF-β presence alters the circularity of spheroids formed (Figure 5.17 B). Confirmation of HCV infection was performed via the detection of the HCV 5'UTR (Figure 5.17 C). Interestingly, the circularity of Huh7 and LX-2 cell spheroids reduction in circularity is significantly reduced in the presence of DBN3a. These results suggest a change in cell type characteristic of Huh7 cell and LX-2 cells between monolayer and spheroid cultures in the presence of fibrosis inducing stimuli. In relation to spheroid formation and growth during a 96 h time course, spheroid phenotype does not change in the presence of HCV, however analysis of stress and fibrosis markers are required to confirm the activation of fibrotic pathways.

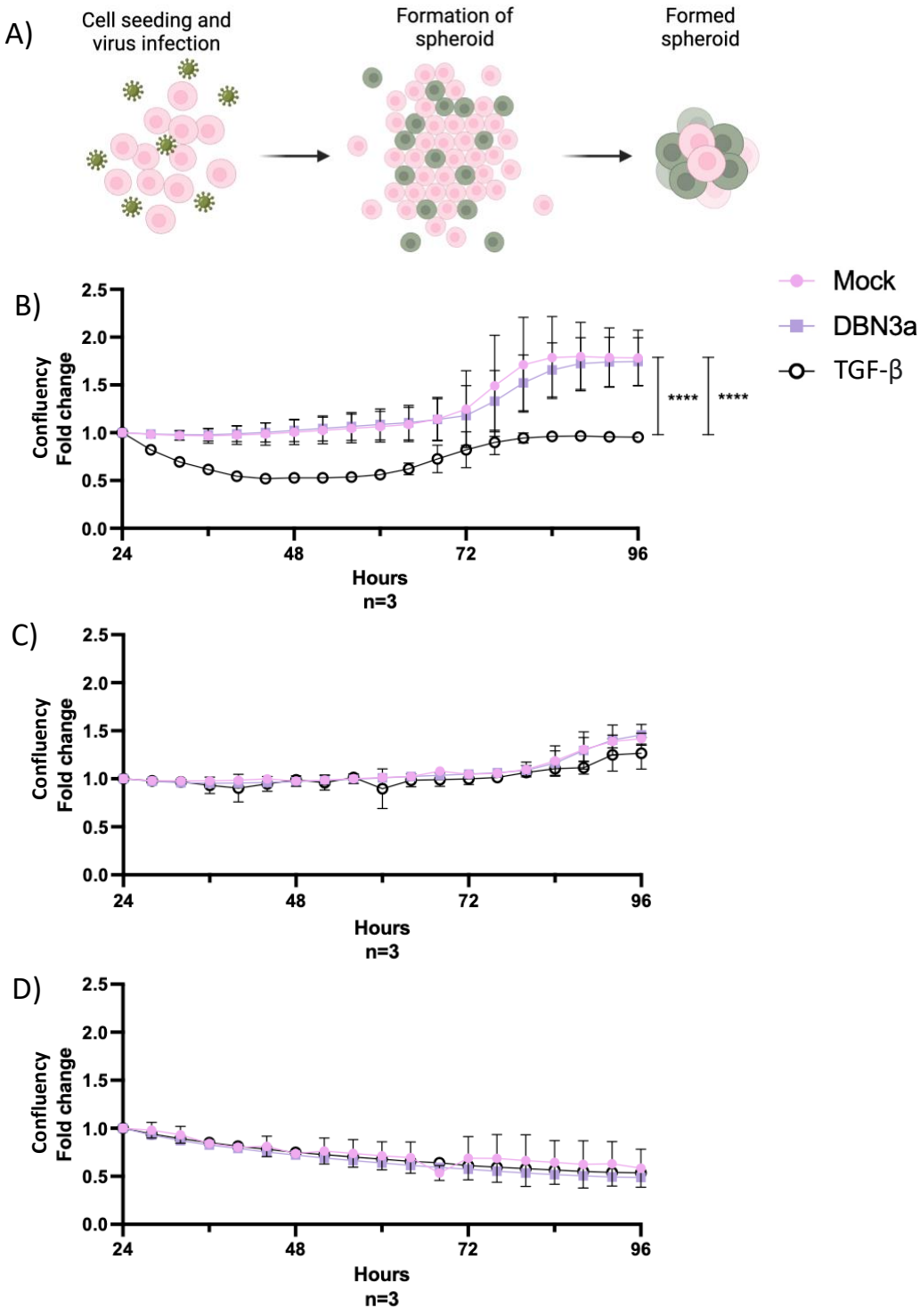

Figure 5.16 HCV GT3 does not alter spheroid growth regardless of cell types present.

A) Schematic of spheroid formation and virus infection. Spheroid growth analysed by IncuCyte S3 B) Huh7 cells only, C) co-cultured Huh7 and LX-2 cells and D) LX-2 cells only. Spheroid growth normalised to spheroid area 24 hours post seeding. Statistical analysis was completed 96 hours post seeding. Data are presented as mean with standard deviation. Statistical significance was tested using one-way ANOVA with the Bonferroni's multiple comparison test, with a single pooled variance. P values; ns, P ≥0.05; ****, P <0.00005.

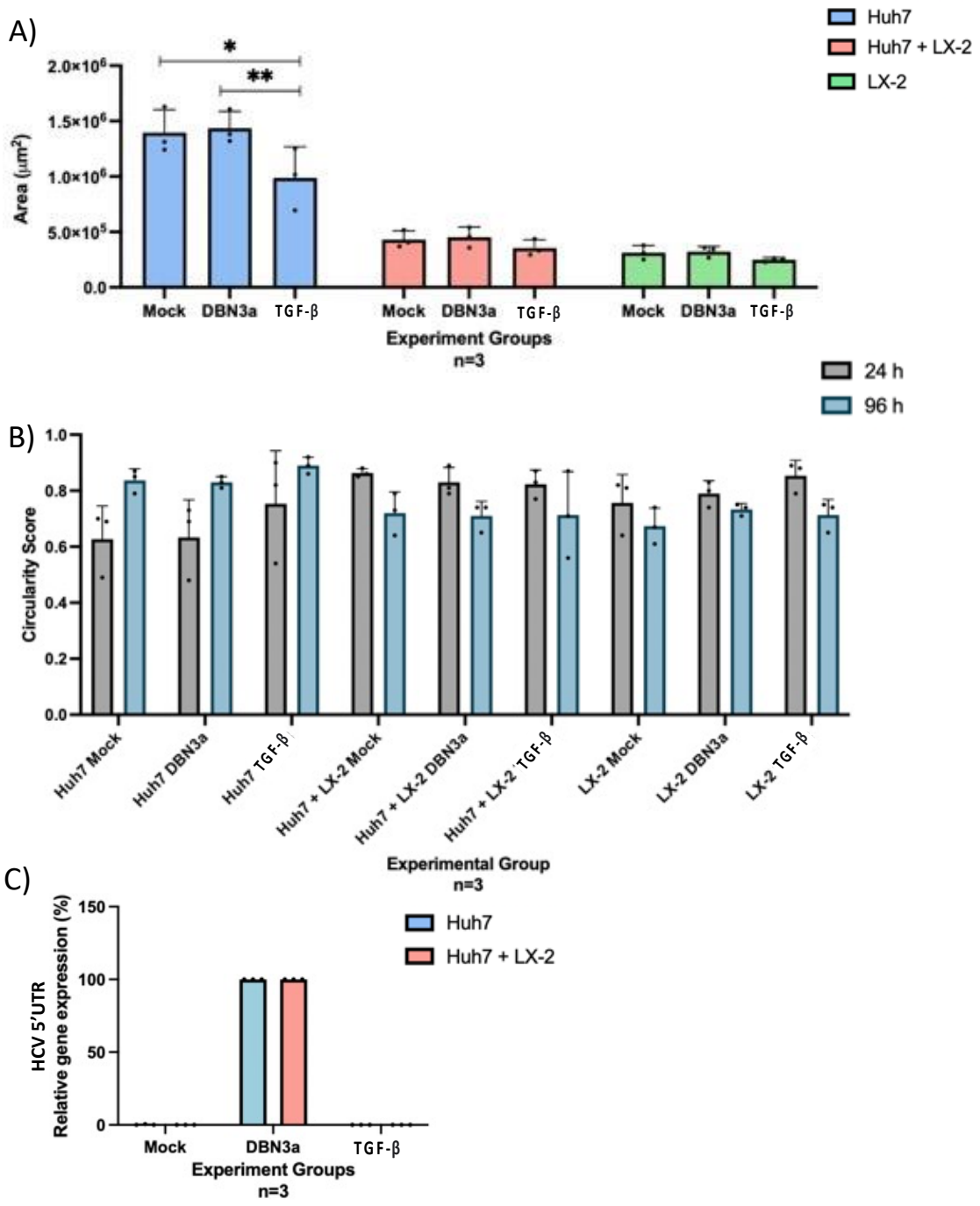

Figure 5.17 HCV GT3 does not impact spheroid formation.

Spheroid growth analysed by IncuCyte S3 A) Spheroid area 24 hours post seeding. B) Circularity score of spheroids compared 24 and 96 hours post seeding analysed via SpheroidJ Fiji plug-in. Spheroids were formed in the presence of DBN3a (MOI 0.2) or TGF-β (10 ng/mL). C) Confirmation of HCV infection via qRT-PCR detecting the presence of the HCV 5'UTR. Data are presented as mean with standard deviation. Statistical significance was tested using one-way ANOVA with the Bonferroni's multiple comparison test, with a single pooled variance. P values; ns, P ≥0.05; *, P <0.05; **, P <0.005.

5.2.8. Spheroids do not contain a necrotic core

Unlike in the context of cancer research, a necrotic core in the centre of the spheroids would result in a misrepresentation of results as I desired to study the progression of fibrosis in a healthy non-diseased liver which does not contain a necrotic core. To confirm the spheroids did not contain a necrotic core, spheroids were stained with Hoechst 33342 and propidium iodide (PI). Classically used in spheroid research to confirm a necrotic core, as well as cell viability assays in a range of cell models, Hoechst 33342 is cell permeable stain for double stranded DNA of both live and dead cells, whereas PI is excluded from live cells and thus only able to stain the DNA of dead cells. If a necrotic core was present, it would be expected to see PI staining in the centre of the spheroid. The presence of a necrotic core was investigated in all spheroid types at 96 h post seeding; Huh7 only (Figure 5.18), Huh7 and LX-2 mixed culture (Figure 5.19) and LX-2 only (Figure 5.20), acquiring cross-sectional images of the spheroids using confocal microscopy. Doxorubicin, a chemotherapy drug used to slow or stop the growth of cancer cells, was used as a positive control for PI staining (Ncube et al., 2023). Phase images were gathered for non-stained samples to ensure the spheroid was within the field of view as could not be detected with the use of fluorescence signal. Interestingly, visualisation of individual Huh7 only spheroids appear very different from LX-2 only or co-cultured spheroids. I believe this is due to the magnification being too high to observe the whole spheroid; the same magnification lens was used to maintain consistency between experimental groups. Furthermore, Huh7 only spheroids were more fragile when handling the spheroids, easily breaking when washing and transferring from wells to cover slips. Images for all spheroid types confirm the absence of a necrotic core ensuring spheroids harvested 96 h post seeding are representative of a healthy liver.

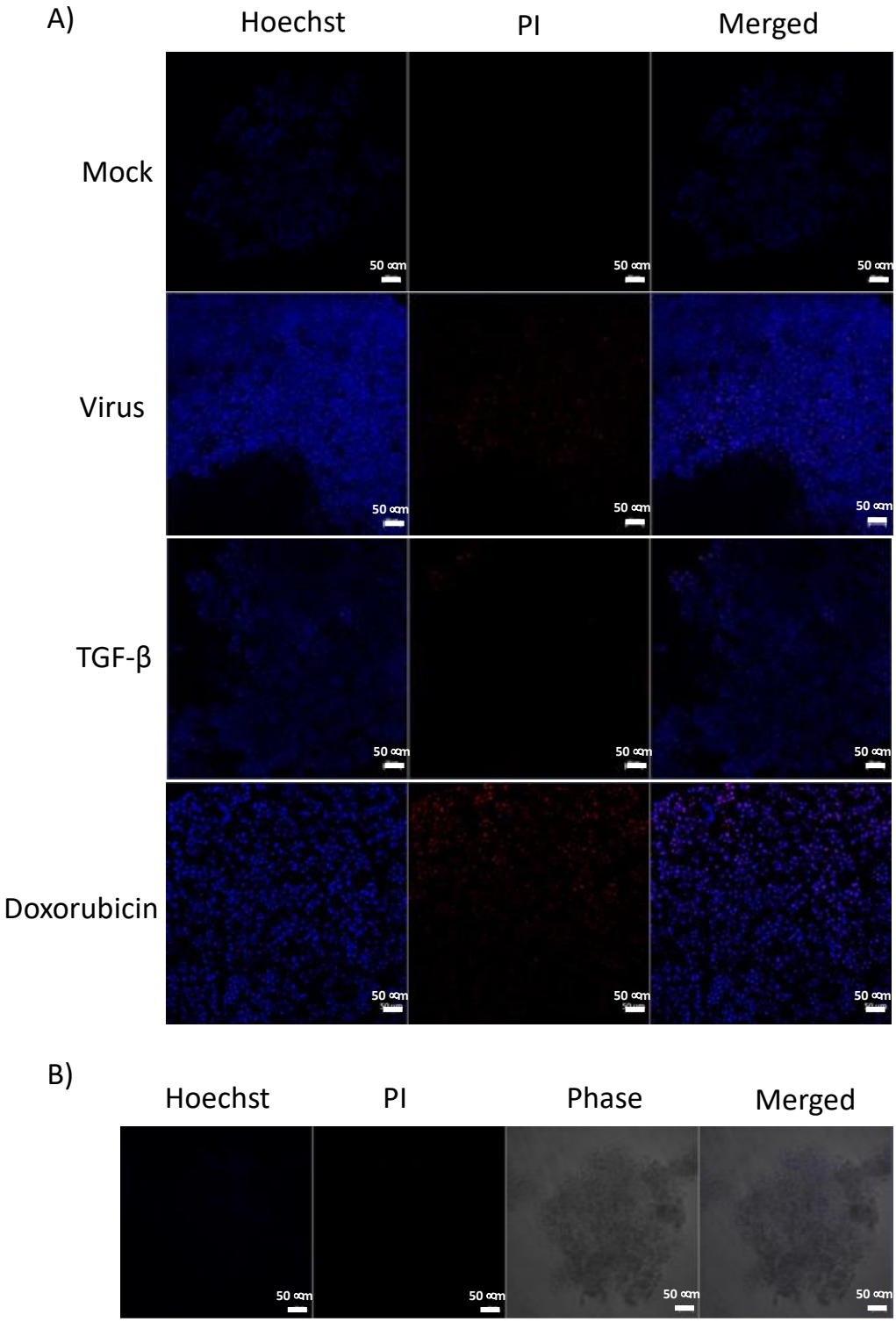

Figure 5.18 Absence of a necrotic core within Huh7 cell spheroids.

Spheroids formed containing only Huh7 cells were cultured for 96 hours post seeding either in the presence of DBN3a (MOI 0.2), TGF-β (10 ng/mL) or doxorubicin 200 nM (treated 12 hours post-harvest). A) Spheroids were stained with Hoechst 33342 and propidium iodide (PI) prior to fixation via 4% PFA. B) Non-stained spheroids directly fixed. Cross-sectional Images acquired with the Zeiss Inverted Confocal microscope LSM 880 magnification 20x and scale bar = 50 microns.

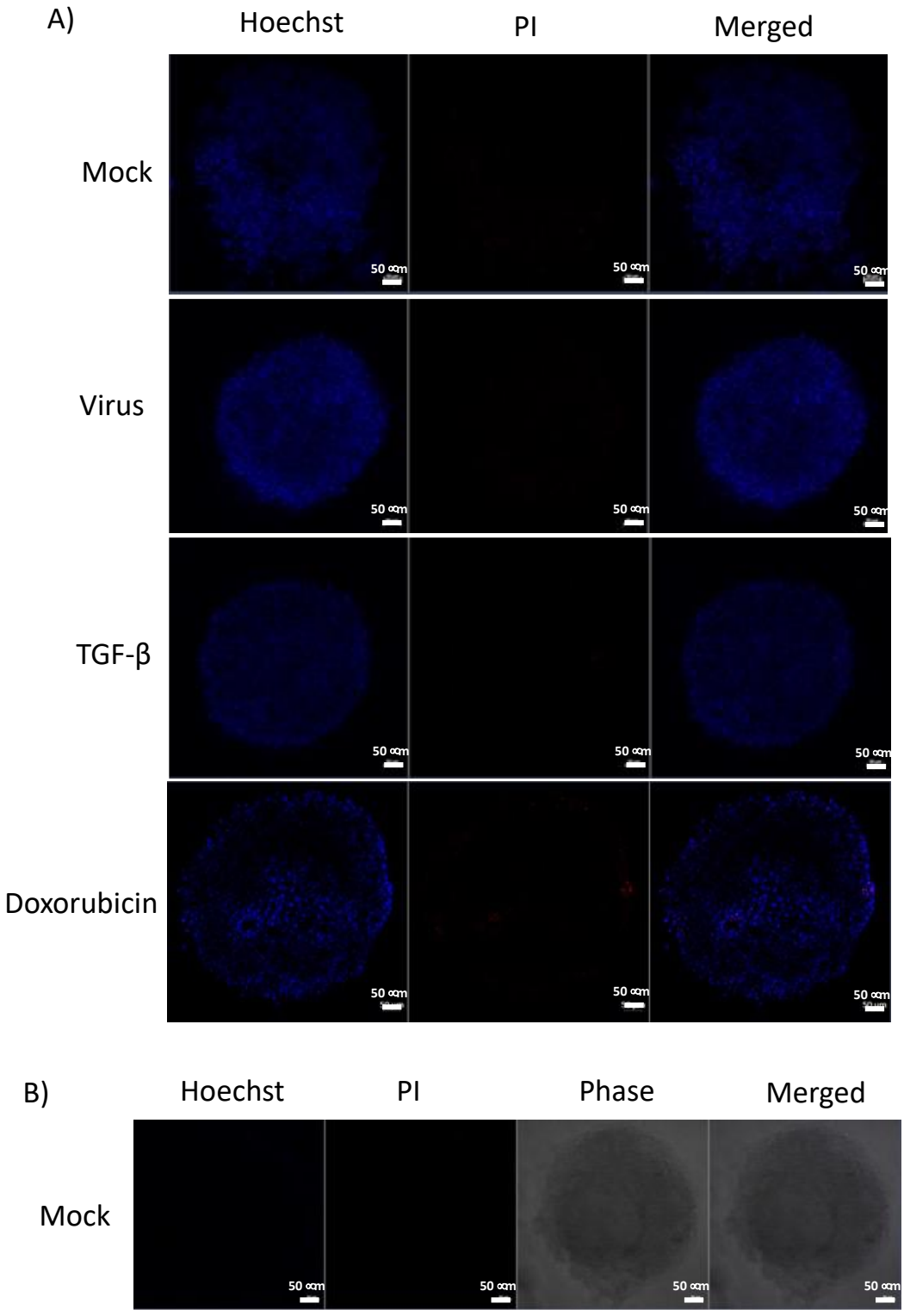

Figure 5.19 Absence of a necrotic core within Huh7 and LX-2 cell spheroids.

Spheroids formed containing Huh7 and LX-2 cells were cultured for 96 hours post seeding either in the presence of DBN3a (MOI 0.2), TGF-β (10 ng/mL) or doxorubicin 200 nM (treated 12 hours post-harvest). A) Spheroids were stained with Hoechst 33342 and propidium iodide (PI) prior to fixation via 4% PFA. B) Non-stained spheroids directly fixed. Cross-sectional Images acquired with the Zeiss Inverted Confocal microscope LSM 880 magnification 20x and scale bar = 50 microns.

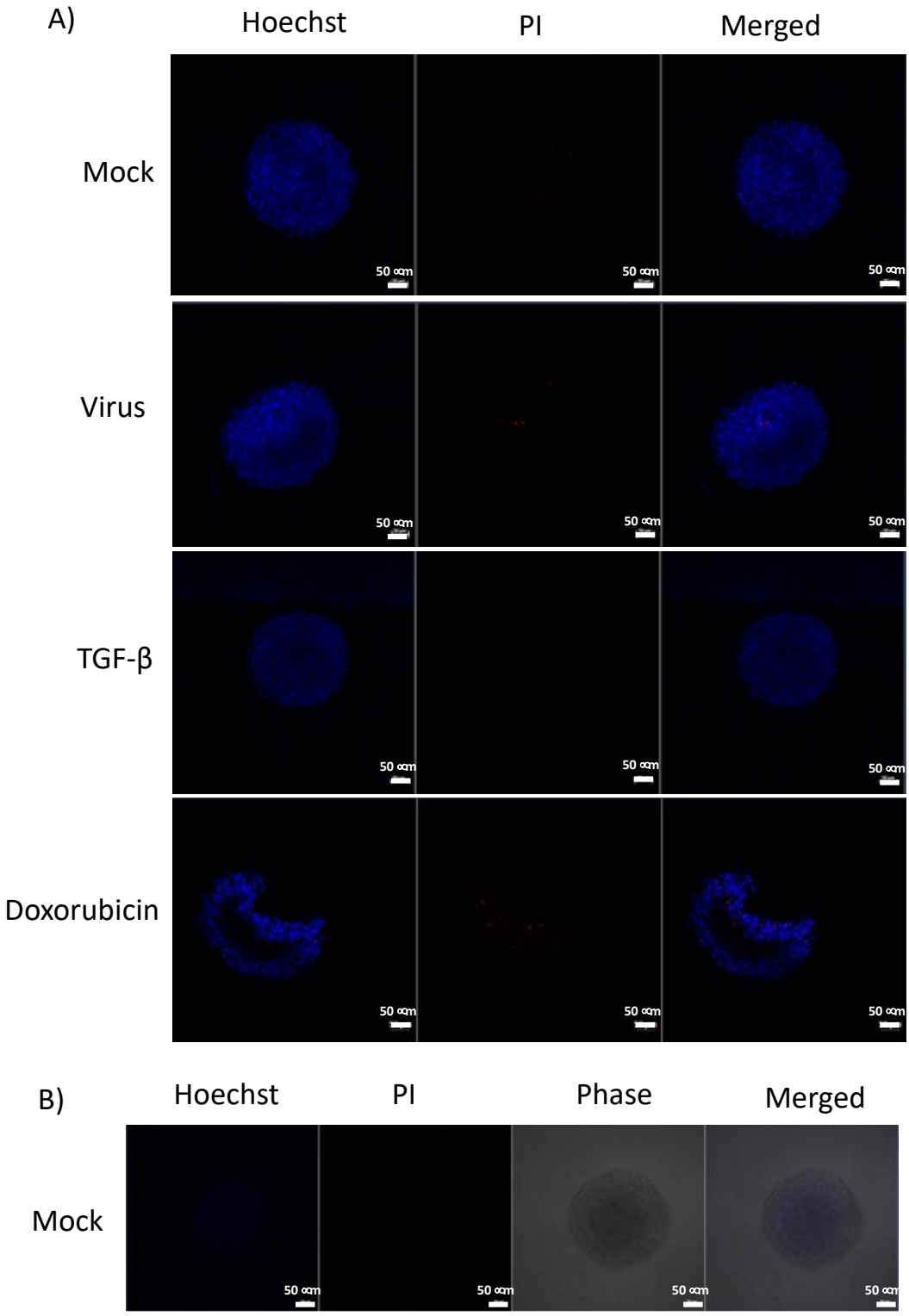

Figure 5.20 Absence of a necrotic core within LX-2 cell spheroids.

Spheroids formed containing only LX-2 cells were cultured for 96 hours post seeding either in the presence of DBN3a (MOI 0.2), TGF-β (10 ng/mL) or doxorubicin 200 nM (treated 12 hours post-harvest). A) Spheroids were stained with Hoechst 33342 and propidium iodide (PI) prior to fixation via 4% PFA. B) Non-stained spheroids directly fixed. Cross-sectional Images acquired with the Zeiss Inverted Confocal microscope LSM 880 magnification 20x and scale bar = 50 microns.

5.2.9. Spheroids alter the cellular response to fibrosis stimuli

When comparing cell growth of monolayer and spheroids experiments, it was noted cell lines behave differently when not adhering to plastic and maintained within a 3D culture. For example, Huh7 cell growth is not significantly impacted by the presence of TGF-β in monolayer contrary to 3D culture cell growth, where spheroid volume is significantly reduced in comparison to mock. Variations of spheroid volume may not be used as a factor of fibrosis activation as LX-2 cell containing spheroid volume does not change in the presence of TGF-β. Therefore, stress and fibrosis markers were analysed for spheroids formed and cultured in the presence of HCV and TGF-β. Like monolayer cell culture, the presence of HCV and TGF-β did not result to significant changes in the expression of stress or fibrosis markers, regardless of the cell type present. Like the analysis of monolayer stress markers, the presence of both Huh7 and LX-2 cells did not significantly enhance gene expression in comparison to Huh7 cell only spheroids (Figure 5.21). Interestingly, the increased expression of stress and fibrosis markers observed in monolayer cells stimulated by TGF-β was not observed for both Huh7 cell mono and bi- spheroid cultures but shows general decrease compared with monolayer. Particularly the expression of ZEB-1 is significantly reduced in the presence of TGF-β (Figure 5.21 B). Fibrosis markers of LX-2 cell only spheroids, showing very little variation between biological repeats and expression levels similar to the mock control confirms LX-2 cells are not impacted by the presence of HCV however, the presence of TGF-β also does not significantly induce the expression of fibrosis markers. There appears to be greater variation of general gene expression in co- cultures in comparison to mono- LX-2 cell spheroids (Figure 5.22). Gene analysis of spheroids in the presence of HCV supports monolayer infection results, HCV does not induce fibrogenic pathways during early stages of infection however, differences between gene expression in the presence of TGF-β within spheroids suggests 3D cell cultures alter the cellular response to fibrosis stimuli. Overall, the presence of TGF-β inducing stress and fibrosis markers appear reduced in spheroids in comparison to monolayer experiments.

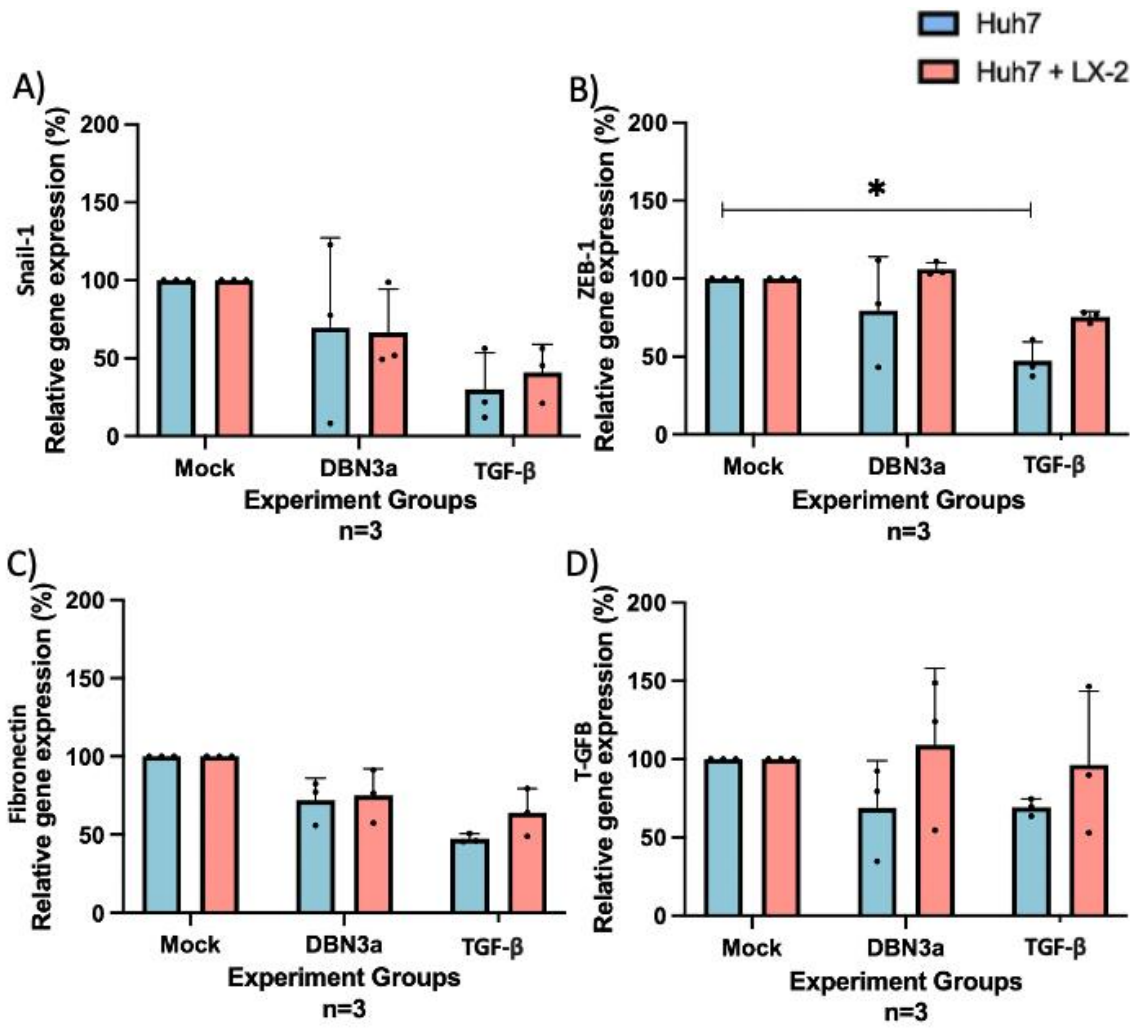

Figure 5.21 3D cell culture does not enhance HCV induction of stress markers.

mRNA expression of spheroids formed using Huh7 cells infected by DBN3a (MOI 0.2) or TGF-β (10 ng/mL) analysed for stress markers; A) Snail-1 B) ZEB-1, C) fibronectin and D) TGF-β. Data are presented as mean with standard deviation. Statistical significance was tested using one-way ANOVA with the Bonferroni's multiple comparison test, with a single pooled variance. P values; ns, P ≥0.05; *, P <0.05.

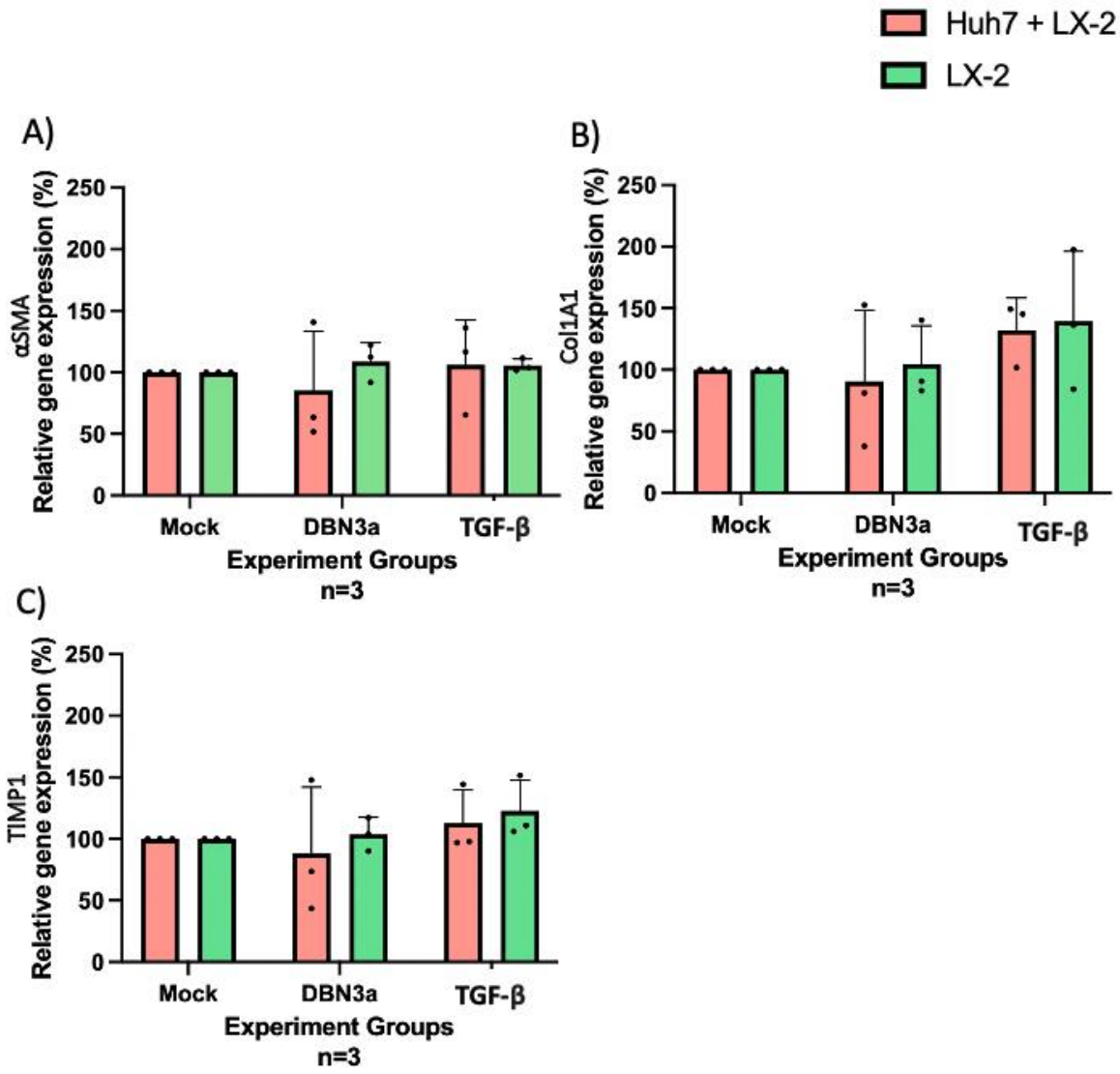

Figure 5.22 3D cell culture does not enhance HCV induction of fibrosis markers.

mRNA expression of spheroids formed using Huh7 cells only or Huh7 cells with LX-2 cells infected by DBN3a (MOI 0.2) or treated with TGF-β (10 ng/mL) analysed for fibrosis markers A) αSMA B) Col1A1 and C) TIMP1. Data are presented as mean with standard deviation. Statistical significance was tested using one-way ANOVA with the Bonferroni's multiple comparison test, with a single pooled variance. P values; ns, P ≥0.05.

5.2.10. Presence of macrophages do not induce fibrosis during early stages of HCV infection

As macrophages have been defined as a major cell type involved in fibrosis, I aimed to investigate the role of macrophages in the presence of different HCV GTs in the co- monolayer cell culture. Non-differentiated THP1 cells (in suspension) were combined to the adherent monolayer culture of Huh7 cell and LX-2 cell cultured (ratio 1:1:1) in the presence of JFH-1, DBN3a or TGF-β; differentiating monocytes into macrophages. Cells were harvested and downstream analysis was only conducted on the adherent monolayer of Huh7 cells and LX-2 cells. Replicating previous monolayer cell culture results, HCV infection does not result in reduced cell growth (Figure 5.23 A). Cell growth analysis of Huh7 cell and LX-2 cells in the presence of macrophages suggests a reduction of cell growth in the presence of TGF-β (Figure 5.23 B). To confirm HCV early stages of HCV infection does not induce pro-fibrogenic pathways, stress (Figure 5.24) and fibrosis markers (Figure 5.25) were analysed and compared to monolayer culture. Stress markers in the presence of THP1 cells and TGF-β stimulant suggests marginal differences in comparison to mono- and co- cultures. Likewise, in the presence of HCV, there appears to be no significant difference or trends relating to the expression of stress markers dependent on the cell type and specific HCV GT present. This is comparable to the results of fibrosis markers. These results suggest THP1 cells do not play a role in mediating the expression of stress and fibrosis markers.

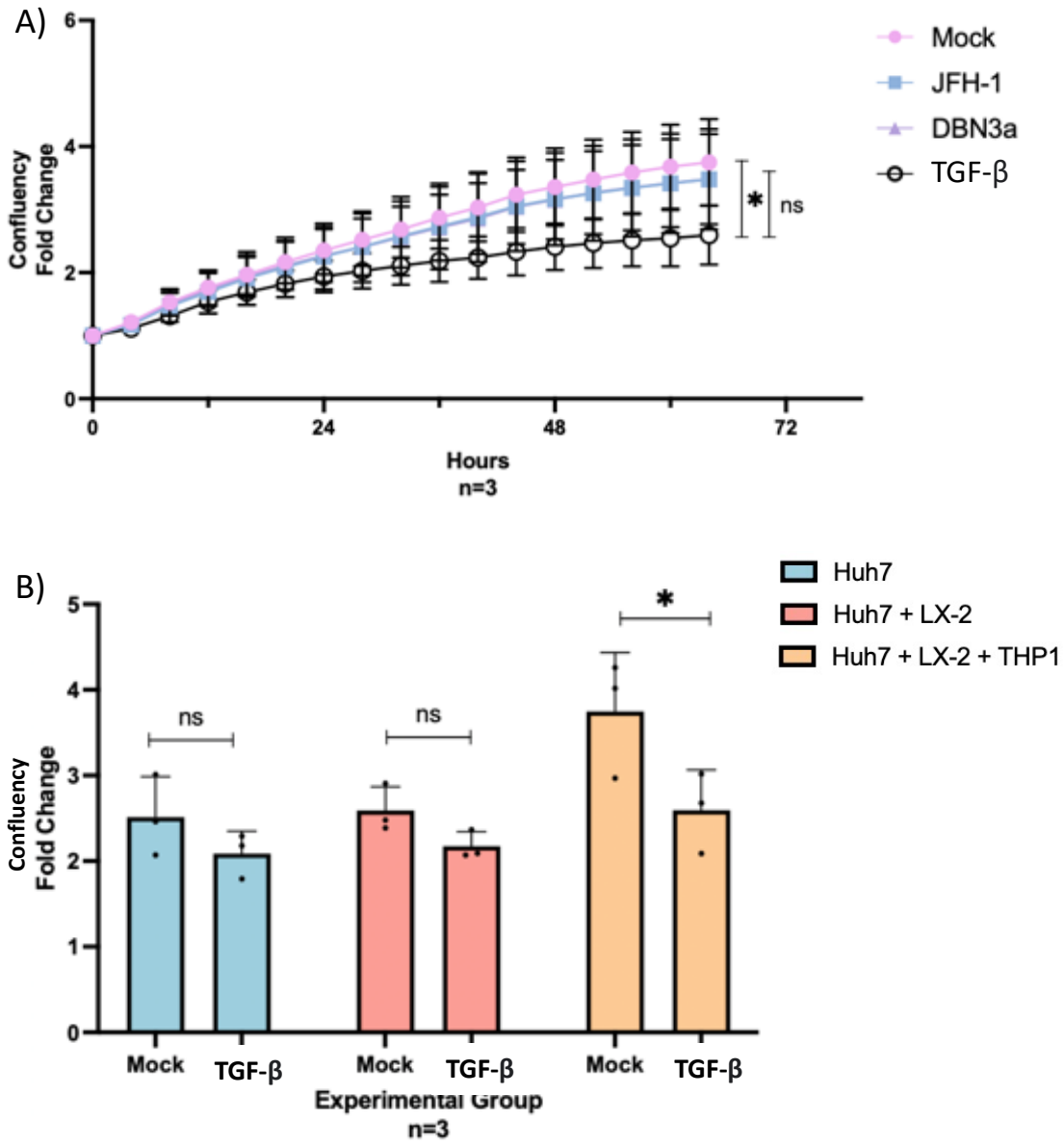

Figure 5.23 Cell growth of co-cultured Huh7, LX-2 and THP1 cells is not affected by HCV infection.

Cell cultures were grown in the presence of HCV JFH-1, DBN3a (MOI 0.2) and TGF-β (10 ng/mL). A) Cell growth analysed by confluency changes overtime and normalised to 4 hour post seeding confluency. B) Comparison of mono- cultured Huh7 cells, co- cultured Huh7 cell and LX-2 cells and, Huh7, LX-2 and THP1 cells co- cultured in the presence of fibrosis stimulant TGF-β. Cell growth analysed by IncuCyte S3. Statistical analysis was completed for fold change confluency values at 68 hours post seeding. Data are presented as mean with standard deviation. Statistical significance was tested using one-way ANOVA with the Bonferroni's multiple comparison test, with a single pooled variance. P values; ns, P ≥0.05; *, P <0.05.

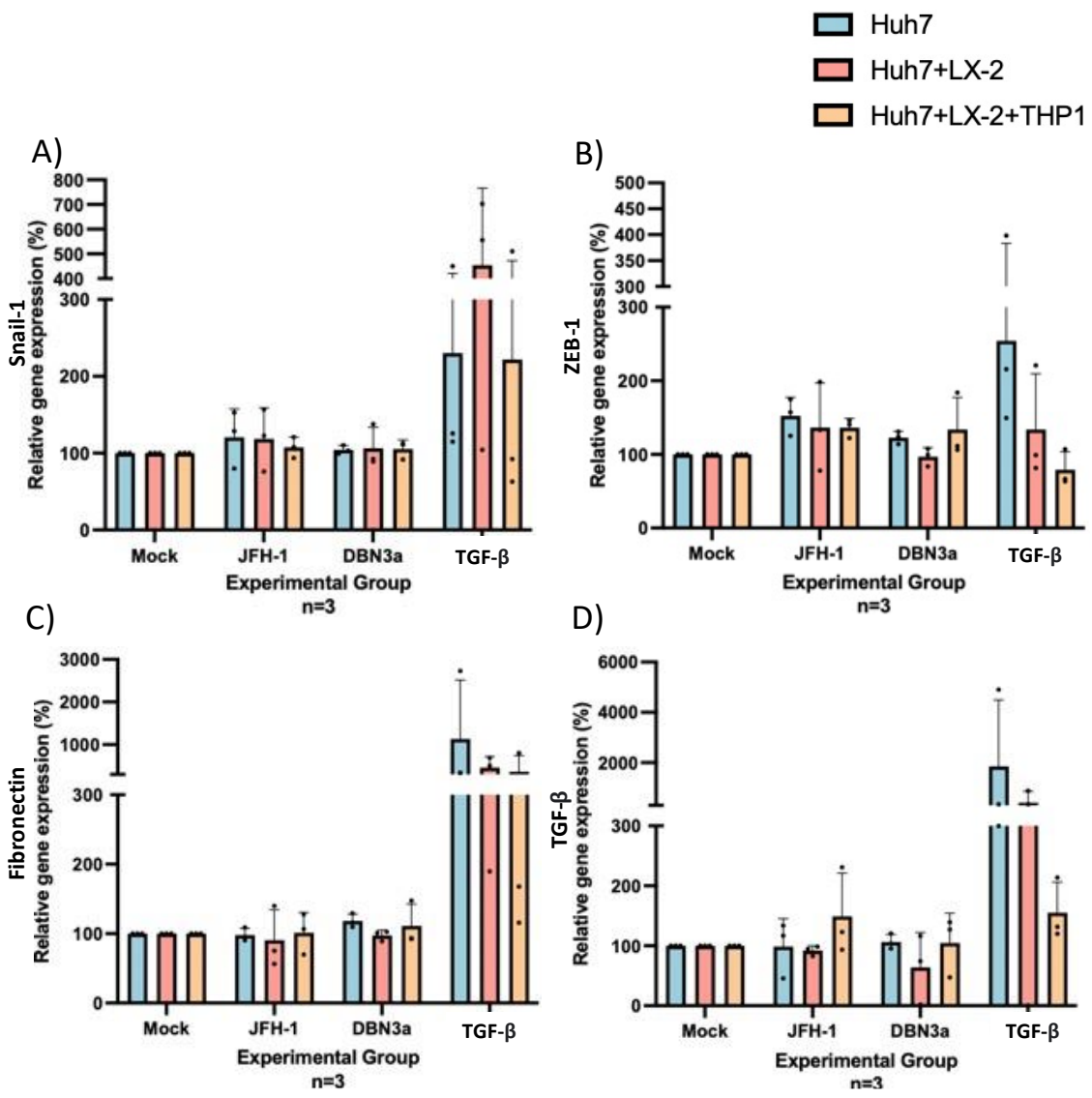

Figure 5.24 Co-culturing of Huh7 cells with LX-2 and THP1 cells does not induce stress markers during HCV infection.

Co-cultured Huh7, Huh7 and LX-2 cells, and Huh7, LX-2 and THP1 cells infected with JFH-1 and DBN3a infectious virus (MOI 0.2) and TGF-β (10 ng/mL) harvested 72 h.p.i. mRNA expression of stress markers A) Snail-1 B) ZEB-1, C) fibronectin and D) TGF-β was analysed. Data are presented as mean with standard deviation. Statistical significance was tested using one-way ANOVA with the Bonferroni's multiple comparison test, with a single pooled variance. P values; ns, P ≥0.05.

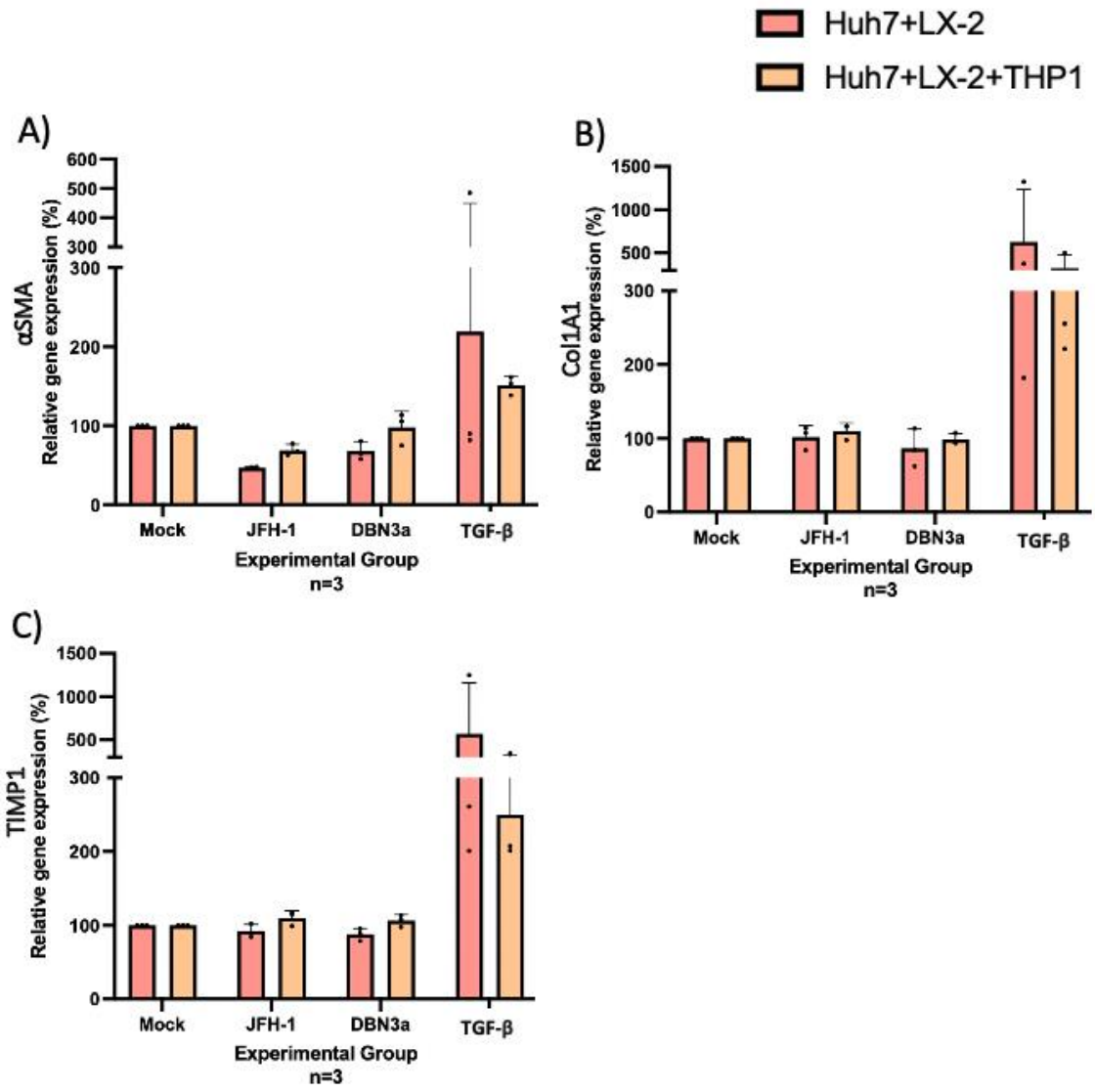

Figure 5.25 Co-culturing of Huh7 cells with LX-2 and THP1 cells does not induce fibrosis markers during HCV infection.

Co-cultured Huh7 and LX-2 cells, and Huh7, LX-2 and THP1 cells infected with JFH-1 and DBN3a infectious virus (MOI 0.2) and TGF-β (10 ng/mL) harvested 72 h.p.i. mRNA expression of fibrosis markers A) αSMA B) Col1A1 and C) TIMP1 was analysed. Data are presented as mean with standard deviation. Statistical significance was tested using one-way ANOVA with the Bonferroni's multiple comparison test, with a single pooled variance. P values; ns, P ≥0.05.

5.2.11. Presence of THP1 restricts DBN3a infection

To determine if THP1 cells play a direct protective role during HCV infection not linked to the expression of stress and fibrosis markers, the number of NS5A infected cells was analysed. To investigate if this was HCV GT specific, cells were infected with either JFH-1 or DBN3a and the number of cells infected was calculated by anti-NS5A immunostaining analysed on the IncuCyte S3 and normalised to Huh7 containing 100% susceptible cells (Figure 5.26). Results suggest in the presence of THP1 cells, DBN3a has a reduced infection efficiency in comparison to JFH-1 infection which appears to infect the same proportion of cells regardless of THP1 cell presence. This data suggests DBN3a infection may trigger an immune response not related to the stress and fibrosis markers analysed. It is important to note, the number of Huh7 cells susceptible to infection has not been quantified between experimental and may be a variable altering the results.

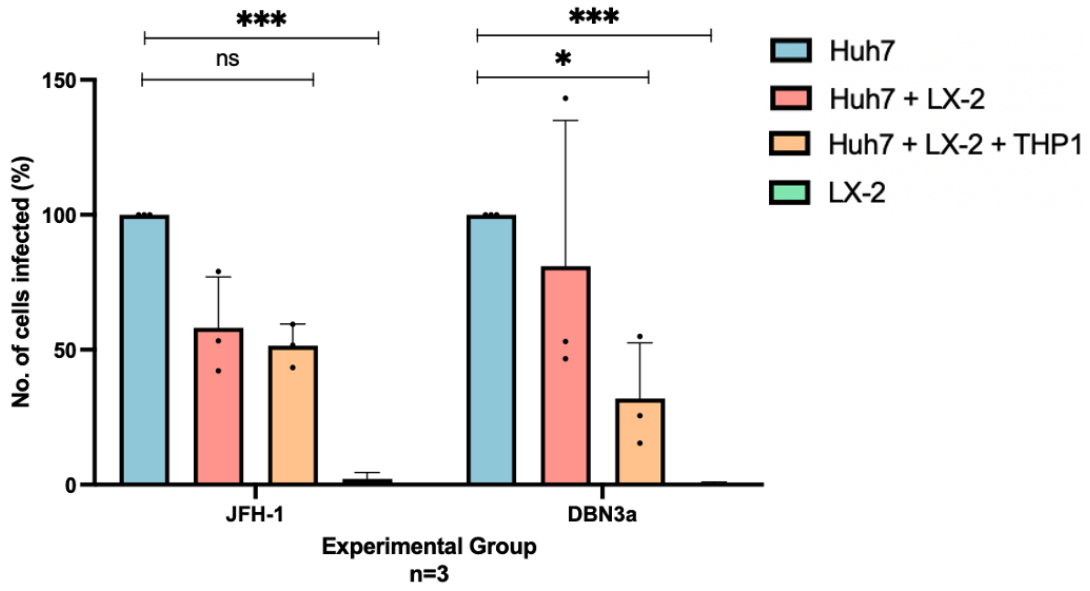

Figure 5.26 THP1 cell presence reduced DBN3a infection efficiency.

Co-cultured Huh7, Huh7 and LX-2 cells, and Huh7, LX-2 and THP1 cells infected with JFH-1 and DBN3a infectious virus (MOI 0.2) harvested 72 h.p.i. The number of NS5A positive cells was normalised to Huh7 and LX-2 co-culture. Data are presented as mean with standard deviation. Statistical significance was tested using one-way ANOVA with the Bonferroni's multiple comparison test, with a single pooled variance. P values; ns, P ≥0.05; *, P <0.05; ***, P <0.0005.

5.2.12. PCLS as an effective model to visualise *ex vivo* liver fibrosis

Using rat derived PCLS, I aimed to illustrate the promotion of fibrosis *ex vivo* using TGF-β and platelet-derived growth factor (PDGF), demonstrating PCLS as an effective model to investigate liver fibrosis containing all cell types and cell architecture of a native liver. Slices were cultured for 24 h prior to the addition of fibrosis stimulants for 72 h. Histological staining was conducted to observe changes to αSMA and picrosirius red staining, allowing the evaluation of organised collagen fibres, and promotion of a fibrotic matrix in PCLS (Figure 5.27). In t=0 slices, obtained at the time of slicing from healthy rats, both αSMA and picrosirius red staining is restricted to vessels. By 96 h, control slices obtained minimal HM observed via αSMA staining and picrosirius red staining illustrated thickening of collagen surrounding central veins. Particularly in Rat1 control, minimal perisinusoidal fibrosis was observed. Contrastingly, TGF-β and PDGF treated PCLS resulted to the increased presence of HM as a result of stellate activation (observed by αSMA staining) and more extensive perisinusoidal fibrosis in combination with increased collagen presence surrounding vessels (observed by picrosirius red staining). Results illustrate the PCLS bioreactor developed within the Oakley group introduces minimal fibrosis activation in control slices as well as efficient fibrosis activation in fibrotic stimulated samples.

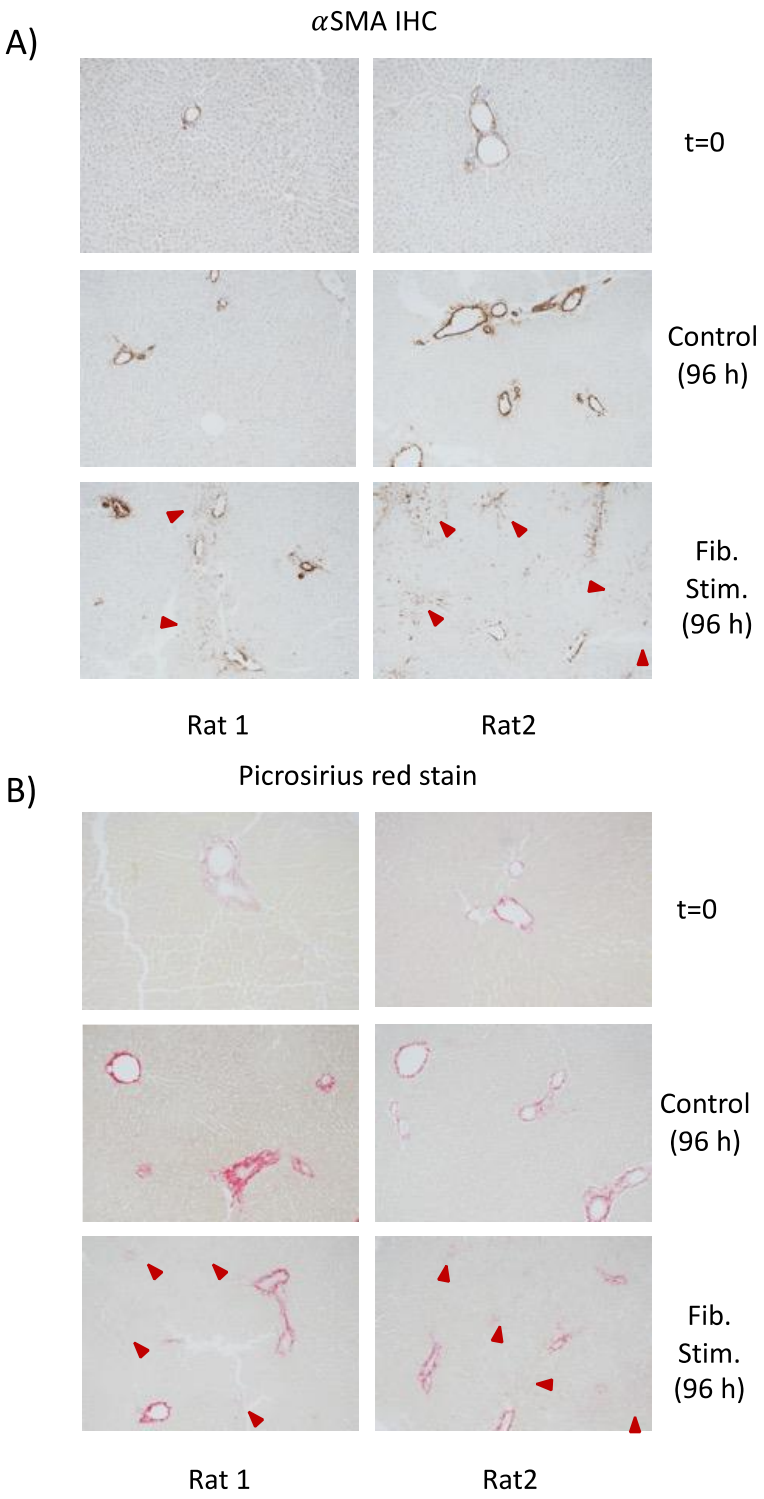

Figure 5.27 Fibrosis modelling in healthy rat liver slices.

Representative 10x magnification images of A) αSMA (immunohistochemical staining) and B) picrosirius red staining from two different rats collected directly at time of slicing (t=0) and after 24 hour rest + 72 hour culture with or without fibrotic stimulus (Fib. Stim.) TGF-β (3 ng/mL) and PDGF (50 ng/mL) treatment was conducted daily for a positive Fib. Stim. control sample. Red arrows indicate αSMA hepatic myofibroblasts and picrosirius red staining fibrosis regions.

5.2.13. Preparation for PCLS virus infection

Prior to performing BSL-3 infection of human PCLS, multiple contingencies had to be accounted for such as cell viability of PCLS when cultured in PBS for 4 h and virus inactivation methods allowing reliable downstream analysis of PCLS. Testing of cell viability of PCLS cultured in media containing either 17% PBS (500 μL of total media) or 33% PBS (1 mL of total media) was required as concentrated virus was resuspended in PBS. To test cell viability, healthy rat PCLS rested for 24 h were treated with PBS 4 h prior to culturing in complete Williams E media for 72 h and measuring the metabolic capacity of PCLS cell via the colourimetric resazurin assay. Results suggest that 4 h incubation of PCLS with 17% or 33% v/v of PBS does not negatively impact the cell viability of PCLS (Figure 5.28). To ensure reliable results of downstream analysis of media samples collected from virally infected PCLS cultured in BSL-3, multiple inactivation techniques were analysed; 5 minute incubation of media samples at 80 °C, 10 minute incubation of media samples at 65 °C and 30 minute incubation of media samples containing 1% Triton X-100 (Pfaender et al., 2015; Song et al., 2010). Media samples collected from human PCLS (control and fibrotic stimulated) collected at 96 h were treated with the inactivation technique or used directly (non-treated) prior to the completion of various assays to detect soluble factors. Assays detected the presence of the liver damage marker aspartate aminotransferase (AST), the fibrogenic marker soluble collagen 1A1 (Col1A1), a marker of hepatocyte function; albumin and a cell death marker; lactate dehydrogenase (LDH) (Figure 5.29). Results suggest that heat inactivation of 65 °C for 10 minutes may be used for the detection of all soluble factors except the detection of LDH. Treatment with 1% Triton X-100 may be used for the detection of AST, Col1A1 and LDH with a considerable reduction in the detection of albumin. Heat treatment, irrespective of the temperature and time incubation could not be used for the detection of LDH. These results suggest infection with the virus stored in PBS will not impact cell viability of the

PCLS during a 4 h primary infection period and 1% Triton X-100 inactivation method results to the most versatile downstream analysis of media samples.

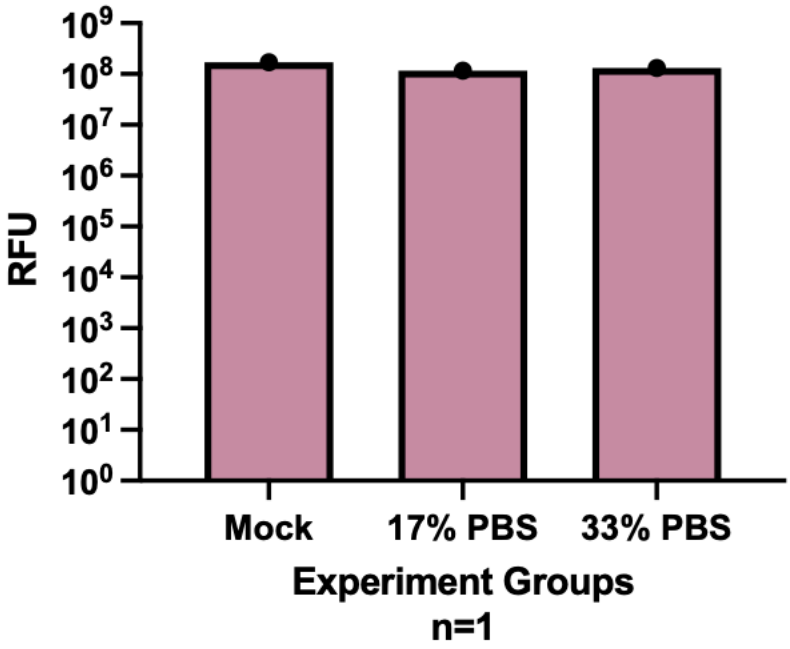

Figure 5.28 Viability of rat PCLS is not negatively impacted by 4 h PBS incubation.

Graph shows the metabolic activity of PCLS cultured in 17% (500 μL) and 33% (1 mL) PBS 24 hours resting slice post-cutting. PCLS remained in culture for 72 hours prior to completion of the Resazurin assay.

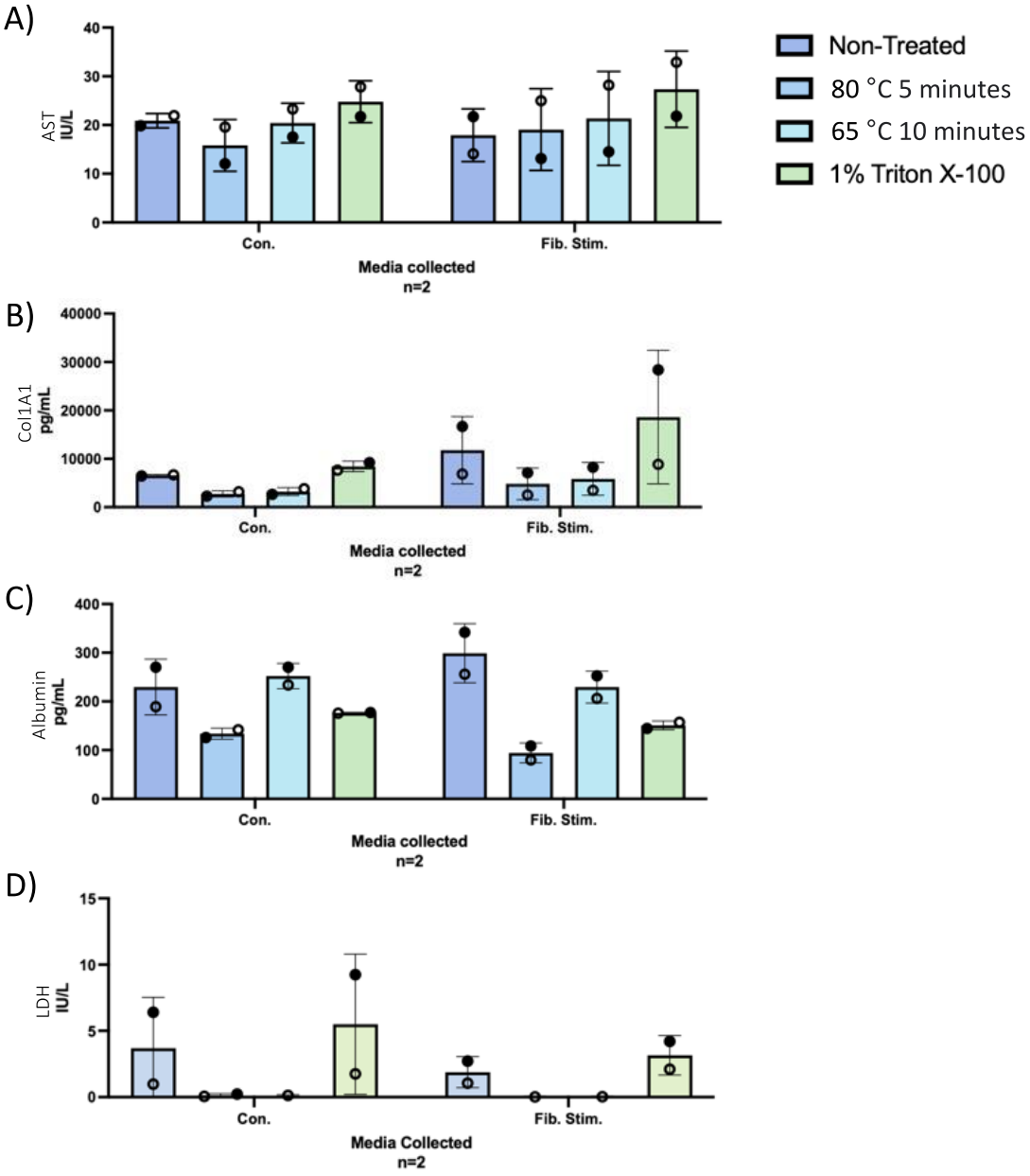

Figure 5.29 Heat treatment of media samples inhibits detection of LDH.

Graphs shows average levels of A) AST (IU/L), B) Col1A1 (pg/mL), C) albumin (pg/mL) and D) LDH (IU/L) of media samples collected from human PCLS cultured with a 24 hour rest period prior to the addition of fibrotic stimulus (Fib. Stim) for 72 hours. Fib. Stim; TGF-β (3 ng/mL) and PDGF (50 ng/mL) treatment was conducted daily for a positive control for fibrogenesis. Different symbols identify the relationship of biological repeats; circle and triangle are separate biological repeats obtained from different patients.

5.2.14. HCV infection of human PCLS decreases the expression of stress and fibrosis markers

To investigate if human PCLS is susceptible to HCV infection in the model and changes to stress and fibrosis markers after infection. Human PCLS were infected with HCV DBN3a (MOI 0.6) for 4 h post 24 h rest period after slicing. Slices were cultured for a further 72 h with regular media changes with complete RPMI. Slices were harvested for mRNA expression of stress and fibrosis markers. When comparing stress markers (Figure 5.30), the presence of HCV does not induce gene expression in comparison to the fibrotic stimulated control samples which result to a notable increase of all stress markers. Interestingly, the presence of DBN3a reduces the expression stress markers, in particular Snail-1 (22% reduction) and fibronectin (53% reduction) in comparison to the mock control. Similarly, DBN3a presence reduces the expression of all fibrosis markers (Figure 5.31); αSMA – 27 %, Col1A1 – 59 % and TIMP1 57% in comparison to the mock control and the fibrotic stimulated control sample increased all fibrogenic genes as expected. To confirm HCV infection of slices, RNA expression of the HCV 5'UTR was analysed and normalised to the mock control (Figure 5.32 A). Results confirm the presence of HCV in the virus only infected slices. However, this cannot be used to confirm the number of cells infected. Interestingly, bearing in mind these results are based on only one biological repeat, when I compare HCV 5'UTR expression in comparison to monolayer Huh7 cells infected by HCV containing 1/3 of the cells present in a PCLS, the amount of 5'UTR detected is more than 600-fold higher (Figure 5.32 B). Results suggest, despite a low expression level of HCV, presence of the virus alters host gene expression eliciting an anti-fibrotic response.

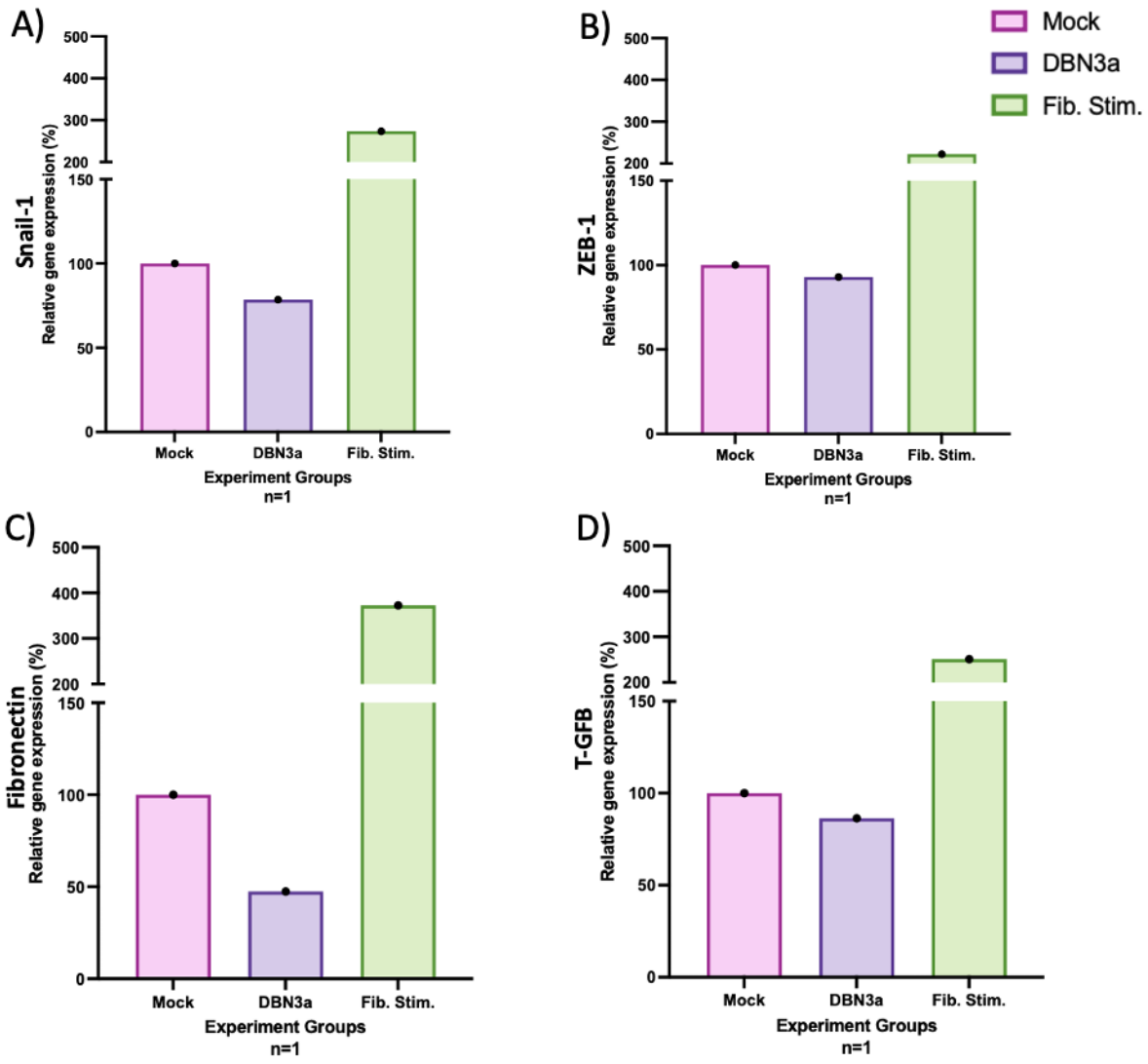

Figure 5.30 HCV infection does not induce stress markers in human PCLS.

Human PCLS infected with HCV DBN3a (MOI 0.6) after 24 hour rest + 72 hour culture. TGF-β (3 ng/mL) and PDGF (50 ng/mL) treatment was conducted daily for a positive fibrosis stimulated (Fib. Stim.) control sample. mRNA expression of stress markers A) Snail-1 B) ZEB-1, C) fibronectin and D) TGF-β was analysed.

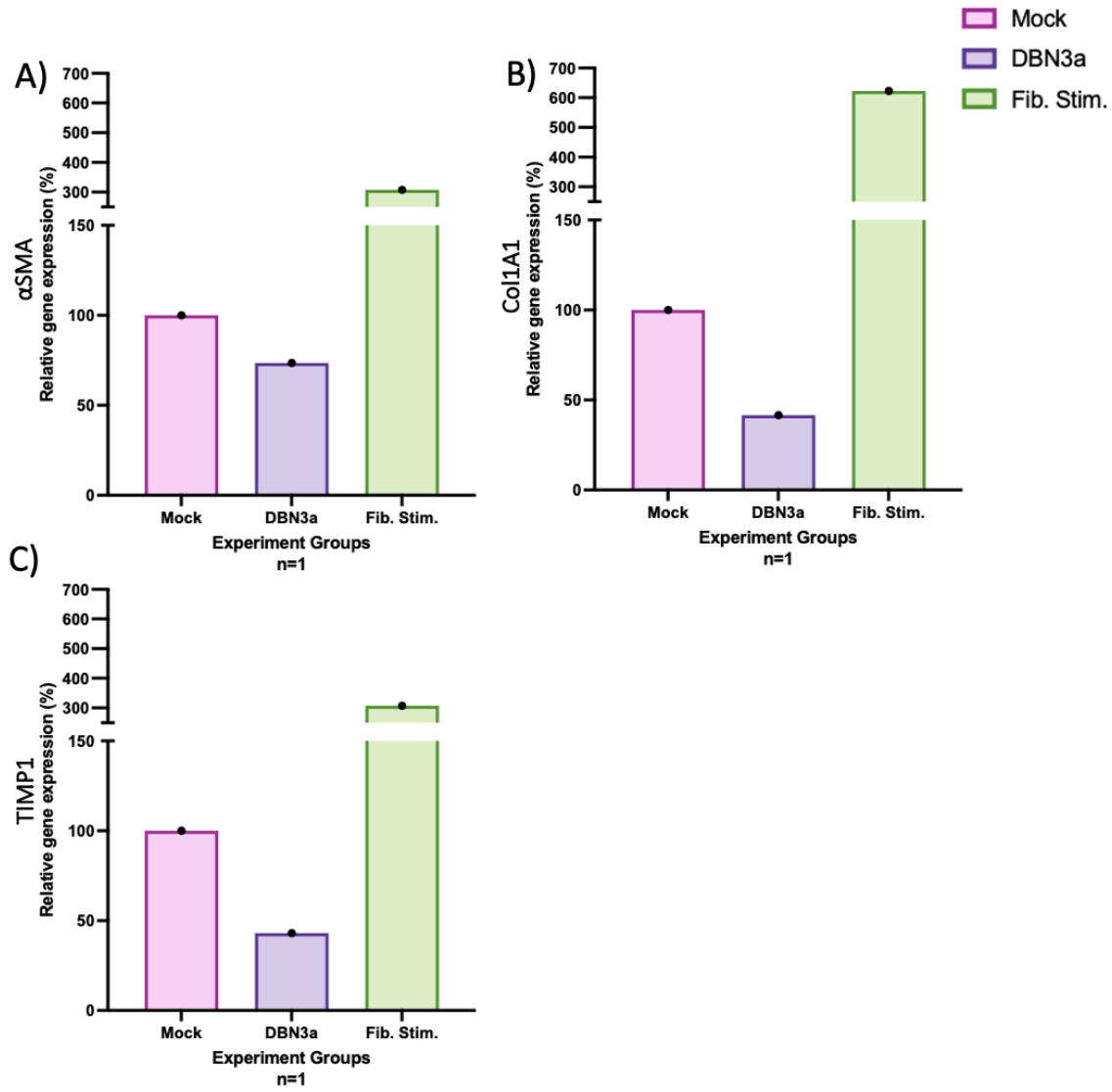

Figure 5.31 HCV infection reduces mRNA expression of fibrosis markers in human PCLS.

Human PCLS infected with HCV DBN3a (MOI 0.6) after 24 hour rest + 72 hour culture. TGF-β (3 ng/mL) and PDGF (50 ng/mL) treatment was conducted daily for a positive fibrosis stimulated (Fib. Stim.) control sample. mRNA expression of fibrosis markers A) αSMA, B) Col1A1 and C) TIMP1 was analysed.

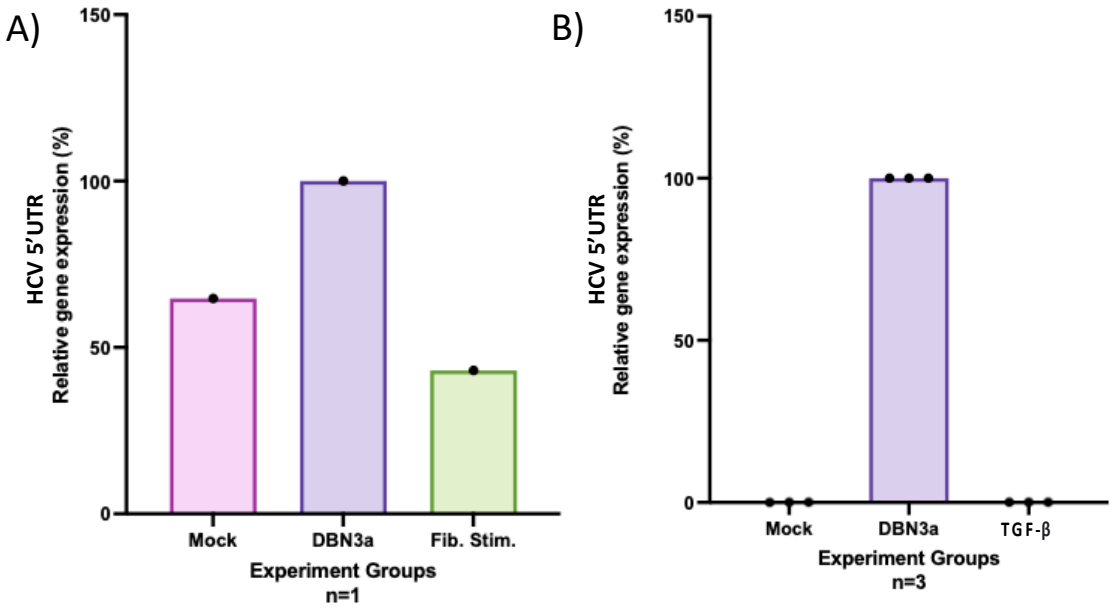

Figure 5.32 Detection of 5'UTR HCV RNA within infected human PCLS.

mRNA expression of the HCV 5'UTR within A) human PCLS infect with HCV DBN3a (MOI 0.06) for 4 hours prior to media removal and further culturing of the slices for 72 hours. TGF-β (3 ng/mL) and PDGF (50 ng/mL) treatment was conducted daily for a positive fibrosis stimulated (Fib. Stim.) control sample. Slices contained approximately $1.53x10^6$ cells. B) Monolayer HCV infection of Huh7 cells (approximate cell number when confluent $0.5x10^6$). Results normalised to DBN3a infection. For experiments containing at least three biological repeats, data are presented as mean with standard deviation. Statistical significance was tested using one-way ANOVA with the Bonferroni's multiple comparison test, with a single pooled variance. P values; 0.1234 (ns).

5.2.15. Evidence of HCV NS5A presence within human PCLS

To confirm the presence of NS5A within cells of the PCLS, two microscopy techniques were utilised; confocal and multiphoton microscopy. Fixed PCLS were stained with sheep anti-NS5A and Hoechst 33342 nuclear stain. Confocal microscopy allows fine tuning of excitation and emission wavelengths to reduce background fluorescence and focusing of objects using a pinhole removing the detection of secondary fluorescent signals, a common artefact of tissue imaging, resulting in a clean-cut image. However, confocal microscopy is not able to penetrate deep into the tissue as most of the excitation is absorbed or scattered by the tissue before it reaches the focal plane, thus limiting the depth acquisition on a confocal microscope to 50-100 μm (tissue dependent). As a user tries to maximise the depth of a confocal microscope, phototoxicity can occur. Images acquired by confocal microscope confirm the presence of NS5A only in the virus infected PCLS (Figure 5.33). However, depending on the area of slice in view, there is varying presence of nuclei and NS5A staining (Figure 5.34). This suggests optimisation of PCLS staining is required. Despite limited tissue depth of approximately 30 μM, z-stacking can capture images of cells clearly illustrating NS5A puncta located only in the cytoplasm (Figure 5.35).

Multiphoton microscopy, conducted at the University of York, was used as it does not require a pinhole as fluorescence is limited to more precise focal plane which allows deeper tissue imaging with greater resolution and precision. A fine focal point is created using multiple photons as, however many photons being used, meet each other at the focal point and selectively excite the tissue. This optimises the acquisition of images to a depth up to 450 μM, tissue dependent. Photobleaching is reduced as instead of one standard photon fluorescence in confocal microscopy, multiphoton uses the excitation of two or more photons of near-infrared light. Near-infrared light minimizes tissue scattering and ensures a signal is only produced from objects that acquire the correct excitation when two or photons are absorbed creating the energy required for a single photon excitation event. A 100 μm z-stack of the PCLS within the

virus infected sample demonstrates limited virus infiltration of the tissue. As images are acquired deeper into the tissue, staining of the nuclei and NS5A become more diffused suggesting penetration of the multiphoton is limited to 100 μm depth or inefficient tissue staining. (Figure 5.36). As such, mock, fibrosis stimulated and virus images of tissue was collected at a depth of 50 μM, to compare clear distinct images of virus infection greater than surface level (Figure 5.37). Virus acquired images at 50 μm depth confirms z-stack images that virus infection occurs within the tissue and not restricted to the surface. Mock stain images confirm NS5A staining is specific to the presence of the virus. However, the fibrotic stimulated tissue samples express a high level of autofluorescence as red puncta is observed in the stained and non-stained sample. The collection of images gathered by confocal and multiphoton microscopy confirm the presence of virus infected cells at least 50 μm deep into the tissue.

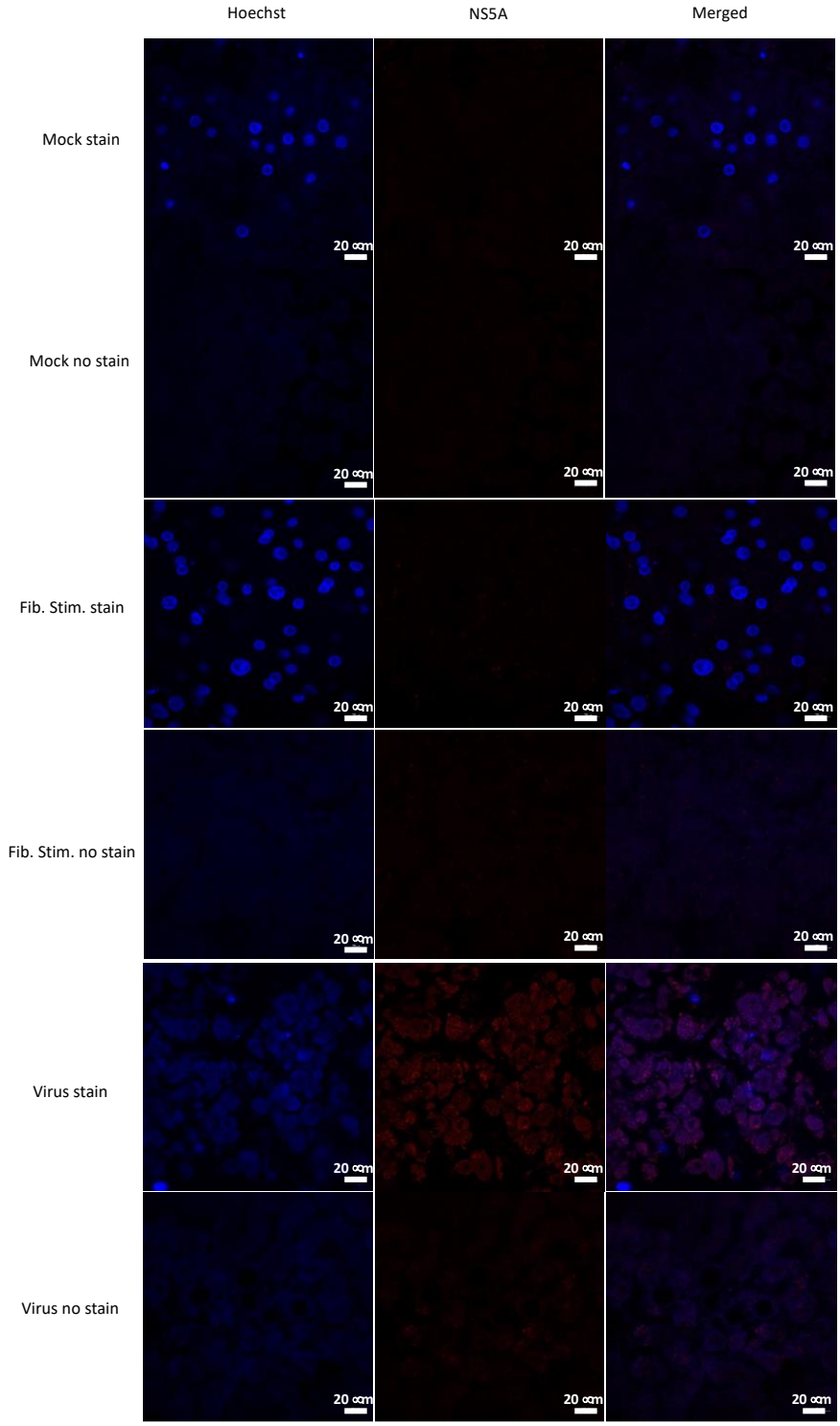

Figure 5.33 Presence of NS5A puncta within PCLS cells.

Human PCLS rested for 24 hours was infected with HCV DBN3a (MOI 0.06) for 4 hours prior to media removal and culturing of the slices for 72 hours. TGF-β (3 ng/mL) and PDGF (50 ng/mL) treatment was conducted daily for a positive fibrosis stimulated (Fib. Stim.) control sample. The samples were fixed with 4% PFA and stained with sheep anti-NS5A and Hoechst 33342. Non-stained samples were mounted after blocking with 3% BSA. Images acquire with the Zeiss Inverted Confocal microscope, LSM 880, magnification 40x and scale bar = 20 microns.

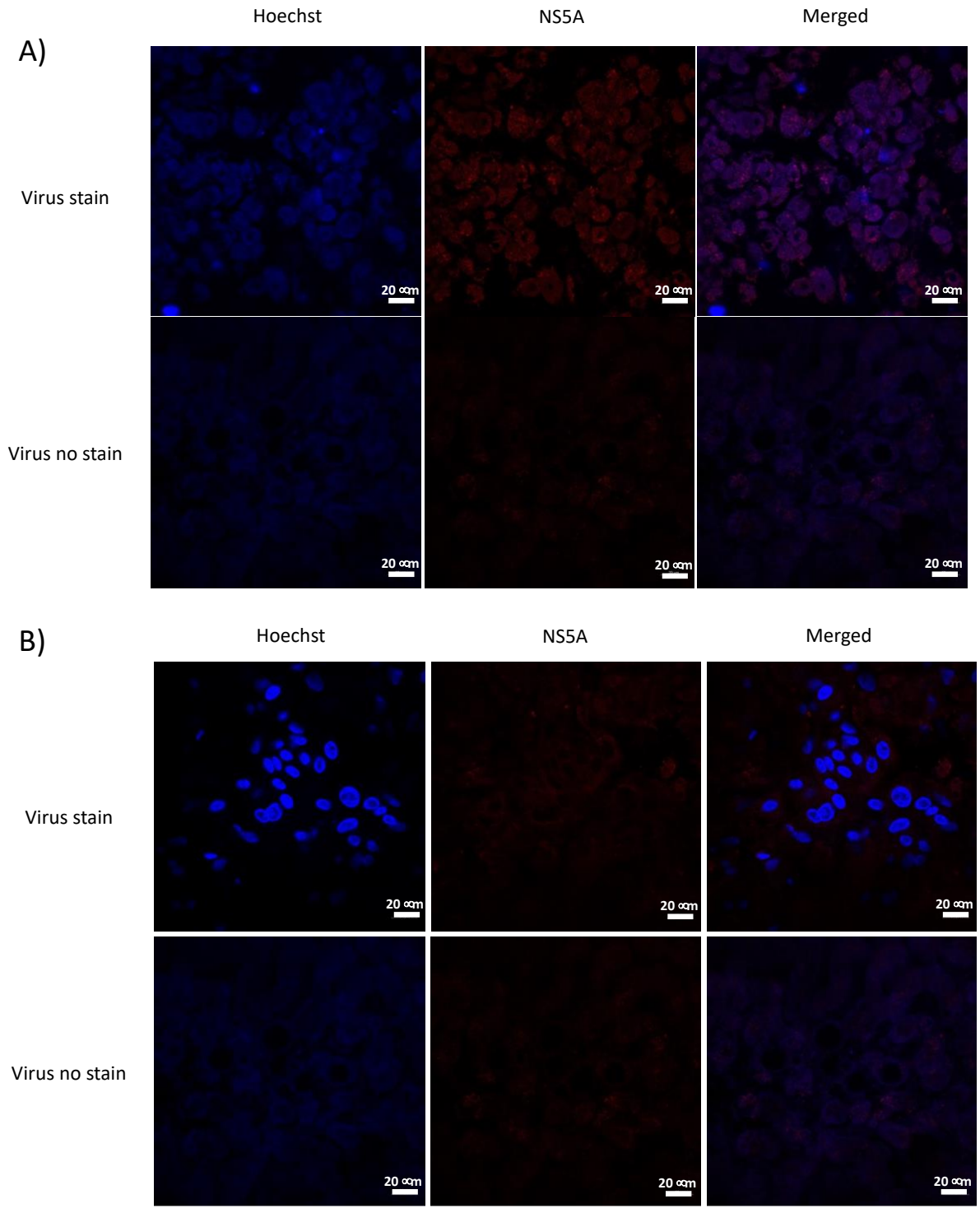

Figure 5.34 Staining efficiency varied at different areas of the PCLS.

Human PCLS rested for 24 hours was infected with HCV DBN3a (MOI 0.06) for 4 hours prior to media removal and culturing of the slices for 72 hours. TGF-β (3 ng/mL) and PDGF (50 ng/mL) treatment was conducted daily for a positive fibrosis stimulated (Fib. Stim.) control sample. The samples were fixed with 4% PFA and stained with sheep anti-NS5A and Hoechst 33342. Non-stained samples were mounted after blocking with 3% BSA. Images acquire with the Zeiss Inverted Confocal microscope, LSM 880, magnification 40x and scale bar = 20 microns.

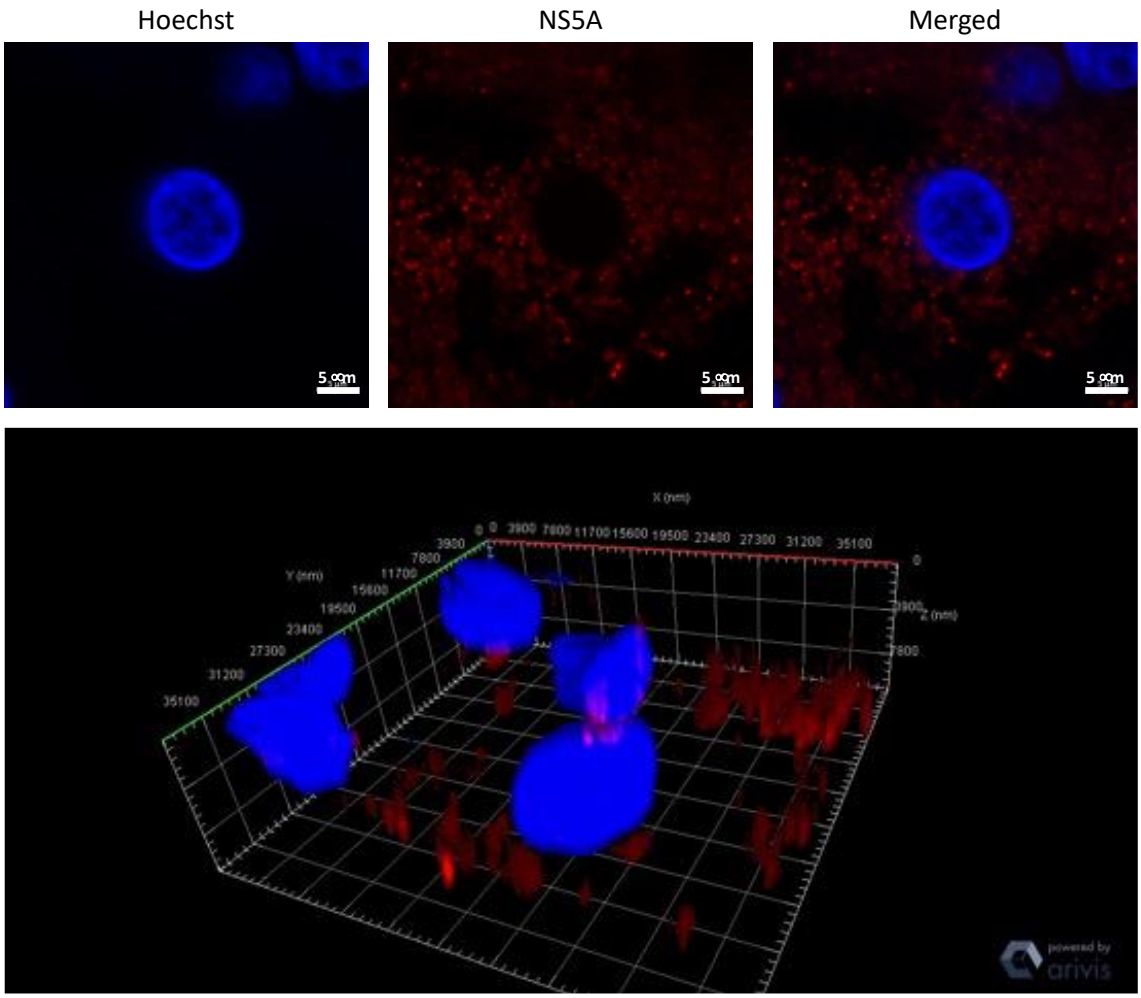

Figure 5.35 NS5A puncta visualised by z-stack.

Human PCLS rested for 24 hours was infected with HCV DBN3a (MOI 0.06) for 4 hours prior to media removal and culturing of the slices for 72 hours. The samples were fixed with 4% PFA and stained with sheep anti-NS5A and Hoechst 33342. Non-stained samples were mounted after blocking with 3% BSA. Images acquire with the Zeiss Inverted Confocal microscope, LSM 880, magnification 40x and scale bar = 5 microns. Z-stacking was performed for 11.8 microns.to capture NS5A puncta within one cell.

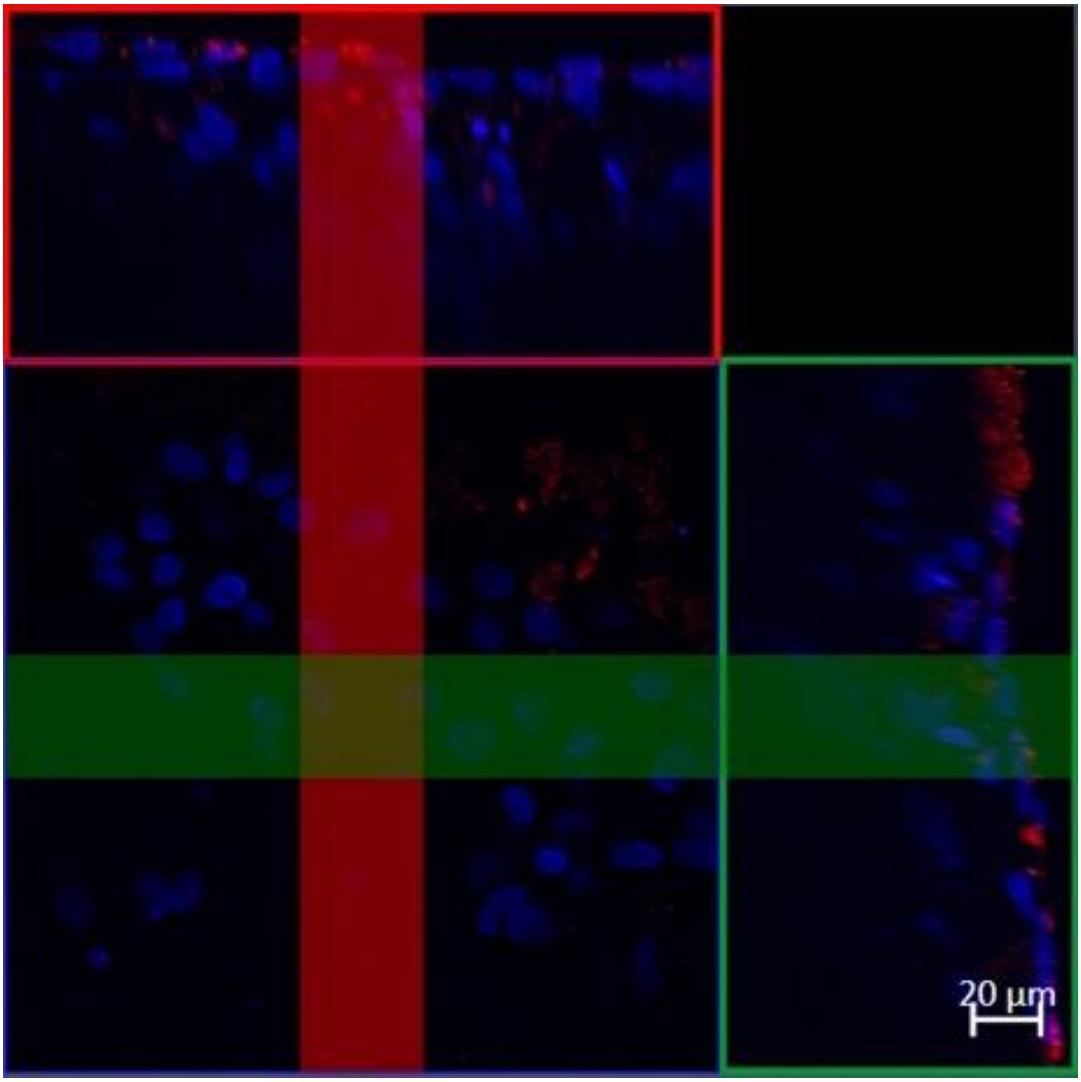

Figure 5.36 NS5A presence visualised by multiphoton z-stack of PCLS.

Human PCLS rested for 24 hours was infected with HCV DBN3a (MOI 0.06) for 4 hours prior to media removal and culturing of the slices for 72 hours. TGF-β (3 ng/mL) and PDGF (50 ng/mL) treatment was conducted daily for a positive fibrosis stimulated (Fib. Stim.) control sample. The samples were fixed with 4% PFA and stained with sheep anti-NS5A and Hoechst 33342. Images acquire with the Zeiss Inverted/Observer microscope, LSM 980, with the Coherent Chameleon Ultra II, main beam splitter M-BS760 and BS-MP760. Magnification 40x and scale bar = 20 microns. Z-stacking was performed for 100 µm to capture NS5A presence within the tissue. LSM-Plus 3D processing was performed to collate all images. Cross-sectional view of the z-stack is shown; green representing the x axis and red representing the y-axis.

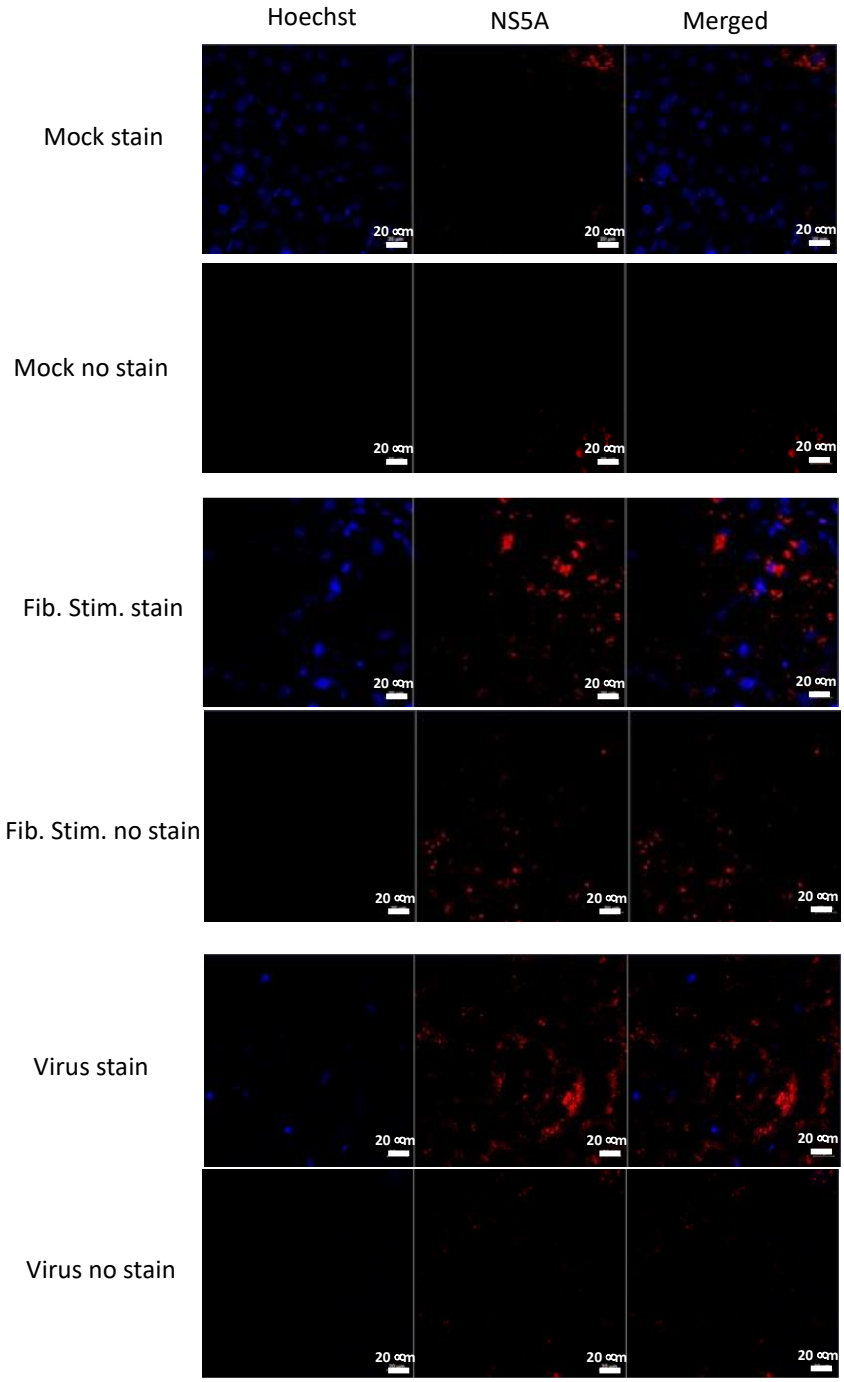

Figure 5.37 NS5A presence within 50 μm of PCLS.

Human PCLS rested for 24 hours was infected with HCV DBN3a (MOI 0.06) for 4 hours prior to media removal and culturing of the slices for 72 hours. TGF-β (3 ng/mL) and PDGF (50 ng/mL) treatment was conducted daily for a positive fibrosis stimulated (Fib. Stim.) control sample. The samples were fixed with 4% PFA and stained with sheep anti-NS5A and Hoechst 33342. Images acquire with the Zeiss Inverted/Observer microscope, LSM 980, with the Coherent Chameleon Ultra II, main beam splitter M-BS760 and BS-MP760, conducting using two-photon capacity. Magnification 40x and scale bar = 20 microns. Z-stacking was performed 2 μm either side of the 50 μm total depth to allow LSM-Plus 3D processing to collate all images.

5.3. Discussion

This chapter explores the use of various cell culture models to mimic the architecture of the native liver, comparing varying levels of complexity to the promotion of possible HCV driven fibrosis. The introduction of different cell models and cell:cell contact results in changes to gene expression in the presence of HCV with clear distinct differences between cell models using a fibrosis stimulant as a positive control. When comparing different cell models, additional contingencies are introduced resulting in a level of limitation when directly comparing cell model results. Here I discuss those contingencies with possible explanation to varying results between cell models.

5.3.1. HCV driven fibrosis is marginally altered by the presence of LX-2 cells

Primarily, a comparison of Huh7 cells stably harbouring the SGR and virus infected cells was produced. Within the literature, there is currently the belief that stably expressed SGR within Huh7 cells may be continuously cultured, with the ability to freeze stocks and maintain the SGR and that the model may be used to represent chronic HCV infection *in vitro*. Anticoli *et al*. (2019) describes an acute and chronic *in vitro* model as HCV infection occurring at a low MOI with an acute phase occurring up to 8 dpi and a chronic phase occurring at 28 dpi. Stably expressed cell lines used in this study had been established and continuously grown for a longer period than 28 days. Relevant to this Anticoli *et al*. (2019) describes changes between the acute and chronic phase via changes in ROS levels being elevated in the acute phase and conversely, downregulated ROS in the chronic phase. It was also described, during the acute phase of infection, an increased rate of apoptotic cell death which was not observed during chronic infection. In these models, no significant changes in the cell growth of Huh7 cells in the presence of HCV was observed, regardless of the model used (Figure 5.2). Interestingly, the presence of

TGF-β does not significantly change Huh7 cell growth, conversely to Kim *et al.* (2018), who described the inhibition of Huh7 cell growth in the presence of TGF-β. Additionally, did not see any notable differences between the gene expression for the stress markers of Huh7 cells between stably expressed SGR and Huh7 cells infected with HCV and harvested 72 h.p.i (Figure 5.3 and Figure 5.4). Possible differences between the Huh7 cell HCV results and these results are likely differences in the Huh7 cell lines used. Sainz *et al.* (2009) describes changes in Huh7 cell phenotype and infectivity to HCV varies between different laboratories. As no changes were observed, the infectious HCV model was used when comparing different cell models as I believed it mimicked a natural infection and would allow direct comparison to models which could not benefit from a stable cell line such as PCLS. Morphological changes were observed in Huh7 cells infected with HCV and treated with TGF-B (Figure 5.5) demonstrating limitations to the stress markers selected, as despite the presence of morphological changes there were no changes to stress marker expression during HCV infection, in addition to measuring stress markers, inflammatory markers could be analysed. Inflammatory markers such as TNF-α are expressed as a classic example of viral infection, in particular HCV (J. Lee et al., 2015). Morphological changes demonstrate a physical reaction to a stimulus as they are not observed in mock cells. Conversely, the phenotypic change is not universally observed; I believe it is harder to identify morphological changes when observing cells which are almost at 100% confluency.

In the presence of a fibrosis stimulant, LX-2 cells change phenotype and reduced cell growth during observation of the monolayer adherent culture (Figure 5.6 and 5.7). Therefore, I determined a reduction of cell growth as a signature of LX-2 cell activation into a myofibroblast-like phenotype and promotion of fibrosis pathways within the cell. Related to this, the literature suggests hepatocytes release soluble factors such as TGF-β and TNF-α during HCV infection (Chusri et al., 2016; Knobler & Schattner, 2005; Li et al., 2018; Shin et al., 2005) suggesting if I culture LX-2 cells in conditioned media from HCV infected Huh7 cells I should observe a reduction in LX-2 cells growth. However, I observed no changes to LX-2 cell growth when

cultured in the media of infected Huh7 cells (Figure 5.8). This suggests soluble factors are not released during HCV infection as despite LX-2 cells being cultured in 100% conditioned media for 72 h from Huh7 cells cultured for 72 h (media age a total of 6 days old), the mock LX-2 cell growth is comparable to the conditioned media from mock Huh7 cells. This suggests the age of the media did not impact LX-2 cell growth. It is possible soluble factors are released, however at too low a concentration to observe a change in LX-2 cell growth. To confirm this, ELISAs detecting TGF-β and TNF-α could be performed. The only change in cell growth observed within conditioned media samples was LX-2 cells cultured in Huh7 cells treated with TGF-β resulting in a non-significant reduction in cell growth. Upon treatment of Huh7 cells with TGF-β I expected to see comparable if not a greater reduction in LX-2 cells growth in the presence of conditioned TGF-β due to the presence of additional soluble factors released by Huh7 cells and residual TGF-β. Treatment of Huh7 cells with TGF-β induces the expression of p38 MAP kinase and Smad group of proteins. p38 MAP kinase mediates connective tissue growth factor (CTGF) expression in Huh7 cells resulting in the increased production of CTGF activating stellate cells (Nagaraja et al., 2012; Trampuž et al., 2023). To define whether the effects of TGF-β conditioned media are due to released soluble factors or residual TGF-β, media containing TGF-β could be stored at 37°C for 72 h prior to being used to culture LX-2 cells and changes in LX-2 cell growth observed. This would determine if the LX-2 cell growth changes I observed was not as efficient in activating LX-2 cells due to degradation of TGF-B during the primary 72 h incubation with Huh7 cells.

To investigate the requirement of cell contact or release of soluble factors directly in the presence of LX-2 cells, a mixed cell culture of LX-2 and Huh7 cells was established. In the presence of TGF-β, I did not observe significant changes to cell growth, however, I did observe changes to cell phenotypes (Figure 5.9). Analysis of Huh7 only (Figure 5.2) and LX-2 only (Figure 5.7) cell lines in the presence of TGF-β suggests LX-2 cell growth is reduced; thus, creating large spaces between elongated cells. It is possible I do not observe a reduction in cell growth of the mixed monolayer cell culture as Huh7 cells are growing inside the large spaces produced by LX-

2 cells. To confirm this, Huh7 cells and LX-2 cells could be stained for cell specific markers to define cell types, localisation of cells and cell line specific cell counts. Generation of reporter cell lines containing a fluorescent protein for Huh7 and LX-2 cells would allow further characterisation of cells with live cell imaging. Comparison of mono- Huh7 cell only and co-cultured – Huh7 and LX-2 cell lines in the presence of HCV JFH-1 and DBN3a, and TGF-β are comparable (Figure 5.11) however, as I cannot distinguish differences between Huh7 cell and LX-2 cell growth, promotion of a pro-fibrotic state was characterised by mRNA expression of stress and fibrosis markers. No significant changes were observed in the expression of stress markers suggesting LX-2 cells are not required to induce greater cell stress. Importantly, I was not able to decipher the expression of stress markers specific to Huh7 cells or LX-2 cells (Figure 5.12). To separate mRNA expression of cells line, cells could be magnetically sorted prior to harvesting cell lysates. Post-harvest, cells may be analysed by FACS with markers selected to define cell populations such as activated LX-2 cells expressing TIMP-1. Results suggest there are no significant changes of fibrosis markers dependent on the HCV GT present, however there is a trend of αSMA reduction of gene expression in the presence of JFH-1 (Figure 5.13 A). This is particularly interesting as the trend is not observed in the expression of Col1A1 or TIMP1 suggesting JFH-1 may disrupt a component of the αSMA pathway independent of other fibrosis markers. Conversely, this may be an anti-fibrotic response by the host of which DBN3a is able to interrupt. However, as Col1A1 and TIMP1 are not affected by the presence of JFH-1, I believe the reduction is not inhibiting the progression of a pro-fibrotic state. To further investigate the requirement of direct cell contact between Huh7 and LX-2 cells in co-cultures, transwell membranes could be used allowing the free exchange of soluble factors between the cell types without direct interaction (Akil et al., 2019; Salloum et al., 2016). Analysis of stress and fibrosis markers was limited to the cell line present; LX-2 cells were not analysed for stress markers. Analysis of LX-2 cells expression of stress markers could provide additional information regarding the state of LX-2 cells during HCV infection despite not seeing significant changes in

fibrosis markers. Conversely, fibrosis markers could be analysed in Huh7 cell mono- cultures as was conducted by Salloum *et al.* (2016).

5.3.2. Spheroid phenotype dependent on the cell types present

To greater understand the requirement of cell:cell contact, I investigated the production of spheroids which I hypothesised would have cell:cell interactions more comparable to those present in the intact liver, in comparison to adherent monolayer cell culture. The IncuCyte S3 allowed regular intervals of images to be acquired allowing comparisons of spheroid phenotypes (Figure 5.14). Results demonstrated spheroid area changes over time may be dependent on the cell type present; spheroids containing LX-2 cells reduce or stay stagnant over 10 days culturing period (Figure 5.15) which is conversely different to monolayer cell culture where LX-2 cells continue to grow unless in the presence of TGF-β (Figure 5.7).

Changes to LX-2 cells grown in spheroids may be linked to changes in tissue culture pressure, measured in elastic modulus (*E*) kilopascal (kPa) pressure, which varies between adherent cell culture of monolayer cells grown on plastic ($E > \sim 3$ kPa) and cells grown on soft substrates ($E < \sim 3$ kPa), such as hydrogels based on hyaluronic acid and Matrigel (Gaca et al., 2005; Guvendiren et al., 2014). Liver stiffness has been described as a key factor driving the progression of fibrosis, research conducted on the culturing of primary stellate cells describes HSCs as quiescent when cultured on soft substances and can only partially transdifferentiate into myofibroblasts-like cells. In the presence of TGF-β, a stimulant of HSC activation, can only partial differentiate LX-2 cells in low elastic modulus pressure states however, partially activated HSCs can fully differentiate when exposed to a stiff high elastic modulus pressure surface (Olsen et al., 2011). This may also be reversed, differentiated HSCs can revert back to a quiescent state when placed on soft substrates (Guvendiren et al., 2014). I hypotheses in the absence of a stiff substrate, such as monolayer growing on plastic, LX-2 cells contract with low proliferative

characteristics producing a spheroid area with stagnant growth. Huh7 cells proliferation is not impacted by elastic modulus pressure therefore, the combination of LX-2 cells and Huh7 cells mimics some of the spheroid growth characteristics observed by Huh7 cell only spheroids, but spheroid growth is limited by loss of LX-2 cell proliferative ability. This complements spheroid growth in the presence of TGF-β, LX-2 cells are not able to fully differentiate therefore I do not see a significant change of LX-2 cell only spheroid growth and observe a marginal change in Huh7 and LX-2 cell mixed spheroids due to the presence of Huh7 cells accounting for 50% of the cell population. Furthermore, the fragility of Huh7 cell only spheroids may be related to the absence of LX-2 cells.

The variation of gene expression between biological repeats of co-cultured spheroids but not mono- cultured LX-2 cells may be accounted for by the activation of Huh7 cells but not LX-2 cells with the mixed spheroids (Figure 5.22). Interestingly Huh7 cell only spheroids in the presence of TGF-β results to a significant reduction in spheroid area. This suggests cell:cell contact of Huh7 cells within spheroids can enhance phenotypic changes observed in monolayer culture suggesting spheroids may be a more realistic model than monolayer culture for Huh7 cells. This supports previous data that the presence of HCV does not alter cell growth of monolayer Huh7 cells (Figure 5.16, Figure 5.17 A).

Multiple aspects of spheroids can be further investigated, images acquired suggested Huh7 cell spheroids may alter in circularity in the presence of TGF-β resulting in another signature of phenotypic changes in the presence of different stimuli (Figure 5.17 B). To investigate this, a circularity score was generated via the SpheroidJ plug-in using Fiji ImageJ software. In the presence of LX-2 cells, spheroid circularity reduces overtime and Huh7 cell only spheroids circularity index increases. As proliferative ability of Huh7 cells decreases in the presence of TGF-β, I do not believe the circularity of spheroids is dependent on the proliferative capacity of cells. Monolayer Huh7 cell phenotype changes in the presence of TGF-β becoming more contracted and spindle-like suggesting circularity scores increases as TGF-β contracts Huh7

cells together creating a more circular object. In co-cultured spheroids, Huh7 cells maintain proliferative ability perhaps creating an imbalanced growth of spheroids as LX-2 cells are not proliferating at the same rate or phenotypically changing. LX-2 cell only spheroids marginally change during the 24 h and 96 h timepoints, with the greatest difference of circularity possibly occurring in the presence of TGF-β. This could be due to partial differentiation of LX-2 cells altering the phenotype creating irregular contracting of cells. To greater understand the role of cell proliferation within spheroids, 5-Ethynyl-2'-deoxyuridine (EdU) staining could be conducted whereby a thymidine analogue is incorporated into the DNA of dividing cells and analysed by fluorescence microscopy. Cell specific markers or the use of reporter cell lines expressing fluorescent proteins could identify specific cell types and compare proliferative ability of each cell type in co-cultured spheroids.

A necrotic core was not observed in spheroids 4 days post culture (Figure 5.18, 5.19, 5.20). Published data suggests the formation of a necrotic core varies depending on the number of cells seeded, the number of days the spheroids have been cultured and cell types present (Browning et al., 2021; Murphy et al., 2023). Browning *et al.* (2021) describes the variation of cell dynamics present within a spheroid while forming a necrotic core, based on the Greenspan model (Greenspan, 1972), such as the presence of cell cycle arrest. Incorporation of EdU as well as Hoechst 33342 and PI staining observed daily could detect the formation of a necrotic core to greater understand the viability of spheroids during infection biology studies. The positive control for PI staining was doxorubicin treatment for 12 h prior to cell staining for 30 minutes prior to cell fixation. The images may suggest greater optimisation of Hoechst 33342 and PI staining is required or a longer treatment period of doxorubicin to observe greater staining of PI specifically. Relevant to this, cell viability assays may be conducted.

To greater improve the reliability of spheroids mimicking the native liver, spheroids could be cultured using hydrogels greater mimicking liver stiffness, particularly for the culturing of LX-2 cells however, also impactful to the growth of Huh7 cells. By increasing the mechanical

stiffness, LX-2 cells can differentiate which may result to changes in spheroid growth in the presence of pro-fibrogenic stimuli. Lee *et al.* (2015) describes the alteration of hydrogel stiffness in the presence of fibrinogen-modified poly(ethylene glycol)-diacrylate (PEG-DA) based hydrogels, that can alter the mechanotransduction representing different stiffness to present a normal liver or a diseased cirrhotic liver. The formation of Huh7.5 cell spheroids changes in size and expression of fibrosis markers when varying the elastic modulus pressure. I believe this may be required to see greater change of mRNA expression of stress (Figure 5.21) and fibrosis markers (Figure 5.22). Interestingly, despite observing changes to Huh7 cell only spheroid growth in the presence of TGF-β, stress markers were not upregulated, with specific attention drawn to the stimulated TGF-β spheroid mRNA analysis. As virus and TGF-β treatment occurred during spheroid formation, all cells were exposed to the stimulants. Only a small subset of genes were analysed, to gain a greater understanding of gene expression changes within Huh7 cell spheroids, transcriptomic analysis could be performed to gain a universal understanding of mRNA expression changes in comparison to mock and HCV infection.

5.3.3. Presence of THP1 cells alters the efficiency of HCV infection

Macrophages are known to play a key role during the progression of fibrosis during HCV infection via the production of pro-fibrotic factors TGF-β, TNF-α and PDGF (Friedman & Arthur, 1989; Ignat et al., 2020; Saha et al., 2016) as well as anti-fibrotic effects such as the production of enzymes and factors important for ECM breakdown and turnover, including MMP9, MMP12 and MMP13 (Ramachandran et al., 2012; Zigmond et al., 2014). The pro- and anti- fibrogenic effects are dependent of the cytokines released and interactions with HSCs and hepatocytes (Gao et al., 2022). As THP1 cells are a suspension cell line, the IncuCyte S3 can only determine the cell growth of adherent Huh7 cells and LX-2 cells in the co-culture (Figure 5.22). No change in cell growth is observed in the presence of HCV GTs, comparable to mono- cultures, however the presence of TGF-β results to a significant reduction in Huh7 and LX-2 mixed cell culture. This

result suggests in the presence of TGF-β monocytes may become activated, differentiating into macrophages, and communicate with Huh7 and LX-2 cells affecting cell growth to a greater extent than TGF-β in the co-culture (Figure 5.23 B). Zhang *et al.* (2016) describes the presence of TGF-β and Snail-1 as driving factors of THP1 cells becoming activated into a M2-like phenotype. Zhu *et al.* (2022) describes the presence of M2 macrophages as a driving factor of LX-2 cell activation via the secretion of prostaglandin E2 (PGE2). Despite a significant difference in cell growth, gene expression of stress (Figure 5.24) and fibrosis (Figure 5.25) markers of Huh7 and LX-2 cells stimulated by TGF-β, suggest in the presence of THP1 cells, no notable differences in comparison to co-cultures. To greater understand the communication of cells within a co-culture, specific cell lines could be cultured in transwells allowing easy observation of phenotypic changes and harvesting of particular cell types, as performed in the co-culture by Akil *et al.* (2019) . This would allow gene expression analysis of individual cell types instead of analysing Huh7 and LX-2 cells collectively.

Upon analysis of NS5A positive cells, the efficiency of HCV infection in the presence of THP1 cells appear to vary depending on the HCV GT present, there is a reduction of cell line susceptibility to DBN3a infection in the presence of THP1 cells (Figure 5.26). As LX-2 cells are not susceptible to HCV infection, in the co- culture of Huh7 and LX-2 cells, I expect a 50% reduction of NS5A expression which is observed for both HCV GTs. In the co- culture including THP1 cells, only the adherent Huh7 and LX-2 cells were stained for NS5A detection, and there was a reduction of DBN3a infection of adherent monolayer cells. These results assume Huh7 and LX-2 cell growth do not alter in the presence of THP1 cells. To greater understand cell growth kinetics in the presence of different cell types, cell lines could be identified using cell line specific markers to count the number of cells present. As Huh7 cells were only identified by the presence of HCV antigen, I cannot determine if the number of Huh7 cells infected is due to a reduction of infection efficiency or a reduction in the number of Huh7 cells present during DBN3a infection. Fletcher *et al.* (2014) describes the expression of TNF-α by activated macrophages as a promoter

of HCV entry, utilising HCV GT1 pseudotypes and GT2 cell-culture infectious virus model within polarised HepG2 cells expressing CD81 allowing HCV entry. However, the expression of IL-1B, also secreted by activated macrophages, may also inhibit HCV replication (Guo et al., 2020; Zhu & Liu, 2003). To decipher the impact of factors released by macrophages in the presence of HCV JFH-1 and DBN3a infection, infection of Huh7 cells could be performed in the presence of TNF-α and IL-1B and the number of HCV infected cells could be compared between the two GTs. Additionally, soluble factors, TNF-α and IL-1B expression, in the tri- culture could be examined by ELISAs. Crucially, there was no characterisation of THP1 cells and possible differentiation into macrophages after HCV infection. The infection of THP1 cells should be analysed and monocytes/macrophages could be characterised by flow cytometry utilising macrophage specific markers such as TLR2 to define M1 activated macrophages and CD163 to define M2 activated macrophages (Mily et al., 2020) and NS5A to detect HCV infection. During HCV infection, there is a mixed population of macrophage subsets; macrophages in the liver may be described as resident or tissue-infiltrating and up-taking foreign antigen, known as phagocytosis, does not typically result in an inflammatory response (Horst et al., 2016). However, signals during HCV infection may surpass the activation threshold directing macrophages to produce immune activating factors such as TNF-α, IL-6 and IL-1B (Horst et al., 2016). Ahmed et al. describes the presence of M1 macrophages in chronic HCV infection acquiring M2 characteristics such as increased CD86 expression and IL-10 secretion.

5.3.4. HCV DBN3a infection of PCLS suggests an anti-fibrotic environment

Initially, rat liver slices were stimulated with TGF-β and PDGF to demonstrate the ability of maintaining liver slices without the introduction of cell culture artefacts and efficient induction of histological fibrosis characteristics using the bioreactor developed within the Oakley group (Figure 5.27). Results supported previously published data by Paish *et al.* (2019).

Prior to the primary experiment, infection of PCLS with a BSL-3 category virus required confirmation the infection protocol would not induce cell damage (Figure 5.28) and comparing inactivation techniques ensuring reliable downstream outputs after inactivation of the virus sample (Figure 5.29). The resazurin assay confirmed the presence of PBS within PCLS culturing media for 4 h does not induce tissue damage and that inactivation of media samples with Triton X-100 results as the most versatile method in comparison to heat inactivation. The most inaccurate assay performed using Triton X-100 inactivation was the detection of albumin by ELISA. Alternatively, another commonly assessed metabolic product of the liver acting as a functional marker, may be analysed such as, urea. Relevant to this, different biological samples are identified as variation between biological may be a results of variation of individual liver health between patients.

Access to human liver is severely limited. Tissue is obtained from the normal margins of a colorectal metastasis liver resection that is surplus to pathology requirements and used with full informed patient consent. The viability of the tissue is significantly reduced when isolated from livers greater than 3 h post-hepatectomy (Bhogal et al., 2011). To minimise the ischemic time and preserve tissue viability, the maximum timing to generate the PCLS is limited to 2 h (Paish et al., 2019). The number of slices generated varies depending on the size of liver tissue obtained. As the introduction of fibrosis within HCV infected patients is observed years after infection and data within the Oakley group supported the ideology that histological changes in the liver would be minimal without a strong fibrosis stimulant, the limited number of PCLS were harvested for qRT-PCR analysis (Figure 5.30) and stained for the detection of NS5A (Figure 5.31) for completion of a preliminary experiment. Stress marker analysis suggests minimal changes of stress markers in DBN3a infected slices with a notable reduction in the mRNA expression of Snail-1 and fibronectin. This result complements the reduction of all fibrosis markers in the presence of DBN3a. In addition to the variation of gene expression in the presence of DBN3a, Snail-1 and ZEB-1 were enhanced within the fibrotic stimulated slices which are changes to gene

expression not observed within any of the *in vitro* cell culture models. The fibrotic stimulated sample, acting as a positive control, confirms sufficient induction of both stress and fibrosis markers. In comparison to my *in vitro* results, variation within the fibrotic stimulated samples could be due to the presence of both TGF-β and PDGF. Additionally, gene expression changes in comparison to the *in vitro* cell cultures could be a result of a greater number of cells within PCLS, cells maintained in the appropriate organisation, or the use of primary cells instead of a transformed cell line. Within PCLS many cell types are present which were not explored in the *in vitro* cell culture models; endothelial cells, cholangiocytes, Kupffer cells and immune cells within the tissue at the time of resection.

qRT-PCR detection of HCV 5'UTR confirms infection of the PCLS, however the relative gene expression was remarkably lower than gene expression within monolayer Huh7 cell infection (Figure 5.32). As qRT-PCR counts all viral genome copies within a cell, it cannot be used to measure the number of cells infected as there is typically multiple viral genomes present within one HCV infected cell. It is also well documented that the number of HCV viral genome copies within infected livers is estimated as a few copies per cell in comparison to *in vitro* cell culture conditions (Quinkert et al., 2005; Stiffler et al., 2009; Zhu et al., 2003). This means qPCR cannot be a determinant of the number of cells infected. Despite a greater number of cells present within the PCLS, than *in vitro* cell culture, the reduction of 5'UTR expression may be due to a greater number of cells present not susceptible to HCV infection, alteration to the MOI, 0.06 instead of 0.1, or inability for the virus to access to all HCV susceptible cells. To greater understand the number of cells infected, PCLS were stained for the presence of NS5A via confocal (Figures 5.32-5.35) and multiphoton (Figures 5.36 and 5.37) microscopy.

Confocal microscopy confirmed NS5A presence at a surface level, with Z-stacking performed at a single cell capacity confirming the puncta of NS5A within an infected cell confined to the cytoplasm. Variation of NS5A and Hoechst staining across the PCLS I believe is caused by inefficient staining of the tissue slice. Optimisation of antibody concentration,

permeability of tissue and incubation times may be optimised to obtain a more universal stain. Multiphoton microscopy confirmed the requirement to optimise antibody staining as greater than approximately 50 μm depth, there is a loss of Hoechst nuclei staining (Figure 5.36). Therefore, I was unable to confirm the presence of HCV greater than 50 μm into the tissue. Multiphoton was conducted with two photon beams. Additional photon beams were tested to acquire images deeper into the tissue however, autofluorescence restricted the ability to confirm NS5A presence. Auto-fluorescence was particularly problematic within the fibrotic stimulated sample. I was able to confirm red puncta observed within the fibrotic stimulated samples as autofluorescence due to red puncta present within the non-stained sample. Additionally, red puncta is not observed in the mock stained and non-stained sample nor the non-stained virus sample. I hypothesis the confocal does not present autofluorescence within the fibrotic stimulated sample as the laser beam strength is much weaker. Additionally, I cannot fine tune the excitation and emission wavelength on the Coherent Chameleon Ultra II, with physical M-BS760 and BS-MP760 lasers being placed in the machine, which is not a limitation of all multiphotons. For example, the Leica TCS SP8 MP has fully integrated infrared excitation lasers. By using both the confocal and multiphoton microscopy techniques. If the virus was unable to penetrate fully through the tissue, the results from the resazurin assay suggests re-introduction of concentrated virus could be performed daily to maximise the number of infected cells. Similarly, cell viability could be analysed after incubating PCLS with PBS containing media for 24 h.

I hypothesise, due to a reduction of stress and, in particularly fibrosis markers of PCLS obtained from the same patient, DBN3a can manipulate the host response to suppress activation of an immune response driving fibrosis during the early stages of HCV infection. Results concerning DBN3a are particularly impactful considering the low viral genome expression (Figure 5.32). I believe this may be GT3 dependent as results published by Kartasheva-Ebertz et al. (2021) suggests, HCV increases the expression of fibrosis markers.

However, upon comparisons of the different bioreactor systems predicting PCLS viability of 21 days in comparison to 6 days, within the Oakley group, is very different resulting in clear distinctions between experiments and results obtained. Additionally, initial virus infection was incubated overnight instead of 4 h and used the GT1b HCV cell culture virus instead of GT3 DBN3a. Primarily, I desired to infect PCLS with JFH-1 and DBN3a to draw direct comparisons between GT2 and GT3 HCV infection. However, as propagation of JFH-1 to achieve a high virus titre was difficult and the number of HCV infected cells during monolayer infection is not comparable to DBN3a infection, primary PCLS infection had a "proof of concept" approach.

To further explore the concept of DBN3a downregulating the expression of the innate immune response, innate immune markers should be explored such as TLR3, RIG-I and a range of soluble factors such as IFNs and cytokines (K. Li et al., 2012; Loo et al., 2006; Saito et al., 2008; Sumpter et al., 2005). The use of PCLS being used to exploit both liver pathology and innate immunity, as demonstrated by Wu et al. (2022). However, as PCLS are obtained from patients undergoing treatment of colorectal cancer, direct comparisons of the results and predictions of the response of HCV infection in a healthy liver should be considered.

Completion of PCLS experiments utilising tissue from fibrotic patients, patients infected with different genotypes of HCV or PCLS infected with patient-derived virus representing different HCV GTs could be explored. Such experiments have been conducted by Wu et al. (2022); comparing the innate immune response of DAA treated patient PCLS to non-infected patient PCLS and, Kartasheva-Ebertz et al. (2021); comparing the progression of liver fibrosis driven by HCV, alcohol and steatosis utilising PCLS from patients with varying degrees of liver fibrosis. Accessing human tissue representing different fibrosis phases, infected by different HCV GTs and the collection of patient serum with high virus titres to infect PCLS would allow greater interrogation of PCLS as an *ex vivo* model to study HCV and fibrosis pathology however, is limited by access to patient tissue.

To conclude, JFH-1 and DBN3a did not induce a significant expression of stress or fibrosis markers independent of the cell model used. Increasing the complexity of cell models from monolayer, mixed cell cultures, spheroids and PCLS suggests during early stages of HCV infection, HCV does not fibrosis. As the complexity of cell model increases, greater contingencies should be accounted when analysing results, such as LX-2 cell activation in spheroids and differences between biological repeats of PCLS infection.

5.3.5. Summary

- Culture of Huh7 cells with different cell types (LX-2 cells and THP1 cells) does not result to notable changes of stress and fibrosis markers and is not HCV GT dependent during monolayer cell culture experiments.
- Huh7 cell only spheroid volume is significantly reduced in the presence of TGF-β, this suggests cell:cell interactions alter the response of cells in comparison to monolayer cells where TGF-β does not significantly reduce cell growth.
- Greater understanding of spheroid dynamics, such as hydrogel composition, is required to optimise the activation of LX-2 cells, in particular, to greater exploit hepatocyte and HSC interactions during HCV.
- PCLS can be infected with genotype 3a HCV, isolate DBN3a.
- *Ex vivo* PCLS infection supports *in vitro* analysis, HCV does not induce fibrosis markers during early stages of HCV infection.

Chapter 6. Concluding remarks and future perspectives

6.1. Project Outcomes

The main focus and primary aim of this project was to compare HCV GT2 and GT3 in relation to the promotion of liver fibrosis, with particular focus on the NS5A plasticity and proteome, and exploitation of different cell culture models to greater investigate induction of fibrosis.

6.1.1. Key differences between JFH-1 and DBN3a

At the beginning of the project, I sought to identify key differences between the infection efficiency of JFH-1 and DBN3a, this was important to identify the differences between these cell culture adapted viruses prior to comparing their proteomes or modification to host gene expression. Direct comparison of JFH-1 and DBN3a beyond the comparison of virus propagation, such as infection efficiency, has not been compared before. I identified that the number of cells infected at 72 h.p.i differed between the different cell culture virus genotypes. By performing a time course analysis of cells infected throughout a 72 h period, data suggests equal infection efficiency, however, there were discrepancies between the production of virus particles. Specifically, DBN3a is more efficient at producing virus particles in comparison to JFH-1 tested in monolayer Huh7 cell infection. Additionally, to facilitate the identification of potential NS5A binding partners through an immunoprecipitation and mass spectrometry approach, the insertion of a small epitope tag at four sites across the C-terminus of NS5A alludes to different plasticity, and potentially function, between GT2 and GT3 (Chapter 3). Identified tolerable sites were limited by the size of gene insertions. This impacted both RNA replication and virus particle production resulting in limitations of inserting a fluorescent protein tag which

could have aided future experiments comparing JFH-1 and DBN3a infection, particularly during the exploration of different cell culture models (Chapter 5).

Successful insertion of an epitope tag allowed the completion of LC-MS/MS proteomics to compare the protein interactome of NS5A within JFH-1 and DBN3a (Chapter 4). Primarily, optimisation of NS5A co-immunoprecipitation assays was essential to ensure successful pulldown. Secondly, completion of LC-MS/MS via TMT labelling resulted in the identification of only three differential NS5A protein interactions between JFH-1 and DBN3a. I believed this number is very low due to high bleed-through of TMT-labelling between non-tagged NS5A controls and tagged NS5A samples. Confirmation of proteomic results was focussed on NAP1L1, demonstrating the requirement of both JFH-1 and DBN3a NS5A interaction for efficient virus production, utilising infectious HCV, but not required for genome replication, utilising Huh7 cell harbouring the SGR. Upon investigating discrepancies of proteomic results and confirmatory experiments, the phosphorylation status of NS5A was observed and demonstrated differences in the presence of phosphorylated NS5A within SGR and infectious virus models between JFH-1 and DBN3a. This may allude to the poor pull down of DBN3a NS5Aa interactions or differences between proteomic results performed using SGR samples. As NS5A is a phosphoprotein with over 130 host protein interactions described (Ross-Thriepland & Harris, 2015), I believe differences in the presence of a hyper and hypo phosphorylated form between SGR and infectious virus may alter the detection of virus to host protein interactions.

6.1.2. Difficulties recapitulating the liver architecture *in vitro* and investigation of HCV induced fibrosis

To explore the progression of *in vitro* fibrosis, various models were compared utilising the presence of different cell types, cell:cell interactions and PCLS as an *ex vivo* model (Chapter 5). The presence of Huh7, LX-2 and THP1 cells does not induce greater expression of stress or fibrosis markers, however this data suggests THP1 may reduce the efficiency of DBN3a infection.

Formation of spheroids highlights additional experimental factors acquired during alteration of cell:cell contact, such as failure of LX-2 cells to fully activate low elastic modulus pressure states. This is cell line specific as it not observed during the formation of Huh7 cell spheroid which appear to have induced TGF- β responses. The exploration of different cell culture models, varying in complexity, highlights the importance of analysing multiple experimental outputs, such as cell viability and proliferative ability within spheroids that may alter gene expression. The infection of *ex vivo* PCLS supports *in vitro* experimental results, DBN3a does not induce fibrosis during the early stages of infection. To greater understand the level of HCV infection within the PCLS, NS5A staining was conducted and observed by confocal and multiphoton microscopy. Optimisation of antibody is required, however results confirm the presence of NS5A greater than surface depth, at least 50 μm within the slice.

6.2. Future Studies

The importance of HCV research is highlighted by the resistance to the newly developed DAAs and the inability to eradicate the progression of HCC within cured patients. HCV GT3 in particular has been associated with increasing resistance DAA treatment as well as associations with a more rapid progression of fibrosis, steatosis and increased risk of developing HCC. As HCV is typically diagnosed over 10 years after infection, together with increasing screening programmes as part of the WHO initiative to eradicate HCV infections, greater understanding of HCV progression of liver pathology is required for the development of new DAAs. This will allow for treatment specifically targeting fibrosis in HCV infected patients. Caligiuri *et al.* (2021) describes the factors underpinning liver fibrosis regression such as removal of the injury causing agent. Relevant to this, there is increasing speculation of monolayer cell culture inability to recapitulate key organ dynamics which alter the investigation of disease pathology. As such, there has been a rapid development of *in vitro* spheroids, organoids and *ex vivo* models (Blutt & Estes, 2022).

6.2.1. Understanding NS5A phosphorylation status in different cell culture models

The identification of susceptible insertion sites within DBN3a suggests significant differences between the C terminal site of NS5A differing within GT3 and other HCV GTs. Greater expansion of this research could prove variation of protein plasticity, differences of tolerable insertion sites within the C terminus of NS5A between JFH-1 and DBN3a, as functional differences, intolerable regions important to interact with a host or viral protein not required in different HCV GTs. Classic molecular biology studies could be conducted mirroring that of Appel *et al.* (2008), discovering the functional properties of the GT2 C terminus through amino acid deletions. Confirmation of protein interactions to host proteins can also identify different NS5A functions promoting host manipulation of progression of liver pathology. Proteomic analysis within this thesis, suggested DBN3a protein interactions may be transient requiring techniques such as crosslinking reactions to be observed via SDS-PAGE. I believed this to be the case for DBN3a interaction with NAP1L1 which I deemed essential to produce virus particles. The proteomic results failed to recapitulate the extensive amount of results captured from other proteomic analysis within JFH-1 such as that of Goonawardane et al. (2017) and Smirnov *et al.* (2023). Variations of the phosphorylation status dependent on the HCV model used, requires investigation to decipher the most clinically relevant model to greater understand the most likely HCV NS5A interactions occurring *in vivo*. Further study of the DBN3a cell culture produced virus may be required as one the most recent HCV cell culture virus GT to be developed. Relevant to this, this thesis focussed heavily on the differences of NS5A between different HCV GTs as I believed NS5A multi-functional ability drives liver pathology, without investigating other HCV proteins also known to play a role in disease pathology.

6.2.2. Exploring the progression of fibrosis to HCV proteins, not limited to NS5A only

Examples of other HCV proteins driving disease pathology include the core protein blocking NF-KB to suppress an inflammatory response (Nguyen et al., 2006; Shrivastava et al., 1998) and targeting the JAK/STAT pathways via STAT1 and STAT2 inhibiting the induction ISGs (Blindenbacher et al., 2003; Larrea et al., 2006). Likewise, NS3 and NS4A induce the degradation of STAT1 impairing the expression of antiviral effectors (Lin et al., 2005) and NS4B interacts with stimulator of interferon genes (STING) impairing the expression of IFNs (Nitta et al., 2013). The targeting of STAT1 and PKR is an example of multiple HCV proteins targeting the same pathway. This suggests complete inhibition of one HCV protein would not stop or exacerbate the progression of liver pathology as there is not one sole protein responsible. This demonstrates the requirement to take a more universal approach.

6.2.3. Expanding the cell lines used

To gain a greater understanding of changes to host gene expression in the presence of HCV when altering cell:cell interactions, simple cell line monolayer cultures to 3D cell cultures was compared. A limiting factor in this project was the analysis of a small number of selected stress and fibrosis markers. As the progression of fibrosis is greatly controlled by the immune response, further exploration into the immune response changes during GT3 infection would be of interest. This can be exploited via PCLS, and spheroid models. Additionally, Omura *et al.* (2019) describes the establishment of a hepatocellular carcinoma cell line, KH, susceptible to HCV infection that provides greater insight into the innate immune response than Huh7 cells. The use of co-culture systems have also been used to uncover HCV mechanisms of pathology other than fibrosis, such as HCV-induced iron depletion, iron is crucial for effective regulation of the host immune response and outcome of infections. Using a tri- cell culture system,

hepatocytes, enterocytes and macrophages, Foka *et al.* (2021) describes the mechanism as advantageous to HCV during early stages of infection to support viral persistence and propagation. Metabolomics should be explored to gain the greatest insight when comparing cell models, exploiting variations within the metabolites of cells connected to biochemical pathways, has been hallmarked as a tool for biomarker discovery (Alseekh et al., 2021). Relevant to this is the use of primary hepatocyte cells which have gene and protein expression in comparison to immortal cancerous cell lines (Pan et al., 2009).

PCLS allows infection of an *ex vivo* model which maintains primary cells in the precise and intricate architecture of the native liver however, I was limited in this project to fully exploit the infection of PCLS by HCV. This was partially due to the accessibility of tissue. Greater optimisation and biological repeats are required to confirm the anti-fibrotic response observed during DBN3a infection of PCLS. However, expression of the HCV genome within PCLS highlights distinct difference between *in vitro* and *ex vivo* HCV genome expression. Significant differences between the expression of the HCV genome within the native liver and *in vitro* HCV infection suggests the level of HCV observed within cancerous cell lines, such as Huh7 cells, are not representative of infection elicited by HCV in the native liver. Wu *et al.* (2012) describes the use of differentiated human hepatocyte-like cells derived from pluripotent stem cells as a more physiologically relevant model which can support patient serum-derived HCV infection, as well as identification of cellular transitions impacting cell susceptibility to HCV infection. I would like to explore the use of primary cells and patient sera from GT3 infected patients to bridge the gap between laboratory results and *in vivo* infection utilising the most representative *in vitro* cell culture model, such as spheroids or generation of organoids, as performed by Natarajan *et al.* (2022). Direct comparisons of HCV GTs has not be exploited however, greater investigation is required to understand DBN3a cell culture clinical relevance. Due to the increasing clinical manifestations of GT3, I believe it is imperative to understand GT3 infection using the most clinically relevant models which will increase the impact of all results discovered.

6.2.4. Greater models to study chronic HCV infection

Importantly, due to the extensive manifestation of HCV infection prior to the progression of liver pathology, GT differences promoting liver fibrosis may only be observed in hindsight through bioinformatic studies. Analysis of cell models at only 72 h.p.i may only exploit viral mechanisms promoting a persistent infection and not the promotion of liver pathology. However, the exploration of different cell cultures highlights the importance of increasing the complexities of cell culture models to greater mimic the native organ for infectious agents which directly elicit disease pathology mechanisms. For example, Chikungunya and influenza viruses, whereby symptoms may occur as early as 2 days post infection.

6.3. Summary

Work from this PhD provides new insights into the characterisation of HCV GT-specific mechanisms of infection and the requirement to explore different cell culture models when investigating disease pathology. I have provided a strong basis for the future study of HCV GT characterisation specific to JFH-1 and DBN3a. In addition to the exploration of different cell culture models that may drive disease pathology studies in infection biology. Understanding both the molecular differences of HCV GTs and utilisation of appropriate cell culture models is important to develop future HCV treatment specific to disease pathology, such as fibrosis.

Chapter 7. Appendices

7.1. Oligonucleotides

7.1.1. Overlapping PCR Oligonucleotides

Primers	Sequence (5' → 3')	Purpose
JFH-1 NS5A Forward	TAACTGAGGACTGCCCCATCCCATGC	Amplification of the complete NS5A between restriction sites *BamHI* and *AfeI* with JFH-1.
JFH-1 NS5A Reverse	CTTTTCCTCTTCGGGGCTACAGGG	
DBN3a NS5A Forward	TAACTGAGGACTGCCCCATCCCATGC	Amplification of the complete NS5A between restriction sites *BspE*I and *BsiWI* with DBN3a.
DBN3a NS5A Reverse	CTTTTCCTCTTCGGGGCTACAGGG	

Table 7.1 Oligonucleotide sequences for the amplification of NS5A.

Primers	Sequence (5' → 3')	Purpose
JFH-1 Isn418 Forward	GGTTCAGGAGGTGGATCGGGAGGTGGATCGTGGAGCCACCCGC AGTTCGAAAAAGACCTGGAGTCTGATCAG	Insertion of TST at McCormick *et al.* (2006) site.
JFH-1 Isn418 Reverse	CCGATCCACCTCCTGAACCTCCACCTTTCTCGAACTGCGGGTGGC TCCACGGATCTCCAGGCTCCCCCTCGA	
JFH-1 Isn426 Forward	GGTTCAGGAGGTGGATCGGGAGGTGGATCGTGGAGCCACCCGC AGTTCGAAAAACTCGAGGGGGAGCCTGGAGA	Insertion of TST at Goonawardane *et al.* (2017) site.
JFH-1 Isn426 Reverse	CCGATCCACCTCCTGAACCTCCACCTTTCTCGAACTGCGGGTGGC TCCAGGGGGGCATAGAGGAGGCGGAA	
JFH-1 Isn431 Forward	GGTTCAGGAGGTGGATCGGGAGGTGGATCGTGGAGCCACCCGC AGTTCGAAAAACAGGTAGAGCTTCAACCTCC	Insertion of TST at Ross-Thriepland *et al.* (2015) site.
JFH-1 Isn431 Reverse	CCGATCCACCTCCTGAACCTCCACCTTTCTCGAACTGCGGGTGGC TCCAATCAGACTCCAGGTCCGGAT	
JFH-1 Isn463 Forward	CCGATCCACCTCCTGAACCTCCACCTTTCTCGAACTGCGGGTGGC TCCAGGTGGTATCGTCCTCCTCGGAG	Insertion of TST at novel site by the C-terminus.
JFH-1 Isn463 Reverse	GGTTCAGGAGGTGGATCGGGAGGTGGATCGTGGAGCCACCCGC AGTTCGAAAAAGTGTGCTGCTCCATGTCATAC	
DBN3a Isn423 Forward	ATGATGATGAGATCTGGGAAGTAGCGGGTCATCGTGGAGCCACC CGCATTCG	Insertion of TST at McCormick *et al.* (2006) site.
DBN3a Isn423 Reverse	CATCATCATAGATCTGGCGATGACCCGCTACTTCCTTTTTCGAACT GCGGGTGGFCTCC	
DBN3a Isn431 Forward	GGTTCAGGAGGTGGATCGGGAGGTGGATCGTGGAGCCACCCGC AGTTCGAAAAACTCGAGGGAGAGCCGGG	Insertion of TST at Goonawardane *et al.* (2017) site.
DBN3a Isn431 Reverse	CCGATCCACCTCCTGAACCTCCACCTTTCTCAACTGCGGGTGGCTCCAAG GAGGCATAGACGAACACGAC	
DBN3a Isn436 Forward	GGTTCAGGCGGTGGATCGGGAGGTGGATCGTGGAGCCACCCGC AGTTCGAAAAATCCTGGTCCACCGTTAGTGACAGC	Insertion of TST at Ross-Thriepland *et al.* (2015) site.
DBN3a Isn436 Reverse	CCGATCCACCTCCTGAACCTCCACCTTTCTCGAACTGCGGGTGGC TCCAGTCACAACTCAAGTCTGGATCGCC	
DBN3a Isn449 Forward	GGTTCAGGAGGTGGATCGGGAGGTGGATCGTGGAGCCACCCGC AGTTCGAAAAAGTCTGCTGCTCTATGTCATACTCCTGG	Insertion of TST at novel site by the C-terminus.
DBN3a Isn449 Reverse	CCGATCCACCTCCTGAACCTCCACCTTTCTCGAACTGCGGGTGGC TCCACACTCTCTGCTCCTCGCTCCTCGCTGTCACTAAC	

Table 7.2 Oligonucleotide sequences for the insertion of TST into NS5A.

Primers	Sequence (5' → 3')	Purpose
Product 1 DBN3a Isn423 Forward	GCCCTAGGCTCTGAAGGTGA	Insertion of eGFP at McCormick *et al.* (2006) site.
Product 1 DBN3a Isn423 Reverse	ACAGCTCCTCGCCCTTGCTCACTGGATCGCCCGGCTCTCCCTCGA	
Product 2 DBN3a Isn423 Forward	TCGAGGGAGAGCCGGGCGATCCAGTGAGCAAGGGCGAGGAGC TGT	
Product 2 DBN3a Isn423 Reverse	GGACCAGGAGTCACAACTCAAGTCCTTGTACAGCTCGTCCATGCC GAG	
Product 3 DBN3a Isn423 Forward	CTCGGCATGGACGAGCTGTACAAGGACTTGAGTTGTGACTCCTG GTCC	
Product 3 DBN3a Isn423 Reverse	AACGCGCTTAGACCATGGAG	
Product 1 DBN3a Isn431 Forward	GCCCTAGGCTCTGAAGGTGA	Insertion of eGFP at Goonawardane *et al.* (2017) site.
Product 1 DBN3a Isn431 Reverse	ACAGCTCCTCGCCCTTGCTCACAGGAGGCATAGACGAACACGAC	
Product 2 DBN3a Isn431 Forward	GTCGTGTTCGTCTATGCCTCCTGTGAGCAAGGGCGAGGAGCTGT	
Product 2 DBN3a Isn431 Reverse	CCCGGCTCTCCCTCGAGCTTGTACAGCTCGTCCATGCCGAGAGTG AT	
Product 3 DBN3a Isn431 Forward	ATCACTCTCGGCATGGACGAGCTGTACAAGCTCGAGGGAGAGCC GGG	
Product 3 DBN3a Isn431 Reverse	AACGCGCTTAGACCATGGAG	
Product 1 DBN3a Isn436 Forward	GCCCTAGGCTCTGAAGGTGA	Insertion of eGFP at Ross-Thriepland *et al.* (2015) site.
Product 1 DBN3a Isn436 Reverse	ACAGCTCCTCGCCCTTGCTCACGTCACAACTCAAGTCTGGATCGC C	
Product 2 DBN3a Isn436 Forward	GGCGATCCAGACTTGAGTTGTGACGTGAGCAAGGGCGAGGAGC TGT	
Product 2 DBN3a Isn436 Reverse	GCTGTCACTAACGGTGGACCAGGACTTGTACAGCTCGTCCATGCC GAGAGTGAT	
Product 3 DBN3a Isn436 Forward	ATCACTCTCGGCATGGACGAGCTGTACAAGTCCTGGTCCACCGTT AGTGACAGC	
	AACGCGCTTAGACCATGGAG	

Product 3 DBN3a Isn436 Reverse		
Product 1 DBN3a Isn449 Forward	GCCCTAGGCTCTGAAGGTGA	Insertion of eGFP at novel site by the C-terminus.
Product 1 DBN3a Isn449 Reverse	ACAGCTCCTCGCCCTTGCTCACCACTCTCTGCTCCTCGCTGTCACTA	
Product 2 DBN3a Isn449 Forward	TAGTGACAGCGAGGAGCAGAGAGTGGTGAGCAAGGGCGAGGAGCTGT	
Product 2 DBN3a Isn449 Reverse	CCAGGAGTATGACATAGAGCAGCAGACCTTGTACAGCTCGTCCATGCCGAGAGTGAT	
Product 3 DBN3a Isn449 Forward	ATCACTCTCGGCATGGACGAGCTGTACAAGGTCTGCTGCTCTATGTCATACTCCTGG	
Product 3 DBN3a Isn449 Reverse	AACGCGCTTAGACCATGGAG	

Table 7.3 Oligonucleotide sequences for the insertion of eGFP into NS5A.

Primers	Sequence (5' → 3')	Purpose
Product 1 JFH-1 Isn463 Forward	TAACTGAGGACTGCCCCATCCCATGC	Insertion of eGFP flanked by linkers at McCormick *et al.* (2006) site.
Product 1 JFH-1 Isn463 Reverse	TGAACAGCTCCTCGCCCTTGCTCACCGATCCACCTCCCGATCCACC TCCTGAACCTCCACCGGTGGTATCGTCCTCCTCGGAG	
Product 2 JFH-1 Isn463 Forward	CTCCGAGGAGGACGATACCACCGGTGGAGGTTCAGGAGGTGGA TCGGGAGGTGGATCGGTGAGCAAGGGCGAGGAGCTGTTCA	
Product 2 JFH-1 Isn463 Reverse	GTATGACATGGAGCAGCACACCGATCCACCTCCCGATCCACCTCC TGAACCTCCACCCTTGTACAGCTCGTCCAT	
Product 3 JFH-1 Isn463 Forward	ATGGACGAGCTGTACAAGGGTGGAGGTTCAGGAGGTGGATCGG GAGGTGGATCGGTGTGCTGCTCCATGTCATAC	
Product 3 JFH-1 Isn463 Reverse	CTTTTCCTCTTCGGGGCTACAGGG	
Product 1 DBN3a Isn423 Forward	GCCCTAGGCTCTGAAGGTGA	Insertion of eGFP flanked by linkers at McCormick *et al.* (2006) site.
Product 1 DBN3a Isn423 Reverse	CTCGCCCTTGCTCACCGATCCACCTCCCGATCCACCTCCTGAACCT CCACCTGGATCGCCCGGCTCTC	
Product 2 DBN3a Isn423 Forward	GAGAGCCGGGCGATCCAGGTGGAGGTTCAGGAGGTGGATCGG GAGGTGGATCGGTGAGCAAGGGCGAG	
Product 2 DBN3a Isn423 Reverse	CAGGAGTCACAACTCAAGTCCGATCCACCTCCCGATCCACCTCCT GAACCTCCACCCTTGTACAGCTCGTCCAT	
Product 3 DBN3a Isn423 Forward	ATGGACGAGCTGTACAAGGGTGGAGGTTCAGGAGGTGGATCGG GAGGTGGATCGGACTTGAGTTGTGACTCCTG	
Product 3 DBN3a Isn423 Reverse	AACGCGCTTAGACCATGGAG	
Product 1 DBN3a Isn431 Forward	GCCCTAGGCTCTGAAGGTGA	Insertion of eGFP flanked by linkers at Goonawardane *et al.* (2017) site.
Product 1 DBN3a Isn431 Reverse	CAGCTCCTCGCCCTTGCTCACCGATCCACCTCCCGATCCACCTCCT GAACCTCCACCAGGAGGCATAGACGAACACG	
Product 2 DBN3a Isn431 Forward	GTCGTGTTCGTCTATGCCTCCTGTGAGCAAGGGCGAGGAGCTGT CGTGTTCGTCTATGCCTCCTGGTGGAGGTTCAGGAGGTGGATCG GGAGGTGGATCGGTGAGCAAGGGCGAGGAGCTG	
Product 2 DBN3a Isn431 Reverse	CCGGCTCTCCCTCGAGCGATCCACCTCCCGATCCACCTCCTGAAC CTCCACCCTTGTACAGCTCGTCCATGCC	
	GGCATGGACGAGCTGTACAAGGGTGGAGGTTCAGGAGGTGGAT CGGGAGGTGGATCGCTCGAGGGAGAGCCGG	

Product 3 DBN3a Isn431 Forward **Product 3 DBN3a Isn431 Reverse**	AACGCGCTTAGACCATGGAG	
Product 1 DBN3a Isn436 Forward **Product 1 DBN3a Isn436 Reverse** **Product 2 DBN3a Isn436 Forward** **Product 2 DBN3a Isn436 Reverse** **Product 3 DBN3a Isn436 Forward** **Product 3 DBN3a Isn436 Reverse**	GCCCTAGGCTCTGAAGGTGA AGCTCCTCGCCCTTGCTCACCGATCCACCTCCCGATCCACCTCCTG AACCTCCACCGTCACAACTCAAGTCTGGATCGC GCGATCCAGACTTGAGTTGTGACGGTGGAGGTTCAGGAGGTGG ATCGGGAGGTGGATCGGTGAGCAAGGGCGAGGAGCT CTGTCACTAACGGTGGACCAGGACGATCCACCTCCCGATCCACCT CCTGAACCTCCACCCTTGTACAGCTCGTCCATGCCG CGGCATGGACGAGCTGTACAAGGGTGGAGGTTCAGGAGGTGGA TCGGGAGGTGGATCGTCCTGGTCCACCGTTAGTGACAG AACGCGCTTAGACCATGGAG	Insertion of eGFP flanked by linkers at Ross-Thriepland *et al.* (2015) site.
Product 1 DBN3a Isn449 Forward **Product 1 DBN3a Isn449 Reverse** **Product 2 DBN3a Isn449 Forward** **Product 2 DBN3a Isn449 Reverse** **Product 3 DBN3a Isn449 Forward** **Product 3 DBN3a Isn449 Reverse**	GCCCTAGGCTCTGAAGGTGA CTCCTCGCCCTTGCTCACCGATCCACCTCCCGATCCACCTCCTGAA CCTCCACCCACTCTCTGCTCCTCGCT AGCGAGGAGCAGAGAGTGGGTGGAGGTTCAGGAGGTGGATCG GGAGGTGGATCGGTGAGCAAGGGCGAGGAG GTATGACATAGAGCAGCAGACCGATCCACCTCCCGATCCACCTCC TGAACCTCCACCCTTGTACAGCTCGTCCATGCC GGCATGGACGAGCTGTACAAGGGTGGAGGTTCAGGAGGTGGAT CGGGAGGTGGATCGGTCTGCTGCTCTATGTCATAC AACGCGCTTAGACCATGGAG	Insertion of eGFP flanked by linkers at novel site by the C-terminus.

Table 1. Oligonucleotide sequences for the insertion of eGFP flanked by linkers into NS5A.

Primers	Sequence (5' → 3')	Purpose
Product 1 DBN3a Isn449 Forward	GCCCTAGGCTCTGAAGGTGA	Insertion of with a methionine at the start of eGFP at novel site by the C-terminus.
Product 1 DBN3a Isn449 Reverse	CGCCCTTGCTCACCATCACTCTCTGCTCCTCGCT	
Product 2 DBN3a Isn449 Forward	AGCGAGGAGCAGAGAGTGATGGTGAGCAAGGGCG	
Product 2 DBN3a Isn449 Reverse	TGACATAGAGCAGCAGACCTTGTACAGCTCGTCCATG	
Product 3 DBN3a Isn449 Forward	CATGGACGAGCTGTACAAGGTCTGCTGCTCTATGTCA	
Product 3 DBN3a Isn449 Reverse	AACGCGCTTAGACCATGGAG	

Table 7.4 Oligonucleotide sequences for the insertion of a methionineprior to eGFP into NS5A.

Primers	Sequence (5' → 3')	Purpose
Product 1 DBN3a Isn449 Forward	GCCCTAGGCTCTGAAGGTGA	Insertion of hrGFP at novel site by the C-terminus.
Product 1 DBN3a Isn449 Reverse	GGATCTGCTTGCTCACCATCACTCTCTGCTCCTCGCT	
Product 2 DBN3a Isn449 Forward	AGCGAGGAGCAGAGAGTGATGGTGAGCAAGCAGATCC	
Product 2 DBN3a Isn449 Reverse	CTGCACGAGTGGGTGGTCTGCTGCTCTATGTCA	
Product 3 DBN3a Isn449 Forward	TGACATAGAGCAGCAGACCACCCACTCGTGCAG	
Product 3 DBN3a Isn449 Reverse	AACGCGCTTAGACCATGGAG	

Table 7.5 Oligonucleotide sequences for the insertion of hrGFP into NS5A.

Primers	Sequence (5' → 3')	Purpose
eGFP *BglII* FMDV 2A Forward	ATGGTGAGCAAGGGCGAGGA	Amplification of eGFP with the insertion of a unique restriction site, *BglII*, followed by the sequence of FMDV 2A.
eGFP *BglII* FMDV 2A Forward	GGGCCCTGGGTTGGACTCGACGTCGCCGGCCAACTTGAGAAGGTCAAAGTTAGATCTCTTGTACAGCTCGTCCATG	
Product 1 JFH-1 Forward	GGAGAGCCATAGTGGTCTG	Insertion of a unique restriction site, *MluI*, between the 5'UTR delta core region and the insertion of eGFP followed the presence of the FMDV 2A sequence within JFH-1.
Product 1 JFH-1 Reverse	TGGGCGACGGTTGGTGTTTCTTT	
Product 2 JFH-1 Forward	AAAGAAACACCAACCGTCGCCCAACGCGTATGGTGAGCAAGGGCGAGGA	
Product 2 JFH-1 Reverse	GAGGTTTAGGATTTGTGCTCATGGGCCCTGGGTTGGACTCGACGTCGCCGGCCAACTTGAGAAGGTCAAAGTT	
Product 3 JFH-1 Forward	AACTTTGACCTTCTCAAGTTGGCCGGCGACGTCGAGTCCAACCCAGGGCCCATGAGCACAAATCCTAAACCTC	
Product 3 JFH-1 Reverse	CGCTAACGATGTCTATGATGACCT	
Product 1 DBN3a Forward	CTAGCCGAGTAGTGTTGG	Insertion of a unique restriction site, *SpeI*, between the 5'UTR delta core region and the insertion of eGFP followed the presence of the FMDV 2A sequence within DBN3a.
Product 1 DBN3a Reverse	TGGGCGGCGGATGGTGTTTCTT	
Product 2 DBN3a Forward	AAGAAACACCATCCGCCGCCCAACTAGTATGGTGAGCAAGGGCGAGGAGCTGTT	
Product 2 DBN3a Reverse	TGAGGTTTAGGAAGTGTGCTCATGGGCCCTGGGTTGGACTCGACGTCGCCGGCCAACTTGAGAAGGTCAAAGTTAGAT	
Product 3 DBN3a Forward	ATCTAACTTTGACCTTCTCAAGTTGGCCGGCGACGTCGAGTCCAACCCAGGGCCCATGAGCACACTTCCTAAACCTCA	
Product 3 DBN3a Reverse	CTGAACGTGAAGGCTTG	

Table 7.6 Oligonucleotide sequences for the insertion of eGFP flanked by unqieu restriction sites and the presence of the FMDV 2A seqeunce upstream of the HCV genome.

7.1.2. qRT-PCR oligonucleotides

Primers	Sequence (5' → 3')	Purpose
αSMA Forward	GCGTGGCTATTCCTTCGTTACT	Detection of human alpha smooth muscle actin.
αSMA Reverse	CCGATGAAGGATGGCTGGAACA	
Col1A1 Forward	CAAGAGGAAGGCCAAGTCGAGG	Detection of human collagen 1A1.
Col1A1 Reverse	CGTTGTCGCAGACGCAGAT	
Fibronectin Forward	CCGAGGGACCTGGAAGTT	Detection of human fibronectin.
Fibronectin Reverse	ACTTGCTCCCAGGCACAG	
HRPT1 Forward	CTCAACTTGAACTCTCATCTTAGG	Detection of human hypoxanthine phosphoribosyltransferase 1, acting as a housekeeper control gene.
HRPT1 Reverse	ATAAGCCAGACTTTGTTGGA	
Snail-1 Forward	TCGGAAGCCTAACTACAGCGA	Detection of human zinc finger protein Snail1.
Snail-1 Reverse	AGATGAGCATTGGCAGCGAG	
TGF-β Forward	TGACAGCAGGGATAACACACT	Detection of human transforming growth factor beta.
TGF-β Reverse	CGCAGGCAGCAGTTCTTCTCC	
TIMP1 Forward	ACTTTCCACAGGTCCACAAC	Detection of human TIMP metallopeptidase inhibitor 1.
TIMP1 Reverse	CATTCCTCACAGCCAACAGT	
ZEB1 Forward	GCACCTGAAGAGGACCAGAG	Detection of human zinc finger E-box-binding homeobox 1
ZEB1 Reverse	TGCATCTGGTGTTCCATTTT	
HCV 5'UTR/Core Forward	ACTGCCTGATAGGG	Detection of a universal region of the 5'untranslated region through to the core protein of HCV.
HCV 5'UTR/Core Reverse	TTTGGTTTTTCTTTGAGG	
AKR1C2 Forward	CTGTGAGGGAGGAAGAAACATTTGCTAA	Detection of human aldo-keto reductase family 1 member C2.
AKR1C2 Reverse	GGCTTCTATTGCCAATTTGACGGC	
NAP1L1 Forward	TTTGCCCCTCCTGAAGTTCC	Detection of human nucleosome assembly protein 1-like 1.
NAP1L1 Reverse	CCCAACACAACTTGAGACATCC	
GRP78 Forward	GCCTGTATTTCTAGACCTGCC	Detection of human glucose-Regulated Protein 78.
GRP78 Reverse	TTCATCTTGCCAGCCAGTTG	

Table 7.7 Oligonucleotide sequences for the detection of mRNA by qRT-PCR.

7.2. IncuCyte Parameters

Segmentation	Classic confluence	Adjustment: 1.2
Clean-up	Hole fill (μm²): 0	Adjust size (pixels): 0
Filters	Area (μm²) min: 140	Area (μm²) max: N/A

Table 7.8 IncuCyte parameters of monolayer phase analysis.

Segmentation	Sensitivity: 50	
Clean-up	Hole fill (μm²): 0	Adjust size (pixels): 0
Filters	Area (μm²) min: 5000	Area (μm²) max: N/A

Table 7.9 IncuCyte parameters of spheroid analysis.

General Analysis	**Segmentation**	Top-hat	Radius (μm): 100	Threshold (RCU): 0.8
	Edge Split	On	Edge sensitivity: -30	
	Clean-up	Hole fill (μm²): 0	Adjust size (pixels): 0	
	Filters	Area (μm²) min: 35	Area (μm²) max: 5000	
Large area	Segmentation	Top-hat	Radius (μm): 100	Threshold (RCU): 0.8
	Edge Split	On	Edge sensitivity: -30	
	Clean-up	Hole fill (μm²): 0	Adjust size (pixels): 0	
	Filters	Area (μm²) min: 150	Area (μm²) max: 5000	
High background	Segmentation	Surface fit		Threshold (RCU): 2.0
	Edge Split	On	Edge sensitivity: -30	
	Clean-up	Hole fill (μm²): 0	Adjust size (pixels): 0	
	Filters	Area (μm²) min: 100	Area (μm²) max: 5000	

Table 7.10 IncuCyte parameters of red fluorescence.

Segmentation	Top-hat	Radius (μm): 100	Threshold (RCU): 0.5
Edge Split	On	Edge sensitivity: -20	
Clean-up	Hole fill (μm^2): 0	Adjust size (pixels): 0	
Filters	Area (μm^2) min: 80	Area (μm^2) max: N/A	

Table 7.11 IncuCyte parameters of green fluorescence.

References

Adinolfi, L. E., Gambardella, M., Andreana, A., Tripodi , M. F., Utili, R., & Ruggiero, G. (2001). Steatosis accelerates the progression of liver damage of chronic hepatitis C patients and correlates with specific HCV genotype and visceral obesity. *Hepatology*, *33*(6), 1358-1364. https://doi.org/10.1053/jhep.2001.24432

Adinolfi, L. E., Utili, R., Andreana, A., Tripodi, M. F., Marracino, M., Gambardella, M., . . . Ruggiero, G. (2001). Serum HCV RNA levels correlate with histological liver damage and concur with steatosis in progression of chronic hepatitis C. *Dig Dis Sci*, *46*(8), 1677-1683. https://doi.org/10.1023/a:1010697319589

Akil, A., Endsley, M., Shanmugam, S., Saldarriaga, O., Somasunderam, A., Spratt, H., . . . Yi, M. (2019). Fibrogenic Gene Expression in Hepatic Stellate Cells Induced by HCV and HIV Replication in a Three Cell Co-Culture Model System. *Sci Rep*, *9*(1), 568. https://doi.org/10.1038/s41598-018-37071-y

Alazard-Dany, N., Denolly, S., Boson, B., & Cosset, F. L. (2019). Overview of HCV Life Cycle with a Special Focus on Current and Possible Future Antiviral Targets. *Viruses*, *11*(1). https://doi.org/10.3390/v11010030

Aledo, J. C. (2019). Methionine in proteins: The Cinderella of the proteinogenic amino acids. *Protein Sci*, *28*(10), 1785-1796. https://doi.org/10.1002/pro.3698

Alseekh, S., Aharoni, A., Brotman, Y., Contrepois, K., D'Auria, J., Ewald, J., . . . Hall, R. D. (2021). Mass spectrometry-based metabolomics: a guide for annotation, quantification and best reporting practices. *Nature methods*, *18*(7), 747-756.

Ananthanarayanan, A., Nugraha, B., Triyatni, M., Hart, S., Sankuratri, S., & Yu, H. (2014). Scalable spheroid model of human hepatocytes for hepatitis C infection and replication. *Mol Pharm*, *11*(7), 2106-2114. https://doi.org/10.1021/mp500063y

Ananthaswamy, N., Fang, Q., AlSalmi, W., Jain, S., Chen, Z., Klose, T., . . . Chand, S. (2019). A sequestered fusion peptide in the structure of an HIV-1 transmitted founder envelope trimer. *Nature communications*, *10*(1), 873.

Aninat, C., Piton, A., Glaise, D., Le Charpentier, T., Langouët, S., Morel, F., . . . Guillouzo, A. (2006). Expression of cytochromes P450, conjugating enzymes and nuclear receptors in human hepatoma HepaRG cells. *Drug Metab Dispos*, *34*(1), 75-83. https://doi.org/10.1124/dmd.105.006759

Anthony, B., Allen, J. T., Li, Y. S., & McManus, D. P. (2010). Hepatic stellate cells and parasite-induced liver fibrosis. *Parasites & vectors*, *3*(1), 1-7.

Anticoli, S., Amatore, D., Matarrese, P., De Angelis, M., Palamara, A. T., Nencioni, L., & Ruggieri, A. (2019). Counteraction of HCV-induced oxidative stress concurs to establish chronic infection in liver cell cultures. *Oxidative Medicine and Cellular Longevity*, *2019*.

Aoudjehane, L., Gautheron, J., Le Goff, W., Goumard, C., Gilaizeau, J., Nget, C. S., . . . Conti, F. (2020). Novel defatting strategies reduce lipid accumulation in primary human culture models of liver steatosis. *Dis Model Mech*, *13*(4). https://doi.org/10.1242/dmm.042663

Appel, N., Pietschmann, T., & Bartenschlager, R. (2005). Mutational analysis of hepatitis C virus nonstructural protein 5A: potential role of differential phosphorylation in RNA replication and identification of a genetically flexible domain. *J Virol*, *79*(5), 3187-3194. https://doi.org/10.1128/JVI.79.5.3187-3194.2005

Appel, N., Zayas, M., Miller, S., Krijnse-Locker, J., Schaller, T., Friebe, P., . . . Bartenschlager, R. (2008). Essential role of domain III of nonstructural protein 5A for hepatitis C virus infectious particle assembly. *PLoS Pathog*, *4*(3), e1000035. https://doi.org/10.1371/journal.ppat.1000035

Arnaud, N., Dabo, S., Maillard, P., Budkowska, A., Kalliampakou, K. I., Mavromara, P., . . . Meurs, E. F. (2010). Hepatitis C virus controls interferon production through PKR activation. *PLoS One*, *5*(5), e10575. https://doi.org/10.1371/journal.pone.0010575

Arpino, J. A., Rizkallah, P. J., & Jones, D. D. (2012). Crystal structure of enhanced green fluorescent protein to 1.35 Å resolution reveals alternative conformations for Glu222. *PLoS One*, *7*(10), e47132. https://doi.org/10.1371/journal.pone.0047132

Aslam, B., Basit, M., Nisar, M. A., Khurshid, M., & Rasool, M. H. (2017). Proteomics: Technologies and Their Applications. *J Chromatogr Sci*, *55*(2), 182-196. https://doi.org/10.1093/chromsci/bmw167

Atwell, S., Ultsch, M., De Vos, A. M., & Wells, J. A. (1997). Structural plasticity in a remodeled protein-protein interface. *Science*, *278*(5340), 1125-1128.

Axley, P., Ahmed, Z., Ravi, S., & Singal, A. K. (2018). Hepatitis C Virus and Hepatocellular Carcinoma: A Narrative Review. *J Clin Transl Hepatol*, *6*(1), 79-84. https://doi.org/10.14218/JCTH.2017.00067

Azuma, H., Hirose, T., Fujii, H., Oe, S., Yasuchika, K., Fujikawa, T., & Yamaoka, Y. (2003). Enrichment of hepatic progenitor cells from adult mouse liver. *Hepatology*, *37*(6), 1385-1394. https://doi.org/10.1053/jhep.2003.50210

Baktash, Y., & Randall, G. (2019). Live Cell Imaging of Hepatitis C Virus Trafficking in Hepatocytes. *Methods Mol Biol*, *1911*, 263-274. https://doi.org/10.1007/978-1-4939-8976-8_18

Barisam, M., Saidi, M. S., Kashaninejad, N., & Nguyen, N. T. (2018). Prediction of Necrotic Core and Hypoxic Zone of Multicellular Spheroids in a Microbioreactor with a U-Shaped Barrier. *Micromachines (Basel)*, *9*(3). https://doi.org/10.3390/mi9030094

Bataller, R., & Brenner, D. A. (2005). Liver fibrosis. *J Clin Invest*, *115*(2), 209-218. https://doi.org/10.1172/JCI24282

Baxter, M., Withey, S., Harrison, S., Segeritz, C.-P., Zhang, F., Atkinson-Dell, R., . . . Jenkins, R. (2015). Phenotypic and functional analyses show stem cell-derived hepatocyte-like cells better mimic fetal rather than adult hepatocytes. *Journal of hepatology*, *62*(3), 581-589.

Bell, M. R., Engleka, M. J., Malik, A., & Strickler, J. E. (2013). To fuse or not to fuse: what is your purpose? *Protein Sci*, *22*(11), 1466-1477. https://doi.org/10.1002/pro.2356

Benga, W. J., Krieger, S. E., Dimitrova, M., Zeisel, M. B., Parnot, M., Lupberger, J., . . . Schuster, C. (2010). Apolipoprotein E interacts with hepatitis C virus nonstructural protein 5A and determines assembly of infectious particles. *Hepatology*, *51*(1), 43-53. https://doi.org/10.1002/hep.23278

Bernardi, P., Gerle, C., Halestrap, A. P., Jonas, E. A., Karch, J., Mnatsakanyan, N., . . . Soukas, A. A. (2023). Identity, structure, and function of the mitochondrial permeability transition pore: controversies, consensus, recent advances, and future directions. *Cell Death Differ*, *30*(8), 1869-1885. https://doi.org/10.1038/s41418-023-01187-0

Bhatnagar, B. S., Bogner, R. H., & Pikal, M. J. (2007). Protein stability during freezing: separation of stresses and mechanisms of protein stabilization. *Pharm Dev Technol*, *12*(5), 505-523. https://doi.org/10.1080/10837450701481157

Bhattacharya, D., Aronsohn, A., Price, J., Lo Re, V., Heald, J., Demisashi, G., . . . Diseases, A. A. f. t. S. o. L. (2023). Hepatitis C Guidance 2023 Update: American Association for the Study of Liver Diseases–infectious diseases society of America recommendations for testing, managing, and treating hepatitis C virus infection. *Clinical Infectious Diseases*.

Bhogal, R. H., Hodson, J., Bartlett, D. C., Weston, C. J., Curbishley, S. M., Haughton, E., . . . Afford, S. C. (2011). Isolation of primary human hepatocytes from normal and diseased liver tissue: a one hundred liver experience. *PLoS One*, *6*(3), e18222. https://doi.org/10.1371/journal.pone.0018222

Bigger, C. B., Guerra, B., Brasky, K. M., Hubbard, G., Beard, M. R., Luxon, B. A., . . . Lanford, R. E. (2004). Intrahepatic gene expression during chronic hepatitis C virus infection in chimpanzees. *J Virol*, *78*(24), 13779-13792. https://doi.org/10.1128/JVI.78.24.13779-13792.2004

Bility, M. T., Nio, K., Li, F., McGivern, D. R., Lemon, S. M., Feeney, E. R., . . . Su, L. (2016). Chronic hepatitis C infection–induced liver fibrogenesis is associated with M2 macrophage activation. *Scientific reports*, *6*(1), 39520.

Blanchard, E., Belouzard, S., Goueslain, L., Wakita, T., Dubuisson, J., Wychowski, C., & Rouillé, Y. (2006). Hepatitis C virus entry depends on clathrin-mediated endocytosis. *J Virol*, *80*(14), 6964-6972. https://doi.org/10.1128/JVI.00024-06

Blight, K. J., Kolykhalov, A. A., & Rice, C. M. (2000). Efficient initiation of HCV RNA replication in cell culture. *Science*, *290*(5498), 1972-1974. https://doi.org/10.1126/science.290.5498.1972

Blight, K. J., McKeating, J. A., & Rice, C. M. (2002). Highly permissive cell lines for subgenomic and genomic hepatitis C virus RNA replication. *Journal of virology*, *76*(24), 13001-13014.

Blindenbacher, A., Duong, F. H., Hunziker, L., Stutvoet, S. T., Wang, X., Terracciano, L., . . . Tripodi, M. (2003). Expression of hepatitis C virus proteins inhibits interferon α signaling in the liver of transgenic mice. *Gastroenterology*, *124*(5), 1465-1475.

Blouin, A., Bolender, R. P., & Weibel, E. R. (1977). Distribution of organelles and membranes between hepatocytes and nonhepatocytes in the rat liver parenchyma. A stereological study. *The Journal of cell biology*, *72*(2), 441-455.

Blutt, S. E., & Estes, M. K. (2022). Organoid Models for Infectious Disease. *Annu Rev Med*, *73*, 167-182. https://doi.org/10.1146/annurev-med-042320-023055

Borgia, S. M., Hedskog, C., Parhy, B., Hyland, R. H., Stamm, L. M., Brainard, D. M., . . . Shafran, S. D. (2018). Identification of a Novel Hepatitis C Virus Genotype From Punjab, India: Expanding Classification of Hepatitis C Virus Into 8 Genotypes. *J Infect Dis*, *218*(11), 1722-1729. https://doi.org/10.1093/infdis/jiy401

Boulant, S., Montserret, R., Hope, R. G., Ratinier, M., Targett-Adams, P., Lavergne, J. P., . . . McLauchlan, J. (2006). Structural determinants that target the hepatitis C virus core protein to lipid droplets. *J Biol Chem*, *281*(31), 22236-22247. https://doi.org/10.1074/jbc.M601031200

Brass, V., Bieck, E., Montserret, R., Wölk, B., Hellings, J. A., Blum, H. E., . . . Moradpour, D. (2002). An amino-terminal amphipathic alpha-helix mediates membrane association of the hepatitis C virus nonstructural protein 5A. *J Biol Chem*, *277*(10), 8130-8139. https://doi.org/10.1074/jbc.M111289200

Brenner, D. A. (2009). Molecular pathogenesis of liver fibrosis. *Transactions of the American clinical and Climatological Association*, *120*, 361.

Browning, A. P., Sharp, J. A., Murphy, R. J., Gunasingh, G., Lawson, B., Burrage, K., . . . Simpson, M. (2021). Quantitative analysis of tumour spheroid structure. *Elife*, *10*, e73020.

Butt, T. R., Edavettal, S. C., Hall, J. P., & Mattern, M. R. (2005). SUMO fusion technology for difficult-to-express proteins. *Protein Expr Purif*, *43*(1), 1-9. https://doi.org/10.1016/j.pep.2005.03.016

Cable, E. E., & Isom, H. C. (1997). Exposure of primary rat hepatocytes in long-term DMSO culture to selected transition metals induces hepatocyte proliferation and formation of duct-like structures. *Hepatology*, *26*(6), 1444-1457. https://doi.org/10.1002/hep.510260611

Cai, H., Yao, W., Li, L., Li, X., Hu, L., Mai, R., & Peng, T. (2016). Cell-death-inducing DFFA-like Effector B Contributes to the Assembly of Hepatitis C Virus (HCV) Particles and Interacts with HCV NS5A. *Sci Rep*, *6*, 27778. https://doi.org/10.1038/srep27778

Cai, W., Tucholski, T. M., Gregorich, Z. R., & Ge, Y. (2016). Top-down Proteomics: Technology Advancements and Applications to Heart Diseases. *Expert Rev Proteomics*, *13*(8), 717-730. https://doi.org/10.1080/14789450.2016.1209414

Caliari, S. R., Perepelyuk, M., Cosgrove, B. D., Tsai, S. J., Lee, G. Y., Mauck, R. L., . . . Burdick, J. A. (2016). Stiffening hydrogels for investigating the dynamics of hepatic stellate cell mechanotransduction during myofibroblast activation. *Scientific reports*, *6*(1), 21387.

Caligiuri, A., Gentilini, A., Pastore, M., Gitto, S., & Marra, F. (2021). Cellular and Molecular Mechanisms Underlying Liver Fibrosis Regression. *Cells*, *10*(10). https://doi.org/10.3390/cells10102759

Carson, J. P., Robinson, M. W., Ramm, G. A., & Gobert, G. N. (2021). RNA sequencing of LX-2 cells treated with TGF-β1 identifies genes associated with hepatic stellate cell activation. *Mol Biol Rep*, *48*(12), 7677-7688. https://doi.org/10.1007/s11033-021-06774-3

Chan, A., Patel, K., & Naggie, S. (2017). Genotype 3 Infection: The Last Stand of Hepatitis C Virus. *Drugs*, *77*(2), 131-144. https://doi.org/10.1007/s40265-016-0685-x

Chang, H. H., Oh, P. Y., Ingber, D. E., & Huang, S. (2006). Multistable and multistep dynamics in neutrophil differentiation. *BMC Cell Biol*, *7*, 11. https://doi.org/10.1186/1471-2121-7-11

Chanput, W., Mes, J. J., & Wichers, H. J. (2014). THP-1 cell line: an in vitro cell model for immune modulation approach. *Int Immunopharmacol*, *23*(1), 37-45. https://doi.org/10.1016/j.intimp.2014.08.002

Chen, S., & Harris, M. (2023). NS5A domain I antagonises PKR to facilitate the assembly of infectious hepatitis C virus particles. *PLoS Pathog*, *19*(2), e1010812. https://doi.org/10.1371/journal.ppat.1010812

Chen, S. L., & Morgan, T. R. (2006). The natural history of hepatitis C virus (HCV) infection. *Int J Med Sci*, *3*(2), 47-52. https://doi.org/10.7150/ijms.3.47

Cheung, W. M., Ng, W. W., & Kung, A. W. (2006). Dimethyl sulfoxide as an inducer of differentiation in preosteoblast MC3T3-E1 cells. *FEBS Lett*, *580*(1), 121-126. https://doi.org/10.1016/j.febslet.2005.11.062

Chhatwal, J., Chen, Q., Ayer, T., Bethea, E. D., Kanwal, F., Kowdley, K. V., . . . Gordon, S. C. (2018). Hepatitis C virus re-treatment in the era of direct-acting antivirals: projections in the USA. *Aliment Pharmacol Ther*, *47*(7), 1023-1031. https://doi.org/10.1111/apt.14527

Chong, W. M., Hsu, S. C., Kao, W. T., Lo, C. W., Lee, K. Y., Shao, J. S., . . . Yu, M. J. (2016). Phosphoproteomics Identified an NS5A Phosphorylation Site Involved in Hepatitis C Virus Replication. *J Biol Chem*, *291*(8), 3918-3931. https://doi.org/10.1074/jbc.M115.675413

Christoforou, A. L., & Lilley, K. S. (2012). Isobaric tagging approaches in quantitative proteomics: the ups and downs. *Anal Bioanal Chem*, *404*(4), 1029-1037. https://doi.org/10.1007/s00216-012-6012-9

Chung, Y. L., Sheu, M. L., & Yen, S. H. (2003). Hepatitis C virus NS5A as a potential viral Bcl-2 homologue interacts with Bax and inhibits apoptosis in hepatocellular carcinoma. *Int J Cancer*, *107*(1), 65-73. https://doi.org/10.1002/ijc.11303

Chusri, P., Kumthip, K., Hong, J., Zhu, C., Duan, X., Jilg, N., . . . Cai, D. (2016). HCV induces transforming growth factor β1 through activation of endoplasmic reticulum stress and the unfolded protein response. *Scientific reports*, *6*(1), 22487.

Clément, S., Pascarella, S., Conzelmann, S., Gonelle-Gispert, C., Guilloux, K., & Negro, F. (2010). The hepatitis C virus core protein indirectly induces alpha-smooth muscle actin expression in hepatic stellate cells via interleukin-8. *J Hepatol*, *52*(5), 635-643. https://doi.org/10.1016/j.jhep.2009.10.035

Coenen, M., Nischalke, H. D., Krämer, B., Langhans, B., Glässner, A., Schulte, D., . . . Spengler, U. (2011). Hepatitis C virus core protein induces fibrogenic actions of hepatic stellate cells via toll-like receptor 2. *Lab Invest*, *91*(9), 1375-1382. https://doi.org/10.1038/labinvest.2011.78

Cordek, D. G., Croom-Perez, T. J., Hwang, J., Hargittai, M. R., Subba-Reddy, C. V., Han, Q., . . . Cameron, C. E. (2014). Expanding the proteome of an RNA virus by phosphorylation of an intrinsically disordered viral protein. *J Biol Chem*, *289*(35), 24397-24416. https://doi.org/10.1074/jbc.M114.589911

Craig, V. J., Zhang, L., Hagood, J. S., & Owen, C. A. (2015). Matrix metalloproteinases as therapeutic targets for idiopathic pulmonary fibrosis. *American journal of respiratory cell and molecular biology*, *53*(5), 585-600.

Cui, J., Zhou, X., Liu, Y., Tang, Z., & Romeih, M. (2003). Wnt signaling in hepatocellular carcinoma: analysis of mutation and expression of beta-catenin, T-cell factor-4 and glycogen synthase kinase 3-beta genes. *Journal of gastroenterology and hepatology*, *18*(3), 280-287.

Cui, M., Cheng, C., & Zhang, L. (2022). High-throughput proteomics: a methodological mini-review. *Lab Invest*, *102*(11), 1170-1181. https://doi.org/10.1038/s41374-022-00830-7

Cui, X., Zhang, X., Yin, Q., Meng, A., Su, S., Jing, X., . . . Cheng, M. (2014). F-actin cytoskeleton reorganization is associated with hepatic stellate cell activation. *Mol Med Rep*, *9*(5), 1641-1647. https://doi.org/10.3892/mmr.2014.2036

Date, T., Morikawa, K., Tanaka, Y., Tanaka-Kaneko, K., Sata, T., Mizokami, M., & Wakita, T. (2012). Replication and infectivity of a novel genotype 1b hepatitis C virus clone. *Microbiol Immunol*, *56*(5), 308-317. https://doi.org/10.1111/j.1348-0421.2012.00437.x

de Chassey, B., Meyniel-Schicklin, L., Vonderscher, J., André, P., & Lotteau, V. (2014). Virus-host interactomics: new insights and opportunities for antiviral drug discovery. *Genome Med*, *6*(11), 115. https://doi.org/10.1186/s13073-014-0115-1

de Chassey, B., Navratil, V., Tafforeau, L., Hiet, M. S., Aublin-Gex, A., Agaugué, S., . . . Lotteau, V. (2008). Hepatitis C virus infection protein network. *Mol Syst Biol*, *4*, 230. https://doi.org/10.1038/msb.2008.66

de Gottardi, A., Pazienza, V., Pugnale, P., Bruttin, F., Rubbia-Brandt, L., Juge-Aubry, C. E., . . . Negro, F. (2006). Peroxisome proliferator-activated receptor-alpha and -gamma mRNA levels are reduced in chronic hepatitis C with steatosis and genotype 3 infection. *Aliment Pharmacol Ther*, *23*(1), 107-114. https://doi.org/10.1111/j.1365-2036.2006.02729.x

de Lamballerie, X., Charrel, R. N., Attoui, H., & De Micco, P. (1997). Classification of hepatitis C virus variants in six major types based on analysis of the envelope 1 and nonstructural 5B genome regions and complete polyprotein sequences. *Journal of General Virology*, *78*(1), 45-51.

De Minicis, S., Seki, E., Uchinami, H., Kluwe, J., Zhang, Y., Brenner, D. A., & Schwabe, R. F. (2007). Gene expression profiles during hepatic stellate cell activation in culture and in vivo. *Gastroenterology*, *132*(5), 1937-1946.

Demone, J., Maltseva, M., Nourimand, M., Nasr-Sharif, M., Galipeau, Y., Alarcon, E. I., . . . MacLean, A. M. (2022). Scalable agroinfiltration-based production of SARS-CoV-2 antigens for use in diagnostic assays and subunit vaccines. *PLoS One*, *17*(12), e0277668.

Deng, L., Nagano-Fujii, M., Tanaka, M., Nomura-Takigawa, Y., Ikeda, M., Kato, N., . . . Hotta, H. (2006). NS3 protein of Hepatitis C virus associates with the tumour suppressor p53 and inhibits its function in an NS3 sequence-dependent manner. *Journal of general virology*, *87*(6), 1703-1713.

Despres, H. W., Mills, M. G., Shirley, D. J., Schmidt, M. M., Huang, M. L., Roychoudhury, P., . . . Bruce, E. A. (2022). Measuring infectious SARS-CoV-2 in clinical samples reveals a higher viral titer:RNA ratio for Delta and Epsilon vs. Alpha variants. *Proc Natl Acad Sci U S A*, *119*(5). https://doi.org/10.1073/pnas.2116518119

Dharancy, S., Malapel, M., Perlemuter, G., Roskams, T., Cheng, Y., Dubuquoy, L., . . . Desreumaux, P. (2005). Impaired expression of the peroxisome proliferator-activated receptor alpha during hepatitis C virus infection. *Gastroenterology*, *128*(2), 334-342. https://doi.org/10.1053/j.gastro.2004.11.016

Dolganiuc, A., Oak, S., Kodys, K., Golenbock, D. T., Finberg, R. W., Kurt-Jones, E., & Szabo, G. (2004). Hepatitis C core and nonstructural 3 proteins trigger toll-like receptor 2-mediated pathways and inflammatory activation. *Gastroenterology*, *127*(5), 1513-1524.

Dooley, S., Hamzavi, J., Ciuclan, L., Godoy, P., Ilkavets, I., Ehnert, S., . . . Geier, A. (2008). Hepatocyte-specific Smad7 expression attenuates TGF-β–mediated fibrogenesis and protects against liver damage. *Gastroenterology*, *135*(2), 642-659. e646.

Duan, Y., Catana, A., Meng, Y., Yamamoto, N., He, S., Gupta, S., . . . Zern, M. A. (2007). Differentiation and enrichment of hepatocyte-like cells from human embryonic stem cells in vitro and in vivo. *Stem Cells*, *25*(12), 3058-3068. https://doi.org/10.1634/stemcells.2007-0291

Dubuisson, J. (2007). Hepatitis C virus proteins. *World J Gastroenterol*, *13*(17), 2406-2415. https://doi.org/10.3748/wjg.v13.i17.2406

Duke, C. G., Bach, S. V., Revanna, J. S., Sultan, F. A., Southern, N. T., Davis, M. N., . . . Day, J. J. (2020). An Improved CRISPR/dCas9 Interference Tool for Neuronal Gene Suppression. *Front Genome Ed*, *2*, 9. https://doi.org/10.3389/fgeed.2020.00009

Durantel, D., & Zoulim, F. (2007). Going towards more relevant cell culture models to study the in vitro replication of serum-derived hepatitis C virus and virus/host cell interactions? *Journal of hepatology*, *46*(1), 1-5.

Dustin, L. B., Bartolini, B., Capobianchi, M. R., & Pistello, M. (2016). Hepatitis C virus: life cycle in cells, infection and host response, and analysis of molecular markers influencing the outcome of infection and response to therapy. *Clin Microbiol Infect*, *22*(10), 826-832. https://doi.org/10.1016/j.cmi.2016.08.025

Dáder, B., Burckbuchler, M., Macia, J. L., Alcon, C., Curie, C., Gargani, D., . . . Drucker, M. (2019). Split green fluorescent protein as a tool to study infection with a plant pathogen, Cauliflower mosaic virus. *PLoS One*, *14*(3), e0213087. https://doi.org/10.1371/journal.pone.0213087

Düesberg, U., von dem Bussche, A., Kirschning, C. J., Miyake, K., Sauerbruch, T., & Spengler, U. (2002). Cell activation by synthetic lipopeptides of the hepatitis C virus (HCV)—Core protein is mediated by toll like receptors (TLRs) 2 and 4. *Immunology letters*, *84*(2), 89-95.

Ekstedt, M., Hagström, H., Nasr, P., Fredrikson, M., Stål, P., Kechagias, S., & Hultcrantz, R. (2015). Fibrosis stage is the strongest predictor for disease-specific mortality in NAFLD after up to 33 years of follow-up. *Hepatology*, *61*(5), 1547-1554.

Elaut, G., Henkens, T., Papeleu, P., Snykers, S., Vinken, M., Vanhaecke, T., & Rogiers, V. (2006). Molecular mechanisms underlying the dedifferentiation process of isolated hepatocytes and their cultures. *Curr Drug Metab*, *7*(6), 629-660. https://doi.org/10.2174/138920006778017759

Elshemey, W., Ibrahim, I. M., Elfiky, A. A., & Elgohary, A. M. (2023). Prediction of HCV E2 association with the host-cell chaperone, GRP78. *Informatics in Medicine Unlocked*, *39*, 101257.

Evans, M. J., Rice, C. M., & Goff, S. P. (2004). Phosphorylation of hepatitis C virus nonstructural protein 5A modulates its protein interactions and viral RNA replication. *Proc Natl Acad Sci U S A*, *101*(35), 13038-13043. https://doi.org/10.1073/pnas.0405152101

Evans, M. J., von Hahn, T., Tscherne, D. M., Syder, A. J., Panis, M., Wölk, B., . . . Rice, C. M. (2007). Claudin-1 is a hepatitis C virus co-receptor required for a late step in entry. *Nature*, *446*(7137), 801-805.

Feld, J. J., & Hoofnagle, J. H. (2005). Mechanism of action of interferon and ribavirin in treatment of hepatitis C. *Nature*, *436*(7053), 967-972. https://doi.org/10.1038/nature04082

Feldmann, G., Nischalke, H. D., Nattermann, J., Banas, B., Berg, T., Teschendorf, C., . . . Iwan, A. (2006). Induction of interleukin-6 by hepatitis C virus core protein in hepatitis C–associated mixed cryoglobulinemia and B-cell non–Hodgkin's lymphoma. *Clinical Cancer Research*, *12*(15), 4491-4498.

Feng, X.-H., & Derynck, R. (2005). Specificity and versatility in TGF-β signaling through Smads. *Annu. Rev. Cell Dev. Biol.*, *21*, 659-693.

Ferenci, P., Fried, M. W., Shiffman, M. L., Smith, C. I., Marinos, G., Gonçales, F. L., . . . Reddy, K. R. (2005). Predicting sustained virological responses in chronic hepatitis C patients treated with peginterferon alfa-2a (40 KD)/ribavirin. *J Hepatol*, *43*(3), 425-433. https://doi.org/10.1016/j.jhep.2005.04.009

Fletcher, N. F., Sutaria, R., Jo, J., Barnes, A., Blahova, M., Meredith, L. W., . . . McKeating, J. A. (2014). Activated macrophages promote hepatitis C virus entry in a tumor necrosis factor-dependent manner. *Hepatology*, *59*(4), 1320-1330. https://doi.org/10.1002/hep.26911

Florimond, A., Chouteau, P., Bruscella, P., Le Seyec, J., Mérour, E., Ahnou, N., . . . Pawlotsky, J. M. (2015). Human hepatic stellate cells are not permissive for hepatitis C virus entry and replication. *Gut*, *64*(6), 957-965. https://doi.org/10.1136/gutjnl-2013-305634

Foka, P., Dimitriadis, A., Karamichali, E., Kochlios, E., Eliadis, P., Valiakou, V., . . . Georgopoulou, U. (2021). HCV-Induced Immunometabolic Crosstalk in a Triple-Cell Co-Culture Model Capable of Simulating Systemic Iron Homeostasis. *Cells*, *10*(9). https://doi.org/10.3390/cells10092251

Foster, T. L., Belyaeva, T., Stonehouse, N. J., Pearson, A. R., & Harris, M. (2010). All three domains of the hepatitis C virus nonstructural NS5A protein contribute to RNA binding. *J Virol*, *84*(18), 9267-9277. https://doi.org/10.1128/JVI.00616-10

Foty, R. (2011). A simple hanging drop cell culture protocol for generation of 3D spheroids. *JoVE (Journal of Visualized Experiments)*(51), e2720.

Fraser, C. S., & Doudna, J. A. (2007). Structural and mechanistic insights into hepatitis C viral translation initiation. *Nat Rev Microbiol*, *5*(1), 29-38. https://doi.org/10.1038/nrmicro1558

Freitas, A. I., Domingues, L., & Aguiar, T. Q. (2022). Tag-mediated single-step purification and immobilization of recombinant proteins toward protein-engineered advanced materials. *J Adv Res*, *36*, 249-264. https://doi.org/10.1016/j.jare.2021.06.010

Friedman, S. L. (2008). Hepatic stellate cells: protean, multifunctional, and enigmatic cells of the liver. *Physiological reviews*, *88*(1), 125-172.

Friedman, S. L., & Arthur, M. (1989). Activation of cultured rat hepatic lipocytes by Kupffer cell conditioned medium. Direct enhancement of matrix synthesis and stimulation of cell proliferation via induction of platelet-derived growth factor receptors. *The Journal of clinical investigation*, *84*(6), 1780-1785.

Fukushi, S., Katayama, K., Kurihara, C., Ishiyama, N., Hoshino, F. B., Ando, T., & Oya, A. (1994). Complete 5' noncoding region is necessary for the efficient internal initiation of hepatitis C virus RNA. *Biochem Biophys Res Commun*, *199*(2), 425-432. https://doi.org/10.1006/bbrc.1994.1246

Gaca, M., Georges, P., Hui, J., Janmey, P., & Wells, R. (2005). The role of matrix stiffness in hepatic stellate cell activation and liver fibrosis. *Wound Repair and Regeneration*, *13*(1), A24-A24.

Gamkrelidze, I., Pawlotsky, J. M., Lazarus, J. V., Feld, J. J., Zeuzem, S., Bao, Y., . . . Razavi, H. (2021). Progress towards hepatitis C virus elimination in high-income countries: An updated analysis. *Liver Int*, *41*(3), 456-463. https://doi.org/10.1111/liv.14779

Gane, E., Pianko, S., Roberts, S., Thompson, A., Zeuzem, S., Zuckerman, E., . . . Laursen, A. (2015). Phase 2, Randomized, Open-Label Clinical Trials of the Efficacy and Safety of Grazoprevir and MK-3682 (NS5B Polymerase Inhibitor) with Either Elbasvir or MK-8408 (NS5A Inhibitor) in Patients with Chronic HCV GT1, 2 or 3 Infection (Part A of C-CREST-1 & 2): LB-15. *Hepatology*, *62*(6).

Gao, C. C., Bai, J., Han, H., & Qin, H. Y. (2022). The versatility of macrophage heterogeneity in liver fibrosis. *Front Immunol*, *13*, 968879. https://doi.org/10.3389/fimmu.2022.968879

Garaigorta, U., & Chisari, F. V. (2009). Hepatitis C virus blocks interferon effector function by inducing protein kinase R phosphorylation. *Cell Host Microbe*, *6*(6), 513-522. https://doi.org/10.1016/j.chom.2009.11.004

Gastaminza, P., Cheng, G., Wieland, S., Zhong, J., Liao, W., & Chisari, F. V. (2008). Cellular determinants of hepatitis C virus assembly, maturation, degradation, and secretion. *J Virol*, *82*(5), 2120-2129. https://doi.org/10.1128/JVI.02053-07

Geerts, A., Vrijsen, R., Rauterberg, J., Burt, A., Schellinck, P., & Wisse, E. (1989). In vitro differentiation of fat-storing cells parallels marked increase of collagen synthesis and secretion. *Journal of hepatology*, *9*(1), 59-68.

Gharaati-Far, N., Tohidkia, M. R., Dehnad, A., & Omidi, Y. (2018). Efficiency and cytotoxicity analysis of cationic lipids-mediated gene transfection into AGS gastric cancer cells. *Artif Cells Nanomed Biotechnol*, *46*(5), 1001-1008. https://doi.org/10.1080/21691401.2017.1355311

Gijbels, E., Vanhaecke, T., & Vinken, M. (2019). Establishment of Sandwich Cultures of Primary Human Hepatocytes. *Methods Mol Biol*, *1981*, 325-333. https://doi.org/10.1007/978-1-4939-9420-5_21

Gong, G. Z., Cao, J., Jiang, Y. F., Zhou, Y., & Liu, B. (2007). Hepatitis C virus non-structural 5A abrogates signal transducer and activator of transcription-1 nuclear translocation induced by IFN-alpha through dephosphorylation. *World J Gastroenterol*, *13*(30), 4080-4084. https://doi.org/10.3748/wjg.v13.i30.4080

González-Motos, V., Jürgens, C., Ritter, B., Kropp, K. A., Durán, V., Larsen, O., . . . Jonjic, S. (2017). Varicella zoster virus glycoprotein C increases chemokine-mediated leukocyte migration. *PLoS pathogens*, *13*(5), e1006346.

Goonawardane, N., Gebhardt, A., Bartlett, C., Pichlmair, A., & Harris, M. (2017). Phosphorylation of Serine 225 in Hepatitis C Virus NS5A Regulates Protein-Protein Interactions. *J Virol*, *91*(17). https://doi.org/10.1128/JVI.00805-17

Gottwein, J. M., Scheel, T. K., Callendret, B., Li, Y. P., Eccleston, H. B., Engle, R. E., . . . Bukh, J. (2010). Novel infectious cDNA clones of hepatitis C virus genotype 3a (strain S52) and 4a (strain ED43): genetic analyses and in vivo pathogenesis studies. *J Virol*, *84*(10), 5277-5293. https://doi.org/10.1128/JVI.02667-09

Greenspan, H. P. (1972). Models for the growth of a solid tumor by diffusion. *Studies in Applied Mathematics*, *51*(4), 317-340.

Guo, M., Ye, L., Yu, T., Han, L., Li, Q., Lou, P., . . . Meng, G. (2020). IL-1β enhances the antiviral effect of IFN-α on HCV replication by negatively modulating ERK2 activation. *ACS Infectious Diseases*, *6*(7), 1708-1718.

Guvendiren, M., Perepelyuk, M., Wells, R. G., & Burdick, J. A. (2014). Hydrogels with differential and patterned mechanics to study stiffness-mediated

myofibroblastic differentiation of hepatic stellate cells. *J Mech Behav Biomed Mater*, *38*, 198-208. https://doi.org/10.1016/j.jmbbm.2013.11.008

Hadziyannis, S. J., Sette, H., Morgan, T. R., Balan, V., Diago, M., Marcellin, P., . . . Group, P. I. S. (2004). Peginterferon-alpha2a and ribavirin combination therapy in chronic hepatitis C: a randomized study of treatment duration and ribavirin dose. *Ann Intern Med*, *140*(5), 346-355. https://doi.org/10.7326/0003-4819-140-5-200403020-00010

Haid, S., Windisch, M. P., Bartenschlager, R., & Pietschmann, T. (2010). Mouse-specific residues of claudin-1 limit hepatitis C virus genotype 2a infection in a human hepatocyte cell line. *Journal of virology*, *84*(2), 964-975.

Han, H. (2018). RNA Interference to Knock Down Gene Expression. *Methods Mol Biol*, *1706*, 293-302. https://doi.org/10.1007/978-1-4939-7471-9_16

Hanoulle, X., Verdegem, D., Badillo, A., Wieruszeski, J. M., Penin, F., & Lippens, G. (2009). Domain 3 of non-structural protein 5A from hepatitis C virus is natively unfolded. *Biochem Biophys Res Commun*, *381*(4), 634-638. https://doi.org/10.1016/j.bbrc.2009.02.108

Hao, Y., Song, K., Tan, X., Ren, L., Guo, X., Zhou, C., . . . Zheng, W. (2022). Reactive Oxygen Species-Responsive Polypeptide Drug Delivery System Targeted Activated Hepatic Stellate Cells to Ameliorate Liver Fibrosis. *ACS Nano*, *16*(12), 20739-20757. https://doi.org/10.1021/acsnano.2c07796

Harrison, S. P., Baumgarten, S. F., Verma, R., Lunov, O., Dejneka, A., & Sullivan, G. J. (2021). Liver organoids: Recent developments, limitations and potential. *Frontiers in medicine*, *8*, 574047.

Hauri, A. M., Armstrong, G. L., & Hutin, Y. J. (2004). The global burden of disease attributable to contaminated injections given in health care settings. *Int J STD AIDS*, *15*(1), 7-16. https://doi.org/10.1258/095646204322637182

He, Y., Sun, M. M., Zhang, G. G., Yang, J., Chen, K. S., Xu, W. W., & Li, B. (2021). Targeting PI3K/Akt signal transduction for cancer therapy. *Signal Transduct Target Ther*, *6*(1), 425. https://doi.org/10.1038/s41392-021-00828-5

Heim, R., Cubitt, A. B., & Tsien, R. Y. (1995). Improved green fluorescence. *Nature*, *373*(6516), 663-664. https://doi.org/10.1038/373663b0

Hemmann, S., Graf, J., Roderfeld, M., & Roeb, E. (2007). Expression of MMPs and TIMPs in liver fibrosis–a systematic review with special emphasis on anti-fibrotic strategies. *Journal of hepatology*, *46*(5), 955-975.

Herker, E., Harris, C., Hernandez, C., Carpentier, A., Kaehlcke, K., Rosenberg, A. R., . . . Ott, M. (2010). Efficient hepatitis C virus particle formation requires diacylglycerol acyltransferase-1. *Nat Med*, *16*(11), 1295-1298. https://doi.org/10.1038/nm.2238

Heslop, J. A., Rowe, C., Walsh, J., Sison-Young, R., Jenkins, R., Kamalian, L., . . . Kevin Park, B. (2017). Mechanistic evaluation of primary human hepatocyte culture using global proteomic analysis reveals a selective dedifferentiation profile. *Arch Toxicol*, *91*(1), 439-452. https://doi.org/10.1007/s00204-016-1694-y

Horst, A. K., Neumann, K., Diehl, L., & Tiegs, G. (2016). Modulation of liver tolerance by conventional and nonconventional antigen-presenting cells and regulatory immune cells. *Cellular & molecular immunology*, *13*(3), 277-292.

Huang, X., Cai, H., Ammar, R., Zhang, Y., Wang, Y., Ravi, K., . . . Jarai, G. (2019). Molecular characterization of a precision-cut rat liver slice model for the evaluation of antifibrotic compounds. *Am J Physiol Gastrointest Liver Physiol*, *316*(1), G15-G24. https://doi.org/10.1152/ajpgi.00281.2018

Hughes, M., Griffin, S., & Harris, M. (2009). Domain III of NS5A contributes to both RNA replication and assembly of hepatitis C virus particles. *J Gen Virol*, *90*(Pt 6), 1329-1334. https://doi.org/10.1099/vir.0.009332-0

Hunt, M. A., Currie, M. J., Robinson, B. A., & Dachs, G. U. (2010). Optimizing transfection of primary human umbilical vein endothelial cells using commercially available chemical transfection reagents. *J Biomol Tech*, *21*(2), 66-72.

Hunyady, B., Kovács, B., & Battyáni, Z. (2011). [Side-effects of pegylated interferon plus ribavirin therapy with or without protease inhibitor direct acting antiviral agents during treatment of chronic hepatitis C virus infection]. *Orv Hetil*, *152*(50), 1997-2009. https://doi.org/10.1556/OH.2011.29266

Ibrahim, I. M., Abdelmalek, D. H., & Elfiky, A. A. (2019). GRP78: A cell's response to stress. *Life Sci*, *226*, 156-163. https://doi.org/10.1016/j.lfs.2019.04.022

Ignat, S. R., Dinescu, S., Hermenean, A., & Costache, M. (2020). Cellular Interplay as a Consequence of Inflammatory Signals Leading to Liver Fibrosis Development. *Cells*, *9*(2). https://doi.org/10.3390/cells9020461

Ingiliz, P., Martin, T. C., Rodger, A., Stellbrink, H. J., Mauss, S., Boesecke, C., . . . group, N. s. (2017). HCV reinfection incidence and spontaneous clearance rates in HIV-positive men who have sex with men in Western Europe. *J Hepatol*, *66*(2), 282-287. https://doi.org/10.1016/j.jhep.2016.09.004

Jackel-Cram, C., Babiuk, L. A., & Liu, Q. (2007). Up-regulation of fatty acid synthase promoter by hepatitis C virus core protein: genotype-3a core has a stronger effect than genotype-1b core. *J Hepatol*, *46*(6), 999-1008. https://doi.org/10.1016/j.jhep.2006.10.019

Jacobson, I. M., Gordon, S. C., Kowdley, K. V., Yoshida, E. M., Rodriguez-Torres, M., Sulkowski, M. S., . . . Study, F. (2013). Sofosbuvir for hepatitis C genotype 2 or 3 in patients without treatment options. *N Engl J Med*, *368*(20), 1867-1877. https://doi.org/10.1056/NEJMoa1214854

Jensen, P., Patel, B., Smith, S., Sabnis, R., & Kaboord, B. (2021). Improved Immunoprecipitation to Mass Spectrometry Method for the Enrichment of Low-Abundant Protein Targets. *Methods Mol Biol*, *2261*, 229-246. https://doi.org/10.1007/978-1-0716-1186-9_14

Jhaveri, R., McHutchison, J., Patel, K., Qiang, G., & Diehl, A. M. (2008). Specific polymorphisms in hepatitis C virus genotype 3 core protein associated with intracellular lipid accumulation. *J Infect Dis*, *197*(2), 283-291. https://doi.org/10.1086/524846

Ji, Q., Chang, L., VanDenBerg, D., Stanczyk, F. Z., & Stolz, A. (2003). Selective reduction of AKR1C2 in prostate cancer and its role in DHT metabolism. *Prostate*, *54*(4), 275-289. https://doi.org/10.1002/pros.10192

Jiang, J., & Luo, G. (2009). Apolipoprotein E but not B is required for the formation of infectious hepatitis C virus particles. *J Virol*, *83*(24), 12680-12691. https://doi.org/10.1128/JVI.01476-09

Jiang, X., Kanda, T., Wu, S., Nakamoto, S., Wakita, T., Shirasawa, H., & Yokosuka, O. (2014). Hepatitis C virus nonstructural protein 5A inhibits thapsigargin-induced apoptosis. *PLoS One*, *9*(11), e113499. https://doi.org/10.1371/journal.pone.0113499

Kale, J., Osterlund, E. J., & Andrews, D. W. (2018). BCL-2 family proteins: changing partners in the dance towards death. *Cell Death Differ*, *25*(1), 65-80. https://doi.org/10.1038/cdd.2017.186

Kang, H. E., Malinen, M. M., Saran, C., Honkakoski, P., & Brouwer, K. L. R. (2019). Optimization of Canalicular ABC Transporter Function in HuH-7 Cells by Modification of Culture Conditions. *Drug Metab Dispos*, *47*(10), 1222-1230. https://doi.org/10.1124/dmd.119.087676

Kanwal, F., Kramer, J. R., Ilyas, J., Duan, Z., & El-Serag, H. B. (2014). HCV genotype 3 is associated with an increased risk of cirrhosis and hepatocellular cancer in a national sample of U.S. Veterans with HCV. *Hepatology*, *60*(1), 98-105. https://doi.org/10.1002/hep.27095

Kanzler, S., Baumann, M., Schirmacher, P., Dries, V., Bayer, E., Gerken, G., . . . Lohse, A. (2001). Prediction of progressive liver fibrosis in hepatitis C infection by serum and tissue levels of transforming growth factor-β. *Journal of viral hepatitis*, *8*(6), 430-437.

Kartasheva-Ebertz, D., Gaston, J., Lair-Mehiri, L., Massault, P. P., Scatton, O., Vaillant, J. C., . . . Lagaye, S. (2021). Adult human liver slice cultures: Modelling of liver fibrosis and evaluation of new anti-fibrotic drugs. *World J Hepatol*, *13*(2), 187-217. https://doi.org/10.4254/wjh.v13.i2.187

Kato, T., Date, T., Miyamoto, M., Furusaka, A., Tokushige, K., Mizokami, M., & Wakita, T. (2003). Efficient replication of the genotype 2a hepatitis C virus subgenomic

replicon. *Gastroenterology*, *125*(6), 1808-1817. https://doi.org/10.1053/j.gastro.2003.09.023

Katoh, M., & Katoh, M. (2006). Cross-talk of WNT and FGF signaling pathways at GSK3ß to regulate ß-catenin and SNAIL signaling cascades. *Cancer biology & therapy*, *5*(9), 1059-1064.

Keeble, A. H., Turkki, P., Stokes, S., Khairil Anuar, I. N. A., Rahikainen, R., Hytönen, V. P., & Howarth, M. (2019). Approaching infinite affinity through engineering of peptide-protein interaction. *Proc Natl Acad Sci U S A*, *116*(52), 26523-26533. https://doi.org/10.1073/pnas.1909653116

Keikha, M., Eslami, M., Yousefi, B., Ali-Hassanzadeh, M., Kamali, A., Yousefi, M., & Karbalaei, M. (2020). HCV genotypes and their determinative role in hepatitis C treatment. *Virusdisease*, *31*(3), 235-240. https://doi.org/10.1007/s13337-020-00592-0

Kelly, L., Badhan, A., Roberts, G. C., Mbisa, J. L., & Harris, M. (2017). Manipulation of both virus- and cell-specific factors is required for robust transient replication of a hepatitis C virus genotype 3a sub-genomic replicon. *J Gen Virol*, *98*(10), 2495-2506. https://doi.org/10.1099/jgv.0.000932

Kim, J. B., Lee, S., Kim, H. R., Park, S. Y., Lee, M., Yoon, J. H., & Kim, Y. J. (2018). Transforming growth factor-β decreases side population cells in hepatocellular carcinoma in vitro. *Oncology Letters*, *15*(6), 8723-8728.

Kim, J. H., Lee, C. H., & Lee, S.-W. (2016). Hepatitis C virus infection stimulates transforming growth factor-β1 expression through up-regulating miR-192. *Journal of Microbiology*, *54*, 520-526.

Kim, J. Y., Wang, L., Lee, J., & Ou, J. J. (2017). Hepatitis C Virus Induces the Localization of Lipid Rafts to Autophagosomes for Its RNA Replication. *J Virol*, *91*(20). https://doi.org/10.1128/JVI.00541-17

Kim, S., Date, T., Yokokawa, H., Kono, T., Aizaki, H., Maurel, P., . . . Wakita, T. (2014). Development of hepatitis C virus genotype 3a cell culture system. *Hepatology*, *60*(6), 1838-1850. https://doi.org/10.1002/hep.27197

Kish, T., Aziz, A., & Sorio, M. (2017). Hepatitis C in a New Era: A Review of Current Therapies. *P T*, *42*(5), 316-329.

Knobler, H., & Schattner, A. (2005). TNF-{alpha}, chronic hepatitis C and diabetes: a novel triad. *QJM*, *98*(1), 1-6. https://doi.org/10.1093/qjmed/hci001

Koch, A., Saran, S., Tran, D. D., Klebba-Färber, S., Thiesler, H., Sewald, K., . . . Tamura, T. (2014). Murine precision-cut liver slices (PCLS): a new tool for studying tumor microenvironments and cell signaling ex vivo. *Cell Commun Signal*, *12*, 73. https://doi.org/10.1186/s12964-014-0073-7

Kollmann, D., & Selzner, M. (2017). Recent advances in the field of warm ex-vivo liver perfusion. *Curr Opin Organ Transplant*, *22*(6), 555-562. https://doi.org/10.1097/MOT.0000000000000471

Kouroupis, D., & Correa, D. (2021). Increased mesenchymal stem cell functionalization in three-dimensional manufacturing settings for enhanced therapeutic applications. *Frontiers in bioengineering and biotechnology*, *9*, 621748.

Kowdley, K. V., Gordon, S. C., Reddy, K. R., Rossaro, L., Bernstein, D. E., Lawitz, E., . . . Ryan, M. (2014). Ledipasvir and sofosbuvir for 8 or 12 weeks for chronic HCV without cirrhosis. *New England Journal of Medicine*, *370*(20), 1879-1888.

Kramer, E. D., Tzetzo, S. L., Colligan, S. H., Hensen, M. L., Brackett, C. M., Clausen, B. E., . . . Abrams, S. I. (2023). β-Catenin signaling in alveolar macrophages enhances lung metastasis through a TNF-dependent mechanism. *JCI insight*, *8*(8).

Kumthip, K., Chusri, P., Jilg, N., Zhao, L., Fusco, D. N., Zhao, H., . . . Lin, W. (2012). Hepatitis C virus NS5A disrupts STAT1 phosphorylation and suppresses type I interferon signaling. *J Virol*, *86*(16), 8581-8591. https://doi.org/10.1128/JVI.00533-12

Lacalle, D., Castro-Abril, H. A., Randelovic, T., Domínguez, C., Heras, J., Mata, E., . . . Ochoa, I. (2021). Spheroidj: An open-source set of tools for spheroid segmentation. *Computer methods and programs in biomedicine*, *200*, 105837.

Lachowski, D., Cortes, E., Rice, A., Pinato, D., Rombouts, K., & Del Rio Hernandez, A. (2019). Matrix stiffness modulates the activity of MMP-9 and TIMP-1 in hepatic stellate cells to perpetuate fibrosis. *Sci Rep*, *9*(1), 7299. https://doi.org/10.1038/s41598-019-43759-6

Lagaye, S., Brun, S., Gaston, J., Shen, H., Stranska, R., Camus, C., . . . Pol, S. (2016). Anti-hepatitis C virus potency of a new autophagy inhibitor using human liver slices model. *World J Hepatol*, *8*(21), 902-914. https://doi.org/10.4254/wjh.v8.i21.902

Lagaye, S., Shen, H., Saunier, B., Nascimbeni, M., Gaston, J., Bourdoncle, P., . . . Mallet, V. (2012). Efficient replication of primary or culture hepatitis C virus isolates in human liver slices: a relevant ex vivo model of liver infection. *Hepatology*, *56*(3), 861-872.

Lan, K. H., Lan, K. L., Lee, W. P., Sheu, M. L., Chen, M. Y., Lee, Y. L., . . . Lee, S. D. (2007). HCV NS5A inhibits interferon-alpha signaling through suppression of STAT1 phosphorylation in hepatocyte-derived cell lines. *J Hepatol*, *46*(5), 759-767. https://doi.org/10.1016/j.jhep.2006.11.013

Lange, C. M., Jacobson, I. M., Rice, C. M., & Zeuzem, S. (2014). Emerging therapies for the treatment of hepatitis C. *EMBO Mol Med*, *6*(1), 4-15. https://doi.org/10.1002/emmm.201303131

Larrea, E., Aldabe, R., Molano, E., Fernandez-Rodriguez, C. M., Ametzazurra, A., Civeira, M. P., & Prieto, J. (2006). Altered expression and activation of signal transducers and activators of transcription (STATs) in hepatitis C virus infection: in vivo and in vitro studies. *Gut*, *55*(8), 1188-1196.

Latronico, T., Mascia, C., Pati, I., Zuccala, P., Mengoni, F., Marocco, R., . . . Vullo, V. (2016). Liver fibrosis in HCV monoinfected and HIV/HCV coinfected patients: Dysregulation of matrix metalloproteinases (MMPs) and their tissue inhibitors TIMPs and effect of HCV protease inhibitors. *International journal of molecular sciences*, *17*(4), 455.

Lawitz, E., Sulkowski, M. S., Ghalib, R., Rodriguez-Torres, M., Younossi, Z. M., Corregidor, A., . . . Gitlin, N. (2014). Simeprevir plus sofosbuvir, with or without ribavirin, to treat chronic infection with hepatitis C virus genotype 1 in non-responders to pegylated interferon and ribavirin and treatment-naive patients: the COSMOS randomised study. *The Lancet*, *384*(9956), 1756-1765.

Lee, B. H., Kim, M. H., Lee, J. H., Seliktar, D., Cho, N.-J., & Tan, L. P. (2015). Modulation of Huh7. 5 spheroid formation and functionality using modified PEG-based hydrogels of different stiffness. *PloS one*, *10*(2), e0118123.

Lee, J., Tian, Y., Chan, S. T., Kim, J. Y., Cho, C., & Ou, J.-h. J. (2015). TNF-α induced by hepatitis C virus via TLR7 and TLR8 in hepatocytes supports interferon signaling via an autocrine mechanism. *PLoS pathogens*, *11*(5), e1004937.

Lee, K. Y., Chen, Y. H., Hsu, S. C., & Yu, M. J. (2016). Phosphorylation of Serine 235 of the Hepatitis C Virus Non-Structural Protein NS5A by Multiple Kinases. *PLoS One*, *11*(11), e0166763. https://doi.org/10.1371/journal.pone.0166763

Lee, S., Choi, E. J., Cho, E. J., Lee, Y. B., Lee, J. H., Yu, S. J., . . . Kim, Y. J. (2020). Inhibition of PI3K/Akt signaling suppresses epithelial-to-mesenchymal transition in hepatocellular carcinoma through the Snail/GSK-3/beta-catenin pathway. *Clin Mol Hepatol*, *26*(4), 529-539. https://doi.org/10.3350/cmh.2019.0056n

Lee, S. S., Kim, C. Y., Kim, B. R., Cha, R. R., Kim, W. S., Kim, J. J., . . . Lee, O. J. (2019). Hepatitis C virus genotype 3 was associated with the development of hepatocellular carcinoma in Korea. *J Viral Hepat*, *26*(4), 459-465. https://doi.org/10.1111/jvh.13047

Lee, Y. A., Wallace, M. C., & Friedman, S. L. (2015). Pathobiology of liver fibrosis: a translational success story. *Gut*, *64*(5), 830-841. https://doi.org/10.1136/gutjnl-2014-306842

Lemon, B., & Tjian, R. (2000). Orchestrated response: a symphony of transcription factors for gene control. *Genes & development*, *14*(20), 2551-2569.

Lengler, J., Holzmüller, H., Salmons, B., Günzburg, W. H., & Renner, M. (2005). FMDV-2A sequence and protein arrangement contribute to functionality of CYP2B1-

reporter fusion protein. *Anal Biochem*, *343*(1), 116-124. https://doi.org/10.1016/j.ab.2005.05.004

Lewis, J. E., Brameld, J. M., Hill, P., Barrett, P., Ebling, F. J., & Jethwa, P. H. (2015). The use of a viral 2A sequence for the simultaneous over-expression of both the vgf gene and enhanced green fluorescent protein (eGFP) in vitro and in vivo. *J Neurosci Methods*, *256*, 22-29. https://doi.org/10.1016/j.jneumeth.2015.08.013

Li, C., Wu, X., Zhang, W., Li, J., Liu, H., Hao, M., . . . Zheng, J. (2014). AEG-1 Promotes Metastasis Through Downstream AKR1C2 and NF1 in Liver Cancer. *Oncol Res*, *22*(4), 203-211. https://doi.org/10.3727/096504015X14386062091352

Li, C., Wu, X., Zhang, W., Li, J., Liu, H., Hao, M., . . . Zheng, J. (2016). High-Content Functional Screening of AEG-1 and AKR1C2 for the Promotion of Metastasis in Liver Cancer. *J Biomol Screen*, *21*(1), 101-107. https://doi.org/10.1177/1087057115603310

Li, H., Huang, M. H., Jiang, J. D., & Peng, Z. G. (2018). Hepatitis C: From inflammatory pathogenesis to anti-inflammatory/hepatoprotective therapy. *World J Gastroenterol*, *24*(47), 5297-5311. https://doi.org/10.3748/wjg.v24.i47.5297

Li, H. C., Yang, C. H., & Lo, S. Y. (2021). Cellular factors involved in the hepatitis C virus life cycle. *World J Gastroenterol*, *27*(28), 4555-4581. https://doi.org/10.3748/wjg.v27.i28.4555

Li, K., Li, N. L., Wei, D., Pfeffer, S. R., Fan, M., & Pfeffer, L. M. (2012). Activation of chemokine and inflammatory cytokine response in hepatitis C virus–infected hepatocytes depends on toll-like receptor 3 sensing of hepatitis C virus double-stranded RNA intermediates. *Hepatology*, *55*(3), 666-675.

Li, L., Zheng, Y.-L., Jiang, C., Fang, S., Zeng, T.-T., Zhu, Y.-H., . . . Guan, X.-Y. (2019). HN1L-mediated transcriptional axis AP-2γ/METTL13/TCF3-ZEB1 drives tumor growth and metastasis in hepatocellular carcinoma. *Cell Death & Differentiation*, *26*(11), 2268-2283.

Li, L. Y., Yang, C. C., Yang, J. F., Li, H. D., Zhang, B. Y., Zhou, H., . . . Xu, T. (2019). ZEB1 regulates the activation of hepatic stellate cells through Wnt/β-catenin signaling pathway. *Eur J Pharmacol*, *865*, 172787. https://doi.org/10.1016/j.ejphar.2019.172787

Li, W., Hou, G., Zhou, D., Lou, X., Xu, Y., Liu, S., & Zhao, X. (2016). The roles of AKR1C1 and AKR1C2 in ethyl-3,4-dihydroxybenzoate induced esophageal squamous cell carcinoma cell death. *Oncotarget*, *7*(16), 21542-21555. https://doi.org/10.18632/oncotarget.7775

Li, Y. P., Ramirez, S., Gottwein, J. M., Scheel, T. K., Mikkelsen, L., Purcell, R. H., & Bukh, J. (2012). Robust full-length hepatitis C virus genotype 2a and 2b infectious cultures using mutations identified by a systematic approach applicable to

patient strains. *Proc Natl Acad Sci U S A*, *109*(18), E1101-1110. https://doi.org/10.1073/pnas.1203829109

Li, Y. P., Ramirez, S., Mikkelsen, L., & Bukh, J. (2015). Efficient infectious cell culture systems of the hepatitis C virus (HCV) prototype strains HCV-1 and H77. *J Virol*, *89*(1), 811-823. https://doi.org/10.1128/JVI.02877-14

Liang, Y., Shilagard, T., Xiao, S. Y., Snyder, N., Lau, D., Cicalese, L., . . . Lemon, S. M. (2009). Visualizing hepatitis C virus infections in human liver by two-photon microscopy. *Gastroenterology*, *137*(4), 1448-1458. https://doi.org/10.1053/j.gastro.2009.07.050

Lichtinghagen, R., Michels, D., Haberkorn, C. I., Arndt, B., Bahr, M., Flemming, P., . . . Boeker, K. H. (2001). Matrix metalloproteinase (MMP)-2, MMP-7, and tissue inhibitor of metalloproteinase-1 are closely related to the fibroproliferative process in the liver during chronic hepatitis C. *J Hepatol*, *34*(2), 239-247. https://doi.org/10.1016/s0168-8278(00)00037-4

Lickteig, A. J., Zhang, Y., Klaassen, C. D., & Csanaky, I. L. (2019). Effects of Absence of Constitutive Androstane Receptor (CAR) on Bile Acid Homeostasis in Male and Female Mice. *Toxicol Sci*, *171*(1), 132-145. https://doi.org/10.1093/toxsci/kfz143

Lin, W., Choe, W. H., Hiasa, Y., Kamegaya, Y., Blackard, J. T., Schmidt, E. V., & Chung, R. T. (2005). Hepatitis C virus expression suppresses interferon signaling by degrading STAT1. *Gastroenterology*, *128*(4), 1034-1041.

Lin, W., Tsai, W. L., Shao, R. X., Wu, G., Peng, L. F., Barlow, L. L., . . . Chung, R. T. (2010). Hepatitis C virus regulates transforming growth factor beta1 production through the generation of reactive oxygen species in a nuclear factor kappaB-dependent manner. *Gastroenterology*, *138*(7), 2509-2518, 2518.e2501. https://doi.org/10.1053/j.gastro.2010.03.008

Lin, W., Weinberg, E. M., & Chung, R. T. (2013). Pathogenesis of accelerated fibrosis in HIV/HCV co-infection. *The Journal of infectious diseases*, *207*(suppl_1), S13-S18.

Lin, W., Wu, G., Li, S., Weinberg, E. M., Kumthip, K., Peng, L. F., . . . Chung, R. T. (2011). HIV and HCV cooperatively promote hepatic fibrogenesis via induction of reactive oxygen species and NFkappaB. *J Biol Chem*, *286*(4), 2665-2674. https://doi.org/10.1074/jbc.M110.168286

Lindenbach, B. D., Evans, M. J., Syder, A. J., Wölk, B., Tellinghuisen, T. L., Liu, C. C., . . . Rice, C. M. (2005). Complete replication of hepatitis C virus in cell culture. *Science*, *309*(5734), 623-626. https://doi.org/10.1126/science.1114016

Lindenbach, B. D., Meuleman, P., Ploss, A., Vanwolleghem, T., Syder, A. J., McKeating, J. A., . . . Rice, C. M. (2006). Cell culture-grown hepatitis C virus is infectious in vivo and can be recultured in vitro. *Proc Natl Acad Sci U S A*, *103*(10), 3805-3809. https://doi.org/10.1073/pnas.0511218103

Liu, X. Y., Liu, R. X., Hou, F., Cui, L. J., Li, C. Y., Chi, C., . . . Yin, C. H. (2016). Fibronectin expression is critical for liver fibrogenesis in vivo and in vitro. *Mol Med Rep*, *14*(4), 3669-3675. https://doi.org/10.3892/mmr.2016.5673

Liu, Z., Chen, O., Wall, J. B. J., Zheng, M., Zhou, Y., Wang, L., . . . Liu, J. (2017). Systematic comparison of 2A peptides for cloning multi-genes in a polycistronic vector. *Sci Rep*, *7*(1), 2193. https://doi.org/10.1038/s41598-017-02460-2

Liver, E. A. f. t. S. o. t. (2011). EASL Clinical Practice Guidelines: management of hepatitis C virus infection. *J Hepatol*, *55*(2), 245-264. https://doi.org/10.1016/j.jhep.2011.02.023

Lohmann, V., Körner, F., Koch, J., Herian, U., Theilmann, L., & Bartenschlager, R. (1999). Replication of subgenomic hepatitis C virus RNAs in a hepatoma cell line. *Science*, *285*(5424), 110-113. https://doi.org/10.1126/science.285.5424.110

Loo, Y.-M., Owen, D. M., Li, K., Erickson, A. K., Johnson, C. L., Fish, P. M., . . . Yoneyama, M. (2006). Viral and therapeutic control of IFN-β promoter stimulator 1 during hepatitis C virus infection. *Proceedings of the National Academy of Sciences*, *103*(15), 6001-6006.

Luna-Cuadros, M. A., Chen, H. W., Hanif, H., Ali, M. J., Khan, M. M., & Lau, D. T. (2022). Risk of hepatocellular carcinoma after hepatitis C virus cure. *World J Gastroenterol*, *28*(1), 96-107. https://doi.org/10.3748/wjg.v28.i1.96

Lussignol, M., Kopp, M., Molloy, K., Vizcay-Barrena, G., Fleck, R. A., Dorner, M., . . . Catanese, M. T. (2016). Proteomics of HCV virions reveals an essential role for the nucleoporin Nup98 in virus morphogenesis. *Proc Natl Acad Sci U S A*, *113*(9), 2484-2489. https://doi.org/10.1073/pnas.1518934113

Macdonald, A., Crowder, K., Street, A., McCormick, C., Saksela, K., & Harris, M. (2003). The hepatitis C virus non-structural NS5A protein inhibits activating protein-1 function by perturbing ras-ERK pathway signaling. *J Biol Chem*, *278*(20), 17775-17784. https://doi.org/10.1074/jbc.M210900200

Macdonald, A., & Harris, M. (2004). Hepatitis C virus NS5A: tales of a promiscuous protein. *J Gen Virol*, *85*(Pt 9), 2485-2502. https://doi.org/10.1099/vir.0.80204-0

Mackay, A. M., Beck, S. C., Murphy, J. M., Barry, F. P., Chichester, C. O., & Pittenger, M. F. (1998). Chondrogenic differentiation of cultured human mesenchymal stem cells from marrow. *Tissue engineering*, *4*(4), 415-428.

Mandal, P., Pritchard, M. T., & Nagy, L. E. (2010). Anti-inflammatory pathways and alcoholic liver disease: role of an adiponectin/interleukin-10/heme oxygenase-1 pathway. *World J Gastroenterol*, *16*(11), 1330-1336. https://doi.org/10.3748/wjg.v16.i11.1330

Manns, M. P., & Maasoumy, B. (2022). Breakthroughs in hepatitis C research: from discovery to cure. *Nat Rev Gastroenterol Hepatol*, *19*(8), 533-550. https://doi.org/10.1038/s41575-022-00608-8

Mark, C., Grundy, T. J., Strissel, P. L., Böhringer, D., Grummel, N., Gerum, R., . . . Eckstein, M. (2020). Collective forces of tumor spheroids in three-dimensional biopolymer networks. *Elife*, *9*, e51912.

Marrero, J. A., Kulik, L. M., Sirlin, C. B., Zhu, A. X., Finn, R. S., Abecassis, M. M., . . . Heimbach, J. K. (2018). Diagnosis, Staging, and Management of Hepatocellular Carcinoma: 2018 Practice Guidance by the American Association for the Study of Liver Diseases. *Hepatology*, *68*(2), 723-750. https://doi.org/10.1002/hep.29913

Matthiesen, R., & Bunkenborg, J. (2013). Introduction to mass spectrometry-based proteomics. *Methods Mol Biol*, *1007*, 1-45. https://doi.org/10.1007/978-1-62703-392-3_1

McCormick, C. J., Maucourant, S., Griffin, S., Rowlands, D. J., & Harris, M. (2006). Tagging of NS5A expressed from a functional hepatitis C virus replicon. *J Gen Virol*, *87*(Pt 3), 635-640. https://doi.org/10.1099/vir.0.81553-0

McGivern, D. R., & Lemon, S. M. (2011). Virus-specific mechanisms of carcinogenesis in hepatitis C virus associated liver cancer. *Oncogene*, *30*(17), 1969-1983. https://doi.org/10.1038/onc.2010.594

McHutchison, J. G., Blatt, L. M., de Medina, M., Craig, J. R., Conrad, A., Schiff, E. R., & Tong, M. J. (2000). Measurement of serum hyaluronic acid in patients with chronic hepatitis C and its relationship to liver histology. Consensus Interferon Study Group. *J Gastroenterol Hepatol*, *15*(8), 945-951. https://doi.org/10.1046/j.1440-1746.2000.02233.x

Mee, C. J., Farquhar, M. J., Harris, H. J., Hu, K., Ramma, W., Ahmed, A., . . . McKeating, J. A. (2010). Hepatitis C virus infection reduces hepatocellular polarity in a vascular endothelial growth factor–dependent manner. *Gastroenterology*, *138*(3), 1134-1142.

Mee, C. J., Grove, J., Harris, H. J., Hu, K., Balfe, P., & McKeating, J. A. (2008). Effect of cell polarization on hepatitis C virus entry. *Journal of virology*, *82*(1), 461-470.

Mee, C. J., Harris, H. J., Farquhar, M. J., Wilson, G., Reynolds, G., Davis, C., . . . McKeating, J. A. (2009). Polarization restricts hepatitis C virus entry into HepG2 hepatoma cells. *Journal of virology*, *83*(12), 6211-6221.

Meindl-Beinker, N. M., & Dooley, S. (2008). Transforming growth factor-β and hepatocyte transdifferentiation in liver fibrogenesis. *Journal of gastroenterology and hepatology*, *23*, S122-S127.

Meng, R., Xu, H.-y., Di, S.-m., Shi, D.-y., Qian, A.-r., Wang, J.-f., & Shang, P. (2011). Human mesenchymal stem cells are sensitive to abnormal gravity and exhibit classic apoptotic features. *Acta Biochim Biophys Sin*, *43*(2), 133-142.

Meng, Z., Liu, Q., Sun, F., & Qiao, L. (2019). Hepatitis C virus nonstructural protein 5A perturbs lipid metabolism by modulating AMPK/SREBP-1c signaling. *Lipids Health Dis*, *18*(1), 191. https://doi.org/10.1186/s12944-019-1136-y

Menzel, N., Fischl, W., Hueging, K., Bankwitz, D., Frentzen, A., Haid, S., . . . Pietschmann, T. (2012). MAP-kinase regulated cytosolic phospholipase A2 activity is essential for production of infectious hepatitis C virus particles. *PLoS Pathog*, *8*(7), e1002829. https://doi.org/10.1371/journal.ppat.1002829

Messina, J. P., Humphreys, I., Flaxman, A., Brown, A., Cooke, G. S., Pybus, O. G., & Barnes, E. (2015). Global distribution and prevalence of hepatitis C virus genotypes. *Hepatology*, *61*(1), 77-87. https://doi.org/10.1002/hep.27259

Meyers, V. E., Zayzafoon, M., Gonda, S. R., Gathings, W. E., & McDonald, J. M. (2004). Modeled microgravity disrupts collagen I/integrin signaling during osteoblastic differentiation of human mesenchymal stem cells. *Journal of cellular biochemistry*, *93*(4), 697-707.

Mily, A., Kalsum, S., Loreti, M. G., Rekha, R. S., Muvva, J. R., Lourda, M., & Brighenti, S. (2020). Polarization of M1 and M2 Human Monocyte-Derived Cells and Analysis with Flow Cytometry upon Mycobacterium tuberculosis Infection. *J Vis Exp*(163). https://doi.org/10.3791/61807

Mindnich, R. D., & Penning, T. M. (2009). Aldo-keto reductase (AKR) superfamily: genomics and annotation. *Hum Genomics*, *3*(4), 362-370. https://doi.org/10.1186/1479-7364-3-4-362

Ming-Ju, H., Yih-Shou, H., Tzy-Yen, C., & Hui-Ling, C. (2011). Hepatitis C virus E2 protein induce reactive oxygen species (ROS)-related fibrogenesis in the HSC-T6 hepatic stellate cell line. *J Cell Biochem*, *112*(1), 233-243. https://doi.org/10.1002/jcb.22926

Minskaia, E., & Ryan, M. D. (2013). Protein coexpression using FMDV 2A: effect of "linker" residues. *Biomed Res Int*, *2013*, 291730. https://doi.org/10.1155/2013/291730

Mirabelli, P., Coppola, L., & Salvatore, M. (2019). Cancer Cell Lines Are Useful Model Systems for Medical Research. *Cancers (Basel)*, *11*(8). https://doi.org/10.3390/cancers11081098

Miyanari, Y., Atsuzawa, K., Usuda, N., Watashi, K., Hishiki, T., Zayas, M., . . . Shimotohno, K. (2007). The lipid droplet is an important organelle for hepatitis C virus production. *Nature cell biology*, *9*(9), 1089-1097.

Molina-Jimenez, F., Benedicto, I., Thi, V. L. D., Gondar, V., Lavillette, D., Marin, J. J., . . . Baumert, T. F. (2012). Matrigel-embedded 3D culture of Huh-7 cells as a hepatocyte-like polarized system to study hepatitis C virus cycle. *Virology*, *425*(1), 31-39.

Moradpour, D., Evans, M. J., Gosert, R., Yuan, Z., Blum, H. E., Goff, S. P., . . . Rice, C. M. (2004). Insertion of green fluorescent protein into nonstructural protein 5A allows direct visualization of functional hepatitis C virus replication complexes. *J Virol*, *78*(14), 7400-7409. https://doi.org/10.1128/JVI.78.14.7400-7409.2004

Mori, K. I., Matsumoto, A., Maki, N., Ichikawa, Y., Tanaka, E., & Yagi, S. (2016). Production of infectious HCV genotype 1b virus in cell culture using a novel Set of adaptive mutations. *BMC Microbiol*, *16*(1), 224. https://doi.org/10.1186/s12866-016-0846-9

Moriya, K., Yotsuyanagi, H., Shintani, Y., Fujie, H., Ishibashi, K., Matsuura, Y., . . . Koike, K. (1997). Hepatitis C virus core protein induces hepatic steatosis in transgenic mice. *J Gen Virol*, *78 (Pt 7)*, 1527-1531. https://doi.org/10.1099/0022-1317-78-7-1527

Morozov, V. A., & Lagaye, S. (2018). Hepatitis C virus: Morphogenesis, infection and therapy. *World journal of hepatology*, *10*(2), 186.

Muir, A. J., Strasser, S., Wang, S., Shafran, S., Bonacini, M., Kwo, P., . . . Lin, C.-W. (2016). High SVR rates with ABT-493+ ABT-530 co-administered for 8 weeks in non-cirrhotic patients with HCV genotype 3 infection. *J Hepatol*, *64*(Suppl 2), S186.

Murphy, D. G., Sablon, E., Chamberland, J., Fournier, E., Dandavino, R., & Tremblay, C. L. (2015). Hepatitis C virus genotype 7, a new genotype originating from central Africa. *J Clin Microbiol*, *53*(3), 967-972. https://doi.org/10.1128/JCM.02831-14

Murphy, F. R., Issa, R., Zhou, X., Ratnarajah, S., Arthur, M. J., Benyon, C., . . . Nagase, H. (2002). Inhibition of apoptosis of activated hepatic stellate cells by tissue inhibitor of metalloproteinase-1 is mediated via effects on matrix metalloproteinase inhibition: implications for reversibility of liver fibrosis. *Journal of Biological Chemistry*, *277*(13), 11069-11076.

Murphy, R. J., Gunasingh, G., Haass, N. K., & Simpson, M. J. (2023). Growth and adaptation mechanisms of tumour spheroids with time-dependent oxygen availability. *PLOS Computational Biology*, *19*(1), e1010833.

Mushtaq, S., Hashmi, A. H., Khan, A., Asad Raza Kazmi, S. M., & Manzoor, S. (2022). Emergence and Persistence of Resistance-Associated Substitutions in HCV GT3 Patients Failing Direct-Acting Antivirals. *Front Pharmacol*, *13*, 894460. https://doi.org/10.3389/fphar.2022.894460

Nagaraja, T., Chen, L., Balasubramanian, A., Groopman, J. E., Ghoshal, K., Jacob, S. T., . . . Ganju, R. K. (2012). Activation of the connective tissue growth factor (CTGF)-

transforming growth factor β 1 (TGF-β 1) axis in hepatitis C virus-expressing hepatocytes.

Nagrath, D., Xu, H., Tanimura, Y., Zuo, R., Berthiaume, F., Avila, M., . . . Yarmush, M. L. (2009). Metabolic preconditioning of donor organs: defatting fatty livers by normothermic perfusion ex vivo. *Metab Eng*, *11*(4-5), 274-283. https://doi.org/10.1016/j.ymben.2009.05.005

Nakabayashi, H., Taketa, K., Miyano, K., Yamane, T., & Sato, J. (1982). Growth of human hepatoma cells lines with differentiated functions in chemically defined medium. *Cancer Res*, *42*(9), 3858-3863.

Natarajan, V., Simoneau, C. R., Erickson, A. L., Meyers, N. L., Baron, J. L., Cooper, S., . . . Ott, M. (2022). Modelling T-cell immunity against hepatitis C virus with liver organoids in a microfluidic coculture system. *Open biology*, *12*(3), 210320.

Ncube, K. N., Jurgens, T., Steenkamp, V., Cromarty, A. D., van den Bout, I., & Cordier, W. (2023). Comparative Evaluation of the Cytotoxicity of Doxorubicin in BT-20 Triple-Negative Breast Carcinoma Monolayer and Spheroid Cultures. *Biomedicines*, *11*(5), 1484.

Nelson, D. R., Cooper, J. N., Lalezari, J. P., Lawitz, E., Pockros, P. J., Gitlin, N., . . . Team, A.-S. (2015). All-oral 12-week treatment with daclatasvir plus sofosbuvir in patients with hepatitis C virus genotype 3 infection: ALLY-3 phase III study. *Hepatology*, *61*(4), 1127-1135. https://doi.org/10.1002/hep.27726

Nguyen, H., Sankaran, S., & Dandekar, S. (2006). Hepatitis C virus core protein induces expression of genes regulating immune evasion and anti-apoptosis in hepatocytes. *Virology*, *354*(1), 58-68.

NHS, N. H. S.-. (2021). *Hepatitis C virus - Treatment*. Retrieved 11th December from

Nitta, S., Sakamoto, N., Nakagawa, M., Kakinuma, S., Mishima, K., Kusano-Kitazume, A., . . . Azuma, S. (2013). Hepatitis C virus NS4B protein targets STING and abrogates RIG-I–mediated type I interferon-dependent innate immunity. *Hepatology*, *57*(1), 46-58.

Nkontchou, G., Ziol, M., Aout, M., Lhabadie, M., Baazia, Y., Mahmoudi, A., . . . Beaugrand, M. (2011). HCV genotype 3 is associated with a higher hepatocellular carcinoma incidence in patients with ongoing viral C cirrhosis. *J Viral Hepat*, *18*(10), e516-522. https://doi.org/10.1111/j.1365-2893.2011.01441.x

Noguchi, T., Satoh, S., Noshi, T., Hatada, E., Fukuda, R., Kawai, A., . . . Shimotohno, K. (2001). Effects of mutation in hepatitis C virus nonstructural protein 5A on interferon resistance mediated by inhibition of PKR kinase activity in mammalian cells. *Microbiol Immunol*, *45*(12), 829-840. https://doi.org/10.1111/j.1348-0421.2001.tb01322.x

Novin, M. G., & Nouri, M. (2007). Effect of matrigel on function and morphology of human endometrial epithelial cell in vitro. *Iran Biomed J*, *11*(2), 87-94.

Ojosnegros, S., Garcia-Arriaza, J., Escarmis, C., Manrubia, S. C., Perales, C., Arias, A., . . . Domingo, E. (2011). Viral genome segmentation can result from a trade-off between genetic content and particle stability. *PLoS genetics*, *7*(3), e1001344.

Okamoto, H., Kurai, K., Okada, S.-I., Yamamoto, K., Lizuka, H., Tanaka, T., . . . Mishiro, S. (1992). Full-length sequence of a hepatitis C virus genome having poor homology to reported isolates: comparative study of four distinct genotypes. *Virology*, *188*(1), 331-341.

Olinga, P., & Schuppan, D. (2013). Precision-cut liver slices: a tool to model the liver ex vivo. *J Hepatol*, *58*(6), 1252-1253. https://doi.org/10.1016/j.jhep.2013.01.009

Olsen, A. L., Bloomer, S. A., Chan, E. P., Gaça, M. D., Georges, P. C., Sackey, B., . . . Wells, R. G. (2011). Hepatic stellate cells require a stiff environment for myofibroblastic differentiation. *Am J Physiol Gastrointest Liver Physiol*, *301*(1), G110-118. https://doi.org/10.1152/ajpgi.00412.2010

Omura, H., Liu, F., Shimakami, T., Murai, K., Shirasaki, T., Kitabayashi, J., . . . Sumiyadorj, A. (2019). Establishment and characterization of a new cell line permissive for hepatitis C virus infection. *Scientific reports*, *9*(1), 7943.

Paish, H. L., Reed, L. H., Brown, H., Bryan, M. C., Govaere, O., Leslie, J., . . . Oakley, F. (2019). A Bioreactor Technology for Modeling Fibrosis in Human and Rodent Precision-Cut Liver Slices. *Hepatology*, *70*(4), 1377-1391. https://doi.org/10.1002/hep.30651

Palma, E., Doornebal, E. J., & Chokshi, S. (2019). Precision-cut liver slices: a versatile tool to advance liver research. *Hepatol Int*, *13*(1), 51-57. https://doi.org/10.1007/s12072-018-9913-7

Pan, C., Kumar, C., Bohl, S., Klingmueller, U., & Mann, M. (2009). Comparative proteomic phenotyping of cell lines and primary cells to assess preservation of cell type-specific functions. *Mol Cell Proteomics*, *8*(3), 443-450. https://doi.org/10.1074/mcp.M800258-MCP200

Pankov, R., & Yamada, K. M. (2002). Fibronectin at a glance. *Journal of cell science*, *115*(20), 3861-3863.

Pascussi, J. M., Gerbal-Chaloin, S., Fabre, J. M., Maurel, P., & Vilarem, M. J. (2000). Dexamethasone enhances constitutive androstane receptor expression in human hepatocytes: consequences on cytochrome P450 gene regulation. *Mol Pharmacol*, *58*(6), 1441-1450. https://doi.org/10.1124/mol.58.6.1441

Patterson, M., Chan, D. N., Ha, I., Case, D., Cui, Y., Handel, B. V., . . . Lowry, W. E. (2012). Defining the nature of human pluripotent stem cell progeny. *Cell research*, *22*(1), 178-193.

Pawlotsky, J. M., & Germanidis, G. (1999). The non-structural 5A protein of hepatitis C virus. *J Viral Hepat*, *6*(5), 343-356. https://doi.org/10.1046/j.1365-2893.1999.00185.x

Penin, F., Brass, V., Appel, N., Ramboarina, S., Montserret, R., Ficheux, D., . . . Moradpour, D. (2004). Structure and function of the membrane anchor domain of hepatitis C virus nonstructural protein 5A. *J Biol Chem*, *279*(39), 40835-40843. https://doi.org/10.1074/jbc.M404761200

Perlemuter, G., Sabile, A., Letteron, P., Vona, G., Topilco, A., Chrétien, Y., . . . Bréchot, C. (2002). Hepatitis C virus core protein inhibits microsomal triglyceride transfer protein activity and very low density lipoprotein secretion: a model of viral-related steatosis. *FASEB J*, *16*(2), 185-194. https://doi.org/10.1096/fj.01-0396com

Pfaender, S., Brinkmann, J., Todt, D., Riebesehl, N., Steinmann, J., Steinmann, J., . . . Steinmann, E. (2015). Mechanisms of methods for hepatitis C virus inactivation. *Applied and environmental microbiology*, *81*(5), 1616-1621.

Pflugheber, J., Fredericksen, B., Sumpter, R., Wang, C., Ware, F., Sodora, D. L., & Gale, M. (2002). Regulation of PKR and IRF-1 during hepatitis C virus RNA replication. *Proc Natl Acad Sci U S A*, *99*(7), 4650-4655. https://doi.org/10.1073/pnas.062055699

Pietschmann, T., Zayas, M., Meuleman, P., Long, G., Appel, N., Koutsoudakis, G., . . . Bartenschlager, R. (2009). Production of infectious genotype 1b virus particles in cell culture and impairment by replication enhancing mutations. *PLoS Pathog*, *5*(6), e1000475. https://doi.org/10.1371/journal.ppat.1000475

Pilch, P. F., & Czech, M. P. (1979). Interaction of cross-linking agents with the insulin effector system of isolated fat cells. Covalent linkage of 125I-insulin to a plasma membrane receptor protein of 140,000 daltons. *J Biol Chem*, *254*(9), 3375-3381.

Podevin, P., Carpentier, A., Pène, V., Aoudjehane, L., Carrière, M., Zaïdi, S., . . . Calmus, Y. (2010). Production of infectious hepatitis C virus in primary cultures of human adult hepatocytes. *Gastroenterology*, *139*(4), 1355-1364. https://doi.org/10.1053/j.gastro.2010.06.058

Poole, M. I., Sorribes, I., & Jain, H. V. (2018). Modeling hepatitis C virus protein and p53 interactions in hepatocytes: Implications for carcinogenesis. *Math Biosci*, *306*, 186-196. https://doi.org/10.1016/j.mbs.2018.10.003

Probst, A., Dang, T., Bochud, M., Egger, M., Negro, F., & Bochud, P. Y. (2011). Role of hepatitis C virus genotype 3 in liver fibrosis progression--a systematic review and meta-analysis. *J Viral Hepat*, *18*(11), 745-759. https://doi.org/10.1111/j.1365-2893.2011.01481.x

Purves, K., Reynolds, L. J., Sala-Comorera, L., Martin, N., Dahly, D., Meijer, W., & Fletcher, N. Decay of RNA and Infectious SARS-CoV-2 and Murine Hepatitis Virus in Wastewater. *Available at SSRN 4668621*.

Queiroz, C. J. S., Song, F., Reed, K. R., Al-Khafaji, N., Clarke, A. R., Vimalachandran, D., . . . Jenkins, J. R. (2020). NAP1L1: A Novel Human Colorectal Cancer Biomarker Derived From Animal Models of. *Front Oncol*, *10*, 1565. https://doi.org/10.3389/fonc.2020.01565

Quinkert, D., Bartenschlager, R., & Lohmann, V. (2005). Quantitative analysis of the hepatitis C virus replication complex. *J Virol*, *79*(21), 13594-13605. https://doi.org/10.1128/JVI.79.21.13594-13605.2005

Ramachandran, P., Pellicoro, A., Vernon, M. A., Boulter, L., Aucott, R. L., Ali, A., . . . Gordon-Walker, T. T. (2012). Differential Ly-6C expression identifies the recruited macrophage phenotype, which orchestrates the regression of murine liver fibrosis. *Proceedings of the National Academy of Sciences*, *109*(46), E3186-E3195.

Ramirez, S., & Bukh, J. (2018). Current status and future development of infectious cell-culture models for the major genotypes of hepatitis C virus: Essential tools in testing of antivirals and emerging vaccine strategies. *Antiviral Res*, *158*, 264-287. https://doi.org/10.1016/j.antiviral.2018.07.014

Ramirez, S., Mikkelsen, L. S., Gottwein, J. M., & Bukh, J. (2016). Robust HCV Genotype 3a Infectious Cell Culture System Permits Identification of Escape Variants With Resistance to Sofosbuvir. *Gastroenterology*, *151*(5), 973-985.e972. https://doi.org/10.1053/j.gastro.2016.07.013

Razavi, H., Sanchez Gonzalez, Y., Yuen, C., & Cornberg, M. (2020). Global timing of hepatitis C virus elimination in high-income countries. *Liver Int*, *40*(3), 522-529. https://doi.org/10.1111/liv.14324

Razavi, H., Waked, I., Sarrazin, C., Myers, R. P., Idilman, R., Calinas, F., . . . Estes, C. (2014). The present and future disease burden of hepatitis C virus (HCV) infection with today's treatment paradigm. *J Viral Hepat*, *21 Suppl 1*, 34-59. https://doi.org/10.1111/jvh.12248

Roderfeld, M., Weiskirchen, R., Wagner, S., Berres, M. L., Henkel, C., Grötzinger, J., . . . Roeb, E. (2006). Inhibition of hepatic fibrogenesis by matrix metalloproteinase-9 mutants in mice. *The FASEB journal*, *20*(3), 444-454.

Rong, X., Liu, J., Yao, X., Jiang, T., Wang, Y., & Xie, F. (2019). Human bone marrow mesenchymal stem cells-derived exosomes alleviate liver fibrosis through the Wnt/β-catenin pathway. *Stem cell research & therapy*, *10*, 1-11.

Ross-Thriepland, D., & Harris, M. (2015). Hepatitis C virus NS5A: enigmatic but still promiscuous 10 years on! *J Gen Virol*, *96*(Pt 4), 727-738. https://doi.org/10.1099/jgv.0.000009

Ross-Thriepland, D., Mankouri, J., & Harris, M. (2015). Serine phosphorylation of the hepatitis C virus NS5A protein controls the establishment of replication complexes. *J Virol*, *89*(6), 3123-3135. https://doi.org/10.1128/JVI.02995-14

Roth, S., Gong, W., & Gressner, A. M. (1998). Expression of different isoforms of TGF-beta and the latent TGF-beta binding protein (LTBP) by rat Kupffer cells. *J Hepatol*, *29*(6), 915-922. https://doi.org/10.1016/s0168-8278(98)80119-0

Rowe, R. G., Lin, Y., Shimizu-Hirota, R., Hanada, S., Neilson, E. G., Greenson, J. K., & Weiss, S. J. (2011). Hepatocyte-derived Snail1 propagates liver fibrosis progression. *Mol Cell Biol*, *31*(12), 2392-2403. https://doi.org/10.1128/MCB.01218-10

Rubbia-Brandt, L., Fabris, P., Paganin, S., Leandro, G., Male, P. J., Giostra, E., . . . Negro, F. (2004). Steatosis affects chronic hepatitis C progression in a genotype specific way. *Gut*, *53*(3), 406-412. https://doi.org/10.1136/gut.2003.018770

Sadasivan, S. K., Siddaraju, N., Khan, K. M., Vasamsetti, B., Kumar, N. R., Haridas, V., . . . Pralhada Rao, R. (2015). Developing an in vitro screening assay platform for evaluation of antifibrotic drugs using precision-cut liver slices. *Fibrogenesis Tissue Repair*, *8*(1), 1. https://doi.org/10.1186/s13069-014-0017-2

Saeed, M., Andreo, U., Chung, H. Y., Espiritu, C., Branch, A. D., Silva, J. M., & Rice, C. M. (2015). SEC14L2 enables pan-genotype HCV replication in cell culture. *Nature*, *524*(7566), 471-475. https://doi.org/10.1038/nature14899

Saeed, M., Scheel, T. K., Gottwein, J. M., Marukian, S., Dustin, L. B., Bukh, J., & Rice, C. M. (2012). Efficient replication of genotype 3a and 4a hepatitis C virus replicons in human hepatoma cells. *Antimicrob Agents Chemother*, *56*(10), 5365-5373. https://doi.org/10.1128/AAC.01256-12

Saha, B., Kodys, K., & Szabo, G. (2016). Hepatitis C Virus-Induced Monocyte Differentiation Into Polarized M2 Macrophages Promotes Stellate Cell Activation via TGF-β. *Cell Mol Gastroenterol Hepatol*, *2*(3), 302-316.e308. https://doi.org/10.1016/j.jcmgh.2015.12.005

Sahuc, M. E., Sahli, R., Rivière, C., Pène, V., Lavie, M., Vandeputte, A., . . . Séron, K. (2019). Dehydrojuncusol, a Natural Phenanthrene Compound Extracted from. *J Virol*, *93*(10). https://doi.org/10.1128/JVI.02009-18

Sainz, B., Barretto, N., & Uprichard, S. L. (2009). Hepatitis C virus infection in phenotypically distinct Huh7 cell lines. *PLoS One*, *4*(8), e6561. https://doi.org/10.1371/journal.pone.0006561

Sainz, B., Barretto, N., Yu, X., Corcoran, P., & Uprichard, S. L. (2012). Permissiveness of human hepatoma cell lines for HCV infection. *Virology journal*, *9*, 1-16.

Sainz, B., TenCate, V., & Uprichard, S. L. (2009). Three-dimensional Huh7 cell culture system for the study of Hepatitis C virus infection. *Virol J*, *6*, 103. https://doi.org/10.1186/1743-422X-6-103

Sainz Jr, B., & Chisari, F. V. (2006). Production of infectious hepatitis C virus by well-differentiated, growth-arrested human hepatoma-derived cells. *Journal of virology*, *80*(20), 10253-10257.

Saito, T., Owen, D. M., Jiang, F., Marcotrigiano, J., & Gale Jr, M. (2008). Innate immunity induced by composition-dependent RIG-I recognition of hepatitis C virus RNA. *Nature*, *454*(7203), 523-527.

Salloum, S., Holmes, J. A., Jindal, R., Bale, S. S., Brisac, C., Alatrakchi, N., . . . Luther, J. (2016). Exposure to human immunodeficiency virus/hepatitis C virus in hepatic and stellate cell lines reveals cooperative profibrotic transcriptional activation between viruses and cell types. *Hepatology*, *64*(6), 1951-1968.

Samur, S., Kues, B., Ayer, T., Roberts, M. S., Kanwal, F., Hur, C., . . . Chhatwal, J. (2018). Cost Effectiveness of Pre- vs Post-Liver Transplant Hepatitis C Treatment With Direct-Acting Antivirals. *Clin Gastroenterol Hepatol*, *16*(1), 115-122.e110. https://doi.org/10.1016/j.cgh.2017.06.024

Saran, C., Fu, D., Ho, H., Klein, A., Fallon, J. K., Honkakoski, P., & Brouwer, K. L. R. (2022). A novel differentiated HuH-7 cell model to examine bile acid metabolism, transport and cholestatic hepatotoxicity. *Sci Rep*, *12*(1), 14333. https://doi.org/10.1038/s41598-022-18174-z

Scarpa, M., Grillo, A. R., Brun, P., Macchi, V., Stefani, A., Signori, S., . . . Martines, D. (2011). Snail1 transcription factor is a critical mediator of hepatic stellate cell activation following hepatic injury. *Am J Physiol Gastrointest Liver Physiol*, *300*(2), G316-326. https://doi.org/10.1152/ajpgi.00141.2010

Schaffert, C. S., Duryee, M. J., Bennett, R. G., DeVeney, A. L., Tuma, D. J., Olinga, P., . . . Klassen, L. W. (2010). Exposure of precision-cut rat liver slices to ethanol accelerates fibrogenesis. *Am J Physiol Gastrointest Liver Physiol*, *299*(3), G661-668. https://doi.org/10.1152/ajpgi.00287.2009

Schaller, T., Appel, N., Koutsoudakis, G., Kallis, S., Lohmann, V., Pietschmann, T., & Bartenschlager, R. (2007). Analysis of hepatitis C virus superinfection exclusion by using novel fluorochrome gene-tagged viral genomes. *J Virol*, *81*(9), 4591-4603. https://doi.org/10.1128/JVI.02144-06

Schmidt, T. G., & Skerra, A. (1993). The random peptide library-assisted engineering of a C-terminal affinity peptide, useful for the detection and purification of a functional Ig Fv fragment. *Protein Eng*, *6*(1), 109-122. https://doi.org/10.1093/protein/6.1.109

Schon, H.-T., Bartneck, M., Borkham-Kamphorst, E., Nattermann, J., Lammers, T., Tacke, F., & Weiskirchen, R. (2016). Pharmacological intervention in hepatic stellate cell activation and hepatic fibrosis. *Frontiers in pharmacology*, *7*, 33.

Schulze, R. J., Schott, M. B., Casey, C. A., Tuma, P. L., & McNiven, M. A. (2019). The cell biology of the hepatocyte: A membrane trafficking machine. *J Cell Biol*, *218*(7), 2096-2112. https://doi.org/10.1083/jcb.201903090

Schön, S., Flierman, I., Ofner, A., Stahringer, A., Holdt, L. M., Kolligs, F. T., & Herbst, A. (2014). β-catenin regulates NF-κB activity via TNFRSF19 in colorectal cancer cells. *International journal of cancer*, *135*(8), 1800-1811.

Sekine-Osajima, Y., Sakamoto, N., Mishima, K., Nakagawa, M., Itsui, Y., Tasaka, M., . . . Watanabe, M. (2008). Development of plaque assays for hepatitis C virus-JFH1 strain and isolation of mutants with enhanced cytopathogenicity and replication capacity. *Virology*, *371*(1), 71-85. https://doi.org/10.1016/j.virol.2007.09.019

Serrano-Gomez, S. J., Maziveyi, M., & Alahari, S. K. (2016). Regulation of epithelial-mesenchymal transition through epigenetic and post-translational modifications. *Molecular cancer*, *15*(1), 1-14.

Shah, P. S., Beesabathuni, N. S., Fishburn, A. T., Kenaston, M. W., Minami, S. A., Pham, O. H., & Tucker, I. (2022). Systems Biology of Virus-Host Protein Interactions: From Hypothesis Generation to Mechanisms of Replication and Pathogenesis. *Annu Rev Virol*, *9*(1), 397-415. https://doi.org/10.1146/annurev-virology-100520-011851

Shan, G., Li, Y., Zhang, J., Li, W., Szulwach, K. E., Duan, R., . . . Jin, P. (2008). A small molecule enhances RNA interference and promotes microRNA processing. *Nat Biotechnol*, *26*(8), 933-940. https://doi.org/10.1038/nbt.1481

Shang, X.-Z., Zhu, H., Lin, K., Tu, Z., Chen, J., Nelson, D. R., & Liu, C. (2004). Stabilized β-catenin promotes hepatocyte proliferation and inhibits TNFα-induced apoptosis. *Laboratory investigation*, *84*(3), 332-341.

Shi, L., Qin, E., Zhou, J., Zhao, J., Nie, W., Jiang, T., . . . Liu, L. (2016). HIV and HCV co-culture promotes profibrogenic gene expression through an epimorphin-mediated ERK signaling pathway in hepatic stellate cells. *PLoS One*, *11*(6), e0158386.

Shimizu, K., Soroida, Y., Sato, M., Hikita, H., Kobayashi, T., Endo, M., . . . Ikeda, H. (2018). Eradication of hepatitis C virus is associated with the attenuation of steatosis as evaluated using a controlled attenuation parameter. *Sci Rep*, *8*(1), 7845. https://doi.org/10.1038/s41598-018-26293-9

Shimoike, T., Koyama, C., Murakami, K., Suzuki, R., Matsuura, Y., Miyamura, T., & Suzuki, T. (2006). Down-regulation of the internal ribosome entry site (IRES)-mediated translation of the hepatitis C virus: critical role of binding of the stem-loop IIId

domain of IRES and the viral core protein. *Virology*, *345*(2), 434-445. https://doi.org/10.1016/j.virol.2005.10.013

Shin, J. Y., Hur, W., Wang, J. S., Jang, J. W., Kim, C. W., Bae, S. H., . . . Yoon, S. K. (2005). HCV core protein promotes liver fibrogenesis via up-regulation of CTGF with TGF-beta1. *Exp Mol Med*, *37*(2), 138-145. https://doi.org/10.1038/emm.2005.19

Shirane, M., & Nakayama, K. I. (2003). Inherent calcineurin inhibitor FKBP38 targets Bcl-2 to mitochondria and inhibits apoptosis. *Nat Cell Biol*, *5*(1), 28-37. https://doi.org/10.1038/ncb894

Shrivastava, A., Manna, S. K., Ray, R., & Aggarwal, B. B. (1998). Ectopic expression of hepatitis C virus core protein differentially regulates nuclear transcription factors. *Journal of Virology*, *72*(12), 9722-9728.

Simmonds, P. (2013). The origin of hepatitis C virus. *Curr Top Microbiol Immunol*, *369*, 1-15. https://doi.org/10.1007/978-3-642-27340-7_1

Sinigaglia, A., Lavezzo, E., Trevisan, M., Sanavia, T., Di Camillo, B., Peta, E., . . . Sarcognato, S. (2015). Changes in micro RNA expression during disease progression in patients with chronic viral hepatitis. *Liver International*, *35*(4), 1324-1333.

Sir, D., Chen, W. L., Choi, J., Wakita, T., Yen, T. S., & Ou, J. H. (2008). Induction of incomplete autophagic response by hepatitis C virus via the unfolded protein response. *Hepatology*, *48*(4), 1054-1061. https://doi.org/10.1002/hep.22464

Smirnov, A., Magri, A., Lotz, R., Han, X., Yin, C., Harris, M., . . . Lu, X. (2023). ASPP2 binds to hepatitis C virus NS5A protein via an SH3 domain/PxxP motif-mediated interaction and potentiates infection. *J Gen Virol*, *104*(9). https://doi.org/10.1099/jgv.0.001895

Smirnova, O. A., Ivanova, O. N., Bartosch, B., Valuev-Elliston, V. T., Mukhtarov, F., Kochetkov, S. N., & Ivanov, A. V. (2016). Hepatitis C Virus NS5A Protein Triggers Oxidative Stress by Inducing NADPH Oxidases 1 and 4 and Cytochrome P450 2E1. *Oxid Med Cell Longev*, *2016*, 8341937. https://doi.org/10.1155/2016/8341937

Smith, B. K., & Steinberg, G. R. (2017). AMP-activated protein kinase, fatty acid metabolism, and insulin sensitivity. *Curr Opin Clin Nutr Metab Care*, *20*(4), 248-253. https://doi.org/10.1097/MCO.0000000000000380

Song, H., Li, J., Shi, S., Yan, L., Zhuang, H., & Li, K. (2010). Thermal stability and inactivation of hepatitis C virus grown in cell culture. *Virology journal*, *7*, 1-12.

Spearman, C. W., Dusheiko, G. M., Hellard, M., & Sonderup, M. (2019). Hepatitis C. *Lancet*, *394*(10207), 1451-1466. https://doi.org/10.1016/S0140-6736(19)32320-7

Starokozhko, V., Vatakuti, S., Schievink, B., Merema, M. T., Asplund, A., Synnergren, J., . . . Groothuis, G. M. M. (2017). Maintenance of drug metabolism and transport functions in human precision-cut liver slices during prolonged incubation for 5 days. *Arch Toxicol*, *91*(5), 2079-2092. https://doi.org/10.1007/s00204-016-1865-x

Steinmann, E., Doerrbecker, J., Friesland, M., Riebesehl, N., Ginkel, C., Hillung, J., . . . Pietschmann, T. (2013). Characterization of hepatitis C virus intra- and intergenotypic chimeras reveals a role of the glycoproteins in virus envelopment. *J Virol*, *87*(24), 13297-13306. https://doi.org/10.1128/JVI.01708-13

Stiffler, J. D., Nguyen, M., Sohn, J. A., Liu, C., Kaplan, D., & Seeger, C. (2009). Focal distribution of hepatitis C virus RNA in infected livers. *PLoS One*, *4*(8), e6661. https://doi.org/10.1371/journal.pone.0006661

Street, A., Macdonald, A., Crowder, K., & Harris, M. (2004). The Hepatitis C virus NS5A protein activates a phosphoinositide 3-kinase-dependent survival signaling cascade. *Journal of Biological Chemistry*, *279*(13), 12232-12241.

Su, X., Liu, S., Zhang, X., Lam, S. M., Hu, X., Zhou, Y., . . . Shui, G. (2017). Requirement of cytosolic phospholipase A2 gamma in lipid droplet formation. *Biochimica et Biophysica Acta (BBA)-Molecular and Cell Biology of Lipids*, *1862*(7), 692-705.

Sumpter, R., Loo, Y. M., Foy, E., Li, K., Yoneyama, M., Fujita, T., . . . Gale, M. (2005). Regulating intracellular antiviral defense and permissiveness to hepatitis C virus RNA replication through a cellular RNA helicase, RIG-I. *J Virol*, *79*(5), 2689-2699. https://doi.org/10.1128/JVI.79.5.2689-2699.2005

Takamizawa, A., Mori, C., Fuke, I., Manabe, S., Murakami, S., Fujita, J., . . . Okayama, H. (1991). Structure and organization of the hepatitis C virus genome isolated from human carriers. *Journal of virology*, *65*(3), 1105-1113.

Tan, S. L. (2006). Hepatitis C Viruses: Genomes and Molecular Biology. In. https://doi.org/NBK1630

Tanaka, M., Nagano-Fujii, M., Deng, L., Ishido, S., Sada, K., & Hotta, H. (2006). Single-point mutations of hepatitis C virus NS3 that impair p53 interaction and anti-apoptotic activity of NS3. *Biochem Biophys Res Commun*, *340*(3), 792-799. https://doi.org/10.1016/j.bbrc.2005.12.076

Tayyab, G. U. N., Rasool, S., Nasir, B., Rubi, G., Abou-Samra, A. B., & Butt, A. A. (2020). Hepatocellular carcinoma occurs frequently and early after treatment in HCV genotype 3 infected persons treated with DAA regimens. *BMC Gastroenterol*, *20*(1), 93. https://doi.org/10.1186/s12876-020-01249-4

Tellinghuisen, T. L., Marcotrigiano, J., Gorbalenya, A. E., & Rice, C. M. (2004). The NS5A protein of hepatitis C virus is a zinc metalloprotein. *J Biol Chem*, *279*(47), 48576-48587. https://doi.org/10.1074/jbc.M407787200

Trampuž, S. R., van Riet, S., Nordling, Å., & Ingelman-Sundberg, M. (2023). The Role of CTGF in Liver Fibrosis Induced in 3D Human Liver Spheroids. *Cells*, *12*(2), 302.

Valley, C. C., Cembran, A., Perlmutter, J. D., Lewis, A. K., Labello, N. P., Gao, J., & Sachs, J. N. (2012). The methionine-aromatic motif plays a unique role in stabilizing protein structure. *J Biol Chem*, *287*(42), 34979-34991. https://doi.org/10.1074/jbc.M112.374504

Vassilaki, N., Kalliampakou, K. I., Kotta-Loizou, I., Befani, C., Liakos, P., Simos, G., . . . Mavromara, P. (2013). Low oxygen tension enhances hepatitis C virus replication. *J Virol*, *87*(5), 2935-2948. https://doi.org/10.1128/JVI.02534-12

Vescovo, T., Refolo, G., Vitagliano, G., Fimia, G. M., & Piacentini, M. (2016). Molecular mechanisms of hepatitis C virus–induced hepatocellular carcinoma. *Clinical Microbiology and Infection*, *22*(10), 853-861.

Vrazas, V., Moustafa, S., Makridakis, M., Karakasiliotis, I., Vlahou, A., Mavromara, P., & Katsani, K. R. (2022). A Proteomic Approach to Study the Biological Role of Hepatitis C Virus Protein Core+1/ARFP. *Viruses*, *14*(8). https://doi.org/10.3390/v14081694

Waked, I., Esmat, G., Elsharkawy, A., El-Serafy, M., Abdel-Razek, W., Ghalab, R., . . . Zaid, H. (2020). Screening and Treatment Program to Eliminate Hepatitis C in Egypt. *N Engl J Med*, *382*(12), 1166-1174. https://doi.org/10.1056/NEJMsr1912628

Wakita, T., Pietschmann, T., Kato, T., Date, T., Miyamoto, M., Zhao, Z., . . . Liang, T. J. (2005). Production of infectious hepatitis C virus in tissue culture from a cloned viral genome. *Nat Med*, *11*(7), 791-796. https://doi.org/10.1038/nm1268

Walker, A. J., Peacock, C. J., Pedergnana, V., Irving, W. L., & Consortium, S.-H. (2018). Host genetic factors associated with hepatocellular carcinoma in patients with hepatitis C virus infection: A systematic review. *J Viral Hepat*, *25*(5), 442-456. https://doi.org/10.1111/jvh.12871

Wang, J., Tong, W., Zhang, X., Chen, L., Yi, Z., Pan, T., . . . Yuan, Z. (2006). Hepatitis C virus non-structural protein NS5A interacts with FKBP38 and inhibits apoptosis in Huh7 hepatoma cells. *FEBS Lett*, *580*(18), 4392-4400. https://doi.org/10.1016/j.febslet.2006.07.002

Wang, J. Q., Tang, Q., Parelkar, N. K., Liu, Z., Samdani, S., Choe, E. S., . . . Mao, L. (2004). Glutamate signaling to Ras-MAPK in striatal neurons: mechanisms for inducible gene expression and plasticity. *Molecular neurobiology*, *29*, 1-14.

Wang, M., Wey, S., Zhang, Y., Ye, R., & Lee, A. S. (2009). Role of the unfolded protein response regulator GRP78/BiP in development, cancer, and neurological disorders. *Antioxid Redox Signal*, *11*(9), 2307-2316. https://doi.org/10.1089/ars.2009.2485

Wang, T., Larcher, L. M., Ma, L., & Veedu, R. N. (2018). Systematic Screening of Commonly Used Commercial Transfection Reagents towards Efficient Transfection of Single-Stranded Oligonucleotides. *Molecules*, *23*(10). https://doi.org/10.3390/molecules23102564

Ward, J. C., Bowyer, S., Chen, S., Fernandes Campos, G. R., Ramirez, S., Bukh, J., & Harris, M. (2020). Insights into the unique characteristics of hepatitis C virus genotype 3 revealed by development of a robust sub-genomic DBN3a replicon. *J Gen Virol*, *101*(11), 1182-1190. https://doi.org/10.1099/jgv.0.001486

Waris, G., Livolsi, A., Imbert, V., Peyron, J. F., & Siddiqui, A. (2003). Hepatitis C virus NS5A and subgenomic replicon activate NF-kappaB via tyrosine phosphorylation of IkappaBalpha and its degradation by calpain protease. *J Biol Chem*, *278*(42), 40778-40787. https://doi.org/10.1074/jbc.M303248200

Wei, D., Li, N. L., Zeng, Y., Liu, B., Kumthip, K., Wang, T. T., . . . Li, K. (2016). The Molecular Chaperone GRP78 Contributes to Toll-like Receptor 3-mediated Innate Immune Response to Hepatitis C Virus in Hepatocytes. *J Biol Chem*, *291*(23), 12294-12309. https://doi.org/10.1074/jbc.M115.711598

Wells, R. G. (2013). Tissue mechanics and fibrosis. *Biochimica et Biophysica Acta (BBA)-Molecular Basis of Disease*, *1832*(7), 884-890.

Westin, J., Nordlinder, H., Lagging, M., Norkrans, G., & Wejstål, R. (2002). Steatosis accelerates fibrosis development over time in hepatitis C virus genotype 3 infected patients. *J Hepatol*, *37*(6), 837-842. https://doi.org/10.1016/s0168-8278(02)00299-4

Westra, I. M., Oosterhuis, D., Groothuis, G. M., & Olinga, P. (2014). The effect of antifibrotic drugs in rat precision-cut fibrotic liver slices. *PLoS One*, *9*(4), e95462. https://doi.org/10.1371/journal.pone.0095462

Westra, I. M., Pham, B. T., Groothuis, G. M., & Olinga, P. (2013). Evaluation of fibrosis in precision-cut tissue slices. *Xenobiotica*, *43*(1), 98-112. https://doi.org/10.3109/00498254.2012.723151

Wilhelm, M., Schlegl, J., Hahne, H., Gholami, A. M., Lieberenz, M., Savitski, M. M., . . . Kuster, B. (2014). Mass-spectrometry-based draft of the human proteome. *Nature*, *509*(7502), 582-587. https://doi.org/10.1038/nature13319

Willows, R., Sanders, M. J., Xiao, B., Patel, B. R., Martin, S. R., Read, J., . . . Carling, D. (2017). Phosphorylation of AMPK by upstream kinases is required for activity in mammalian cells. *Biochem J*, *474*(17), 3059-3073. https://doi.org/10.1042/BCJ20170458

Wilson, G. K., Brimacombe, C. L., Rowe, I. A., Reynolds, G. M., Fletcher, N. F., Stamataki, Z., . . . Afford, S. C. (2012). A dual role for hypoxia inducible factor-1α in the hepatitis C virus lifecycle and hepatoma migration. *Journal of hepatology*, *56*(4), 803-809.

Wilson, G. K., & Stamataki, Z. (2012). In vitro systems for the study of hepatitis C virus infection. *Int J Hepatol*, *2012*, 292591. https://doi.org/10.1155/2012/292591

Windisch, M. P., Frese, M., Kaul, A., Trippler, M., Lohmann, V., & Bartenschlager, R. (2005). Dissecting the interferon-induced inhibition of hepatitis C virus replication by using a novel host cell line. *Journal of virology*, *79*(21), 13778-13793.

Wose Kinge, C. N., Espiritu, C., Prabdial-Sing, N., Sithebe, N. P., Saeed, M., & Rice, C. M. (2014). Hepatitis C virus genotype 5a subgenomic replicons for evaluation of direct-acting antiviral agents. *Antimicrob Agents Chemother*, *58*(9), 5386-5394. https://doi.org/10.1128/AAC.03534-14

Wu, F., Wu, D., Ren, Y., Huang, Y., Feng, B., Zhao, N., . . . Xu, A. (2019). Generation of hepatobiliary organoids from human induced pluripotent stem cells. *Journal of Hepatology*, *70*(6), 1145-1158.

Wu, S. C., & Wong, S. L. (2013). Structure-guided design of an engineered streptavidin with reusability to purify streptavidin-binding peptide tagged proteins or biotinylated proteins. *PLoS One*, *8*(7), e69530. https://doi.org/10.1371/journal.pone.0069530

Wu, X., Roberto, J. B., Knupp, A., Greninger, A. L., Truong, C. D., Hollingshead, N., . . . Koelle, D. M. (2022). Response of human liver tissue to innate immune stimuli. *Frontiers in Immunology*, *13*, 811551.

Wu, X., Roberto, J. B., Knupp, A., Kenerson, H. L., Truong, C. D., Yuen, S. Y., . . . Crispe, I. N. (2018). Precision-cut human liver slice cultures as an immunological platform. *J Immunol Methods*, *455*, 71-79. https://doi.org/10.1016/j.jim.2018.01.012

Wu, X., Robotham, J. M., Lee, E., Dalton, S., Kneteman, N. M., Gilbert, D. M., & Tang, H. (2012). Productive hepatitis C virus infection of stem cell-derived hepatocytes reveals a critical transition to viral permissiveness during differentiation. *PLoS pathogens*, *8*(4), e1002617.

Xiaohua Zhu, Xie, Y., Huang, W., Chen, Z., & Guo, S. (2022). NAP1L1 promotes tumor proliferation through HDGF/C-JUN signaling in ovarian cancer. *BMC Cancer*, *22*(1), 339. https://doi.org/10.1186/s12885-022-09356-z

Xu, L., Hui, A. Y., Albanis, E., Arthur, M. J., O'Byrne, S. M., Blaner, W. S., . . . Eng, F. J. (2005). Human hepatic stellate cell lines, LX-1 and LX-2: new tools for analysis of hepatic fibrosis. *Gut*, *54*(1), 142-151. https://doi.org/10.1136/gut.2004.042127

Yin, P., Li, Y., Zhou, L., & Zhang, L. (2018). NAP1L1 Regulates Hepatitis C Virus Entry and Interacts with NS3. *Virol Sin*, *33*(2), 205-208. https://doi.org/10.1007/s12250-018-0006-5

Yoon, E. J., & Hu, K. Q. (2006). Hepatitis C virus (HCV) infection and hepatic steatosis. *Int J Med Sci*, *3*(2), 53-56. https://doi.org/10.7150/ijms.3.53

Yoshiji, H., Kuriyama, S., Miyamoto, Y., Thorgeirsson, U. P., Gomez, D. E., Kawata, M., . . . Tsujinoue, H. (2000). Tissue inhibitor of metalloproteinases-1 promotes liver fibrosis development in a transgenic mouse model. *Hepatology*, *32*(6), 1248-1254.

Yu, M., Peng, B., Chan, K., Gong, R., Yang, H., Delaney, W., & Cheng, G. (2014). Robust and persistent replication of the genotype 6a hepatitis C virus replicon in cell culture. *Antimicrob Agents Chemother*, *58*(5), 2638-2646. https://doi.org/10.1128/AAC.01780-13

Zarębska-Michaluk, D., Lebensztejn, D., Chrapek, M., Paluch, K., Stępień, P., & Kryczka, W. (2016). Predictors of sustained virological response in patients with hepatitis C virus genotype 3 infection. *Clin Exp Hepatol*, *2*(3), 117-124. https://doi.org/10.5114/ceh.2016.62526

Zecha, J., Meng, C., Zolg, D. P., Samaras, P., Wilhelm, M., & Kuster, B. (2018). Peptide Level Turnover Measurements Enable the Study of Proteoform Dynamics. *Mol Cell Proteomics*, *17*(5), 974-992. https://doi.org/10.1074/mcp.RA118.000583

Zein, N. N. (2000). Clinical significance of hepatitis C virus genotypes. *Clinical microbiology reviews*, *13*(2), 223-235.

Zhai, W., Ma, J., Zhu, R., Xu, C., Zhang, J., Chen, Y., . . . Xue, W. (2018). MiR-532-5p suppresses renal cancer cell proliferation by disrupting the ETS1-mediated positive feedback loop with the KRAS-NAP1L1/P-ERK axis. *Br J Cancer*, *119*(5), 591-604. https://doi.org/10.1038/s41416-018-0196-5

Zhang, F., Wang, H., Wang, X., Jiang, G., Liu, H., Zhang, G., . . . Du, J. (2016). TGF-β induces M2-like macrophage polarization via SNAIL-mediated suppression of a pro-inflammatory phenotype. *Oncotarget*, *7*(32), 52294-52306. https://doi.org/10.18632/oncotarget.10561

Zhang, H., Zhang, C., Tang, H., Gao, S., Sun, F., Yang, Y., . . . Li, C. (2018). CD2-Associated Protein Contributes to Hepatitis C, Virus Propagation and Steatosis by Disrupting Insulin Signaling. *Hepatology*, *68*(5), 1710-1725. https://doi.org/10.1002/hep.30073

Zhang, W., Conway, S. J., Liu, Y., Snider, P., Chen, H., Gao, H., . . . Kubal, C. (2021). Heterogeneity of Hepatic Stellate Cells in Fibrogenesis of the Liver: Insights from Single-Cell Transcriptomic Analysis in Liver Injury. *Cells*, *10*(8). https://doi.org/10.3390/cells10082129

Zhang, Y. W., Chen, Q., Li, B., Li, H. Y., Zhao, X. K., Xiao, Y. Y., . . . Zuo, S. (2021). NAP1L1 Functions as a Tumor Promoter. *Front Cell Dev Biol*, *9*, 659680. https://doi.org/10.3389/fcell.2021.659680

Zhao, S. F., Wang, S. G., Zhao, Z. Y., & Li, W. L. (2019). AKR1C1-3, notably AKR1C3, are distinct biomarkers for liver cancer diagnosis and prognosis: Database mining in

malignancies. *Oncol Lett*, *18*(5), 4515-4522. https://doi.org/10.3892/ol.2019.10802

Zhu, H., & Liu, C. (2003). Interleukin-1 inhibits hepatitis C virus subgenomic RNA replication by activation of extracellular regulated kinase pathway. *Journal of virology*, *77*(9), 5493-5498.

Zhu, L., Zhou, Y., Li, R., & Deng, S. (2022). Macrophages produce PGE2 to promote hepatic stellate cell autophagy and liver fibrosis. *Autophagy Reports*, *1*(1), 389-392.

Zhu, Q., Guo, J. T., & Seeger, C. (2003). Replication of hepatitis C virus subgenomes in nonhepatic epithelial and mouse hepatoma cells. *J Virol*, *77*(17), 9204-9210. https://doi.org/10.1128/jvi.77.17.9204-9210.2003

Zigmond, E., Samia-Grinberg, S., Pasmanik-Chor, M., Brazowski, E., Shibolet, O., Halpern, Z., & Varol, C. (2014). Infiltrating monocyte-derived macrophages and resident kupffer cells display different ontogeny and functions in acute liver injury. *The Journal of Immunology*, *193*(1), 344-353.

Çevik, R. E., Cesarec, M., Da Silva Filipe, A., Licastro, D., McLauchlan, J., & Marcello, A. (2017). Hepatitis C Virus NS5A Targets Nucleosome Assembly Protein NAP1L1 To Control the Innate Cellular Response. *J Virol*, *91*(18). https://doi.org/10.1128/JVI.00880-17